Recycled Materials Resource Center

Project No. 27:

Full Scale Monitoring for Assessment of Exothermal Reactions in Waste Tires

Final Report

February 2006

by

Hailey L. Wappett[1]

Jorge G. Zornberg[2]

[1] Graduate Student, Department of Civil, Architectural and Environmental Engineering, University of Texas at Austin

[2] Assistant Professor, Department of Civil, Architectural and Environmental Engineering, University of Texas at Austin, University of Texas at Austin

Table of Contents

Acknowledgements

Financial support for this project was provided by the Recycled Materials Resource Center (RMRC) of the Federal Highway Administration (FHWA). This support is appreciated. The contribution of Tim Fitzgerald and Brent Vollenweider, former students at the University of Colorado at Boulder, and Yuri D. Costa, former graduate student at the University of Sao Paulo at Sao Carlos are also gratefully acknowledged.

Introduction

Nearly 250 million tires per year are added to the 2 billion tires that already exist in landfills in the United States (Edil and Bosscher, 1994). This significant amount of waste has created a major challenge in determining methods of tire disposal that are both environmentally sound and aesthetically pleasing. Civil engineers have tackled the issue and proposed the beneficial reuse of tires into tire products such as tire shreds and tire bales, for use in civil engineering projects including retaining structures, backfill and road sub-grade. The technical issues involved with these applications are varied and difficult, ranging from mechanical properties that affect deformation to the thermal properties of tires that can potentially trigger exothermic reactions within the tire fill.

Tire shreds have been found to provide an economical alternative for lightweight backfill material. Tire shreds have performed well mechanically in over 70 civil engineering projects across the United States. Many of these projects used 100,000 to 1 million scrap tires (Humphrey, 1996). The volume of tires that these relatively small engineering projects utilize can significantly decrease the number of tires disposed of annually and minimize the size of existing tire stockpiles and all the aesthetic, environmental, and health risks associated with large tire stockpiles.

Despite the positive mechanical properties of tire shreds when used as lightweight backfill material, there have been several cases across the United States where the tire shred embankments have experienced internal exothermic reaction that ultimately led to failure of the project. Preliminary evaluations have been conducted to determine the cause of the heating within the embankments in order to minimize the risk of using tire shreds in civil engineering applications (Humphrey, 1996). Several potential causes include: oxidation of the steel wires left exposed when the tires are shredded, biodegradation of petroleum products and/or oxidation of the rubber itself. Although the causes of the exothermic reactions have not being confirmed, two documents have been published that present design guidelines and recommendations for use of tire shreds: *Design Guidelines to Minimize Internal Heating of Tire Shred Fills* (Ad Hoc Civil Engineering Committee, 1997), and *ASTM D6270: Standard Practice for Use of Scrap Tires in Civil Engineering Application*,(ASTM, 1998).

One of the main purposes of this report is to evaluate the mechanical behavior of a prototype embankment fill built with tire shreds and cohesive soil. The embankment consisted of three cross-sections comprising distinct configurations, that is, with successive layers of soil and tire-shreds, with a soil-tire shred mixture, and with pure soil. Immediately after construction, the embankment was submitted to heavy truck traffic and settlements were monitored for over two years at different locations across the surface of each section. Plate load tests were carried out on the embankment in order to assess the stress-settlement behavior of the different sections proceeding traffic exposure. This investigation also provides insight into the *in-situ* compression, compaction and preparation characteristics of soil-tire shred mixtures and pure tire shreds as backfill materials.

Another main purpose of this research is to evaluate design approaches that are expected to *prevent* these heat generating reactions and evaluate existing design recommendations that will minimize the potential for exothermic reactions to occur.

Specifically, this research will attempt to prove that, when mixed or layered with soil, tire shreds do not experience an exothermic reaction. This will be achieved by analysis of data collected from the prototype embankment built with tire shreds using different layouts during construction.

Background

Tire Shredding

Millions of tires are disposed of annually; however, only about 30% end up in landfills, and many thousands are illegally dumped (Lee et al., 1999). This situation has created a need for inventive approaches for recycling and/or reusing scrap tires. Approaches already being used include tire derived fuel for energy generation, highway barriers, crumb rubber asphalt pavement, breakwaters, etc. While these approaches have decreased the number of tires in present stockpiles, the quantities are not significant enough to eliminate the need for additional means of reuse, such as applications in civil engineering projects.

A tire reuse method that can dispose large volumes of tires involves the use of tire shreds. The low unit weight, flexibility, and strength of tire shreds make them a promising alternative in place of more expensive materials used for backfill or drainage layers. Tire shreds have been used as an aggregate replacement in nonstructural sound barriers, lightweight backfill on either normal or soft, unstable ground, and as a drainage material (Edil and Bosscher, 1994). Tire shreds have also been used in landfills as daily cover and as a drainage layer in the leachate collection system. The properties and characteristics of tire shreds make them a favorable alternative to other expensive backfill or reinforcement materials used in civil engineering applications.

Tire shreds are produced by either shearing or tearing scrap tires. The tire shreds are approximately 30 to 300 mm in length (Humphrey et al., 1996) and cost

approximately $30/ton to produce (Rick Welle, personal communication 2003). Shearing and tearing produce tire shreds with slightly different properties, specifically the amount of steel exposed. Typical passenger vehicle tires are 10% steel by weight (Humphrey, 1996); however, the percentage of steel in tire shreds is slightly higher than in new tires due to the wear down of the rubber from use. When tires are shredded many of the steel reinforcing belts are left exposed. Although the steel reinforcements are exposed despite the method of shredding, the shearing method does not expose as much steel as the tearing method and therefore has been the preferred method. It has been hypothesized that oxidation of the exposed steel contributes to the exothermic reactions in tire shred embankments. Therefore, tire shreds produced by shearing are recommended to reduce the potential for this oxidation and ultimately the possibility of exothermic reactions within the embankment.

Mechanical Response of Embankment Background

Tire shreds were first used as fill material to replace a conventional fill over soft organic soil in order to reduce settlements. Since then, numerous projects have employed tire-shreds in the construction of lightweight embankment fills, conventional fills, reinforced retaining wall backfills, and insulation against pavement frost (Humphrey 1997). Tire shreds are also used as drainage material in landfill cover and liner systems (Reddy and Saichek 1998).

Pure tire shreds show high compressibility at low confining stresses. However, once the amount of plastic deformation involved is not irrelevant, the compressibility of the material is significantly reduced after the fist loading cycle (Humphrey and Manion 1992, Edil and Bosscher 1994). As a result, static or vibratory efforts in the field do not significantly improve compaction after the first or second pass of the roller. The initial compressibility appears to be less significant for tire shreds of larger sizes (Dickson et al. 2001).

The compressibility of soil-tire shred mixtures is directly proportional to the content of tire shreds. For tire shred contents typically used in the field, between 10 and 30% by weight, the compressive behavior of the resulting composite is likely to be controlled by the compressive behavior of the tire shreds embedded in the soil matrix. Factors such as compactive effort and water content are known to play a minor role on the compaction of such mixtures (Humphrey and Manion 1992, Ahmed and Lovell 1993, Edil and Bosscher 1994).

Typically, settlement of embankment fills with pure tire shreds or soil-tire shred composites are higher than that of fills of pure soil (Bosscher et al. 1992, Hoppe 1998). Most of the observed settlement takes place during the first few months following construction. For embankments with pure tire shreds, it has been observed that this period is equal to 30-60 days (Tweedie et al. 1998b, Dickson et al. 2001). Due to the high compressibility at low confining stresses, as mentioned above, a soil cover has been found to be very effective in the reduction of settlement of embankment fills containing tire shreds, especially in situations involving pure tire shreds (Bosscher et al. 1992). Bosscher et al. (1997) recommend for design a minimum soil cover thickness of 1 m.

Several laboratorial studies were conducted to investigate the mechanical properties of soil-tire shred mixtures. The shear strength of sand-tire shred mixtures involving large-scale direct shear tests was evaluated by Edil and Bosscher (1994) and Foose et al. (1996). It was noted that the addition of more than 10% by weight of tire shreds improved the shear strength of the sand, particularly at low and intermediate confining stresses. Normal stress, tire shred content and sand matrix unit weight were the factors that mostly affect the shear strength of the mixture. Friction angle increased from 34^0 for pure sand to as much as 67^0 upon addition of tire shreds.

The triaxial behavior of tire shred-soil composites was evaluated by Masad et al. (1996) and Lee et al. (1999). Shreds with approximate dimensions (lower than 4.75 mm) and Ottawa sand were used in both studies. Pure tire shred specimens showed an

approximate linear stress-strain response for confining pressures ranging from 28 to 350 kPa, while sand-tire shred mixtures presented an intermediate response between that of pure sand and pure tire shreds for the same range of confining stresses. The mixtures showed a tendency to decrease in volume followed by expansion, and the range of strains for which contraction manifested was larger in comparison to the observed with pure sand. Zornberg et al. (2003) conducted a comprehensive experimental program involving triaxial tests with sand-tire shred composites in which the optimum dosage and geometry of shreds were evaluated. It was observed that the behavior of sand-tire shred mixtures with respect to volume change shifts from sand-like to tire shred-like at a tire shred content of about 35%. The maximum shear strength is reached at this value. It was also verified that the shear strength of the mixture increases with tire shred aspect ratio.

The aforementioned investigations demonstrate that the contribution of the tire shreds as reinforcement begins to take place for comparatively higher axial strains. For comparatively lower axial strains the presence of the tire shreds has an opposite effect on the composite behavior; that is, it provides lower shear strength in comparison to the shear strength of pure soil. This behavior becomes more apparent with the increase in confining pressure.

Although the mechanical characteristics of pure tire shreds and soil-tire shred composites have been addressed through laboratory studies, information regarding the field behavior of embankment fills made with these materials is still limited, particularly when cohesive soils are involved.

Thermal Response of Embankment Background

Three well documented failures caused by exothermic reactions within civil engineering applications of tire shreds were located in Il Waco, Washington; Garfield County, Washington and Glenwood Canyon, Colorado.

Case Study I: Il Waco, Washington

The SR 100 Loop in Il Waco, Washington is a paved road serving as a scenic route accessing the Fort Canby State Park in the southwest corner of Washington at Cape Disappointment. In late 1994 a landslide occurred along the roadway which left a 140 foot long and 25 foot deep gap in the road. It was determined that the most cost effective method of repair would be to use tire shreds as the lightweight fill used to fill the gap left by the landslide. Due to the properties of the tire shreds, a shear key excavated into the underlying material and/or a buttress at the toe of the fill were deemed unnecessary and thus not constructed (Humphrey, 1996).

The tire shreds used in the repair of SR 100 were produced through the shearing process and were approximately 4 to 6 inches long and 2 inches wide. The shreds were provided by *Waste Recovery* in Portland, Oregon, located south of Il Waco across the Columbia River. The design of the repaired section is shown in Figure 1.

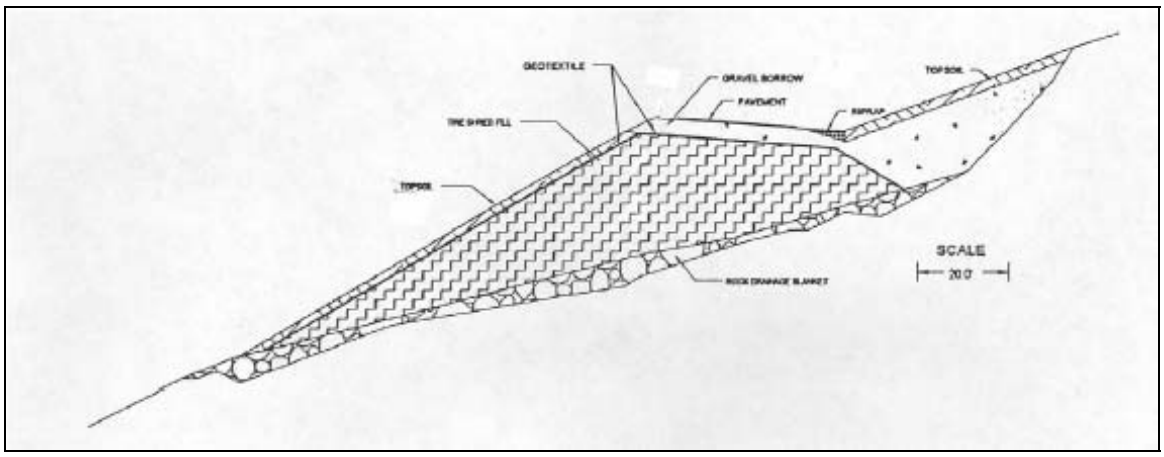

Figure 1: Cross Section of Il Waco Tire Shred Fill

A four foot drainage layer of rock fill was laid down as the base layer, which was then directly overlain by tire shreds. The tire shreds were laid in lifts of approximately ½ to 1 foot thick, which were each compacted with a minimum of three passes by a bulldozer weighing over 70,000 pounds. The overall height of the tire shred layer reached a maximum of 26 feet. The placement of the tire shreds began on October 3,

1995 and was completed by October 18, 1995. The tire shreds were then overlain by a geotextile, 4 feet of granular fill and approximately 0.65 feet of crushed surfacing top course. Approximately 0.35 feet of asphaltic concrete pavement was placed on October 31, 1995.

In retrospect, it is important to note that during the construction of the tire shred embankment along SR 100 there was a significant amount of precipitation recorded. At a weather station located 13 miles from the site nearly 4.8 inches of rain were recorded, with an additional 2 inches recorded in the 12 days after completion of the embankment (Humphrey, 1996).

The top layer of pavement was placed following this period of intense rainfall, completing the roadway. Over a month and a half after completion, in mid-December, a crack approximately 75 feet long (WA DOT, 2003) was observed in the pavement and later on January 3, 1996, steam and heat were observed to rise from the repaired section of the road. On January 17th, a monitoring program was implemented to record temperature, air quality, settlement and water quality (Humphrey, 1996). Figure 2 illustrates the placement of the sensors within the embankment.

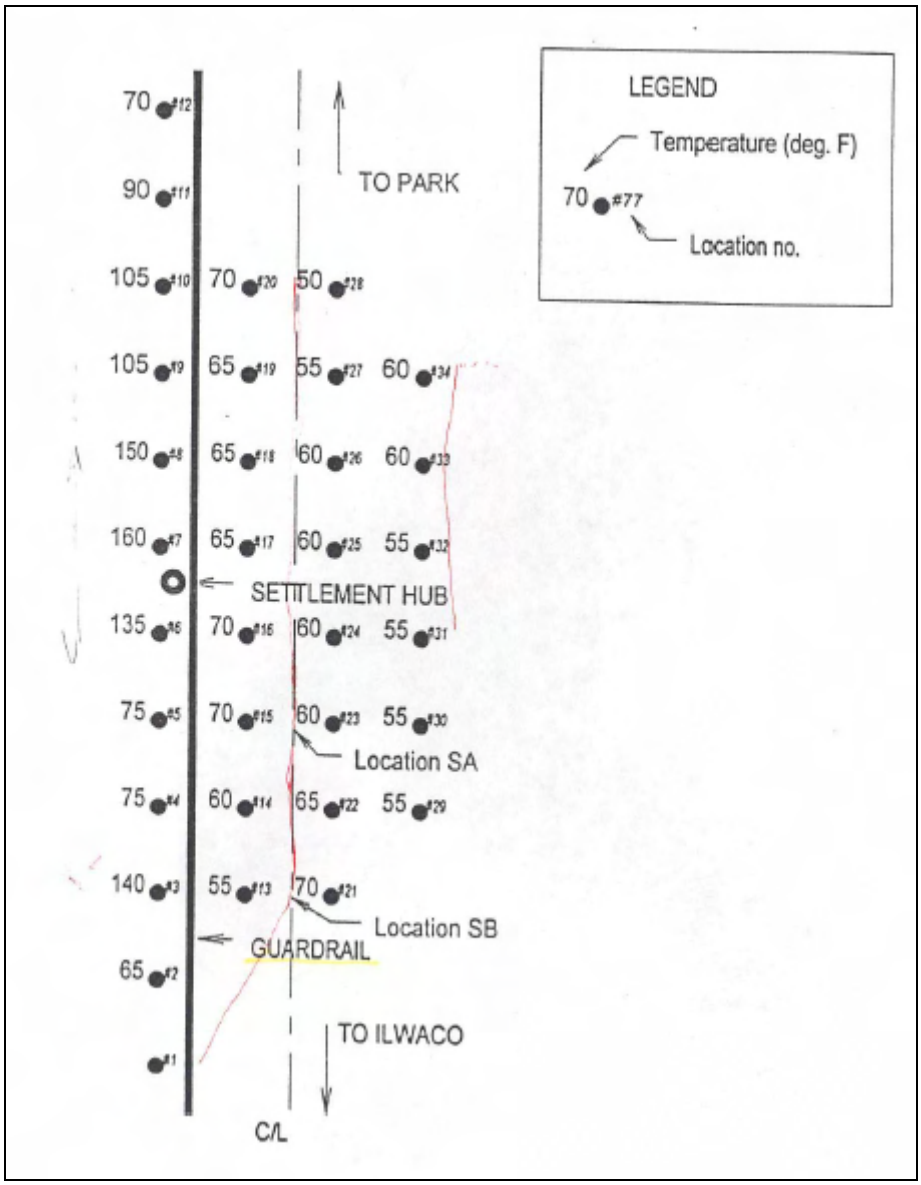

Figure 2: Instrumentation of SR 100 in Il Waco, Washington

The monitoring program continued through February 22nd, at which time the internal temperature readings ranged from 130°F to 160°F at locations 6, 7, and 8 shown in Figure 2. However, the temperature decreased north and south of these sensors to values ranging from 60°F to 90°F.

Monitoring of the embankment continued until March 1996, when significant settlement of the roadway was observed and liquid petroleum products were detected

seeping from the base of the tire shred fill. A spontaneous internal exothermic reaction decomposed the tire shred rubber and generated these waste products (Humphrey, 1996), which contaminated the sump at the base of the fill (WA DOT, 2003).

Figure 3: SR 100 Tire Shred Embankment during Removal

Following these discoveries, the tire shred fill was excavated and reconstructed with a rock shear key. The clean up of the embankment cost approximately $3.2 million which covered the removal of nearly 13,700 tons of tire shreds, native soils, drainage material and other contaminated material. The total cost of clean up and reconstruction totaled over $4.55 million (WA DOT, 2003).

Case Study II: Garfield County, Washington

Falling Springs Road near the eastern Washington community of Pomeroy was a gravel-surfaced road used primarily by farm and local traffic. The roadway had a tight hairpin curve at the head of a ravine which was eliminated by the construction of a tire shred embankment across the ravine. This project was designed and constructed by

Garfield County with funds from the Washington State tire recycling and clean up fund administered by the Department of Ecology (DOE) (WA DOT, 2003).

The tire shreds provided for this project were produced by both the hammermill (i.e. tearing method) shearing methods. The hammermill process typically produces tire shreds with more exposed steel wires than those produced by shearing. The tire shreds for this project were provided by Tire Shredders, Inc. of Goldendale, Washington (WA DOT, 2003).

The embankment was designed to cross the ravine, requiring a length of 225 feet long and a maximum depth of 49.5 feet at the centerline of the proposed roadway. The roadway was 32 feet wide with side slopes of 1.5H: 1V. Figure 4 shows a schematic of this tire shred embankment (Humphrey, 1996).

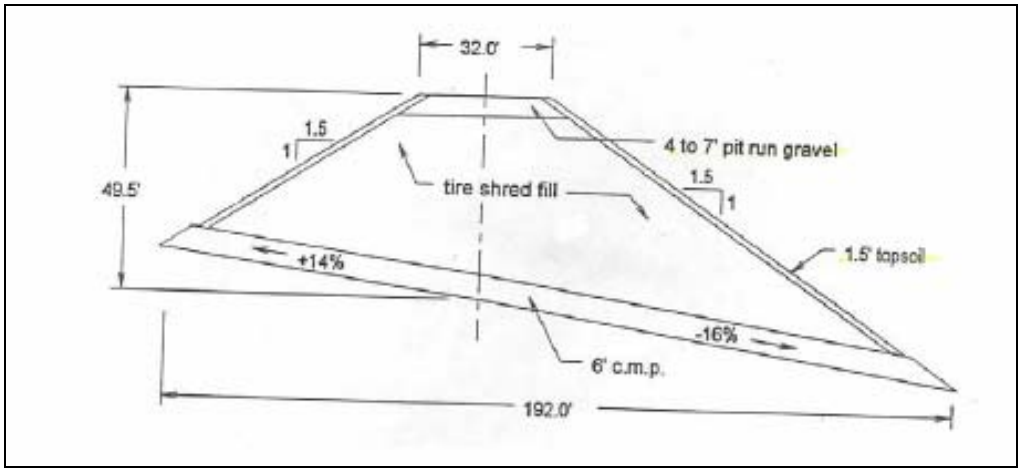

Figure 4: Tire Shred Fill Along Falling Springs Road

The construction of the embankment began in the Fall of 1994 and lasted until the Spring of 1995. The tire shreds were pushed and spread by a D-7 bulldozer into lifts typically greater than 1.5 feet thick. Nearly 16,500 cubic yards of tires were required for the fill (WA DOT, 2003). On top of the tire shreds a 4 to 7 foot layer of gravel was placed to form the surface of the roadway (Humphrey, 1996). As part of the design, a 6-

foot corrugated metal pipe was placed under the fill to facilitate drainage (WA DOT, 2003).

The embankment was monitored for settlement following completion of construction, with only minor changes being observed. On July 6, 1995 a major rainfall event caused a flash flood in the ravine traversed by the new roadway, which lodged a tree stump in the 6 foot culvert, causing nearly 30 feet of water to pond against the upstream side of the embankment (Humphrey, 1996). In October, a local resident reported steam coming from a fissure located 8 feet below the surface of the roadway on the upstream side. Steam continued to be observed coming from this fissure until January 17, 1996 when open flames were reported. It was believed that combustion was taking place internally within the embankment in November, but nothing was done to remediate the problem until January, when flames were observed and the road was shut down (Humphrey, 1996). The fire within the tire shred fill was located near the bottom of the embankment on the downstream side (Humphrey, 1996).

The initial cost for the design and construction of the tire shred embankment and roadway was reported to be $1.0 million by the Washington State DOE. The removal and disposal of the tire shreds cost the DOE nearly $2.5 million (WA DOT, 2003).

Case Study III: Glenwood Canyon, Colorado

A retaining wall was constructed along Interstate 70 in Glenwood Canyon, Colorado near the Hanging Lake Comfort Station in the fall of 1994 by the Colorado Department of Transportation. The retaining wall was a multi-level geogrid reinforced structure with facing elements made of 2’ x 4’ x 16” blocks composed of shredded tire rubber and latex. The backfill was tire shreds, which were covered with a top soil/compost mixture (Fitzgerald, 2003). Figure 5 illustrates the design of this retaining wall.

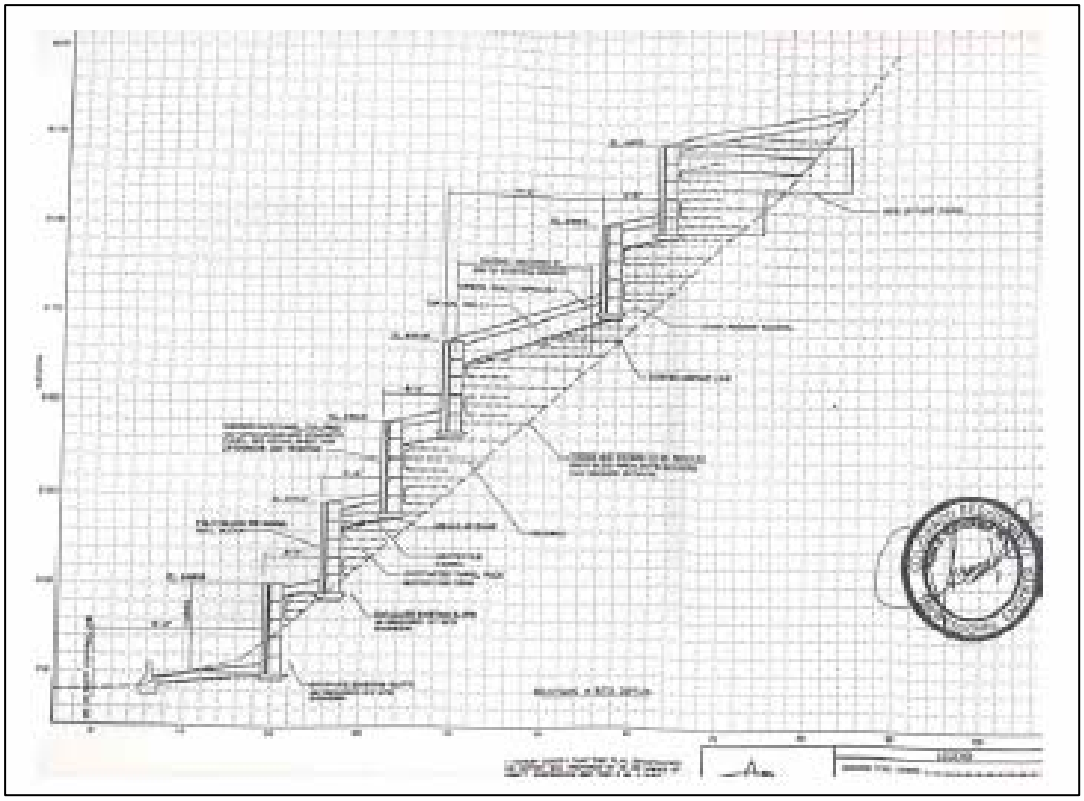

Figure 5: Glenwood Canyon Retaining Wall

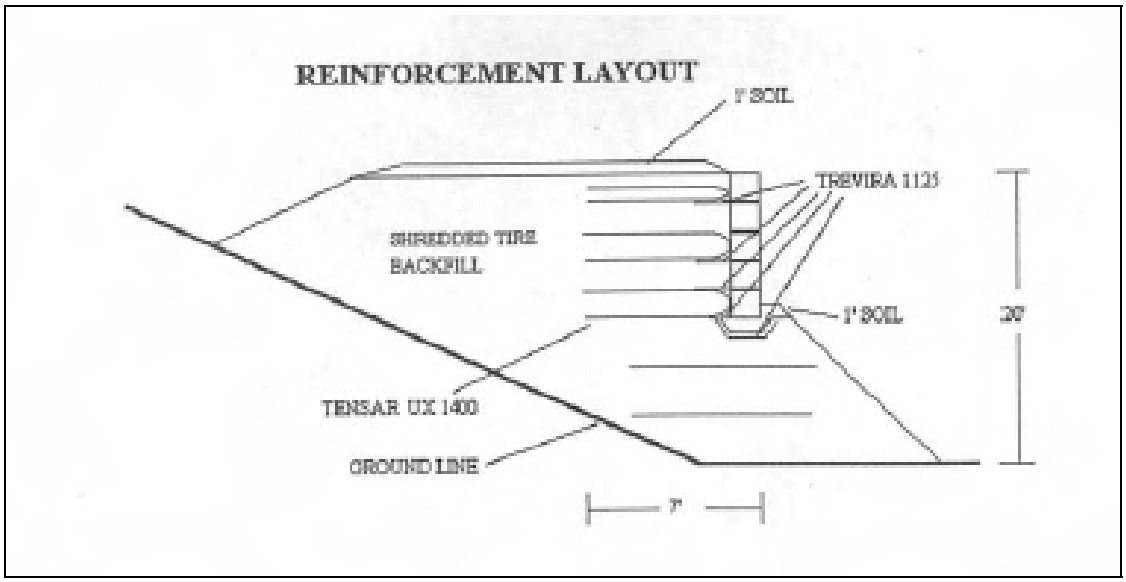

Figure 6: Glenwood Canyon Retaining Wall Detailed View of Layer

During the summer of 1995, various locations within the embankment showed evidence of internal heating of the tire shred backfill. In review, it was noted that during the construction of the retaining wall, the area of the wall received a significant amount of rainfall. On October 30, 1995, fire was clearly observed in the 6th level of the retaining wall.

Remarks Concerning Case Studies

These three case studies represented a setback on the use of tire shreds in civil engineering applications, which had been identified as a promising disposal approach in the 1990's. These episodes also created an urgency to research the performance of civil engineering applications using tire shreds as backfill or road subgrade. The two failures in Washington were especially key in highlighting the negative thermal responses of tire shred embankments. Following these failures the State of Washington placed a moratorium on the use of tire shreds in roadway projects pending further understanding of the mechanisms behind exothermic reactions and the development of design guidelines (WA DOT, 2003). These guidelines were published as *ASTM D6270: Standard Practice for Use of Scrap Tires in Civil Engineering Applications* in 1998.

Previous Exothermic Reaction Research

Past research has investigated the thermal properties of tire shreds and tire shreds when used in civil engineering applications, specifically, in roadways and embankments. Previous research investigated the effect of density and temperature on the insulative and thermal conductivity of tire shreds (Humphrey, 1996, Humphrey, 1997 and Humphrey and Chen, 1996).

Laboratory experiments were conducted to investigate the thermal conductivity of tire shreds in a controlled environment to determine the insulative properties of tire shreds for use as subgrade insulation to limit the depth of frost penetration. The results of these tests were compared to values determined from a field trial constructed in Richmond, Maine. The laboratory testing involved air dried tire chip samples and tire chip-gravel mixtures under a range of different surcharges and densities (Chen, 1996).

Several simplifying assumptions were made to allow the thermal conductivity to be determined from the laboratory test data. The first assumption was that the heat transfer was one-dimensional and uniformly distributed throughout the sample. Measures were taken to minimize edge effects which would affect the one-dimensional flow of heat through the sample. Heterogeneities were also minimized, allowing a constant heat flux within the test volume and leading to the second assumption of the sample having constant thermal properties throughout the entire volume.

Heat is transferred in three modes: conduction, radiation and convection. It was assumed for the purpose of this research that the heat loss caused by radiation was negligible. The heat loss due to convection depends on the air gap between the sample and test apparatus. It was assumed in these calculations that because the gap was less than 10 mm the effects of convection were very small and could be ignored (Chen, 1996).

The difference between free heat convection and heat convection within the tire shred/soil sample is explained as follows:

> Free heat convection is different from the convection between gaps. Heat convection within the voids of the test sample is classified as convection in porous material. The magnitude of the convection in a porous material depends on several factors including temperature gradient, sample thickness, sizes of the voids, direction of heat flow, and temperature level (Gebhart, 1961). It is generally impossible to separate the heat conduction from the convection in a porous material. In practice, the K value is treated as the combination of heat conduction, radiation, and free convection which is called apparent thermal conductivity. This approach was adopted for this study, and as noted previously, it is apparent thermal conductivity which is needed for field design with tire shreds (Chen, 1996).

The most significant element of the use of tire shreds in embankments and roadway projects that was not addressed by Chen was the potential for exothermic reactions. No exothermic reactions were documented in the thermal conductivity testing performed in the laboratory or in the field measurements. Thus, the thermal conductivity was determined through a steady state analysis that did not account for any heat generation within the test volume.

In a report prepared for the Transportation Research Board (Humphrey, et. al, 1997) the findings from these laboratory and field tests on the thermal conductivity of tire shreds (Chen, 1996) are summarized and subsequently compared with additional data collected in the field. The findings and comparisons presented in these two reports are as follows:

- The apparent thermal conductivity of tire shreds decreased from 0.32 Watts per meter degrees Celsius ($^{W}/_{m°C}$) to 0.20 $^{W}/_{m°C}$ as the density increases from 0.58 megagrams per cubic meter (Mg/ m^3) to 0.79 Mg/m^3 at a temperature gradient of about 27 °C/m.
- The thermal conductivity increased about 40% as the temperature gradient increased from 22.3 °C/m to 68.5 °C/m.
- Tire shreds made from glass belted tires had a lower thermal conductivity than tire shreds made from steel belted tires.

- The thermal conductivity determined in the field ranged from 0.19 $^{W}/_{m°C}$ to 0.20 $^{W}/_{m°C}$. The field values were within the range determined in the laboratory experiments for a similar temperature gradient and surcharge

The field values of thermal conductivity were back-calculated using steady state and non-steady state methods based on the subsurface temperature measurements. The steady state analysis assumed a constant temperature gradient through each layer of uniform material. The heat flux was also assumed to be equal in each layer. The temperature gradient was determined from the plots of temperature with depth, from which the thermal conductivity was determined. The non-steady state analysis used the modified Berggren equation, which is used to calculate the depth of frost penetration (Humphrey, et. al, 1997). This approach considers the effect of the volumetric heat of the soils and latent heat of fusion of water as the frost penetrates the ground. The non-steady state analysis was conducted primarily to determine the insulation properties of tire shreds for use in limiting the penetration of frost into the ground and minimizing frost heave of roadways (Humphrey, et. al 1997).

Possible Causes of Exothermic Reactions

Exothermic reactions within a tire shred embankment precede ignition or combustion of tire shreds, which ultimately lead to failure through excessive settlement and open flames. The current understanding of the mechanisms that cause or contribute to exothermic reactions is inconclusive; with no definitive answer to the actual mechanisms that cause these reactions. However, available data does identify possible factors that contribute to or cause exothermic reactions within tire shred fills.

Three major tire shred stockpiles that underwent combustion were investigated to determine potential sources and/or aggravating mechanisms (Humphrey, 1996). Two common characteristics between these stockpiles were identified:

1) Height or depth of the fill was large enough to limit access to air and provide insulation to underlying layers undergoing heating, and
2) Particle size was smaller than typical tire shreds. (WA DOT, 2003).

The size of particles and the height of the embankment appear to be key elements in exothermic reactions, in addition to their access to precipitation and moisture from the atmosphere.

An investigation of the exothermic reaction in the tire shred fill along SR 100 in Il Waco, Washington was conducted for the Federal Highway Administration (Humphrey, 1996), in which the potential causes of exothermic reactions in tire shred fills are outlined. The causes identified include:

1) Oxidation of exposed steel wires
2) Microbes generating acidic conditions
3) Microbes consuming the exposed steel belts
4) Oxidation of the tire rubber
5) Microbes consuming liquid petroleum products

Other sources that could potentially aggravate embankments prone to exothermic reactions include free access to oxygen and organic matter leached into the fill, fertilizer washed through the fill, significant amounts of exposed steel wires, and possibly the amount of fine crumb rubber (Humphrey, 1996).

Oxidation of Exposed Steel Wires

The steel belts that are left exposed from the shearing process are subject to oxidation, which is a reaction that releases heat. Iron, the main constituent of steel, corrodes according to the following reaction, which takes place at an anode.

$$Fe \rightarrow Fe^{2+} + 2e^{-} \qquad (2\text{-}1)$$

The excess electrons that are the product of this anodic reaction are consumed at a cathode, according to the following reaction:

$$\frac{1}{2}O_2 + H_2O + 2e^- \rightarrow 2OH^- \quad (2\text{-}2)$$

The steel wires of adjacent tire shreds may be in contact within a tire shred embankment, creating near electrical continuity throughout the fill (Humphrey, 1996). This would allow the transport of electrons from the anodes to the cathodes throughout the tire shred embankment, furthering the corrosion of the exposed steel. However, when mixed or layered with soil this electrical continuity may be interrupted by soil particles, limiting the transport of electrons and thus decreasing the rate of corrosion.

In addition to the corrosion mechanisms outlined above, iron can also oxidize under neutral pH and aerobic conditions according to the following (Fitzgerald, 2003):

$$Fe^{2+} + \frac{1}{4}O_2 + H^+ \rightarrow Fe^{3+} + \frac{1}{2}H_2O \quad (2\text{-}3)$$

$$Fe^{3+} + 3OH^- \rightarrow Fe(OH)_3 \text{ (precipitates)} \quad (2\text{-}4)$$

The net result being the following reaction (WA DOT, 2003):

$$4Fe + 3O_2 + 6H_2O \rightarrow 4Fe(OH)_3 \quad (2\text{-}5)$$

This reaction is also exothermic and releases approximately 2,623 Btu per pound of iron oxidized. Therefore, knowing that the volumetric heat capacity of tires is 25 Btu/ft^3°F, (i.e., it takes 25 Btu to raise the temperature of 1 cubic foot of tires by 1 degree Fahrenheit), the oxidation of only 0.095 pounds of steel would raise the temperature of 1 cubic foot of tire shreds by 10°F (WA DOT, 2003). If steel oxidation reactions generate heat at a faster rate than it can be dissipated, internal heating and subsequent combustion within a tire shred fill may result.

The product of oxidation, Fe $(OH)_3$ or rust, forms on the surface of the steel belts and provides a protective coating that slows the corrosion of the steel belts and the generation of heat within the tire shreds. Freshly exposed steel belts are most susceptible to corrosion; therefore, the steel belts are most likely to undergo oxidation shortly after being shredded. It is likely that during the construction and placement of tire shred fills this protective rust cover is damaged, exposing un-oxidized steel, and allowing oxidation

reactions to occur at the original higher rate. The oxidation of steel belts is therefore anticipated to be greatest during and immediately after construction and to decrease with time due to the development of this protective rust coating.

Three factors contribute to increasing the corrosion of the exposed steel belts: the presence of neutral salts, high temperature, and an acidic environment. Neutral salts, such as sodium chloride, increase the electrical conductivity of the water that may be present in tire shred embankments; therefore increasing the magnitude of the corrosion current (Fitzgerald, 2003). It has been noted that as the temperature is raised from 65°F to 70°F the corrosion rate is nearly doubled (WA DOT, 2003). In addition, as the pH drops below 4, creating an acidic environment, the corrosion or oxidation rate of the exposed steel belts is increased. In an acidic environment, certain organic acids such as tanic and humic increase the solubility of the protective rust coating, Fe $(OH)_3$, reducing the effectiveness of rust to protect the steel belts from further oxidation and heat generation (WA DOT, 2003).

Microbes Generating Acidic Conditions and Consuming Exposed Steel Belts

Bacteria have been speculated to play a role in the oxidation of exposed steel belts (Humphrey, 1996). Two types of bacteria that are present in the chemical compound formed by the organic acids tanic and humic can oxidize iron. In addition, sulfur oxidizing bacteria can create an acidic environment through the formation of sulfuric acid. The sulfur oxidized is present in the tire rubber in small amounts. Both the oxidation of the sulfur and the steel by the bacteria in the organic acids are exothermic reactions and could potentially contribute to the cause of heat generating reactions within the tire shred embankment (WA DOT, 2003).

Oxidation of the Tire Rubber

The oxidation of rubber is an exothermic reaction that has also been identified as a potential cause of internal heating within tire shred fills. Tire manufacturers report that the compounds used to generate tire rubber are stable up to a temperature of approximately 250°F (Humphrey, 1996). If this information is correct, the oxidation of rubber would be unlikely in an embankment. However, once the initial exothermic reaction or ignition has raised the temperature within the tire shreds above 250°F, the oxidation of rubber may then become a major contributor to the heat generation.

Microbes Consuming Liquid Petroleum Products

Hydrocarbon-consuming microbes are only active under specific temperature and pH conditions, but have the ability to oxidize liquid petroleum products. The contribution of these microbes to exothermic reactions within an embankment is questionable. The hydrocarbons must be from an external source because these microbes cannot oxidize the tire rubber itself to access the hydrocarbon content of the tires. Possible sources include spills during construction of diesel, gasoline or hydraulic oil. Nitrogen and phosphorus must also be present for these microbes to oxidize the hydrocarbons. Therefore, microbe consumption of liquid petroleum products has been identified as a possible cause, but is the least likely cause of exothermic reactions within a tire shred embankment.

Remarks Concerning Possible Causes of Exothermic Reactions

It should be noted that in the three case studies outlined above, the tire shred embankments received a significant rainfall prior to the failure of the fill due to internal heating. Considering the potential causes of exothermic reactions, it is possible that the precipitation increased the rate of corrosion of the exposed steel belts, increasing the exothermic reactions. The increased rate of oxidation may have led to internal heating, which eventually led to ignition and failure of the embankments.

Existing Design Guidelines for Tire Shred Embankments

In response to the three reported cases of embankment failure due to heating, a committee composed of members from government, industry and academia was formed to investigate the tire shred fires and provide design guidelines that would allow the use of tire shreds to continue in highway projects. These design guidelines, which were presented in 1997 as the "Interim Guidelines for Shredded Tire Embankments," (Humphrey, 1997) were later adopted as ASTM D6270 (1998) (WA DOT, 2003).

The guidelines presented in the Standard Practice for *Use of Scrap Tires in Civil Engineering Applications* by the American Society for Testing and Materials are summarized in Table 1 (ASTM D6270 and WA DOT, 2003).

	Tires should be shredded so that the largest shred is the lesser of one quarter circle in shape or 24 inches (0.6 meters) and at least one side wall should be cut from the tread.
	In applications where pavement is to be used or the tire shreds are used for drainage, the tire shred layer should be wrapped completely in either a woven or nonwoven geotextile in order to minimize the infiltration of soil particles into the voids.
	Tire shreds should be free of all contaminants: oil, grease, gasoline, diesel fuel, etc.
	Tire shred fills should not include the remains of tires that have been subjected to a fire
Class I Fill: Height of tire shred layer: < 3.3 feet (1 meter)	Maximum of 50% (by weight) passing the 1.5 in (38 mm) sieve Maximum of 1% (by weight) passing the 1.5 in (38 mm) sieve
Class II Fill: **Height of tire shred layer:** **3.3 feet to 9.8 feet** **(1 to 3 meters)**	Maximum of 25% (by weight) passing the 1.5 in (38 mm) sieve Maximum of 1% (by weight) passing the 0.2 in (4.75 mm) sieve The tire shreds should be free from fragments of wood, wood chips, and other fibrous organic matter Tire shreds should have less than 1% (by weight) of metal fragments, which are not at least partially encased in rubber. Metal fragments that are encased in rubber shall protrude no more than 1 in (25 mm) from

	pieces and no more than 2 in (50 mm) on 100% of the pieces Infiltration of water shall be minimized Infiltration of air shall be minimized No direct contact between the tire shreds and soil containing organic matter, such as topsoil Tire shreds should be separated from the soil with a geotextile Drainage features at the bottom of the fill should be avoided in order to prevent free access to air

Table 1: Standard Practice for the Use of Scrap Tires in Civil Engineering Applications

The guidelines listed in Table 1 were compiled to avoid exothermic reactions in future civil engineering projects utilizing tire shreds. These guidelines, however, do not identify the exact causes of these reactions and fail to provide a rationale that would provide confidence that these reactions will not occur.

Remarks on the State of Knowledge Regarding Exothermic Reactions in Tire Shreds

The information presented in this chapter covers the methods of tire shredding, environmental impacts of using waste tires in civil engineering applications and case histories where tire shreds have been used. Past research into the potential causes of exothermic reactions within tire shred reinforced embankments was also presented. From this information it is clear that there is significant field experience, a few documented case studies and inconclusive information on the potential causes. The lack of any conclusive evidence as to the causes of exothermic reactions cast doubt on the suitability of the existing guidelines and prevention methods.

The most apparent research and knowledge gap concerning tire shred applications are in the understanding of the interaction between soil and tire shreds. There also lies a knowledge gap in the understanding of the potential benefits gained in preventing exothermic reactions through different soil/tire shred reinforcement methods. As

mentioned, the research into the causes of exothermic reactions within tire shred embankments is inconclusive. These gaps in current knowledge are the primary motivation behind the research conducted in this project. Specifically, this study addresses the prevention of the exothermic reactions versus the causes, and compares the interaction of the soil and tire shreds through different design methods.

The research presented in this report has the objective of contributing to design recommendations that will prevent exothermic reactions from occurring. The findings from this research will be used to evaluate the thermal responses of a tire shred-only stockpile versus the properties and responses of a soil embankment reinforced by tire shreds that are either mixed or layered with the soil. These responses will also be compared with a control section comprised of only soil.

Methods and Materials

Site Description

A field study was initiated in Sedalia, Colorado, at the Front Range Tire Recycle, Inc. facility, where a full-scale embankment was designed and built. The embankment was built to measure mechanical and thermal properties and behavior of a tire shred-soil embankment in a frequently used, full-scale roadway. In addition to this embankment, stockpiles of whole tires and tire shreds were also monitored.

Front Range Tire Recycle, Inc. is a tire storage and recycling facility that currently stores approximately 4 million tires. A significant portion of these tires are shredded through the hammermill process and stored on-site or sold for use in civil engineering or other applications. Figure 7 shows an aerial view of the facility in August of 2002, before a new initiative of tire baling began. The piles that can be observed in the figure are mostly whole tires with some tire shred stockpiles.

Figure 7: Front Range Tire Recycle, Inc. August 2002

Over the past two years (since 2002), Front Range Tire Recycle, Inc. has been aggressively pursuing compliance with fire hazard regulations and has thus begun to bale the tires which were stockpiled on site to reduce the volume of stockpiles. Figure 8 and Figure 9 are aerial views of the facility in 2003, showing the transition from tire stockpiles into tire bale piles.

Figure 8: Front Range Recycle, Inc. May 2003

Figure 9: Front Range Recycle, Inc. July 2003

In the photo taken in May of 2003, Figure 8, a large tire shred pile is seen in the lower right corner. This pile was sold in the summer of 2003, and not seen in the July

2003 photo, Figure 9. This tire shred stockpile was monitored for temperature until it was dismantled.

Since the summer of 2003, the site has proceeded with continuous tire baling and tire shredding. A large percentage of tires have been converted to bales and stacked as a storage method. These tire bales have also been used to form tire bale embankments or roadways. The following photos show the site in August 2004. Figure 10 shows a view looking southwest over the facility. In the forefront of the photo can be seen tire bale stacks, which are in the process of being covered with backfill. In the background on the left is a tire stockpile, located adjacent to the tire shredding machine and the tire baler. Figure 11 shows an up close picture of the tire shredder. Figure 12 is a closer view of the tire baler and the tire bale stacks where they are stored. Figure 13 shows a different view of a stack of tire bales that is being covered to form a reinforced embankment.

Figure 10: Front Range Recycle, Inc. August 2004

Figure 11: Front Range Tire Recycle, Inc. Tire Shredder

Figure 12: Front Range Tire Recycle, Inc. Tire Baler

Figure 13: Front Range Tire Recycle, Inc. Tire Bale Embankment

Front Range Tire Recycle, Inc. provided an ideal setting for monitoring of a tire shred-soil embankment and tire shred-only and whole tire stockpiles. The materials and equipment required for construction of the road embankment were provided by Mr. Rick Welle, owner of Front Range Tire Recycle, Inc. The various stockpiles that were monitored were also provided by Mr. Rick Welle. Figure 14 highlights the four locations where monitoring was conducted: 1) the tire shred-soil embankment, 2) the tire shred-only stockpile adjacent to the tire shred-soil embankment, 3) the whole tire stockpile adjacent to the tire shred-soil embankment, and 4) the large tire shred-only stockpile.

Figure 14: Monitoring Locations

Description of Tire Shred-Soil Embankment

The tire shred-soil embankment constructed for this project consists of three sections, each approximately 30 feet long, 5 feet deep and 30 foot wide. The three sections include a soil-only section, a mixed section and a layered section. These sections are shown in Figure 15.

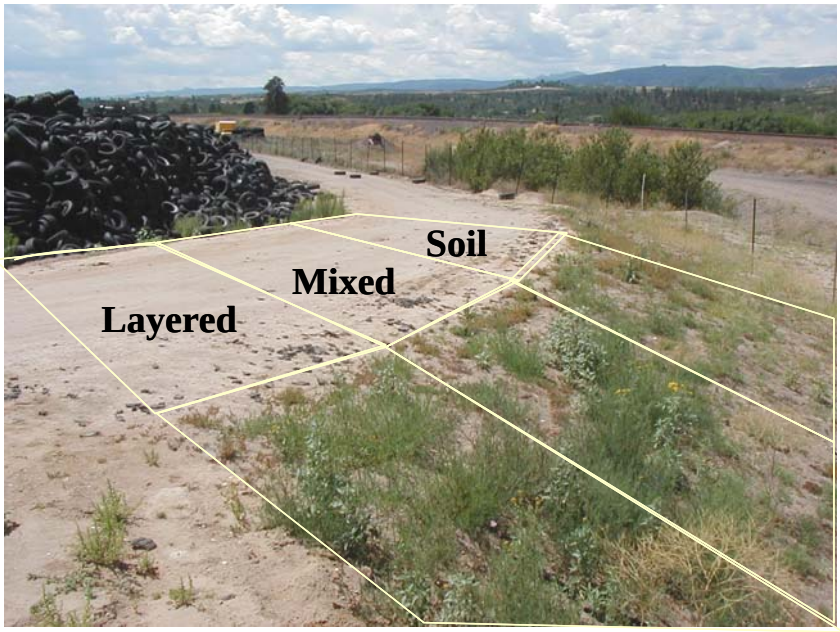

Figure 15: View of the West Slope of the Tire Shred-Soil Embankment

A dimensional representation of the tire shred-soil embankment is presented in Figure 16.

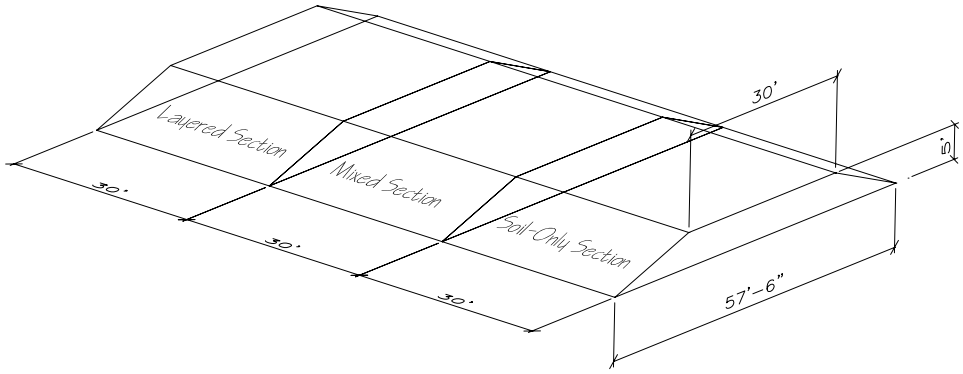

Figure 16: Tire Shred-Soil Embankment Section Dimensions

The owner of Front Range Tire Recycle, Inc., Mr. Richard K. Welle, provided the equipment, tire-shreds, and soil necessary for the construction of the embankment. First, the existing access road upon which the prototype embankment was to be built was excavated to grade. This allowed each section of the new embankment to have the same depth and still achieve an overall grade of 9%. The embankment was constructed in

seven lifts. Despite the different materials used in the different sections of the embankment, the entire embankment was constructed simultaneously. However, each section was compacted individually in order to prevent cross-contamination of materials between embankment sections.

The soil/tire-shred mixture used in the mixed section of the embankment was produced using one WA 120 Komatsu front-end loader with frost points, with a bucket capacity of 1.8 yd^3. The procedure was initiated by dumping a bucket load of tire-shreds onto onsite soil, and then dumping a load of the soil specified for use in the embankment on top of the tire-shreds. Next, the loader dug under the tire-shreds, picked up the shreds and the soil, and then dumped them onto the ground again. This process was repeated until the soil/tire-shred mixture was thoroughly mixed, as determined by visual inspection.

The first lift consisted of a compacted thickness of six inches. This lift consisted of pure soil in the layered and soil-only section, and the soil/tire-shred mixture previously described in the mixed section. Compaction of each section was achieved with eight passes of an Ingersoll-Rand sheepsfoot roller with a load energy of 13,500 pounds. After the compaction of each section, one sand cone test was completed in each section. The second lift also consisted of a 6" compacted thickness. A layer of tire-shreds was used in the layered section, the soil/tire-shred mixture was used in the mixed section, and pure soil was used in the soil-only section. Compaction was achieved through the same process as before, and three more sand cone tests were performed, one in each section. The third lift had a compacted thickness of 12 inches, and consisted of soil in the layered section, the soil/tire-mixture in the mixed section, and soil in the soil-only section. Compaction was achieved and recorded in the same manner as for the previous two lifts. The fourth and fifth lifts had compacted thicknesses of 6 and 12 inches, respectively. For the fourth lift, tires were used in the layered section, while soil was again used in the fifth lift. The sixth lift had a compacted thickness of 6", and consisted of tire-shreds in the

layered section. Finally, the seventh lift had a compacted thickness of one foot, and consisted of pure soil for all three embankment sections. Sand cone tests were performed in each section after the compaction of each lift. The results of these tests are summarized in Table 2.

		Wet Density (PCF)		
Lift #:	**Compacted Thickness (in):**	**Layered Section**	**Mixed Section**	**Soil-Only Section**
1	6	125	110	125
2	6	50	110	125
3	12	128	115	125
4	6	55	110	120
5	12	120	115	125
6	6	50	110	130
7	12	114	112	110

Table 2: Densities of each Lift of Three Embankment Sections
(after Zornberg et al, 2001)

The west side-slope was finished with a 3H:1V slope, while the east side-slope was finished with a slope of 2.5H:1V. Grass seed was planted by hand after the completion of the side-slopes. However, due to inclement weather conditions and a lack of water, the side-slopes never became fully vegetated.

Figure 17 shows the dimensions of a cross-section of the layered section. This figure also indicates the location of the PVC housing for the instrumentation used for the data collection. The instrumentation details will be discussed later.

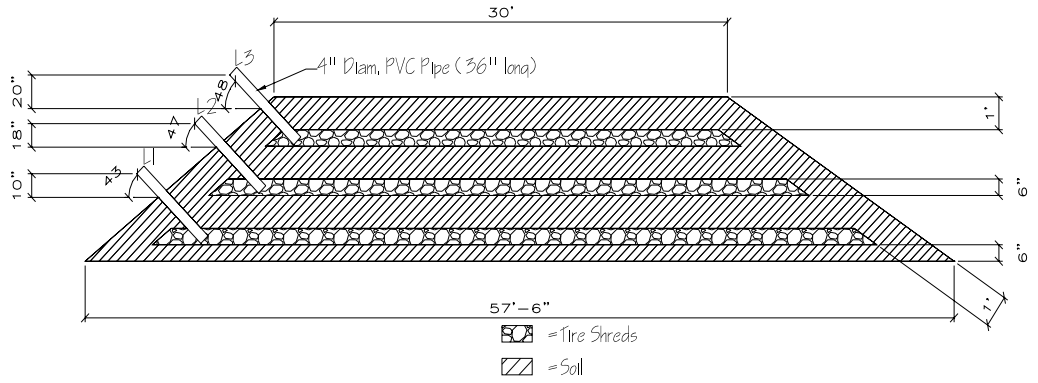

Figure 17: Layered Section Cross-section (not to scale)

The second embankment section consists of a tire shred and soil mixture, with 10% tire shreds by weight. The hammermill produced tire shreds used for the mixture were 2 inches to 6 inches in length and approximately 2 inches in width. Figure 18 shows a cross-section of the mixed section.

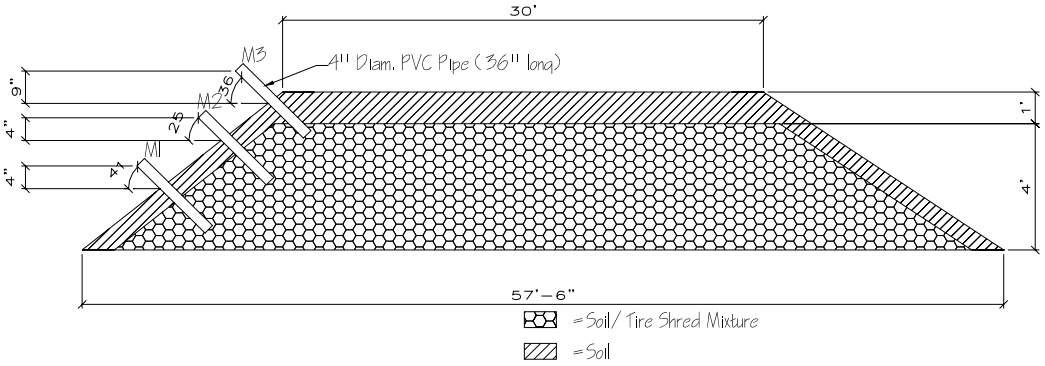

Figure 18: Mixed Section Cross-section (not to scale)

The third section of the embankment was constructed of only soil and constitutes the control section. Figure 19 shows a cross-section of the soil-only section.

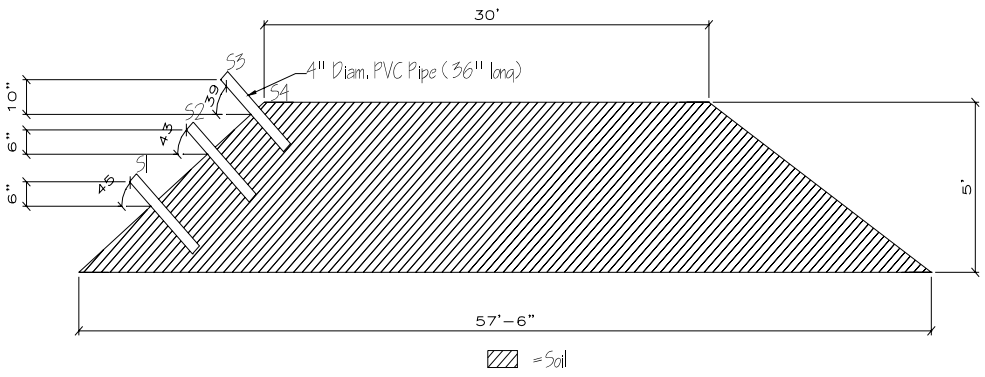

Figure 19: Soil-only section Cross-section (not to scale)

Following completion of the construction of the embankment, periodic surveys were conducted to determine the mechanical behavior of the three sections (Zornberg et al., 2001).

Instrumentation Plan

The instrumentation plan was designed in order to evaluate the potential causes of exothermic reactions. The variables that were identified as potentially influencing exothermic reactions (e.g. the oxidation of steel, the rate of microbial growth) were measured in the tire shred-soil embankment sections. Specifically, the instruments installed included temperature, soil moisture and relative humidity probes. In addition, heat flux monitoring plates were installed in the soil-only section and the whole tire stockpile to assess the quantity of heat transferred through the surface into the embankment.

The instruments were installed with the intention of monitoring the tire shred-soil embankment for several years to determine the thermal behaviour of the three sections through various seasonal changes. The temperature, relative humidity, soil moisture and heat flux were measured for an 18 month monitoring period for the data analysis presented in this thesis. These parameters continue to be monitored. Monitoring of these

parameters is expected to provide insight into the conditions likely to produce exothermic reactions within a tire shred-soil embankment.

The tire shred-soil embankment was prepared during the construction phase for the installation of the monitoring probes. Appendix A includes photos documenting the installation of the instrumentation. As shown in Figures 17, 18 and 19, 4 inch diameter PVC pipes were placed in three holes at different depths augered into the side of the three sections of the tire shred-soil embankment. The holes were located on the west-side slope of the embankment and were approximately 3 feet deep. Bentonite was placed around each of the PVC pipes along the length to seal the hole, preventing air and water from the surface to interfere with the measurements taken by the probes at the end of the tubes. The interiors of the tubes were also sealed for the same reasons.

The three tire shred-soil embankment sections were monitored by 34 sensors, with 13 additional sensors located in the tire shred-only stockpile and the whole tire stockpile. All of the sensors, except those located in the large tire shred-only stockpile, were connected to the same data logger which also collected data from a thermistor attached to the datalogger mount to measure the air temperature. The datalogger was a Campbell Scientific CR10X unit, powered by a solar panel and 12 volt rechargeable battery. A multiplexer is located below the data logger, allowing for all of the sensors to be wired into the same datalogger, which records the data collected by these sensors and stores it with a 2 MB memory. Appendix B includes a copy of the program written to control excitation periods and ranges, and convert the signals from the sensors into the quantities being measured, i.e. voltage into soil suction, etc. (Fitzgerald, 2003). The data is collected every 15 minutes, with the hourly average being stored in the datalogger. In August 2004, a wireless modem was attached to the data logger to allow for remote access to download the data. This eliminates the need to visit the site in Sedalia, Colorado, and connect manually with the data logger to download the data. Instead, the data can now be collected via modem from Austin, Texas. The data continues to be

downloaded at regular intervals. Figure 20 shows the datalogger, solar panel and multiplexer.

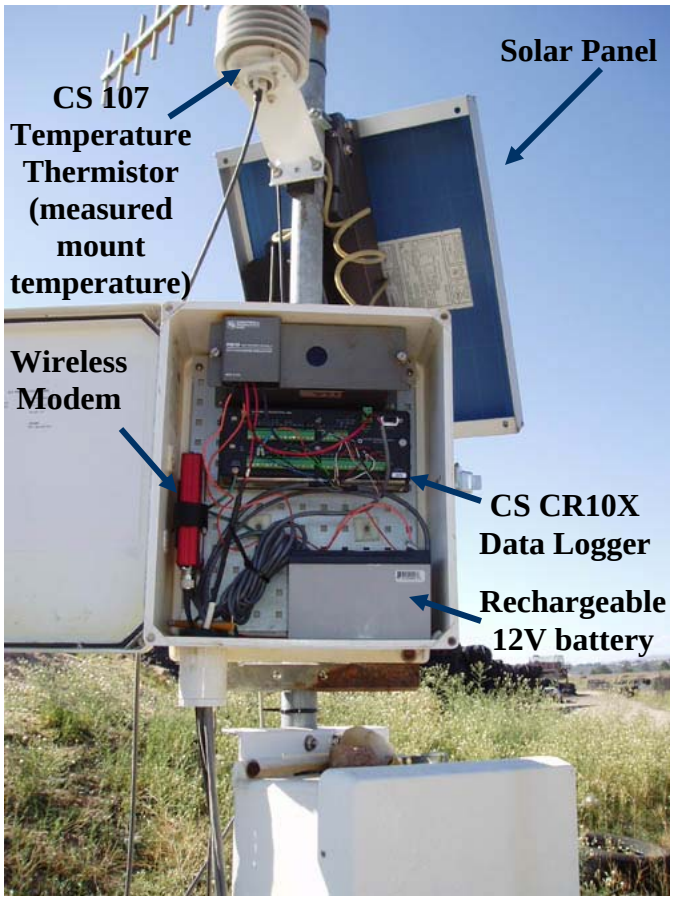

Figure 20: Data Logger and Mount

Table 3 summarizes the locations of the sensors and their input locations (i.e. memory locations) in the data logger (Vollenweider et al. 2002). The designations of L1, M1, and S1 indicate the section the sensor is located in: M being the mixed, L, the layered and S, the soil-only section. The number indicates the depth, with 1 being the deepest sensor, 2, the middle and 3 the sensor closest to the surface of the embankment.

Table 3: Sensor locations in the embankment and stockpiles

Sensor connected to a CR10X data logger via an AM 416 multiplexer	Characteristic	PVC tube # (Input location in multiplexer)[1]
Layered section		
3 interchangeable thermistors (YSI4408)	Attached to rubber chip	L1 (28), L2 (30), L3 (32)
3 interchangeable thermistors (YSI4408)	Attached to metal wire	L1 (29), L2 (31), L3 (33)
3 temperature probes (Model 107)	In soil	L1 (46), L2 (47), L3 (48)
3 Soil Moisture probes (Watermark 200)	In soil; hole drilled besides PVC tube to the same depth	L1 (94), L2 (95), L3 (96)
3 Relative Humidity (+Temp.) probe (CRS 500)	In PVC tube; just above compacted soil in tube; tip protected by jacket	L1 (71; 78)[2], L2 (72; 79), L3 (73; 80)
Mixed section		
3 interchangeable thermistors (YSI4408)	Attached to rubber chip	M1 (22), M2 (24), M3 (26)
3 interchangeable thermistors (YSI4408)	Attached to metal wire	M1 (23), M2 (25), M3 (27)
3 temperature probes (Model 107)	In soil	M1 (43), M2 (44), M3 (45)
3 Soil Moisture probes (Watermark 200)	In soil; hole drilled besides PVC tube to the same depth	M1 (91), M2 (92), M3 (93)
Soil-only section		
3 temperature probes (Model 107)	In soil	S1 (49), S2 (50), S3 (51)
3 Soil Moisture probes (Watermark 200)	In soil; hole drilled besides PVC tube to the same depth	S1 (97), S2 (98), S3 (99)
1 HFT3 Heat Flux Plate	Just below the surface	Not in PVC tube
Tire shred-only stockpile		
3 interchangeable thermistors (YSI4408)	Attached to rubber chip	TS1 (34), TS2 (36), TS3 (38)
3 interchangeable thermistors (YSI4408)	Attached to metal wire	TS1 (35), TS2 (37), TS3 (39)
3 Relative Humidity (+ Temp.) probe (CRS 500)	Cables protected by tires; tip protected by jacket	TS1 (74; 81), TS2 (75; 82), TS3 (76: 83)
1 Heat Flux Plate	Just below the surface of pile	Not in PVC tube
Whole tires stockpile		
2 interchangeable thermistors (YSI4408)	Attached to rubber chip	T1 (40), T2 (41)
1 Relative Humidity (+ Temp.) probe (CRS 500)	Directly inserted inside tire casing; protected at the tip	T1 (84)

Other		
1 temperature probe (Model 107)	On mount, to measure air temperature	Not in PVC tube
Large tire shred-only stockpile (probes connected to a HOBO Outdoor 4-channel data logger)		
4 temperature probes (TMC50-HA)	Directly placed inside tire shred pile	P1, P2, P3, P4

[1] Numbers in parenthesis indicate logger input locations (i.e. memory locations)

[2] CRS 500 requires two channels/probes: one for relative humidity, another for temperature.

Appendix B includes detailed descriptions, specifications and operation manuals for these instruments and probes.

The PVC pipes installed within the west slope of the three embankment sections were placed in similar manners; however, each section had different instrumentation inserted in the PVC tube as shown in Table 3. After installation of the thermistors, a small amount of soil was inserted in the tube and compacted. In the mixed section, a mixture of soil and tire shreds was placed in the PVC tube and compacted. A relative humidity/temperature sensor was then inserted in each PVC tube. Figure 21 shows a schematic section of this probe and its protection from water that would interfere with the readings.

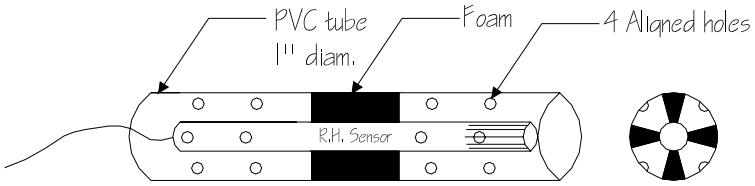

Figure 21: Relative Humidity and Temperature Sensor

Since the soil placement and conditions of the tire shred-soil embankment could not be replicated within the PVC pipe, the soil moisture probe was inserted in each section and level in a separate hole drilled to the same depth neighboring the PVC pipe.

At the base of each of the new holes (drilled for the soil moisture probe) a smaller hole was excavated to allow for a snug fit around the probe. The hole was backfilled with the in-situ soil and compacted to a density consistent with that of the surrounding tire shred-soil embankment. This was done so that the instrument would measure the soil suction of the in-situ compacted embankment. The soil suction is a function of the pore-size distribution and the in-situ density of the soil. From the soil suction read by these probes, the volumetric moisture content can be obtained from a calibrated relationship. Subsequently, the gravimetric moisture content can be determined by knowing the soil unit weight.

A total of five sensors were installed at each depth in the layered section: three thermistors, one relative humidity/temperature probe and one soil moisture probe. Of the three thermistors, one was embedded in the soil to measure the soil temperature, one was glued to a piece of rubber tire and the third was glued to a piece of steel belt. The rubber piece was approximately ½-inch x ½-inch and the steel belt was ½-inch long and about 1 mm in diameter. Figure 22 shows the typical instrumentation as placed in the layered section. It should be noted that the instruments were placed within the tire shred layer. Also, while this figure shows the soil moisture probe as being inserted in the PVC pipe, this probe was indeed inserted adjacent to the PVC pipe.

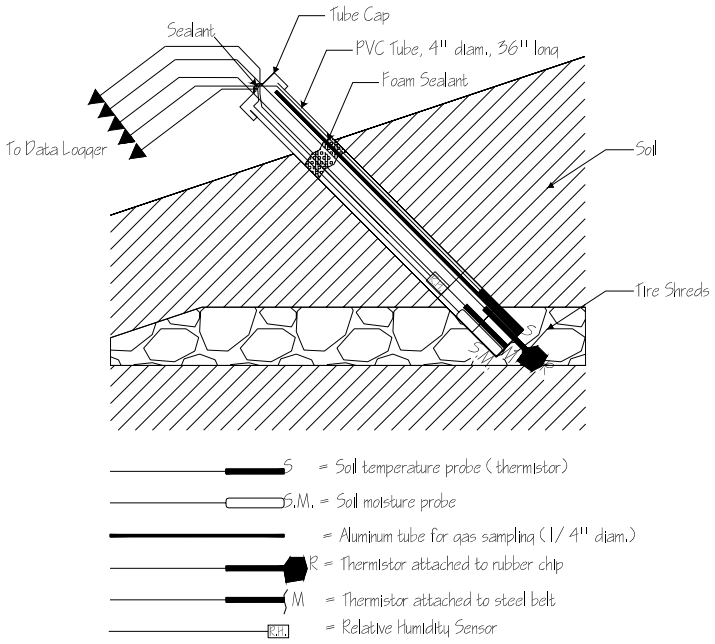

Figure 22: Typical Cross-section of Instrumentation in Layered Section (not to scale)

The instrumentation within the PVC pipe in the mixed section included three thermistors to measure the temperature of the soil, rubber, and steel, and a soil. As in the layered section, a soil moisture probe was located adjacent to the PVC pipe. The mixed section did not include a relative humidity/temperature probe within the PVC housing. Figure 23 shows a typical cross- section of the sensor placement within the mixed section of the tire shred-soil embankment; however, the soil moisture probe was indeed installed adjacent to the PVC pipe and not within it.

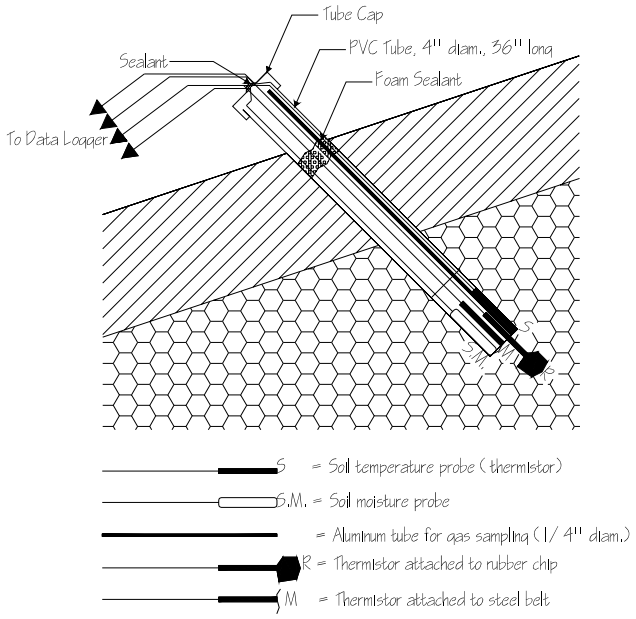

Figure 23: Typical Cross-section of Instrumentation in Mixed Section (not to scale)

The soil-only section only had two thermistors placed to measure the soil temperature and soil moisture. Figure 24 shows the placement of the instrumentation within this section.

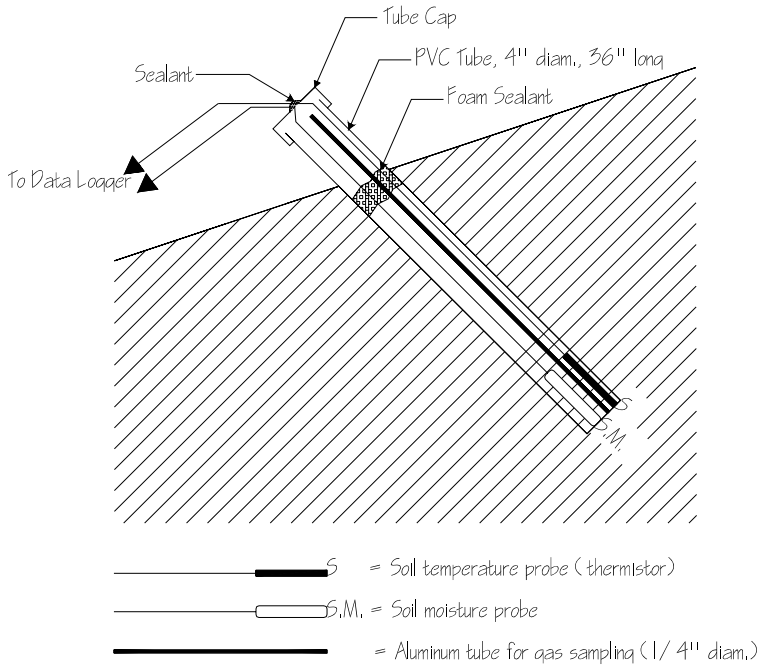

Figure 24: Typical Cross-section of Instrumentation in Soil-only section (not to scale)

A sensor was placed within the PVC pile to measure the in-situ soil temperature at the three different depths. Adjacent to these pipes, similar to the mixed and layered sections, soil moisture probes were placed to measure the soil suction. In addition, a heat flux plate was installed at the surface of the soil-only section to measure the heat transfer rate through the road surface into the embankment. Through the measurement of the internal temperature and the heat flux, the thermal conductivity of the three different sections can be calculated based on heat transfer principles.

Figure 25 shows the placement of the instruments and the PVC pipes directly following installation. Figure 26 shows the PVC pipes in the layered section in August 2004.

Figure 25: Placement of the PVC Pipes in the Layered Section Following Construction

Figure 26: View of the PVC Pipes in the Layered Section (August 2004)

In addition to the layered, mixed and soil-only sections of the tire shred-soil embankment, neighboring stockpiles of whole tires and tire shreds were monitored. An additional large tire shred-only stockpile was monitored to gather the internal temperatures. As shown in Figure 14, this stockpile was located at the southernmost corner of the Front Range Tire Recycle, Inc. facility.

Sensors were placed at three different depths within the tire shred-only stockpile constructed near the embankment. Thermistors were attached to a piece of rubber and a steel belt at three depths to measure the internal temperature. A relative humidity/temperature probe was also placed at each depth. A heat flux plate was placed at the surface of this stockpile to measure the heat transferred through the surface of the stockpile. Through the monitoring of the internal temperature and heat flux through the surface, the heat generated and dissipated within the embankment can be evaluated. Figure 27 shows a typical cross-section of the tire shred-only stockpile, and Figure 28 shows this stockpile with the monitoring devices installed.

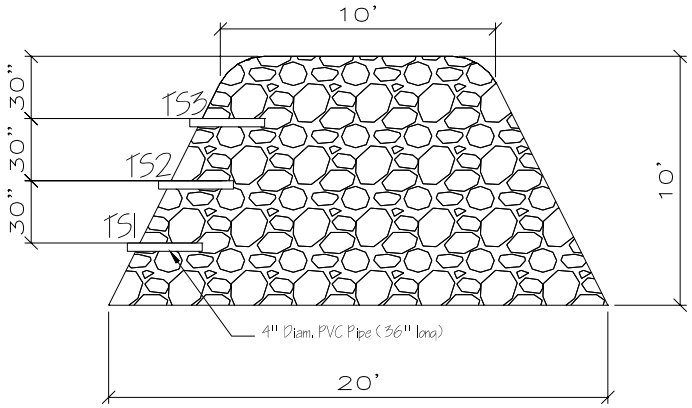

Figure 27: Cross-section of Tire Shred-Only Stockpile Adjacent to the Tire Shred-Soil Embankment (not to scale)

Figure 28: Tire Shred-Only Stockpile with Instrumentation Installed

The whole tire stockpile was constructed between the tire shred-only stockpile and the tire shred-soil embankment. This stockpile was monitored at two locations. At the higher location, a thermistor was attached to a whole tire. At the lower level, a relative humidity/temperature probe was inserted to measure both humidity and temperature changes within the whole tire embankment. Figure 29 illustrates a cross-section of this stockpile.

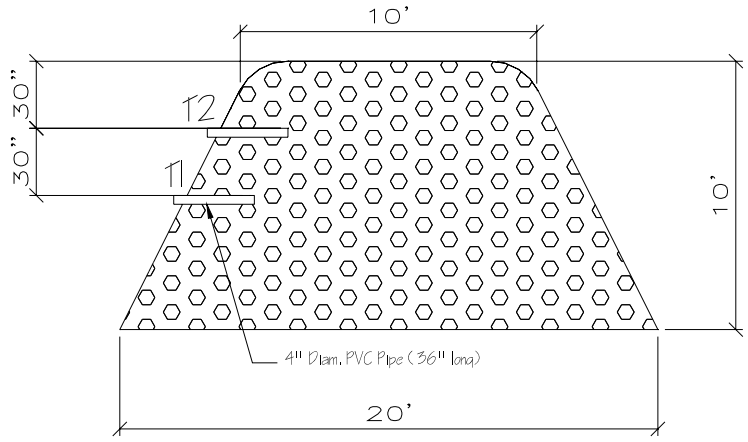

Figure 29: Cross-section of the Whole Tire Shred Stockpile Adjacent to the Tire Shred-Soil Embankment (not to scale)

The large tire shred-only stockpile located at the southern edge of the facility was approximately 300 feet long, 100 feet wide and 30 feet deep. The tire shreds had been shredded using the shearing method, (instead of the tearing method), in order to minimize the amount of steel belts that were exposed. The unit weight of the tire shreds within this stockpile was approximately 40 pounds per cubic foot (pcf) (Fitzgerald, 2003). Sensors were located at four different depths: at the surface, 1.5 feet, 3 feet, and 6 feet. These sensors measured the internal temperature every 30 minutes over a period of 10 months before the large tire shred-only stockpile was dismantled. Figure 30 illustrates the instrumentation placement within the large tire shred-only stockpile. In addition, Appendix A provides photographs documenting the construction and installation of the instrumentation within the large tire shred-only stockpile.

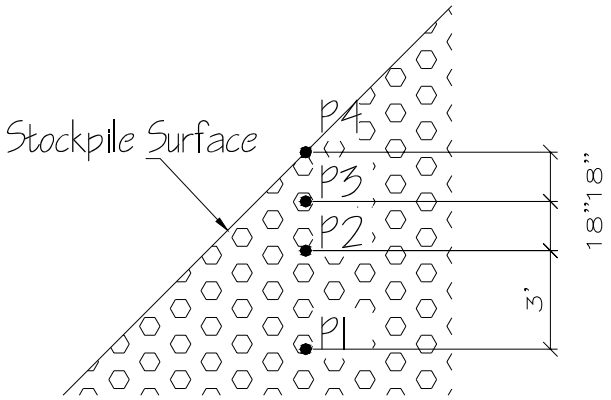

Figure 30: Cross-section of the Large Tire Shred-Only Stockpile (not to scale)

The instrumentation outlined in this chapter has been in place and the collected data has been used in the analysis of the thermal properties of tire shred/soil mixtures and of the likelihood of exothermic reactions within the different tire shred-soil embankment sections.

Mechanical Testing

Preliminary Field Testing

A preliminary testing pad was constructed to evaluate the compaction and compressibility characteristics of the different materials used in the construction of the prototype embankment. An appropriate procedure for mixing the cohesive soil with the tire shreds was also devised. The testing pad consisted of four distinct sections with base dimensions of 3 x 3 m. Each section was constructed in two lifts with thickness equal to 0.15 m. The first two sections were built with mixtures containing 10 and 30% of tire shreds by weight, respectively. The third section was built with pure tire shreds, while the forth section was constructed with pure soil. A sheepsfoot roller weighing 59.8 kN was used for compaction of the materials. Despite the different materials, the sections of the testing pad were compacted simultaneously to facilitate the construction process, following the suggestion of Dickson et al. (2001).

Measurements of unit weight (γ) and water content (w) were taken with a surface nuclear gauge, following ASTM standards D 2933 and D 3017, respectively. Accuracy of the results with pure soil were estimated to be ± 1% for w and ± 0.1 kN/m^3 for γ. Although calibrations in the laboratory were performed with larger samples in an attempt to reduce the influence of material heterogeneity due to the broad range of sizes and shapes of tires shreds, the accuracy of results of γ from field tests involving tire shreds are estimated to be within ± 0.1 and ± 0.8 kN/m^3, depending on the tire shred content.

Figure 31 shows the behavior of the dry unit weight (γ_d) of the tested materials (i.e., pure soil, mixtures, and pure tire shreds) with the number of passes of the compactor equipment, for the second lift of each section. Measurements started after the second pass and were repeated after every single pass (except for the fifth pass). The dry unit weight of the soil increased very slightly from the second to the third pass of the roller, and remained virtually constant after that point. After the third pass, γ_d reached a value of

17.9 kN/m^3, corresponding to a relative compaction of 96% with respect to the maximum dry unit weight achieved in the laboratory. The soil-tire shred mixture with 10% of tire shreds presented slightly lower values of γ_d in comparison to that of pure soil. Very little change in γ_d after the second pass of the roller was also observed with this material, and a value of 17.1 kN/m^3 was achieved after the third pass.

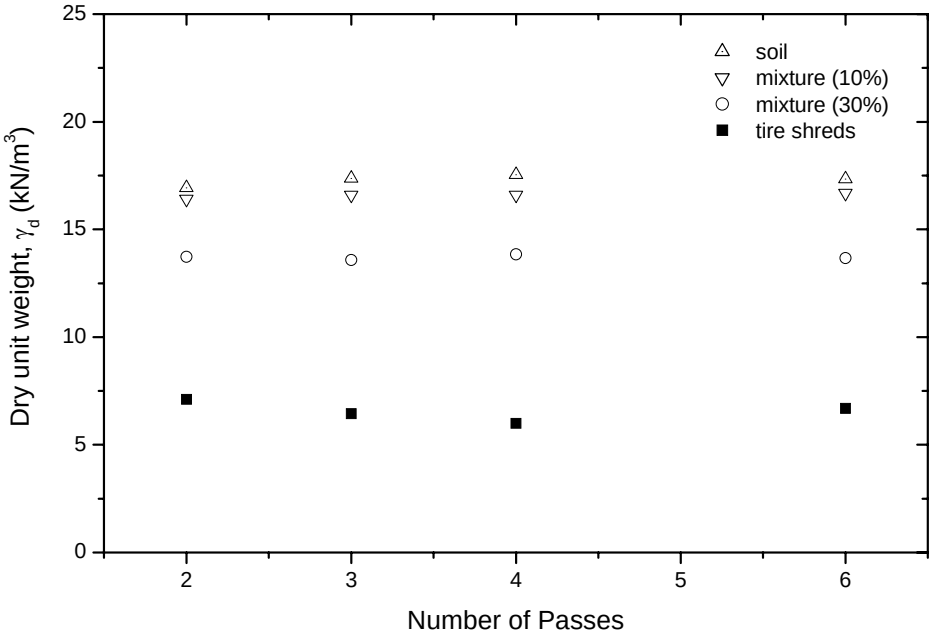

Figure 31: Dry unit weight versus number of passes for the different tested materials

The tests in the tire shred layer and in the 30-% composite revealed some minor scattering in comparison to the previous tested materials, as expected, due to the presence of a larger amount of tire shreds. The mean dry unit weight achieved by the 30-% mixture is equal to 14.1 kN/m^3. Despite the scattering, it is possible to affirm that there were no significant changes in γ_d after the second pass of the roller also with this material. The results with pure tire shreds are a little more scattered than the results of the 30-% mixture. Nevertheless, an average dry unit weight of 6.6 kN/m^3 was found, which is within the range of typical values reported in literature (Reddy and Marella 2001).

As reported by Bosscher et al (1992) in their experiments, most of the observed compression with both mixtures and with pure tire shreds took place until the second pass of the roller, with very small improvement in compaction occurring afterwards. Compactive efforts did not increase the unit weight of pure soil after three passes of the roller. Based on these findings, the optimum number of passes for the construction of the prototype embankment was conservatively established as four.

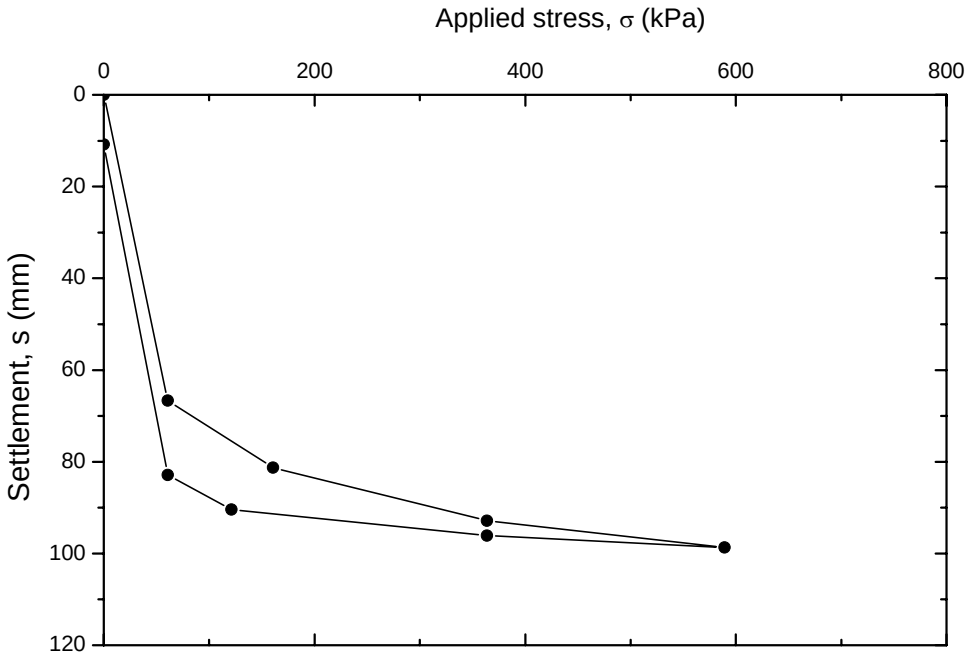

Figure 32: Stress-settlement relationship of pure tire shreds

Figure 32 shows results of a plate load test conducted on the surface of the section of the testing pad containing pure tire shreds. The test was carried out following ASTM Standard D 1196-93, for use in the evaluation and design of airport and highway pavements. The test was performed using a square steel bearing plate with 0.3 m in side and 19 mm in thickness. The plate size and shape were chosen to simulate the loading area of a typical tire of a truck. The bearing plate was loaded in cumulative increments using a hydraulic jack and a hand pump assembly reacting against a wheel loader with an approximate total weight of 133.1 kN. Load measurements were read from the hand

pump manometer. Settlements were obtained using two dial gauges with a maximum stroke of 50 mm and a resolution of 0.01 mm, mounted on two reference beams with articulated magnetic bases. The dial gauges were displaced near the edges of opposite sides of the bearing plate, with the tips positioned directly on the surface of the bearing plate. The magnitude of the loading stages used in the test was previously defined based on a maximum load equal to the standard AASHTO H15 wheel load (53 kN).

Figure 32 shows the stress-settlement relationship obtained in the test. The shape of the curve is quite similar to that of laterally confined tests on pure tire shreds published elsewhere (Edil and Bosscher 1992, Ahmed and Lovell 1993). Markedly high initial settlements are observed for stress increments lower than approximately 65 kPa. However, as the stress level is increased, settlement variations are dramatically reduced, particularly after about 300 kPa. The rebound upon unloading is very significant, with plastic settlement accounting for only about 11% of the total settlement. Since the tire shred layer was previously compacted, settlement is basically due to bending and elastic deformation of individual shreds, once most of settlement due to rearrangement and sliding of the shreds have occurred earlier during the compaction process.

In order to characterize the stiffness of the layer made with pure tire shreds for reference for field design parameters, it is necessary to calculate the modulus of subgrade reaction (K). For the tested material, K computed according to expression (1) is equal to 6 MN/m^3. The stress and settlement values considered in this equation correspond to the final loading stage. For a 0.3-m square footing, typical values of K reported in literature range from 13.5 to 540 MN/m^3 (Fwa 2003).

$$K = \frac{\sigma}{s} \qquad (1)$$

Where: σ = stress level

s = settlement.

Once the stress-displacement response of the system is known, a field Young's modulus (E) can be obtained by back analysis of expression (2), derived from the theory of elasticity. Typical values of Poisson ratio (ν) from uniaxial tests on pure tire shred specimens are in the range between 0.2 and 0.3 (Edil and Bosscher 1994). Considering once again the full loading cycle, and assuming $\nu = 0.25$, $I_d = 1$, and $I_s.I_h = 0.609$ (Harr 1966), a value equal to 307 kPa is obtained for E.

$$E = \frac{\sigma B(1-\upsilon^2)}{s} I_s I_d I_h \qquad (2)$$

Where: B = plate diameter or width

I_s = shape/stiffness factor

I_d = embedment factor

I_h = layer thickness factor.

Settlement Monitoring

After completion of construction of the embankment, a total of 15 steel stakes with 0.45 m in length were properly installed on the surface of the embankment in order to monitor the settlement of the various sections. The location of the survey instrumentation in the embankment is provided in Figures 33. The elevation of the points, measured with a theodolite with accuracy of ± 1 mm, was based on the elevation of a 1.5-m tall plastic pole cemented into the on-site soil. Immediately after installation of the survey instrumentation, the embankment was exposed to heavy truck traffic and settlements were monitored for 824 days. An average of 20 trucks per day crossed the embankment in both directions. The maximum registered weight of an individual truck crossing the embankment was 111 kN.

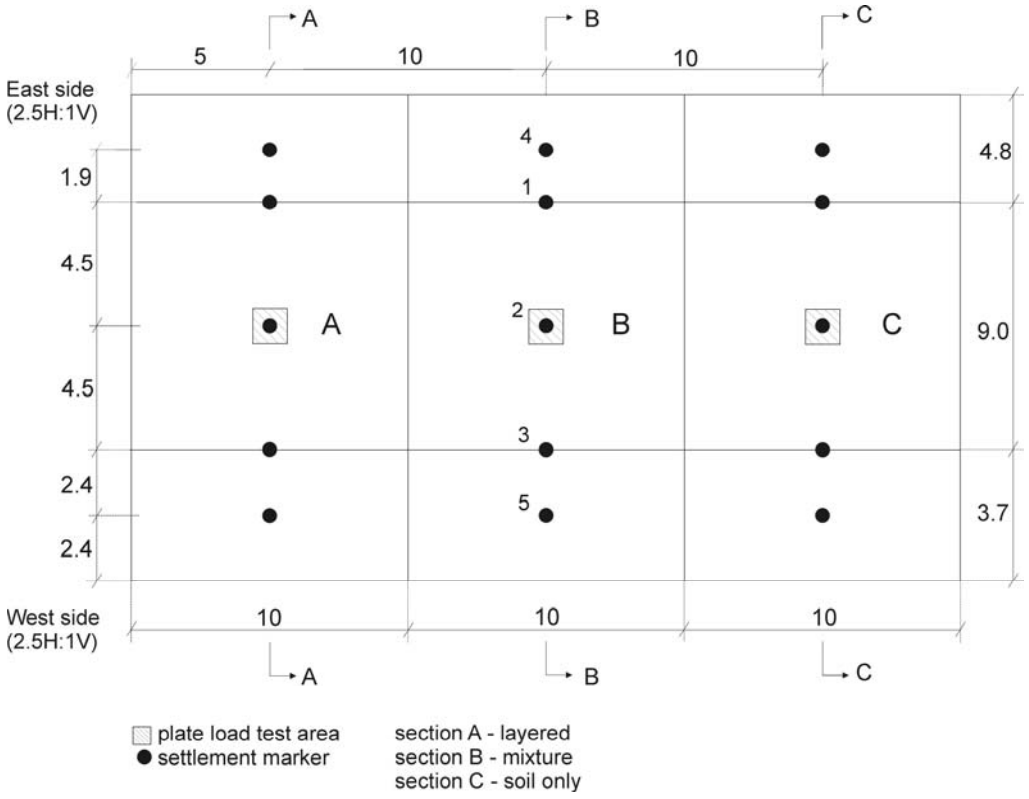

Figure 33: Plan View of the Tire Shred-Soil Embankment (dimensions in meters)

Elevation observations for each of the points have been taken every one to two months over a period of more than two years. Due the long time scale over which the multiple surveys occurred, they were completed by various people of varying surveying experience.

Due to large variations in measured absolute elevations observed during the settlement monitoring process, new settlement hubs were installed during the study. Twenty-one rebar spikes twelve to eighteen inches in length were installed in close proximity (approximately two inches) to the original stakes. The purpose of the installation of these new stakes was to determine if more consistent trends would be produced by the new stakes with greater surface area and correspondingly greater friction between the stakes and the surrounding soil. At the time of installation, a survey was conducted during which the elevations of both the new stakes and the original stakes were recorded. Based on these observations, conversion factors between the original and

the new stakes were determined by calculating the elevation difference between each original stake and the corresponding new stake. These conversion factors were used to correlate the observed elevations of the new stakes to those of the original stakes.

Similarly to pure soil, settlement of fills constructed with soil-tire shred mixtures can be classified into initial, primary consolidation, and secondary compression, and all these components may occur simultaneously. If the composite is in an unsaturated state, consolidation in that case means dissipation of excess of pore-air and pore-water pressures (Fredlund and Rahardjo 1993). Distortion, bending and reorientation of the tire shreds embedded in the soil matrix, as well as elastic deformation of individual tire shreds upon loading are part of the compression mechanisms of such fills. The interaction between tire shreds and soil particles, resulting in interface friction, must also be considered as part of the process. Soil-tire shred interface friction angle is about 26^0 for cohesive soil under drained conditions and 30^0 for dry sand (Garga and O'Shaughnessy 2000). Summed up together, all these mechanisms compose a highly complex scenario.

Settlement of fills of pure tire shreds is basically due to distortion, bending, reorientation, and elastic deformation of tire shreds. In this case, the large voids in the tire shred mass increase the influence of these mechanisms in the overall behavior of the material. As a result, settlement of such fills is generally higher than that of fills of soil-tire shred composites. Moreover, settlement of pure tire shred fills may also be caused by the migration of soil particles from the cover layer (or from upper layers, in the case of layered systems) into the voids of the tire shred mass. This is analogous to a process that takes place in landfills known as raveling (Qian et al. 2002), and the same designation will be used herein.

Raveling is usually accompanied by the formation of potholes on the embankment surface. A geotextile is commonly used as a separation element between the soil and tire shred layers to prevent raveling. In this research, it was chosen to build the embankment without separation elements to evaluate the extent of raveling with cohesive soils. After

over two years of traffic, the layered section (A) developed a few small potholes, comparable to what was observed on the 10-% mixture section (B). This suggests that raveling was negligible in section A. Whenever possible, the design of embankments involving layers of pure tire shreds and cohesive soil should take advantage of the soil cohesion over separation elements.

Settlement as a function of time after the beginning of traffic is presented in Figure 34. The data in this figure was collected at the center of the crest of each section of the embankment (Figure 33). In general, sections A and B showed a satisfactory long-term performance. Settlement measured in section A, built with consecutive layers, was larger than in section B, made with the soil-tire shred composite. However, settlements of both sections were higher than in section C (soil only), which showed settlements not greater than 65 mm. At the end of the survey period (824 days), the final settlements of sections A and B were 87 and 62% larger than the final settlement of section C, respectively.

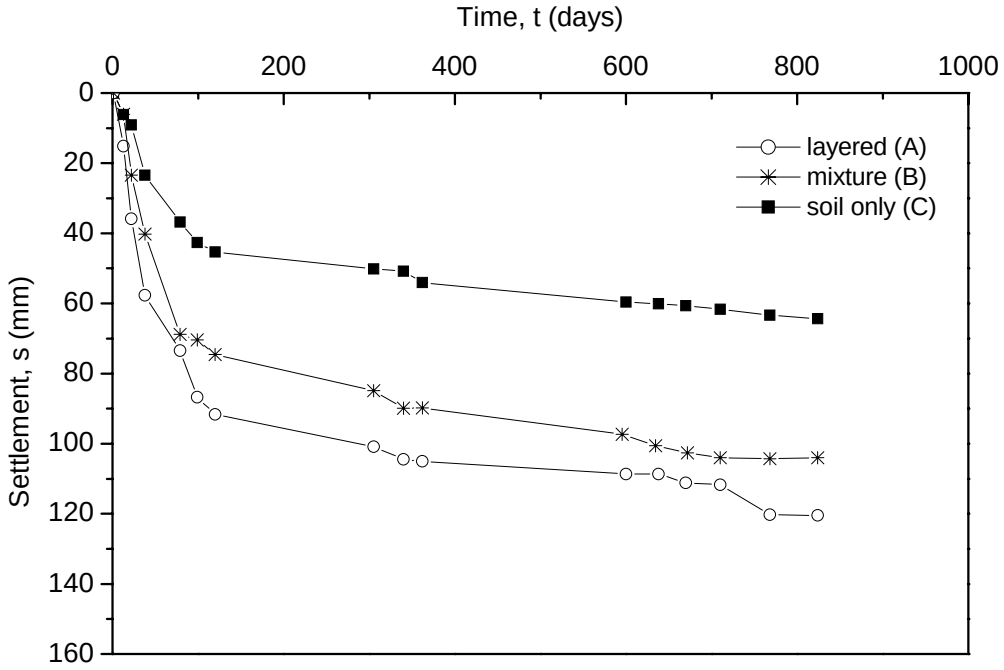

Figure 34: Settlement of each Section after Construction and Subject to Traffic

Results of Figure 34 also indicate that settlements were more pronounced during the first 120 days in all sections, dropping considerably after that period. Settlement rate (m) of each section from the beginning of the survey until the first 120 days (stage I), and from that point to the end of the survey (stage II) is presented in Table 4. During stage I, settlement rate at section A is twice as high as at section C. Accordingly, m at section B is 63% more pronounced than at section C during the same period. Throughout stage II, sections A and B show similar settlement rates, about 0.04 mm/day, less than one tenth of the values of m observed at stage I. This value is very close to that of section C.

Table 4: Settlement Rate of the Embankment Sections

	Settlement rate, m x 10^{-2} (mm/day)		
Period after construction	Section A	Section B	Section C
0 to 120 days (stage I)	76.0	62	38
120 to 824 days (stage II)	4.1	4.2	2.7

According to Figure 32, the portion of settlement in section A due to the initial compression of the two layers of pure tire shreds caused by the self weight of the embankment is about 40 mm. This accounts for almost 45% of the total settlement experienced by this section during the first 120 days after construction and beginning of traffic.

Figure 35 shows profiles composed by settlements measured in five distinct locations across the surface of each section. The data in the figure correspond to 38, 120 and 824 days of survey. In general, section C presented the smallest settlements in all measured locations, followed by sections B and A, respectively. After 38 days (Figure 35a), displacements of sections B and C were very close at the slopes. On the other hand, section A presents slightly higher displacements at the slopes and at the center. A not

very clear pattern is observed at the shoulders. After 120 days (Figure 35b), settlements of section A become noticeably higher in comparison to the other sections, particularly at the slopes. Although settlements of section B became more pronounced at the center and shoulders with respect to section C, settlements of both sections remained very close at the slopes. Figure 35c shows that at the conclusion of the survey period, 824 days, settlements at the slopes and shoulders of section A became markedly pronounced, much larger than at the center. The self-weight of the embankment fill and the presence of the transient loading cause the two layers of pure tire shreds to compresses more near the edges of the embankment, due to the lower confinement in those regions, according to the behavior shown in Figure 32.

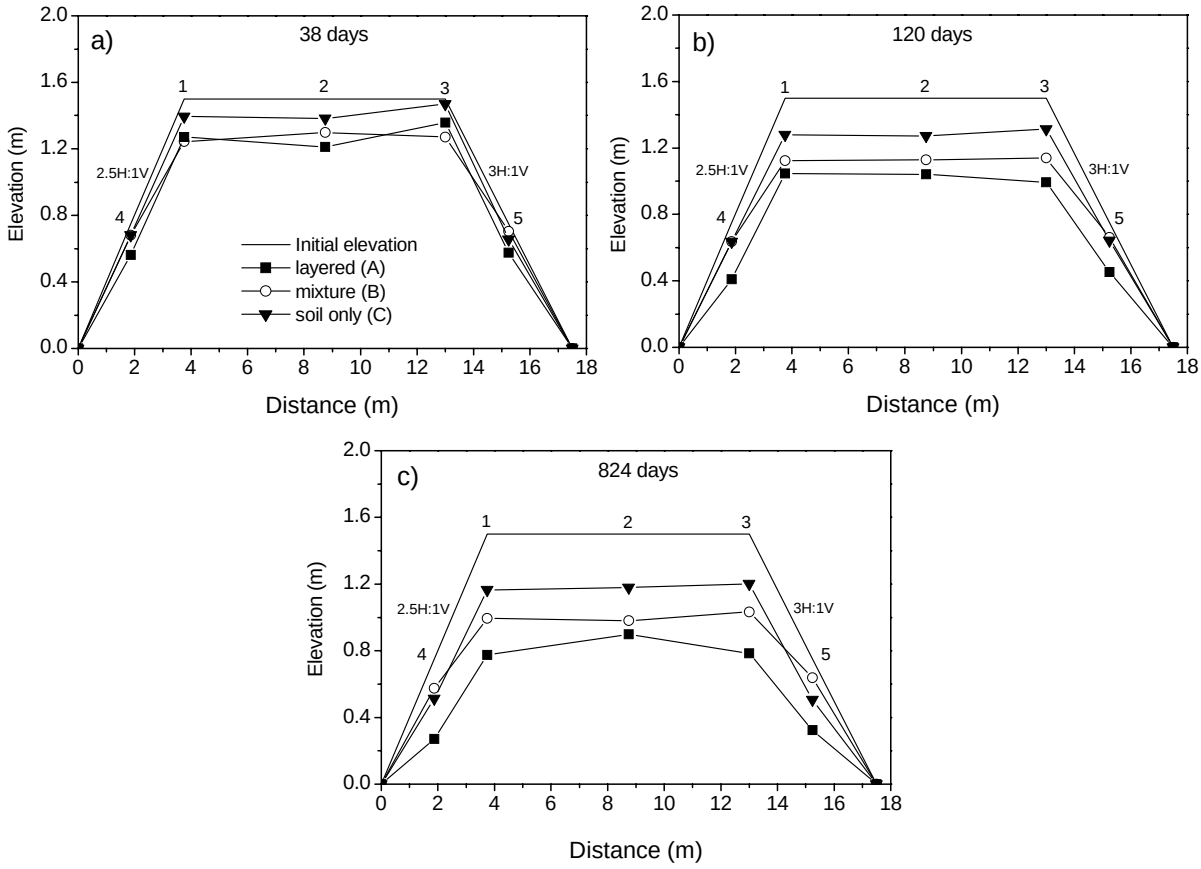

Figure 35: Settlement profiles of the embankment cross-sections at 38, 120 and 824 days. Displacements are magnified by a scale factor of 5.

Angular distortions (β), computed according to expression 3 from the differential settlements observed at the shoulders and the center of the sections (points 1, 2, and 3 in Figures 4, 5 and 7), are shown in Table 3. The settlement data belongs to the final stage of the survey, 824 days.

$$\beta_{ij} = \frac{\Delta s_{ij}}{L_{ij}} \qquad (3)$$

Where: Δs_{ij} = differential settlement between survey points, i and j

L_{ij} = distance between survey points i and j.

Section C presented comparatively small angular distortions, comparable to the safety limit recommended for flexible brick walls, 1/150 (Bjerrum 1963). Except for the distortion between points 2 and 3, which was somewhat elevated, the response of section B was similar to that of section C. As verified previously, section A presented very large differential settlements, with the shoulders settling more than the center.

Plate Load Test Procedure

A total of four plate-load tests were completed, one on each section of the prototype embankment, and one on an area of tire-shreds approximately five feet thick, also located at the Front Range Tire Recycle, Inc. Facility. The standard procedure for nonrepetitive static plate-load tests of soils and flexible pavement components, for use in evaluation and design of airport and highway pavements, as outlined in ASTM Standard D 1196-93, was followed. The same basic procedure was followed for all four tests.

The primary components of the apparatus used to complete the plate-load tests included a loading device, a hydraulic jack assembly, bearing plates, dial gages, a deflection beam, and other miscellaneous tools. The loading device used was a Caterpillar 950B front-end loader, with an approximate operating weight of 30,000 lb. The hydraulic jack assembly used was borrowed from Yenter Companies, a geotechnical engineering and contracting company from Golden, CO. It was a Power Team Hand Pump, model C s/n 0603AD91006. The jack was calibrated by Commercial Testing

Laboratories. The bearing plate used was a ¾" thick steel plate, measuring 12" on each side. It should be noted that the ASTM standard specifies the use of a set of circular bearing plates for testing purposes; the square plate was used because it was the only plate available, and had been used in previous tests completed by the Colorado Department of Transportation (CDOT). Two dial gages, also borrowed from Yenter Companies, were used for deflection measurements. Two deflection beams were used, one to support each dial gage. One deflection beam was a piece of angle iron approximately 6' in length, measuring 1-1/2" x 1-1/2" by 1/8". The other deflection beam was a solid rectangular steel bar approximately 5' in length, measuring 1" x 1". The deflection beams were each mounted on two steel stands, which sat directly on the road surface; the beam/stand connection was secured with tire-wire.

The first plate-load test was completed on the soil-only section of the prototype embankment, in the center of the west-lane of the road, in the approximate center of the section. An area approximately 18" x 18" was excavated by hand to a depth of approximately 3", in order to create a level surface on which to place the bearing plate. The front-end loader was positioned so that the center of its front axle was located directly above the excavated area. A picture of the excavation is shown in Figure 36. Next, a thin layer, approximately 1" thick, of dry plaster was placed in the excavated area and leveled by hand. The purpose of the plaster was to create a smooth contact surface between the bearing plate and the soil so as to maximize the uniformity of the stress distribution over the entire area of the plate. A picture of the excavated area after placing the plaster is shown in Figure 37.

Figure 36: Location of plate-load test, after excavation by hand

Figure 37: Plate-load test area after placement of plaster

The bearing plate was then placed on the plaster, and positioned so that it was directly centered beneath the center of the front axle of the loader. Using a 2' level, the bearing plate was leveled by adding additional plaster as necessary. The hydraulic jack assembly was then placed on the bearing plate and centered, verification of which was achieved through the use of a tape measure. Various steel shims, ranging in shape and thickness, were then placed on top of the hydraulic jack in order to minimize the distance between the jack assembly and the loader axle. Next, the deflection beams were positioned longitudinally beneath the loader, one on either side of the jack assembly. The dial gages were then attached to the deflection beams with magnetic holding devices; the gages were positioned at opposite corners of the bearing plate, approximately 1" from the edge. The jack was then pumped until contact between the jack assembly and the axle was made. A picture of the apparatus set-up is shown in Figure 38. A picture depicting the dial gage positions is shown in Figure 39.

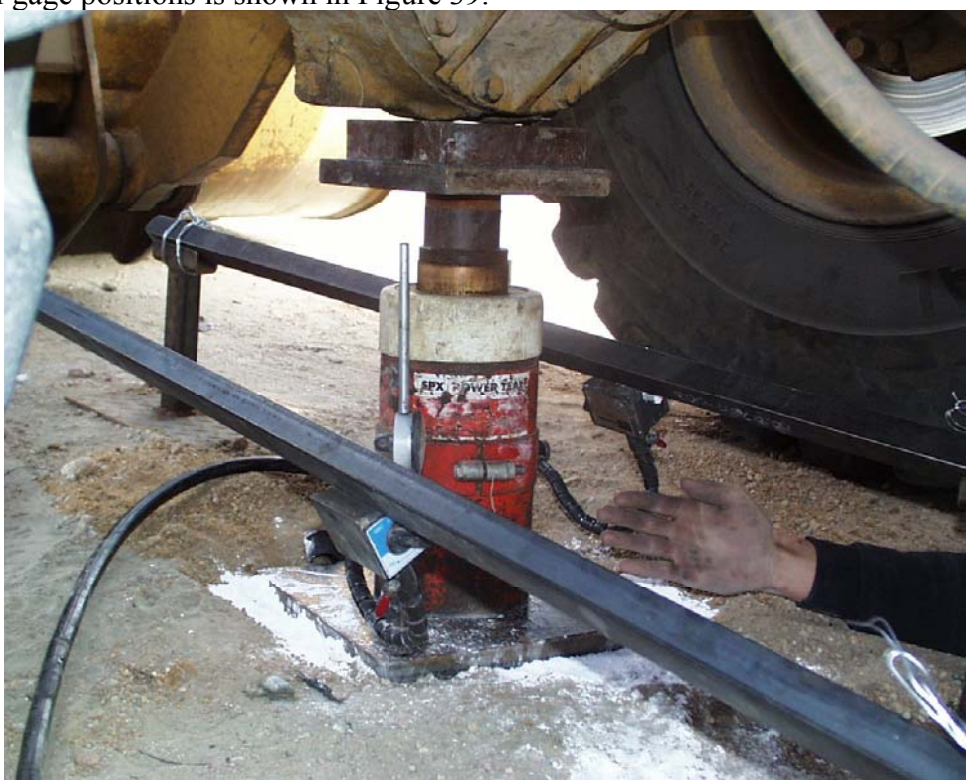

Figure 38: Plate-load test apparatus assembly

The hydraulic jack used for the tests was a 60-ton jack, and the pressure indicator started at 400 psi. Therefore, it was impossible to apply a seating load which produced between 0.01 and 0.02 inches of deflection, and accurately determine the load pressure, as stipulated in the ASTM standard. As such, an initial seating load of 440 psi was used in each test. Dial gage readings were recorded before the application of any load and after the application of the seating load. The dial gage readings after the application of the seating load were taken as the zero-point for purposes of determining total deflections.

Figure 39: Dial gage positions

After the application of the seating load, a constant pressure was maintained until the settlement rate reached a maximum displacement of 0.001" per minute for three consecutive minutes for each dial gage. Then the pressure was increased to 600 psi, and the deflections were recorded in a similar manner. This process continued, with incremental loads of 100 psi, until a maximum load of 1200 psi was achieved. At this point, the tires of the loader were completely off the ground, and the bucket, which was initially placed on the ground, began to lift. After recording the final deflection measurements, the hydraulic jack was unloaded to 400 psi. At this point, deflections were again measured once the rate of recovery reached the rate previously described. The hydraulic jack was then completely unloaded, and final recovery deflections were recorded in the same manner as before. This same process was completed for each of the three tests performed on the prototype embankment.

The test completed on the tire-shred area was performed in the same manner as the three tests performed on the prototype embankment; however, due to the greater magnitude of deflections, the test procedure did not go as smoothly. First, it was extremely difficult to apply a significant load to the tire shreds. Therefore, a seating load of 400 psi was used. At the first incremental load of 500 psi, one dial gage had already bottomed out, as the settlement of the plate was so great. The test was continued, and another reading was made at a load of 600 psi. Then, while pumping the jack, the load increased suddenly from slightly over 600 psi to 1000 psi. Another measurement was recorded at this point. Finally, the jack was unloaded to 600, 500, 400, and 0 psi, with deflection measurements being made at each point. In addition, it should be noted that the stability of the surrounding tire shreds, on which the deflection beam stands were placed, was questionable. The dial gages indicated deflections when people stepped near the deflection beams.

Plate Load Test Results

The results of the plate-load tests were, for the most part, very encouraging. The three tests performed on the sections of the prototype embankment yielded very linear results in almost all cases, with the exception of the test performed in the layered section. Due to the excessive settlements observed during the test in the tire-shred area, the data is relatively meaningless, and will not be presented here. The results of the tests performed in the soil-only section, the soil/tire-shred mixture section, and the layered section are shown together in Figure 40, and individually in Figures 41, 42, and 43.

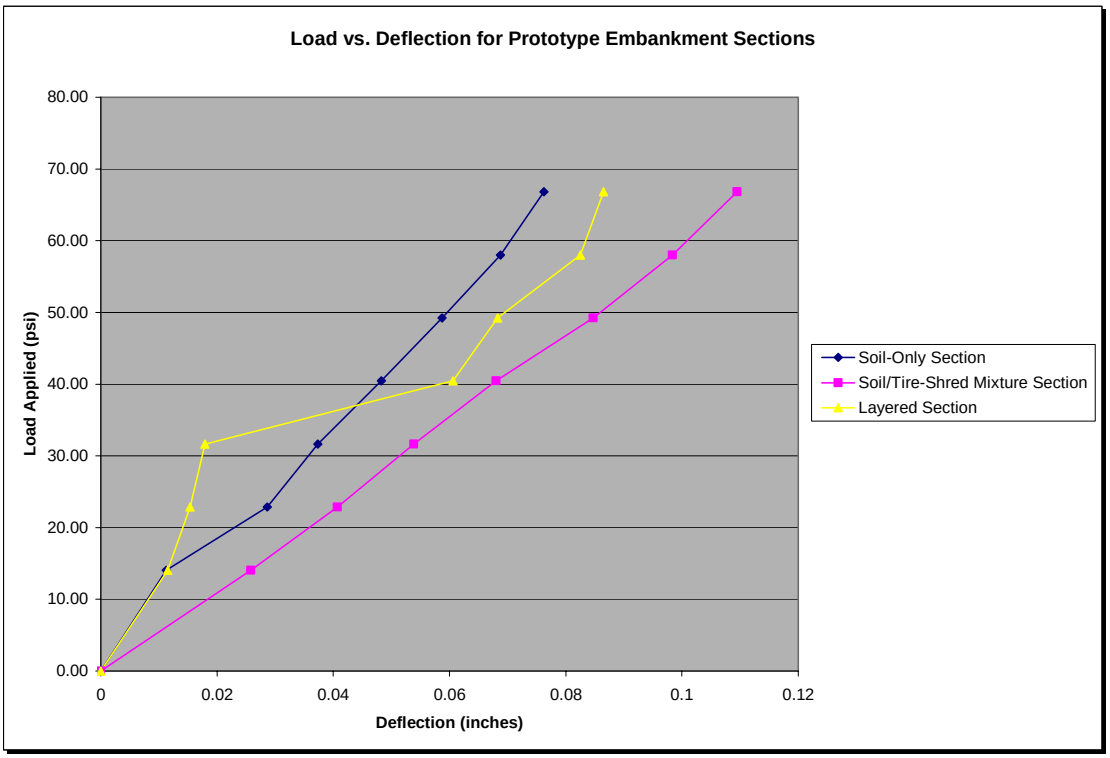

Figure 40: Results of plate-load tests on prototype embankment

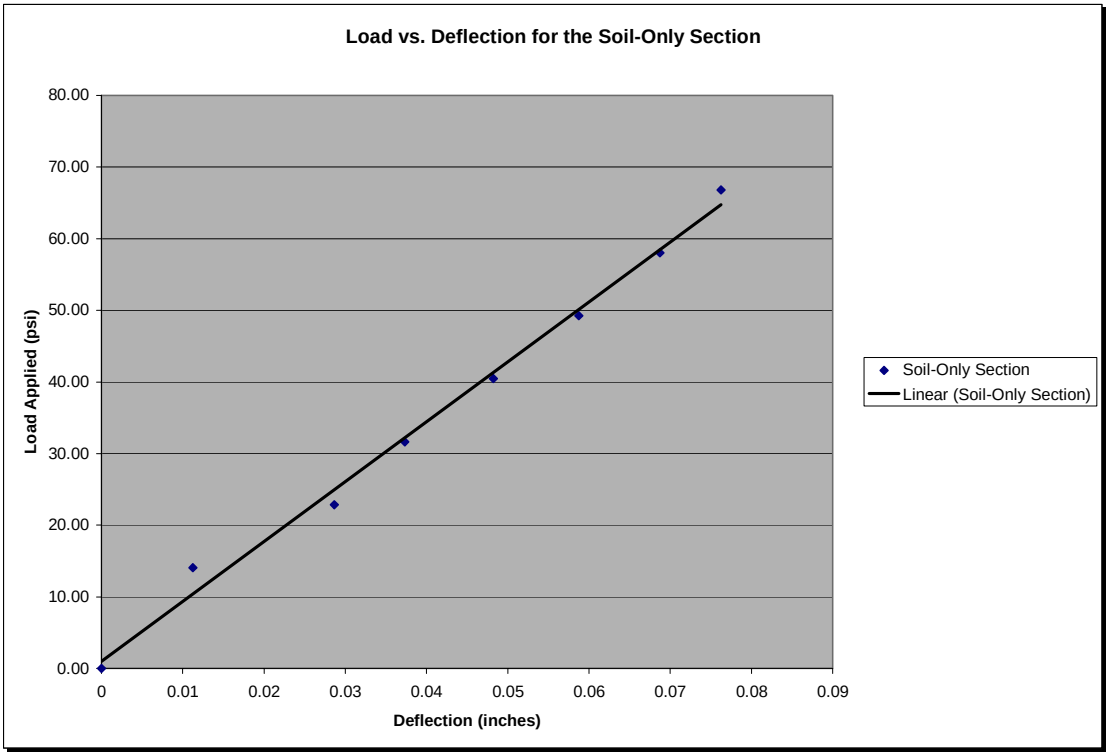

Figure 41: Results of plate-load test on soil-only section

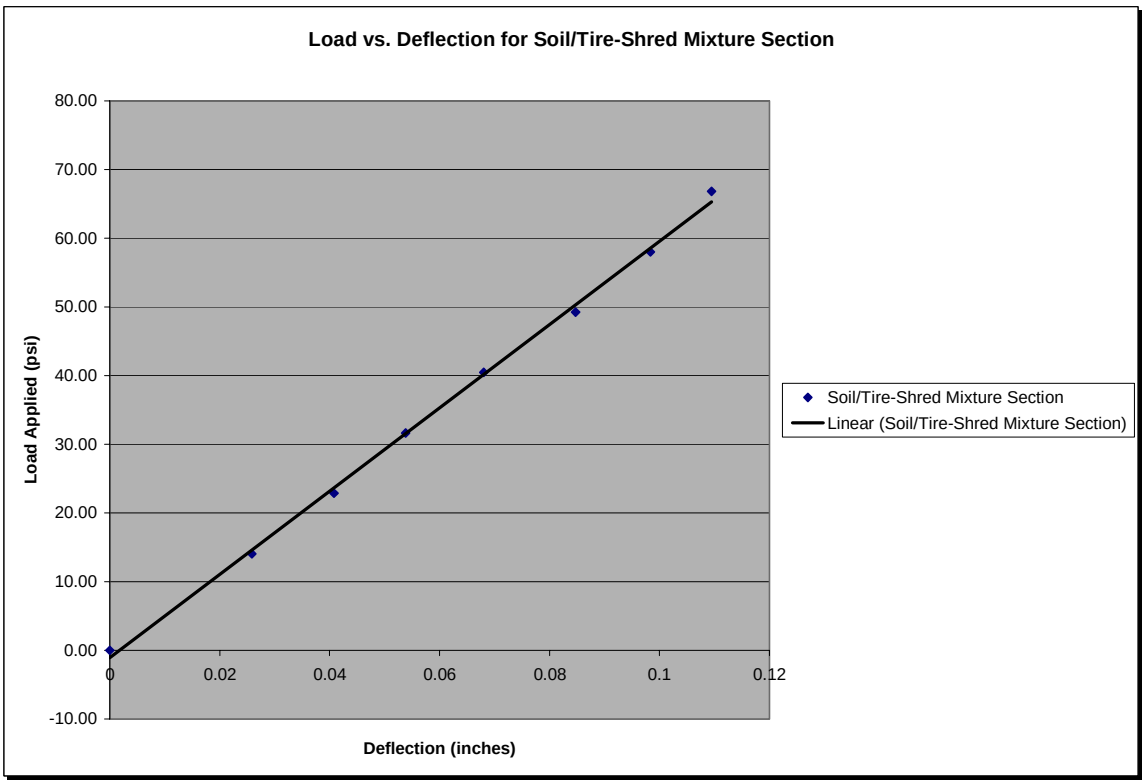

Figure 42: Results of plate-load test on soil/tire-shred mixture section

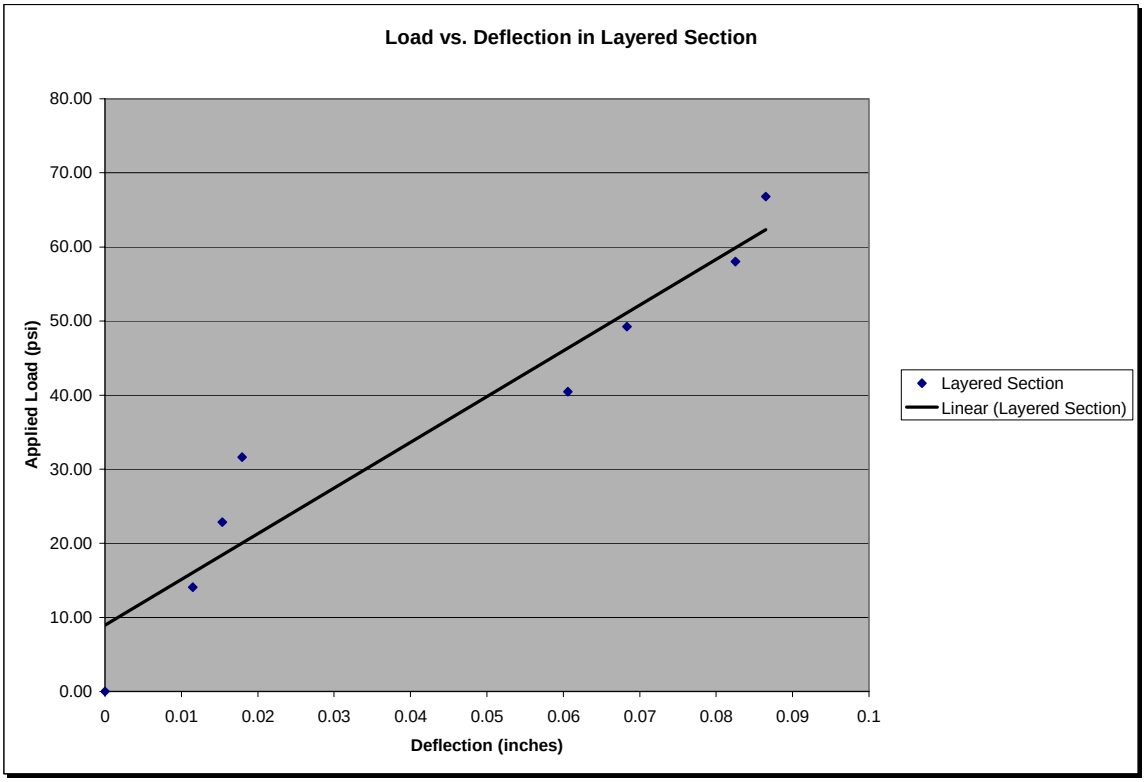

Figure 43: Results of plate-load test on layered section

Summary and Conclusions

A field investigation was conducted to assess the mechanical behavior of an experimental embankment fill built with tire shreds and cohesive soil. Sections including successive layers of soil and tire-shreds, a soil-tire shred composite, and pure soil were evaluated. Immediately after construction, the embankment was submitted to heavy truck traffic and settlements were monitored for over two years at different locations across the surface of each section. Plate load tests were performed to assess the stress-strain behavior of the embankment after the survey period.

The results indicate that the embankment sections built with tire shreds and cohesive soil showed satisfactory long-term performances during traffic exposure. In all sections, most of the compression took place within the first 120 days following construction. Settlements of both fills containing tire shreds were higher than that of the section of pure soil. However, after 120 days, settlement rate in both sections converged to a value close to the observed in the fill section of pure soil. The section containing the soil-tire shred mixture presented a better overall time-dependent performance in comparison to the layered section, including smaller differential settlements.

After more than two years of construction and traffic exposure, the fill sections constructed with tire shreds presented a very good bearing capacity response, very close to that of the fill of pure soil. For the applied loading range, which corresponds to typical truck wheel loads, the elastic phase was not exceeded in none of the tested systems.

Depending on the content of tire shreds and on the cohesion of the soil, large volumes of homogeneous tire shred-cohesive soil composites may be difficult to be prepared in the field with machinery commonly used for embankment construction. Particularly, production of a mixture with 30% of tire shreds was not feasible with the soil tested herein. However, a single wheel loader with a bucket equipped with a tooth edge set proved to be very efficient in making large quantities of a homogeneous mixture with 10% of tire shreds by weight.

The results of the plate-load tests are, for the most part, what was expected. The soil-only section displayed the greatest resistance to deflection for the given loads, and thus is the stiffest of the three types of fill. The soil/tire-shred mixture section illustrated a slightly larger degree of settlement for the same loads, but not an extreme amount. The performance of the soil/tire-shred mixture in terms of its elastic response is most likely acceptable regarding its use as fill material for road embankments. Further analysis is required in order to determine the elastic modulus of the soil/tire-shred mixture, and to compare this with acceptable values for road embankment fill material.

The results of the plate-load test conducted on the layered section may seem a bit strange at first, but can be reasonably explained. As the load is increased, the depth of influence increases. At first, the depth of influence is quite shallow, and the material being tested is really only the soil cover on top of the layered section. The initial portion of the load vs. deflection graph for the layered section matches that for the soil-only section closely. As the depth of influence reaches the layers of tire-shreds, it would be expected to see a greater rate of deflection, which was observed during the test. In order to quantify the overall elastic modulus of the layered section, further analysis is required.

Recommendations for Future Work

Based on this study, it is apparent that soil/tire-shred mixtures can be expected to perform very similar to pure soil in terms of settlement behavior when used as road embankment fill. This study specifically indicates that a mixture 10% tire shreds by volume performs adequately. The use of soil/tire-shred mixtures as road embankment fill represents a significant means of reusing tire shreds. In addition, the total unit weight of the embankment is decreased, which is attractive in many situations, especially when the embankment is constructed upon soft deposits.

The use of layered soil/tire-shred combinations cannot be discounted based on this study only. Indeed, the majority of the settlement in this section took place shortly after the completion of construction. After the initial plastic compression of the tire shreds, the embankment performed similarly to that of the soil/tire-shred mixture and soil-only sections. One way to alleviate this problem in the field would be to apply an additional surcharge to the embankment in the way of additional soil. This surcharge could be removed after a period of a few months. While this may prevent excess settlement in a layered embankment, it also requires additional construction time and costs. Further studies are necessary to validate this approach.

Thermal Analysis of Embankment

Analytical Approach

Thermal Properties of Soil

The thermal properties of soil have been researched since about 1949, when Miles S. Kersten at the University of Minnesota began researching the effect and relative significance of the various factors that influence the thermal properties of soils (Kersten, 1949). Subsequent research in this area has been largely based on the findings and assumptions that Kersten presented. The thermal properties that are of primary interest in geotechnical design are the thermal conductivity, heat capacity, volumetric specific heat, volumetric latent heat and thermal diffusivity. These properties are necessary in determining the heat transfer through a soil mass. A brief introduction to heat transfer within soils will help in understanding the correlations of thermal properties of soils with the other soil properties.

Background

Heat is transferred within soil by conduction, convection and radiation. Conduction is the transfer of energy from the more energetic particles of a substance to the less energetic particles. This transfer of energy is due to the interactions of the particles in a solid or stationary fluid. Convection is the energy transfer due to random molecular motion (diffusion) and by bulk (macroscopic) motion of a fluid. Radiation is the energy emitted by matter that is at a finite temperature and does not require the presence of a material medium (Incropera and DeWitt, 2002). These three heat transfer modes are portrayed in Figure 44.

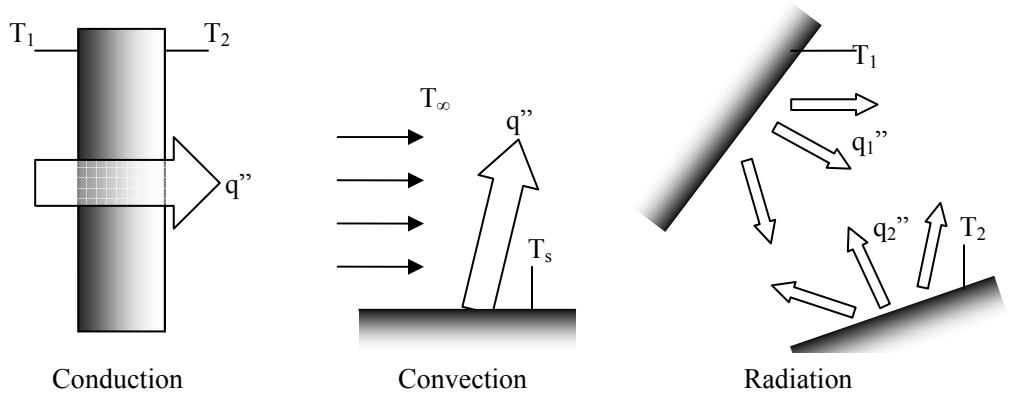

Figure 44: Heat Transfer Modes

Conduction through a medium is determined by measuring the heat flux. The heat flux is the heat transfer rate in the direction of transfer, across a fixed distance. It is calculated per unit area perpendicular to the direction of transfer. The rate is determined by calculating the temperature difference between the two end points and multiplying it by the thermal conductivity, k, of the solid (Incropera and Dewitt, 2002):

$$q'' = \frac{k(T_1 - T_2)}{L} \tag{4}$$

Where: q” = conductive heat flux (W/m^2 or Btu/hr·ft^2)

k = thermal conductivity (W/m·°K or Btu/hr·ft·°F)

T_1 = temperature at point closest to heat source (°K or °F)

T_2 = temperature at point furthest from heat source (°K or °F)

L = distance between two points (m or ft)

The heat rate is the product of the heat flux multiplied by the area, shown in the following expression (Incropera and Dewitt, 2002):

$$q = q'' \times A \tag{5}$$

Where: q = heat rate by conduction (W or Btu/hr)

q” = conductive heat flux (W/m^2 or Btu/hr·ft^2)

A = area (m^2 or ft^2)

Convective heat transfer is determined by the temperature difference between a surface and a fluid above the surface. This temperature gradient is then multiplied by the convection heat transfer coefficient, h (Incropera and Dewitt, 2002):

$$q'' = h(T_s - T_\infty) \tag{6}$$

Where: q" = convective heat flux (W/m^2 or $Btu/hr \cdot ft^2$)

h = convection heat transfer coefficient ($W/m^2 \cdot °K$ or $Btu/hr \cdot ft^2 \cdot °F$)

T_s = surface temperature (°K or °F)

T_∞ = fluid temperature (°K or °F)

Radiation is determined from the emissivity of a surface, ε, and the Stefan-Boltzmann constant multiplied by the difference of the surface temperature and the surrounding temperature (Incropera and Dewitt, 2002):

$$q'' = \varepsilon\sigma(T_s^{\,4} - T_{sur}^{\,4}) \tag{7}$$

Where: q" = radiative heat flux (W/m^2 or $Btu/hr \cdot ft^2$)

ε = emissivity ($0 \leq \varepsilon \leq 1$)

σ = Stefan-Boltzmann constant (5.67×10^{-8} $W/m^2 \cdot °K^4$)

T_s = surface temperature (°K or °F)

T_{sur} = temperature of the surroundings (°K or °F)

These three heat transfer modes can be present within a soil embankment; however, simplifying assumptions are made in order to evaluate the heat transfer in a tire shred-soil embankment. The effect of radiation within the soil mass is considered to be negligible in comparison with the other heat transfer modes. Due to the relatively small pore sizes which contain water and air the effect of convection is also typically assumed to be negligible. Convection may be important if there is a high rate of flow of either water or air through the soil, as in a coarse sand, gravel or rock fill. However, convection is generally considered negligible if the pore sizes are less than 10 millimeters. In addition, it is difficult to separate the conduction heat from the convection heat in a porous medium such as soil. The conduction through the soil mass is considered to be

one dimensional. For the purposes of the thermal conductivity of the soils, the "k" value is often treated as the combination of heat conduction, convection and radiation through the soil constituents-water-air combination, and referred to as the apparent thermal conductivity. The thermal conductivity of the soil is the primary thermal property that describes the heat flow through the soil.

Correlations and Discussion

The thermal conductivity, heat capacity, volumetric specific heat, volumetric latent heat and thermal diffusivity are dependent upon many of the soil mass properties. The research advances in the area of soil thermal properties have been primarily in relation to correlations between the heat transfer in a soil and other soil properties. The important factors that influence the soil thermal properties (e.g. thermal conductivity and heat capacity) include: mineralogy, dry density, gradation, compaction water content, time and temperature. Soils are a combination of various minerals and organic materials, each having their own thermal properties; therefore the percentage of each solid particle constituent affects the overall thermal properties of the soil.

The dry density is an important factor because the volume of the voids and the distance between soil particles affects the conduction of heat through the soil mass. The soil gradation also affects the size of the pores within the soil, with a well graded soil conducting heat better than poorly graded soils due to the particle packing (higher dry density) and mineral-to-mineral contact. Particles within a well graded soil are small enough to fill the pore sizes and increase the mineral-to-mineral contact which in turn increases the heat conduction through the soil. Dry density and soil gradation are relative indicators of the mineral-to-mineral contact and pore sizes within a soil mass, which in turn affect the thermal properties of a soil.

The placement water content during compaction influences the heat conduction through the pore volumes containing water, ultimately affecting the overall heat transfer

within the soil. It has been determined that sands compacted wet and then dried to a lower water content have a higher thermal conductivity than sands compacted with a lower water content. The compaction water content is one of the most significant factors influencing the thermal properties of soil.

Two other influencing factors on soil thermal properties are the presence of cementitious material and temperature. In soils containing silica, carbonates or other cementitious materials, the thermal conductivity may increase with time. It is generally accepted that the thermal conductivity of soils increases slightly as the temperature increases, although this effect is a combined result of the thermal conductivities of water (which increases as the temperature increases), soil minerals (which decreases with increasing temperature), and air (which increases significantly as the temperature increases) in the pore spaces.

Soil Thermal Conductivity

The soil thermal conductivity is often measured to evaluate other soil properties such as water content, shown through correlations determined from past research. Thermal conductivity is a transport property that provides an indication of the rate at which energy is transferred by the diffusive thermal process. It is measured in either calories/sec·cm·°C, W/m·K or Btu/hr·ft·°F. The most relevant soil properties that affect the soil thermal conductivity are the physical structure of the soil (both atomic and molecular), water content, dry density, mineral content and gradation.

The water content of a soil significantly affects the thermal conductivity and is of the most interest in determining thermal correlations for soils. The mechanism by which water content affects the thermal conductivity is related to the mineral-to-mineral contact and the presence of water in the voids. When a soil is completely dry, the heat passes through the grains by conduction and through the air spaces by convection and radiation. As the water content increases, the air voids are filled with water, bridging the gap

between soil particles. The thermal conductivity increases rapidly as the gap is bridged by water, due to the water becoming a continuous medium and conducting heat better than the air in the voids. Figure 44 shows the formation of the water rings that bridge the air gaps between the soil particles (Devries, 1975).

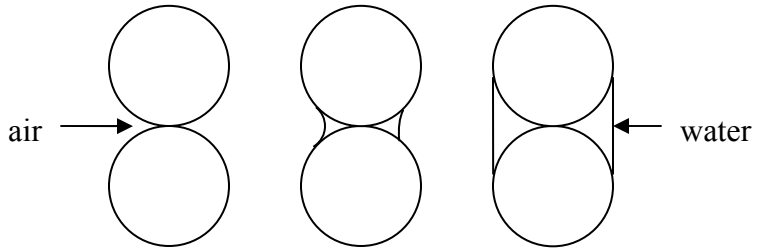

Figure 44: Formation of Water Rings

As the water content increases and the soil nears 100% saturation, the rate of increase in thermal conductivity decreases, as is shown in Figure 45. In this figure Curve 1 is for a quartz sand that is 55% solids by volume; Curve 2, a loam with 50% solids by volume; and, Curve 3, a peat soil with 20% solids by volume. In Figure 45 the x-axis represents the volumetric water content at 10°C, x_w, and the y-axis represents the thermal conductivity, λ, in W/m·°K (Devries, 1975).

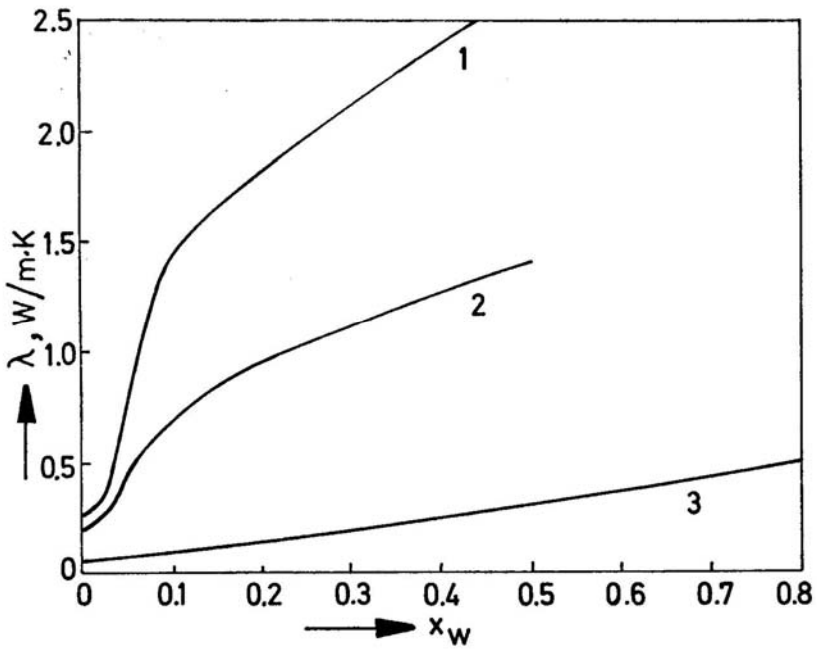

Figure 45: Volumetric Water Content versus Thermal Conductivity (Devries, 1975)

The following correlation has been proposed between the water content and the volumetric water content of the soil (Devries, 1975).

$$\lambda = \frac{x_w \lambda_w + \sum k_i x_i \lambda_i + k_a x_a \lambda_a}{x_w + \sum k_i x_i + k_a x_a} \tag{8}$$

Where: λ = thermal conductivity of soil

λ_w = thermal conductivity of water

λ_i = thermal conductivity of solid particles

λ_a = thermal conductivity of air

x_w = volumetric soil water content

x_i = volumetric soil solid content

x_a = volumetric soil air content

k_i = ratio of the space average of the temperature gradient in the soil grains and the water

k_a = ratio of the space average of the temperature gradient in the air and the water

In equation (8) x_w, x_i, and x_a represent the volumetric fraction of each constituent: water, solid particles of various materials, and air. Multiplication factors are added to the solid and air portions of the equation to account for the ratio of the space average of the temperature gradient through the soil grains and air to the temperature gradient in the water (Devries, 1975).

The dry density has also been determined to affect the thermal conductivity of the soil. As the dry density increases, the mineral-to-mineral contact increases, which enhances the heat transfer by conduction and thus increases the thermal conductivity. Therefore, as the porosity decreases, the thermal conductivity increases. Kersten originally proposed correlations between the dry density, water content and thermal conductivity that are still used today as a reference (Kersten, 1949). Figures 46 and 47 show these correlations for coarse grained soils and fine grained soils.

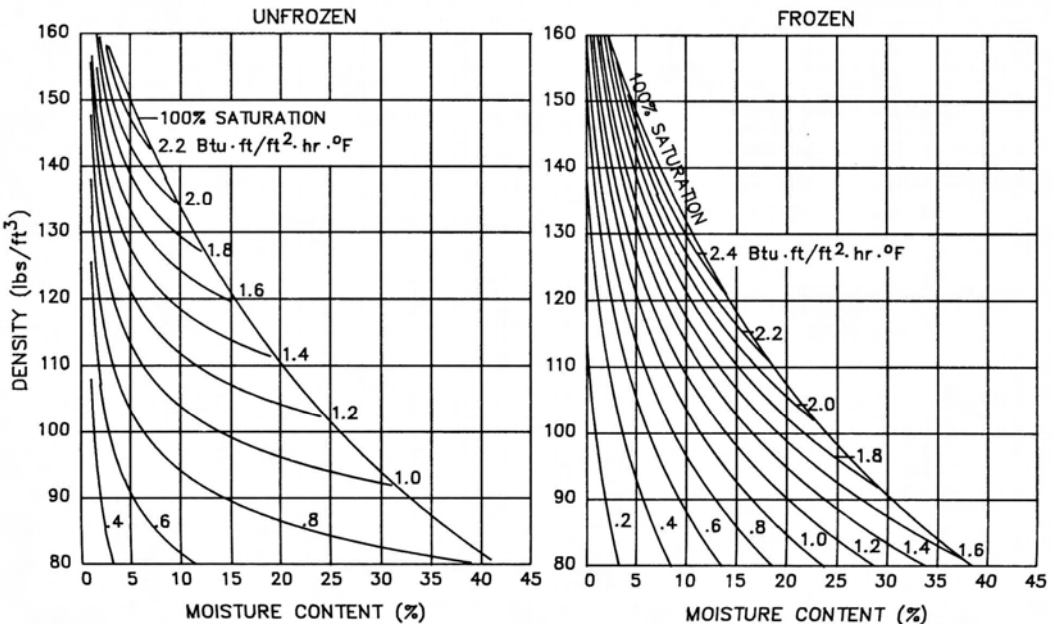

Figure 46: Frozen and Thawed Thermal Conductivities for Coarse Grained Soils (Kersten, 1949)

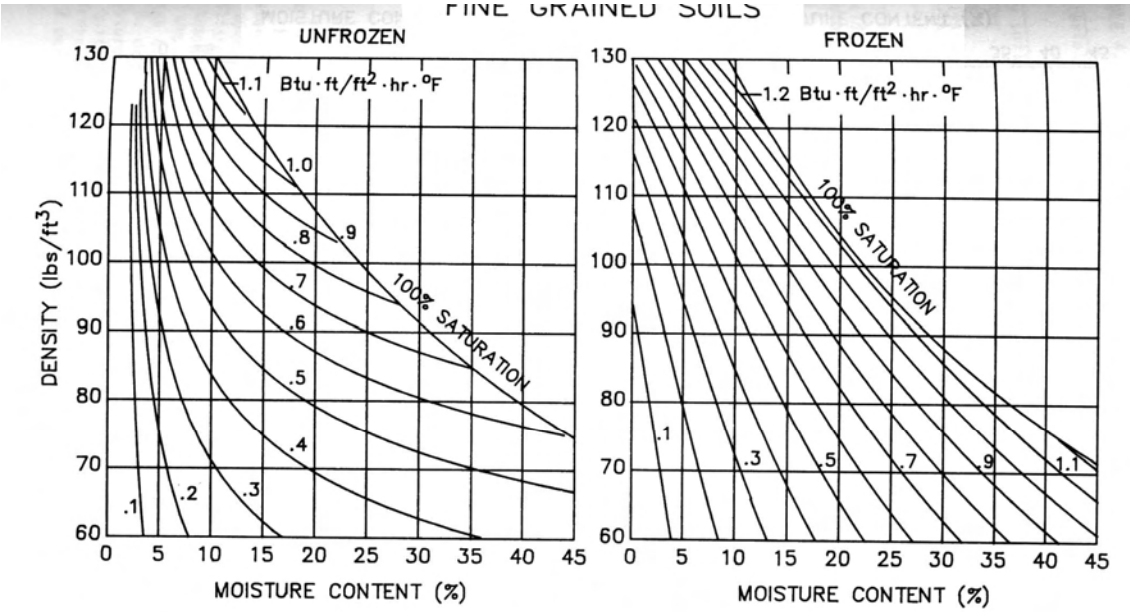

Figure 47: Frozen and Thawed Thermal Conductivities for Fine Grained Soils (Kersten, 1949)

In addition to the dry density and water content, the mineralogy of soils affects the thermal conductivity. The solid particles in a soil are either mineral or organic. Mineral thermal conductivity values range from 2 W/m·°K for feldspar and mica to 8 W/m·°K for quartz. The thermal conductivity of the soil solids has been correlated with the fraction of quartz in the solid particles. This correlation is presented in the following equations, with "q" equaling the fraction of quartz in the soil solids and k_s being the effective thermal conductivity of the solids in an inorganic soil (Farouki, 1985).

$$k_s = 8^q 2^{(1-q)} \quad \text{for q>0.20} \tag{9}$$

$$k_s = 8^q 3^{(1-q)} \quad \text{for q<0.20} \tag{10}$$

Where: k_s = effective thermal conductivity of inorganic solids

q = quartz fraction

The thermal conductivity is the primary thermal property that is used in the determination of soil properties and in the evaluation of other thermal properties such as the soil heat capacity, specific heat and diffusivity.

Soil Specific Heat and Heat Capacity

The soil specific heat is a thermodynamic property unlike thermal conductivity which is a transport property. The heat capacity is a measure of the ability of the soil to store thermal energy. The volumetric heat capacity is equal to the soil density multiplied by the specific heat:

$$C = \rho \times c_p \tag{11}$$

Where: C = volumetric heat capacity (J/m^3·°K or Btu/ft^3·°F)

ρ = density (kg/m^3 or lb/ft^3)

c_p = specific heat (J/kg·°K or Btu/lb·°F)

The heat capacity of soil is determined by assuming a macroscopic approach: the soil is treated as a composite of all the constituents present. A general equation that has been proposed to determine the heat capacity of a soil is as follows (Devries, 1975):

$$C = \sum x_{si} c_s i + x_w c_w + x_a c_a \tag{12}$$

Where: C = volumetric heat capacity (J/m^3·°K or Btu/ft^3·°F)

x_{si} = volumetric percentage of each soil solid constituent

(m=mineral, o=organic)

c_{si} = specific heat of each soil solid constituent

x_w = volumetric percentage of water

c_w = specific heat of water

x_a = volumetric percentage of air

c_a = specific heat of air

Generally, the influence of air and water vapor in the gas-filled pores is assumed to be negligible; therefore equation (12) reduces to the following:

$$C = x_{sm} c_{sm} + x_{so} c_{so} + x_w c_w \tag{13}$$

Where: C = volumetric heat capacity (J/m^3·°K or Btu/ft^3·°F)

x_{sm} = volumetric percentage of the mineral soil solid constituent

c_{sm} = specific heat of mineral soil solid constituent

x_{so} = volumetric percentage of the organic soil solid constituent

c_{so} = specific heat of organic soil solid constituent

x_w = volumetric percentage of water

c_w = specific heat of water

Table 4-1 presents typical values of the heat capacity, C; thermal conductivity, K; and density, ρ, for the different soil constituents.

Table 5: Soil Constituent Heat Capacity and Thermal Conductivity

Soil Constituent	**ρ (kg/m^3)**	**C(J/m^3·K)**	**K (W/m·K)**
Quartz	2.66E3	2.0E6	8.8
Other Minerals	2.65E3	2.0E6	2.98
Organic Matter	1.3E3	2.5E6	0.25
Water	1.0E3	4.2E6	0.57
Ice	0.92E3	1.9E6	2.2
Air	1.25	1.25E3	0.025

Typical values of the heat capacity for a mineral soil with x_{sm}=0.55 ranges from 1.1 MJ/m^3·K for a dry soil to 3.0 MJ/m^3·K for a saturated soil with x_w=0.45. For a typical organic soil with x_{so}=0.20 the heat capacity ranges from 0.5 MJ/ m^3·K for a dry soil to 3.4 MJ/ m^3·K for saturated soil with x_w=0.80.

Soil Latent Heat

The soil latent heat describes the energy transfer associated with no temperature change of a mass. It is of primary importance when soils undergo phase changes, i.e. freeze/thaw cycles. In fine grained soils and soils with saline pore water, the latent heat is released over a range of temperatures, rather than at a specific temperature. This is important in determining the energy released during a phase change due to the range of temperatures present in the soil at that time.

Soil Thermal Diffusivity

The soil thermal diffusivity is defined as the ratio of the soil thermal conductivity to the volumetric specific heat. Therefore, once these values have been determined the thermal diffusivity can be readily calculated. Accordingly, the same factors that influence the thermal conductivity and specific heat of soils also affect the thermal diffusivity. Figure 48 shows a plot of the thermal diffusivity (a in mm^2/sec in the figure) versus the soil water content (x_w in the figure) (Devries, 1975). The solid lines in the figure represent the thermal diffusivity which is along the left y-axis, versus the volumetric water content, x_w along the x-axis. The broken lines are the values of the square root of the thermal conductivity multiplied by the heat capacity in units of $kJ/m^2 \cdot sec^{1/2} \cdot °K$ shown along the right y-axis versus the volumetric water content, x_w along the x-axis. Curve 1 is for a quartz sand that is 55% solids by volume; Curve 2, a loam with 50% solids by volume; and, Curve 3, a peat soil with 20% solids by volume (Devries, 1975).

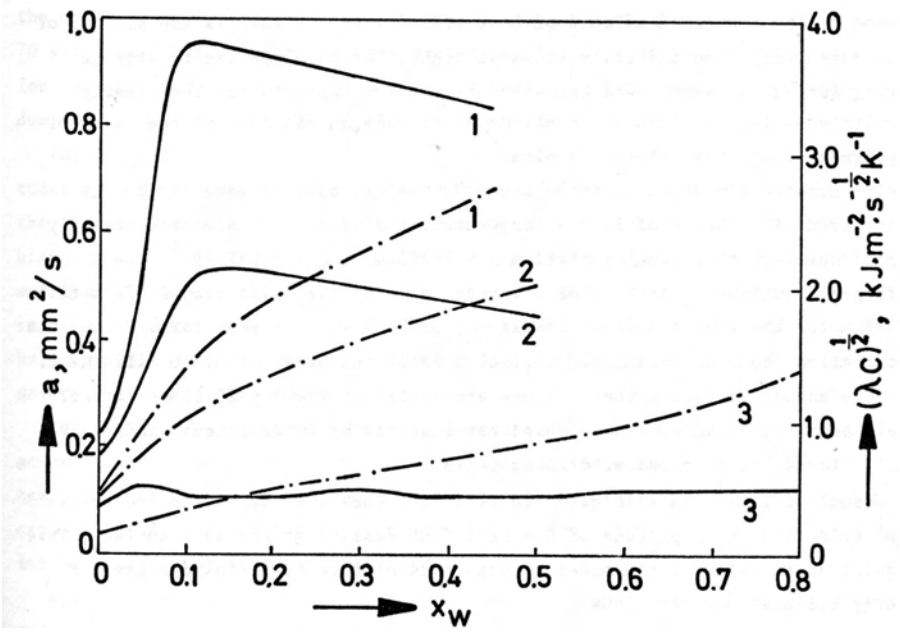

Figure 48: Soil Thermal Diffusivity versus the Volumetric Water Content (Devries, 1975)

This plot illustrates that there is a fairly sharp increase in the thermal diffusivity as the water content increases from zero to about 10%, after which the values decrease. This may be due in part to the sharp increase relative to the water going from being a non-continuous bridge between particles to filling the voids and becoming continuous throughout the soil.

Remarks on Thermal Properties of Soils

Past research has led to correlations between the thermal conductivity and the water content, dry density, and mineralogy of soils. However, further areas have been identified as affecting the thermal properties, including: the effect of ions and salts within the soil mass or pore water on the latent heat and freezing mechanisms of soils; and the effect of atmospheric conditions such as evapo-transpiration, radiation and surface cover effects on the heat conduction through soils. Another area that requires further research is the changes in thermal properties with depth.

Analytical Approach to Determining Thermal Conductivity

The thermal analysis of the tire shred-soil embankment under investigation aims at determining the thermal conductivity of the composite material, tire shreds and soil. In this analysis, the amount of heat generation will be determined and evaluated based on the trends observed in the monitored parameters, with the ultimate goal of determining the potential causes of exothermic reactions in tire shred-soil embankments. The first step in this analysis is to use the collected temperature data at various depths in the different sections of the tire shred-soil embankment to calculate the thermal conductivity.

For this analysis, several simplifying assumptions have been made. The first assumption is that the tire shred-soil embankment can be considered a semi-infinite solid with a periodic surface temperature. This assumption simplifies the geometry by assuming that the solid extends infinitely in all directions but one, the depth, and has one

identifiable surface. The equation relating the thermal properties to the thermal conductivity in a semi-infinite solid is expressed as:

$$k = K\rho C \tag{14}$$

Where: k = thermal conductivity

K = (k/ρC) = thermal diffusivity

ρ = density

C = mass heat capacity

In an approach presented by Zarling (1988), the volumetric specific heat rather than the mass specific heat is used. Zarling states that by using the volumetric specific heat of soil, the effect of the combination of soil, water and air is incorporated. The following equation is presented as a means of estimating the volumetric specific heat:

$$C_u = \gamma_D \left[0.17 + \left(\frac{w}{100} \right) \right] \text{(Btu/ft}^3\cdot\text{°F)} \tag{15}$$

Where: γ_D = dry unit weight of soil (lb/ft^3)

w = gravimetric moisture content

C_u = volumetric specific heat (Btu/ft^3·°F)

Zarling also addresses the issue of phase changes, freezing and thawing, within a soil mass. It is assumed for this research that phase changes within the tire shred-soil embankment are negligible.

A soil mass includes water, air and soil particles, with convective heat transfer within the water and air and conduction and radiation throughout the entire soil mass. It was assumed that the effects of heat transfer via convection and radiation are included within the composite equivalent thermal conductivity value, the apparent thermal conductivity. In a semi-infinite solid with pure conduction, the heat transfer can be expressed as an energy conservation equation as a function of depth and time, T(z,t) (Carslaw, 1959):

$$\frac{\delta}{\delta z}\left[k_z \frac{\delta t}{\delta z}\right] + \frac{\delta}{\delta y}\left[k_y \frac{\delta t}{\delta y}\right] = C\frac{\delta T}{\delta t} \tag{16}$$

Where: z = depth

k_z = thermal conductivity in the z-direction

k_y = thermal conductivity in the y-direction

C = volumetric specific heat

T = temperature

t = time

The left hand side of equation 4-13 represents the net heat conduction and the right hand side represents the energy stored within the soil mass. If the soil is assumed to be isotropic and homogenous, the equation can be further reduced to the two-dimensional heat transfer equation:

$$\frac{\delta^2 T}{\delta z^2} + \frac{\delta^2 T}{\delta y^2} = \frac{1}{K}\frac{\delta T}{\delta t} \tag{17}$$

Where: z = depth

K = material thermal diffusivity

T = temperature

t = time

The heat transfer within the embankment is assumed to be one dimensional, further reducing the equation to the following:

$$\frac{\delta^2 T}{\delta z^2} = \frac{1}{K}\frac{\delta T}{\delta t} \tag{18}$$

The solution to this partial differential equation is as follows:

$$T(z,t) = Ae^{-\alpha \cdot z}\cos(\omega \cdot t - \alpha \cdot z) \tag{19}$$

Where: $\alpha = (\omega/2K)^{1/2}$

ω =1 cycle/time period

A = measurement of the curvature of the temperature profile

e = base of log 10

The value of "A" can be determined from instrumentation data collected of the internal temperature at the various depths of the tire shred-soil embankment. After "A" is determined, the value of α can be calculated, from which "K" can be determined. Once "K" is determined, the original equation for the thermal conductivity (Equation 14) can be used to define the thermal conductivity of the tire shred-soil embankment.

The thermal conductivity can be calculated by assuming conditions of pure conduction within the tire shred-soil embankment; however, heat may have been generated by some type of exothermic reaction. In the case of heat generation, the partial differential equation should incorporate "q," which represents the heat generated that cannot be accounted for by conduction:

$$q + k\frac{\delta^2 T}{\delta z^2} = \rho C\frac{\delta T}{\delta t} \tag{20}$$

Where: C = material mass heat capacity

q = generated heat

To solve this differential equation the derivatives can be approximated using the finite difference method. When using equally spaced nodes the finite difference scheme can be expressed by:

$$\frac{\delta^2 T}{\delta z^2} = \frac{1}{\Delta z^2}T_{n+1} + T_{n-1} - 2T_n \tag{21}$$

$$\frac{\delta T}{\delta t} = \frac{T_n{}^{p+1} - T_n{}^{p}}{\Delta t} \tag{22}$$

Where: Δt = time step

n+1 = node 1

n = node 2

n-1 = node 3

Δz = distance between temperature probes

p = current time

p+1 = one time step into the future

For unequally spaced temperature probes, or nodes, the following finite difference solution can be used:

$$\frac{\delta^2 T}{\delta z^2} = \frac{\frac{T_4 - T_3}{z_4 - z_3} - \frac{T_3 - T_2}{z_3 - z_2}}{\frac{z_3 + z_4}{2} - \frac{z_2 + z_3}{2}} \tag{23}$$

$$\frac{\delta T}{\delta t} = \frac{T_3^{\,p+1} - T_3^{\,p}}{\Delta t} \tag{24}$$

Where: T_n = internal temperature at the unequally spaced sensors

z_n = depth of temperature sensor

If the embankment does not experience an exothermic reaction, the value of "q" should equal zero. The instrumentation data collected as part of this research will be analyzed using these equations. The value of "q" will be plotted versus time, with the average value of "q" determined over the time period. If "q" does not equal zero it may indicate either an exothermic or an endothermic reaction within the tire shred-soil embankment.

As the value of "q" for the various embankment sections is evaluated, the correlation between "q" and the soil moisture content, humidity, and atmospheric conditions may be used to indicate potential causes of the heat generation. The soil moisture and humidity may indicate conditions conducive to the oxidation of the steel belts within the tire shreds, or indicate the possibility of microbial activity within the embankment.

It is anticipated that as the analysis is conducted the soil/tire shred composite material will be found to be more suitable to dissipate any heat generated than the tire shreds alone, due to the greater thermal conductivity of soil.

Results

The primary focus of this chapter will be to provide an overview of the entire 18 month data collection period and a preliminary discussion of the findings from each of the major parameters measured: temperature, soil suction, relative humidity, water content and heat flux.

Temperature

The temperature of the different tire shred-soil embankment sections was monitored at three different depths. The temperature probes are labeled in the following graphs as S1, S2, and S3 for the probes in the soil-only section; L1, L2 and L3 for the probes in the layered section; and M1, M2 and M3 for the mixed section. S1, L1 and M1 indicate the probe at the deepest depth of approximately 4.25 feet; S2, L2 and M2, at 2.75 feet; and S3, L3 and M3 at 1.25 feet. The depth is the distance from the top of the embankment as shown in Figure 5-1.

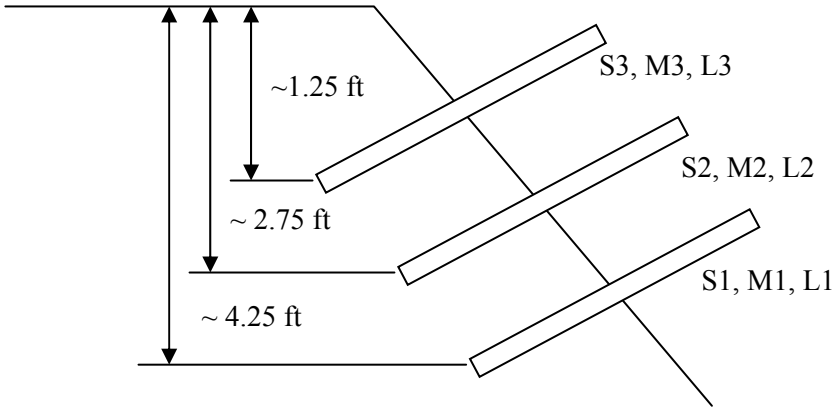

Figure 49: Location of Monitoring Probes (not to scale)

Soil-Only Section

Figure 50 shows the temperature fluctuations through the monitoring period. It is clear the mount, or ambient, temperature and the internal temperatures follow seasonal fluctuations, with the higher temperatures in the summer and the lower temperatures during the cooler winter months. It should be noted from 7/25 to 9/21that no data was recorded, due to problems encountered with the data collection instrumentation. This lack of data is indicated by the flat portion of the curve in Figure 50 and subsequent figures from the different tire shred-soil embankment sections.

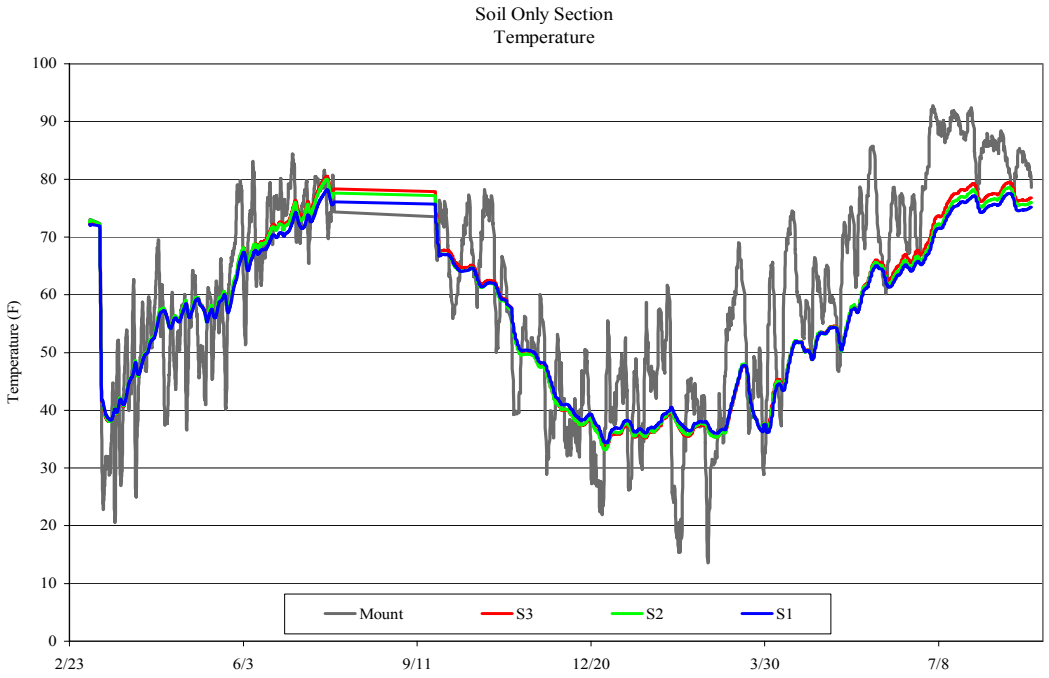

Figure 50: Soil Temperature in the Soil-Only Section

It is also evident from Figure 50 that the internal temperatures also vary slightly with depth. The thermistor located closer to the surface, S3, shows a slightly greater range of temperature variations than the other two thermistors, especially S1. The values of S3 range from approximately 33.5°F to 80.7°F; S2 from 33.0°F to 80.2°F; and S1 from 34.1°F to 79.8°F. The air temperature (mount) shows a greater range of temperatures throughout the seasons, as it does during the day.

Figure 51 is a plot of only one week, which more clearly shows the diurnal fluctuations of temperature at each depth. This plot clearly shows the variation of temperature with depth, with the higher temperatures near the surface and the lower temperatures at the lower depths. This figure also shows the greater diurnal variation of the air temperature than the soil temperature. For example, during the first 24 hour period, the air temperature ranged from about 57°F to 98°F; whereas, the S3 temperature only ranged from 79.5°F to 79.9°F. It is also evident that the temperature fluctuations are not necessarily the same within the embankment as they are in the air. That is, the peak temperatures within the soil-only section of the tire shred-soil embankment (S1, S2, and S3) during each 24 hour period do not align with the peak ambient (mount) temperature. Therefore, it may be concluded that the heat transfer within the embankment induces a time lag between the embankment temperature changes caused by the ambient temperature changes.

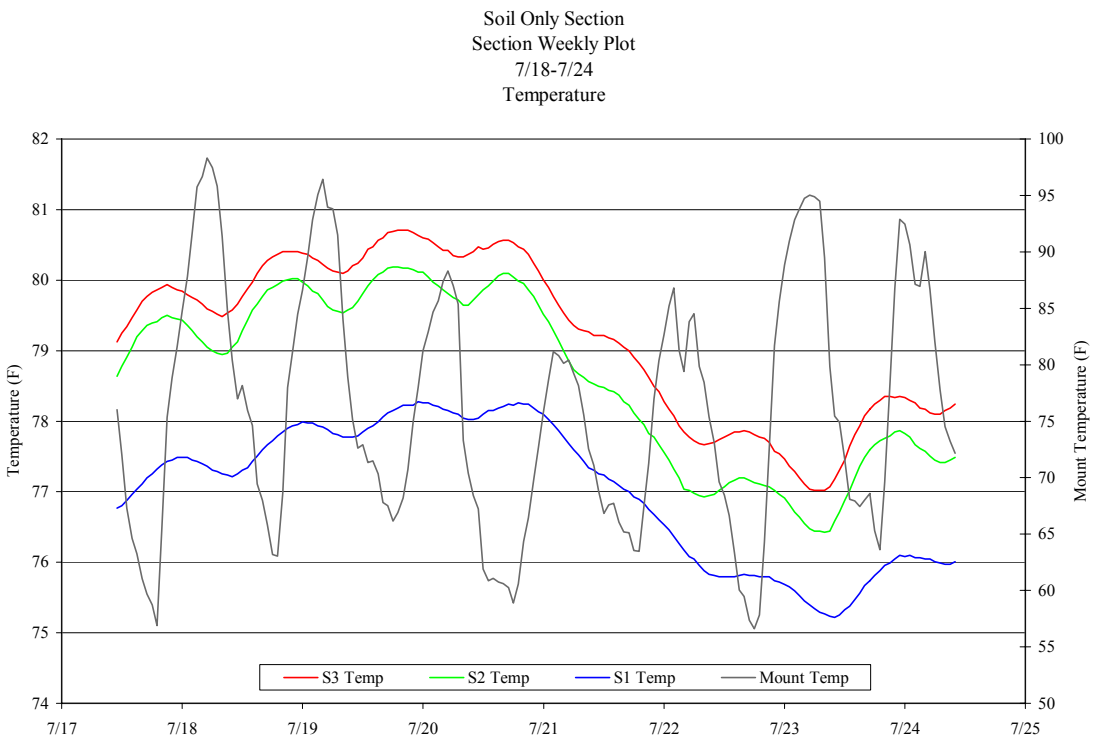

Figure 51: Weekly Soil Temperature in the Soil-Only Section

Figure 52 was generated to better understand the relation between the ambient temperature and the soil temperature within the tire shred-soil embankment. This figure shows the ambient temperature plotted against the internal temperature for the entire 18 month monitoring period for the three soil temperature probes, S1, S2 and S3. This figure indicates that generally as the ambient temperature increases, so also does the internal temperature for the three thermistors at each depth.

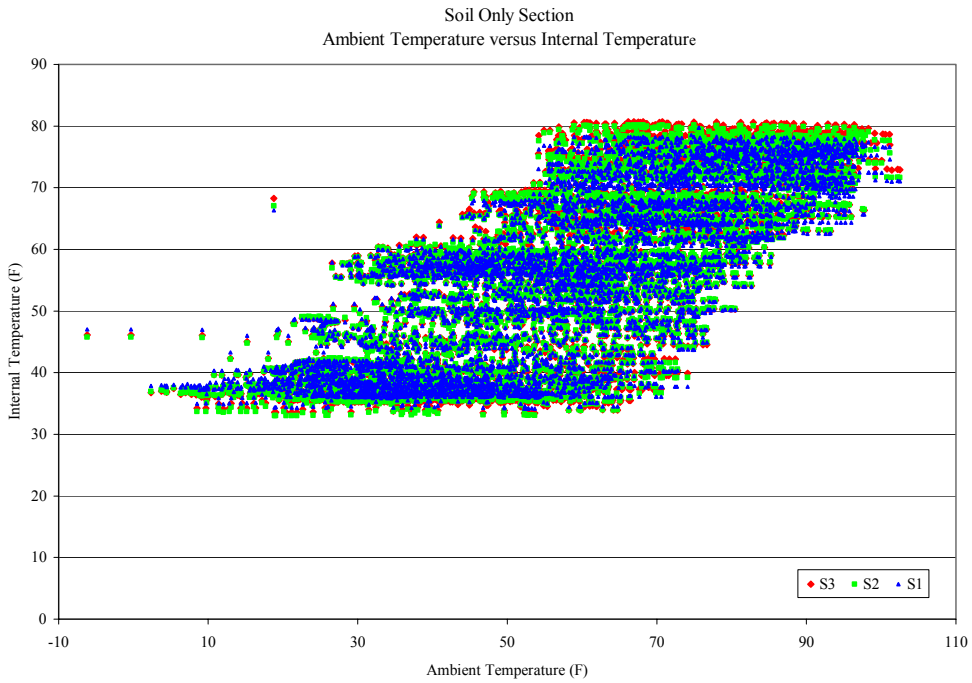

Figure 52: Ambient versus Internal Temperature in Soil-Only Section

Inspection of this plot indicates that there are horizontal trends that slowly increase towards the upper right of the plot. These horizontal trends are the range of ambient temperatures per day. As the ambient temperature increases through the day, the internal temperature remains relatively unchanged, indicated by the zero slope of the internal temperature points. This would suggest that the internal temperature is not directly related to the ambient temperature, but may have a time lag. It is clear that throughout the year as the average ambient temperature increases, so does the average internal temperature.

Further inspection of Figure 53 shows that there is an increasing linear relationship. This trend was investigated to determine the relationship between the ambient temperature and the internal temperature at each depth. Figures 53 through 55 indicate the best-fit linear trend for the data recorded at each depth. The best fit line has error bars that indicate that the internal temperature is generally within $\pm$20°F of the ambient temperature. From the equations of the lines in these figures it can be seen that

the slope is one. A slope of one implies a direct relation between the ambient and internal temperatures, i.e. as the ambient temperature increases so does the internal temperature.

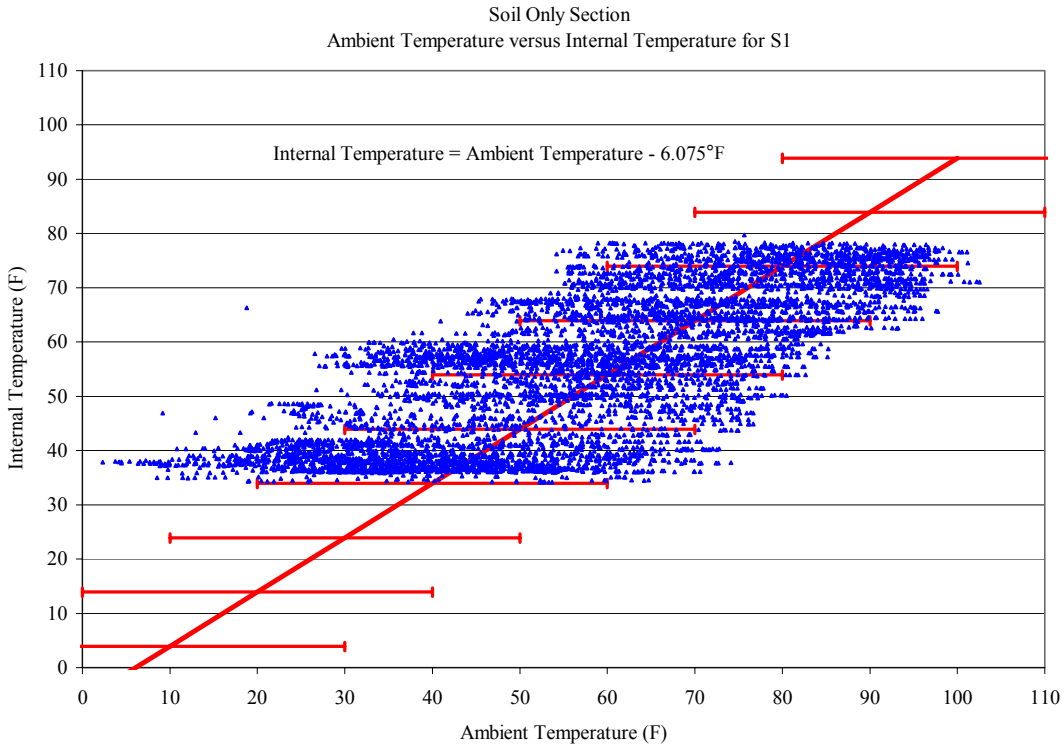

Figure 53: Linear Regression of Ambient versus Internal Temperature for S1

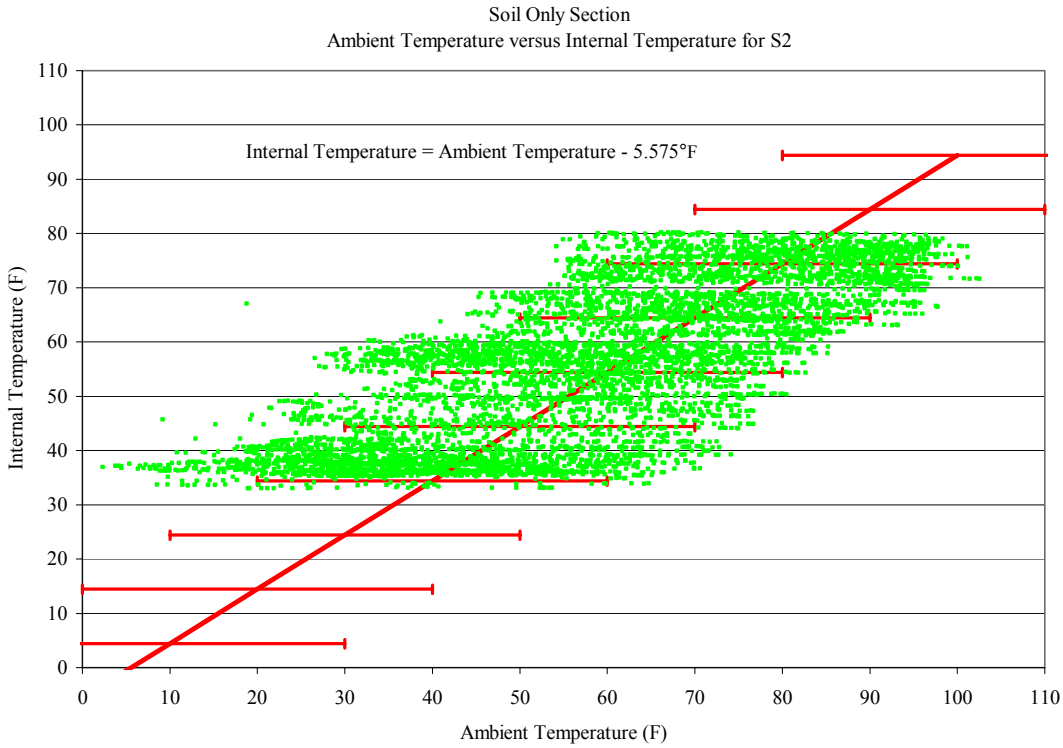

Figure 54: Linear Regression of Ambient versus Internal Temperature for S2

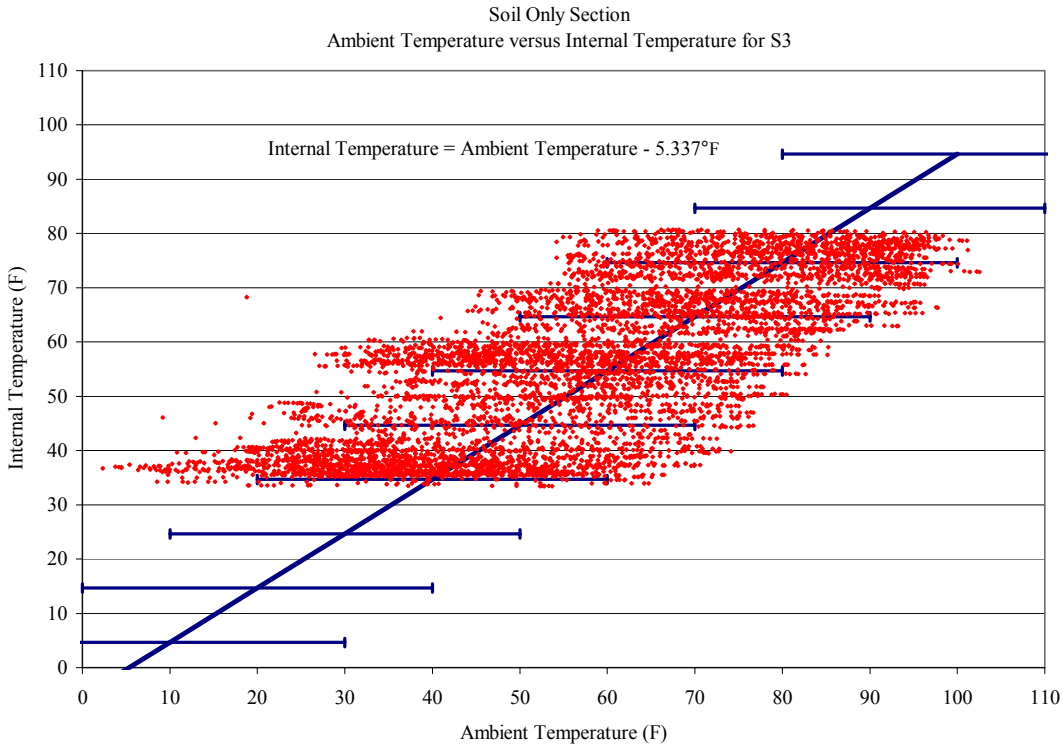

Figure 55: Linear Regression of Ambient versus Internal Temperature for S3

The equations for the best fit lines shown in Figures 53 through 55 have a negative intercept. This negative intercept indicates that the internal temperature is generally lower than the ambient temperature. It is significant to note that the negative intercept for S1 is greater (more negative) than the intercepts for S2 and S3, which is consistent with the knowledge that the temperature at the deeper location, S1, is cooler than at the shallower depths. The constant slope and negative intercept of the best fit lines shown in these plots suggest that the soil-only section dissipates the heat transferred from the atmosphere at a continuous rate within the tire shred-soil embankment.

Mixed Section

Similar to the soil-only section, the mixed section also exhibits the fluctuations that correlate with the seasonal temperature changes. The mixed section however, shows a greater range in temperatures at the shallower depth than within the soil-only section. The shallowest thermistor, M3, shows a range from 25.3°F to 88.5°F, which is a range

over 15°F greater than the thermistor at the same depth within the soil-only section of the embankment. The deeper thermistors experienced ranges of temperatures of 39.9°F for M2 and 48.6°F for M1, each smaller than the range seen by M3 of 63.2°F.

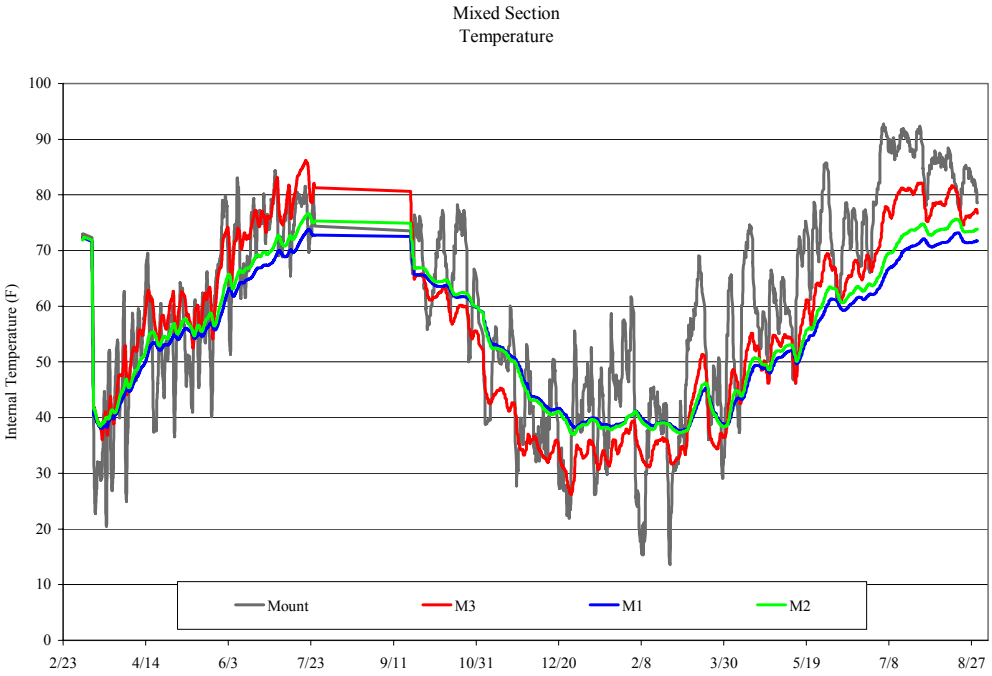

Figure 56: Mixed Section Temperature

Within the mixed section there were two additional thermistors measuring the temperature of a rubber shred and a steel belt at each depth. The temperatures measured by each of thermistors at each depth are illustrated in Figures 57, 58 and 59.

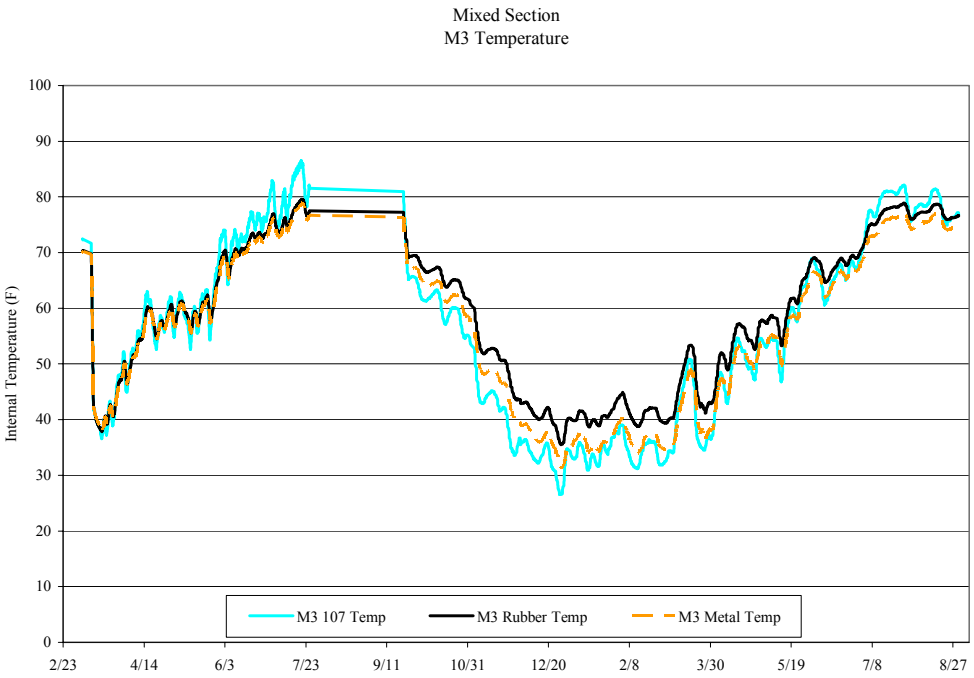

Figure 57: Mixed Section M3 Temperature

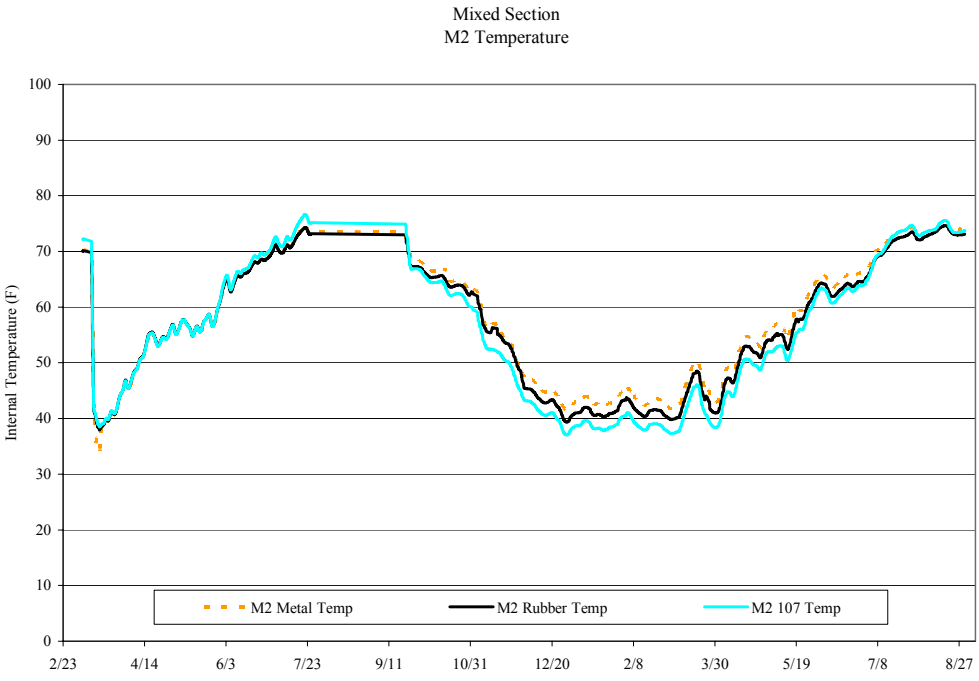

Figure 58 Mixed Section M2 Temperature

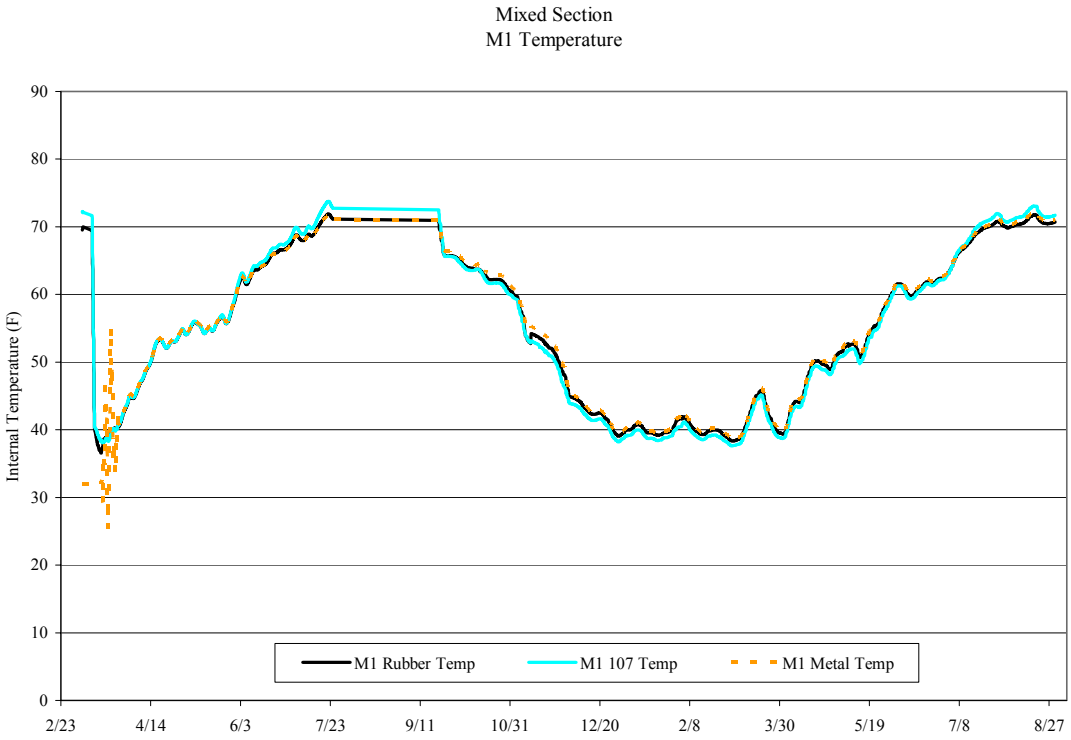

Figure 59: Mixed Section M1 Temperature

Figures 57, 58 and 59 illustrate that the temperature fluctuations were the same for the soil (CS 107), the rubber and the steel belt temperatures. The closer the thermistors were to the surface, the more variation between the three different measurements; however, the deeper the thermistor, such as at location M1, the closer the three temperatures to each other. From these plots, it can be concluded that the temperature variations and values are similar between the three thermistors.

The ambient temperature was plotted against the internal temperature to highlight the correlation between the two measurements. As with the soil-only section, the mixed section displayed a similar trend. As the seasonal temperatures increased, the daily temperatures also increased. Figure 60 highlights randomly selected days to show the daily linear trend and sloped seasonal trend. The lower values for Days 20, 300, and 400 were either during the early spring or winter; whereas, the higher values were during the summer or early fall.

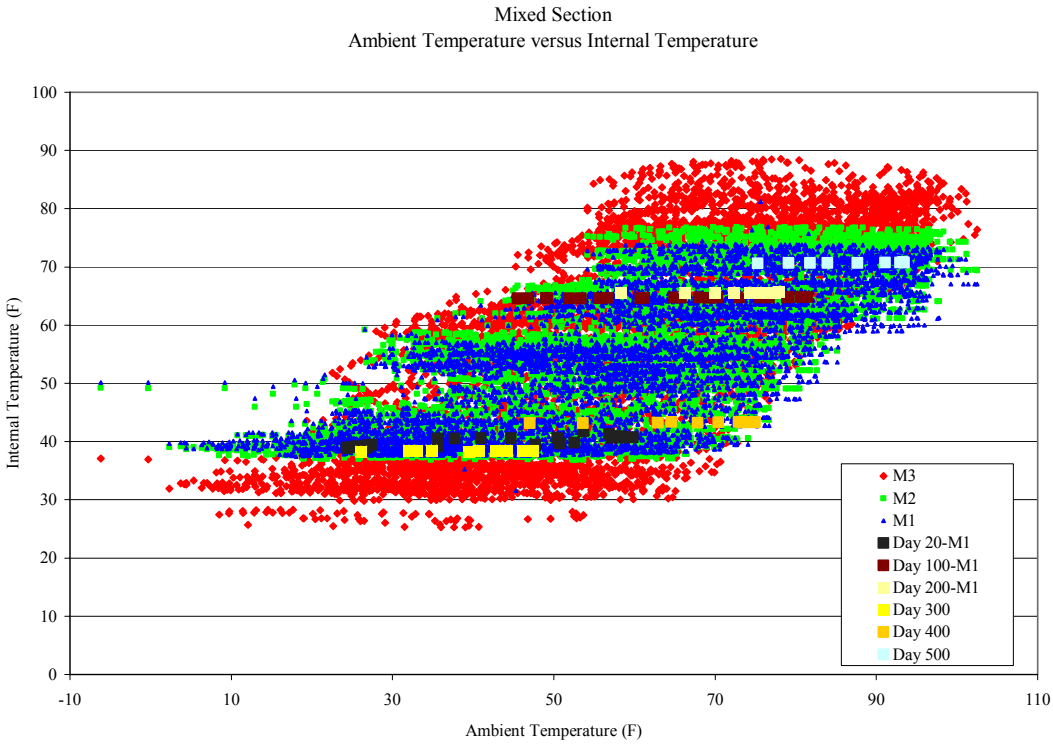

Figure 60: Mixed Section Ambient Temperature versus Internal Temperature

Figure 60 was statistically evaluated for a linear trend, similar to the linear regression analysis done on the soil-only section. Figure 61 shows the best fit lines for each of the mixed section probes at each depth. The best fit lines had a slope of one with a negative intercept similar to the trend line equations for the soil-only section. The values of the intercept were greater for M1 and less for M2 and M3. M1 does have lower internal temperatures in relation to the ambient temperature due to being the deeper probe. The ambient temperatures for each internal temperature were generally within 20°F as seen by the error bars in Figure 61. The internal temperature of the mixed section of the tire shred-soil embankment is generally lower than the ambient temperature, indicative of a constant source of heat dissipation within the embankment.

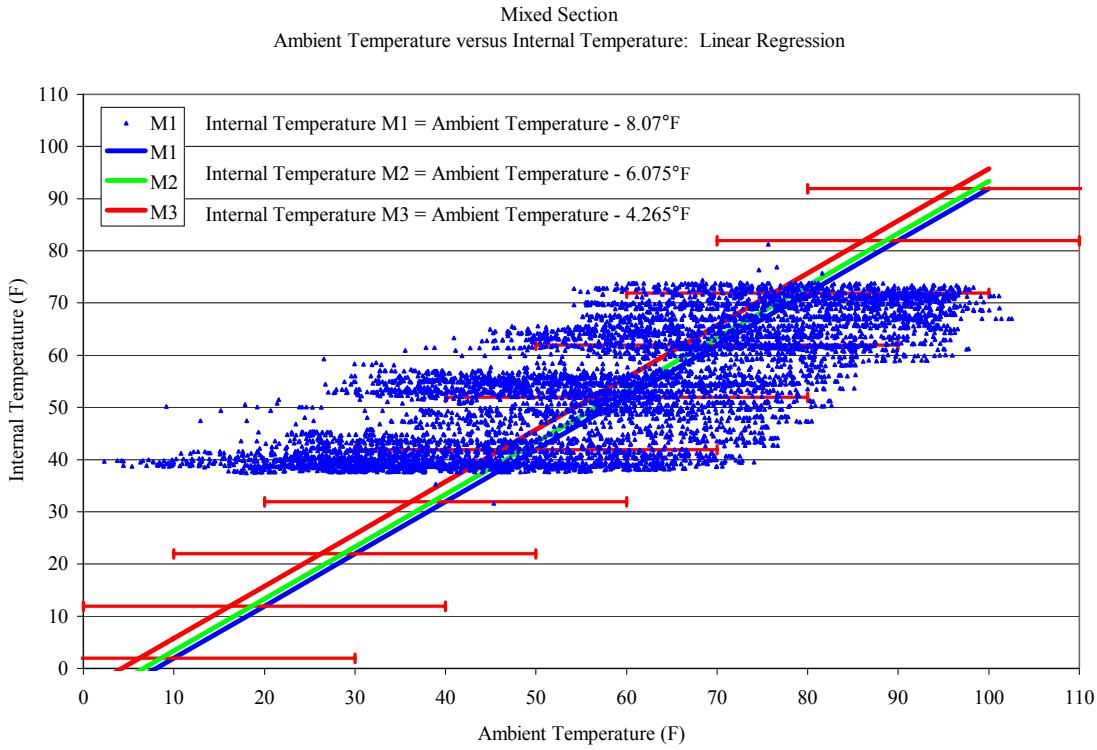

Figure 61: Linear Regression of Ambient versus Internal Temperature of the Mixed Section

Layered Section

The layered section of the embankment was the most instrumented of the three sections, with four different temperature gauges at each depth. The temperature measurements recorded by the CS 107 thermistors were used for the comparison between the tire shred-soil embankment sections, due to this thermistors being the only one that was consistently placed in each tire shred-soil embankment section to measure the soil temperatures. As with the mixed and soil-only sections, the temperature displays seasonal fluctuations: the higher temperatures are in the summer months and the lower temperatures over the winter.

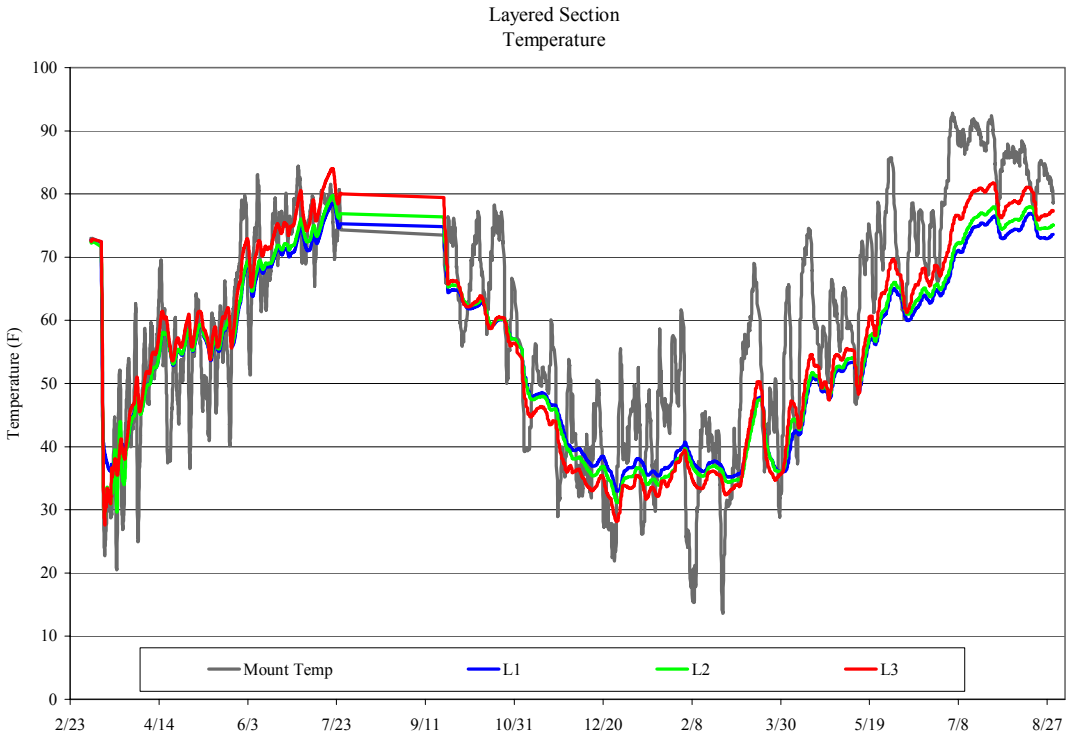

Figure 62: Layered Section Temperature

As shown in prior figures of temperature within both the soil-only and mixed sections, the layered section shows a similar trend in respect to variation of temperature with depth. The shallower thermistor, L3, had temperatures ranging from 18.6°F to 84.7°F, a span of 66.1°F; whereas, L2 and L1 had temperature ranges from 19.9°F to 79.9°F and 32.7°F to 81.4°F, respectively.

The differences in the temperatures measured at each depth by the four thermistors are shown in the Figures 63, 64 and 65. The soil (CS 107), rubber and steel temperatures were measured, in addition to the temperature measurements taken by the relative humidity probe. As can been seen in Figures 63 through 65, there is not a significant difference between the rubber temperature and the steel belt temperature. The relative humidity probe shows a greater range of temperatures, although it does follow the same trends. The difference in the temperatures is shown to be less in the deeper thermistors, similar to the trend seen in similar plots for the mixed section. Due to similar trends and relatively negligible differences in the temperature measurements, the

CS 107 thermistor which measured the soil temperature at each depth in each section, was chosen to be used in the heat generation analysis.

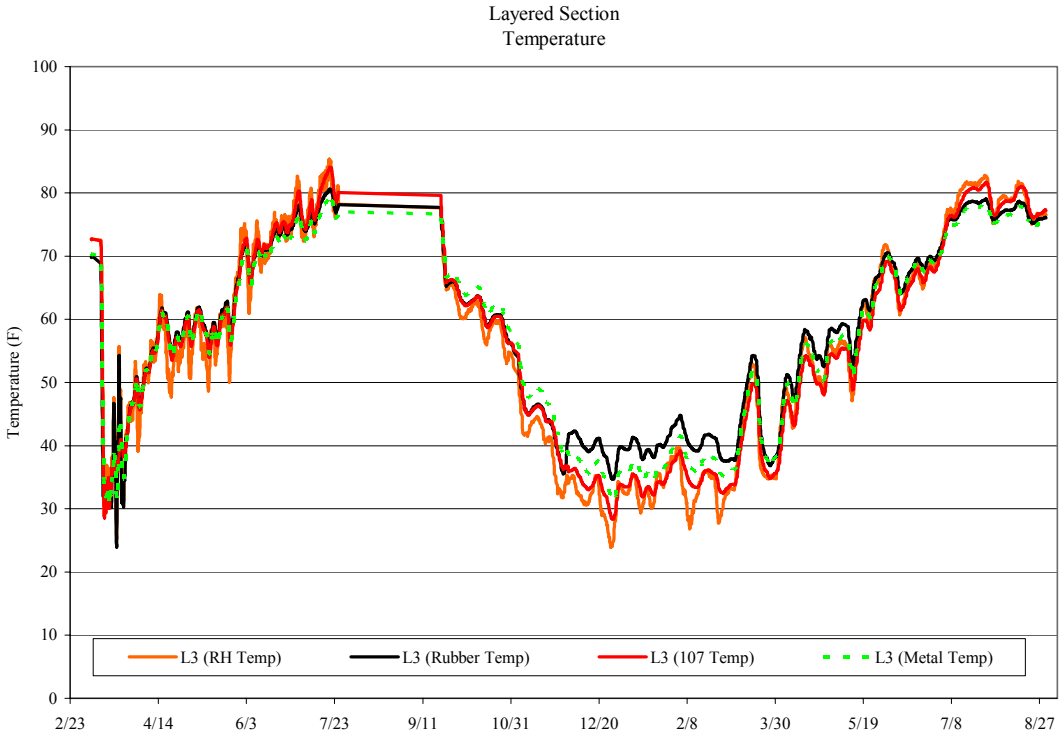

Figure 63: Layered Section L3 Temperatures

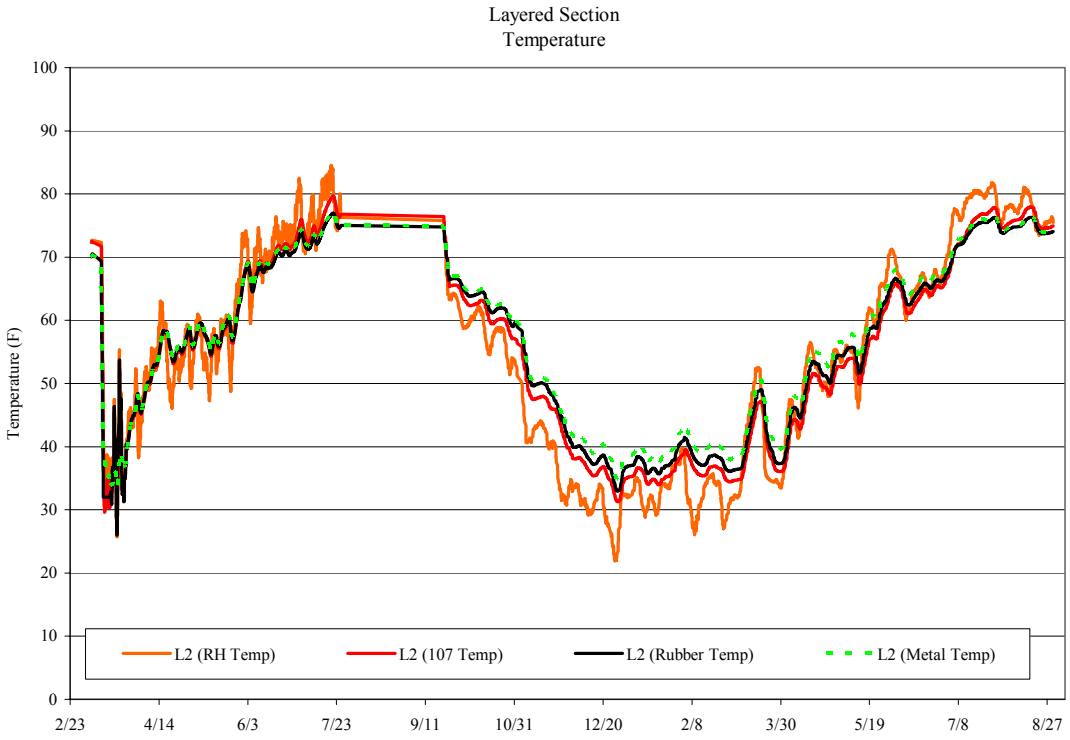

Figure 64: Layered Section L2 Temperature

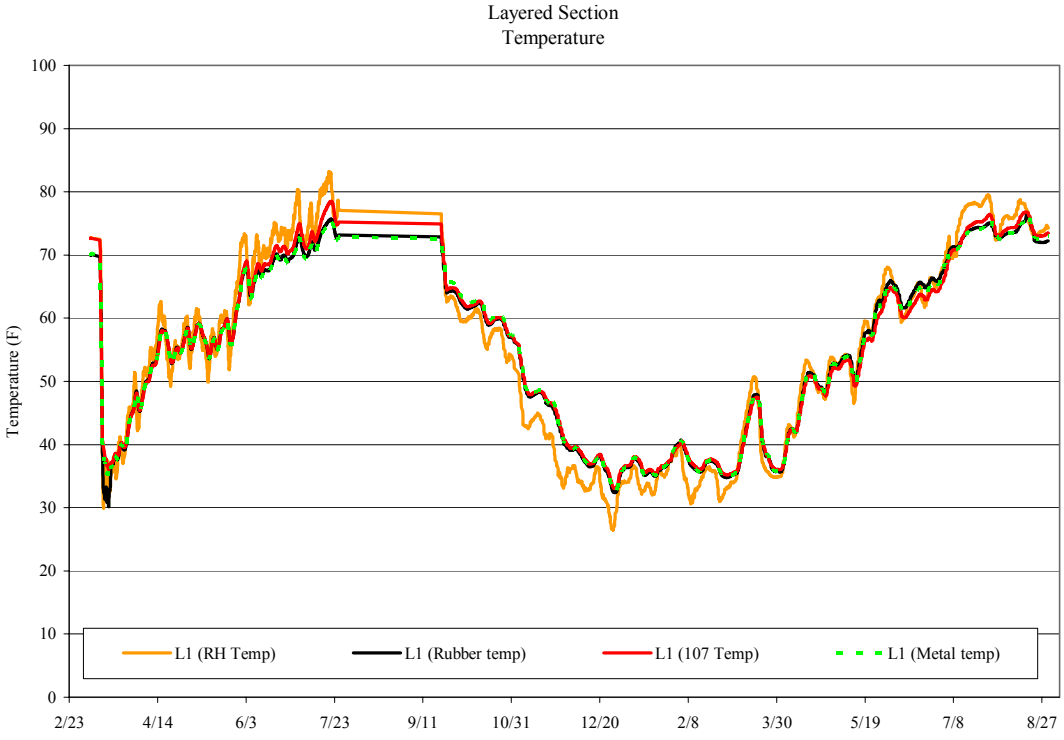

Figure 65: Layered Section L1 Temperature

The layered section temperatures were influenced by the ambient temperature in a similar way as seen in the soil-only and mixed sections of the tire shred-soil embankment. Figure 66 demonstrates the similarities in linear daily trends and increasing seasonal temperatures, as discussed for the mixed section. Figure 67 shows the linear regression, which indicates the same trends as the soil-only and mixed sections. The best fit lines in Figure 67 show negative intercepts and a slope of one. These observations would indicate that the internal temperature of the layered section is generally lower than the ambient temperature with the deeper probe, L1 being cooler than the shallower probes.

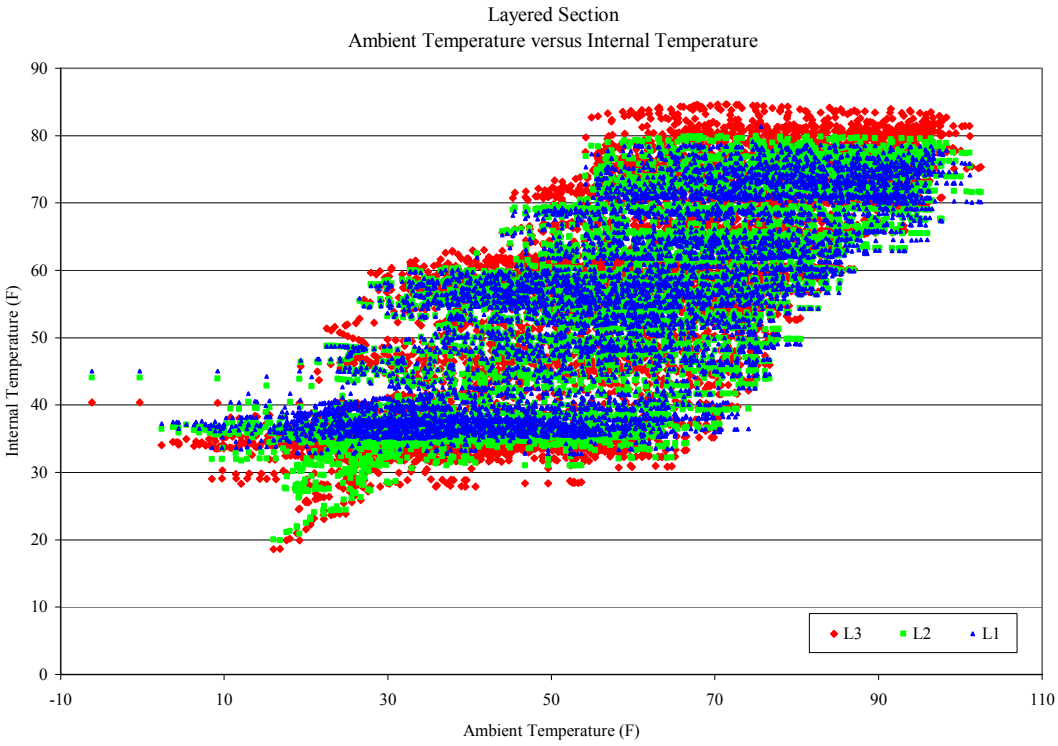

Figure 66: Layered Section Internal Temperature versus Ambient Temperature

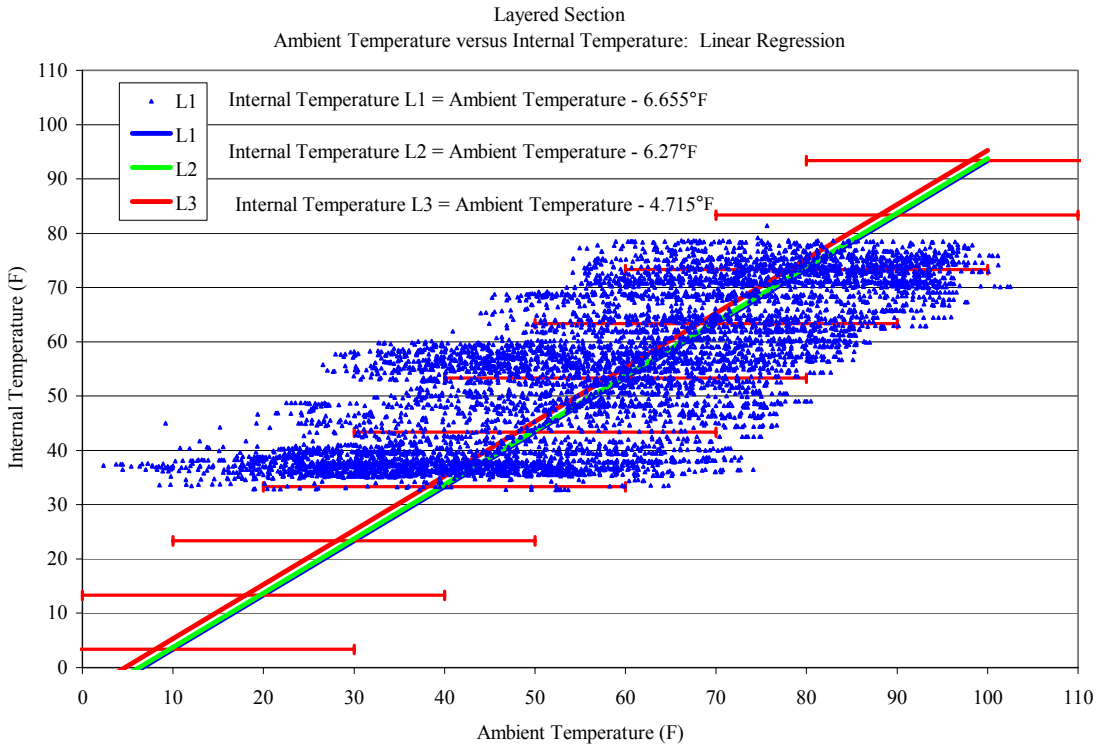

Figure 67: Linear Regression of Ambient versus Internal Temperature of the Layered Section

Large Tire Shred-Only Stockpile

The large tire shred-only stockpile was monitored during a time period slightly shorter than that monitored in the tire shred-soil embankment, but still shows seasonal trends. Figure 68 shows the temperature of the large tire shred-only stockpile. Data for September through October were not recorded due to problems with the datalogger; however, the overall temperature changes are still seen as similar to those in the embankment. The higher temperatures occurred during the summer months with the lower temperatures during the winter months. The range of temperatures for each of the thermistors was 116.6°F for TS 4, which was the deepest thermistor; 132.1°F for TS 3; 151.7°F for TS 2 and 156.6°F for TS 1 which was at the surface. These ranges clearly indicate that the temperatures experienced by the large tire shred-only stockpile were

greater than those in the tire shred-soil embankment, which may be a function of the tire shred thermal properties.

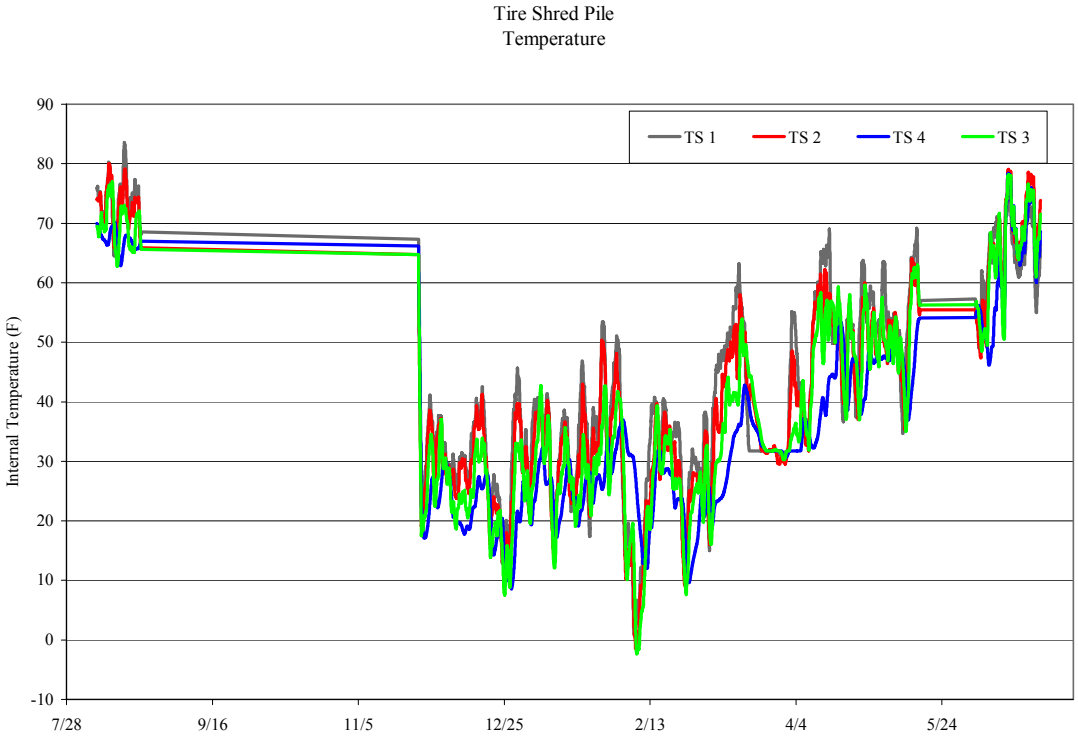

Figure 68: Large Tire Shred-Only Stockpile Temperature

The ambient temperature plotted against the internal temperature shows the internal temperature increasing as the seasonal temperatures increased. Figure 69 illustrates this trend.

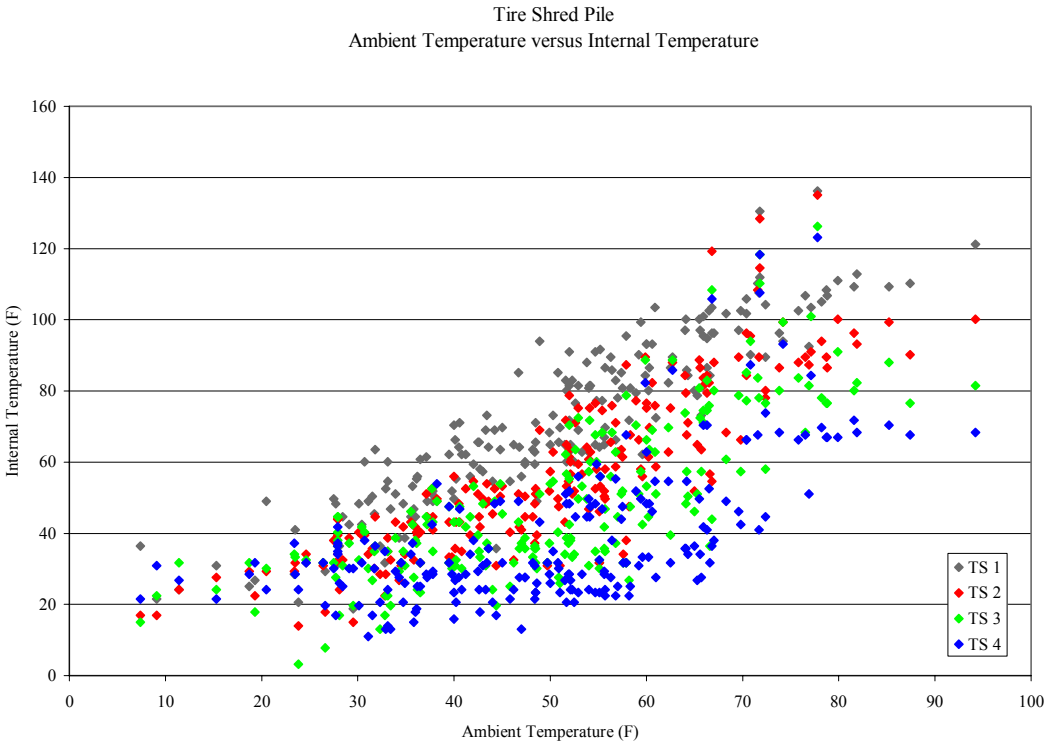

Figure 69: Tire Shred Ambient Temperature versus Internal Temperature

The trends of the large tire shred-only stockpile for ambient temperature versus internal temperature were slightly different than the trends seen in the tire shred-soil embankment. The best fit lines as shown in Figure 70 did not all have negative intercepts, and the slopes for each of the probes were not one. For three of the depths, TS 1, TS 2 and TS 3, the slopes were greater than one, which shows that as the ambient temperature increased, the internal temperature increased at a greater rate, indicative of another heat source or internal heat generation within the stockpile. This evidence of heat generation from the linear regression suggests that the large tire shred-only stockpile undergoes greater heat generation than the tire shred-soil embankment sections. Chapter 6 discusses the analysis of the temperature data that determines if there is heat generation within the stockpile.

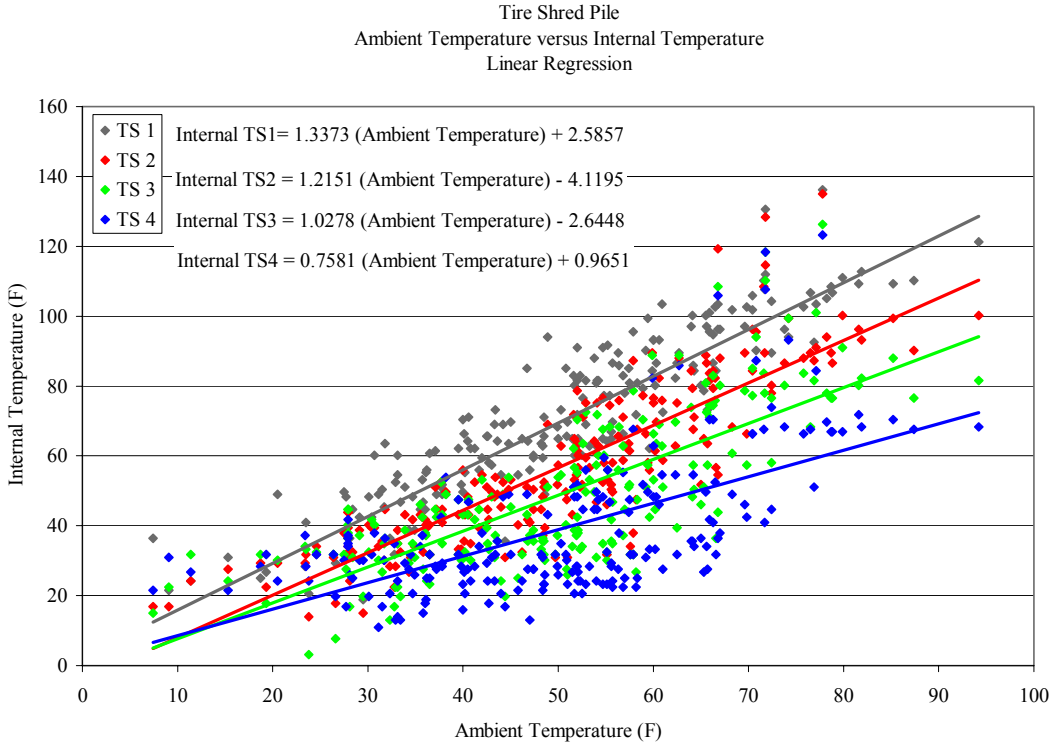

Figure 70: Linear Regression of Ambient Temperature versus Internal Temperature for the Large Tire Shred-Only Stockpile

Soil Suction

Gypsum block soil moisture probes measured the soil suction at the three depths in each of the tire shred-soil embankment sections. These probes were calibrated before being placed to ensure soil-specific readings and in order to correlate the readings to water content. The calibration entailed measuring the in-situ soil density of the tire shred-soil embankment through three sand cone tests. Two of these tests were conducted on the embankment side slope next to the sensor locations and one was on the top of the embankment on the road surface. The average in-situ dry density of the soil was measured from the two tests conducted near the sensor locations and was assumed to be representative of the in-situ dry density. With this dry density as the target density; soil from the site in Sedalia was used in laboratory determination of its soil water characteristic curve. Specifically, the soil was mixed with water to different water

contents and compacted in a standard proctor mold. The same type of soil moisture probe used in the field was then used to measure the soil suction within this sample. This probe was soaked for 48 hours and then subjected to several wetting and drying cycles in order to increase its sensitivity. After these cycles, the probe was inserted within the soil prepared in the laboratory and the soil suction was measured using a digital reader. Readings from the probe were taken every 12 hours until they stabilized. The same procedure was repeated for samples prepared with different water contents in order to define the soil water characteristic curve, from which the volumetric water content of the soil can be determined from the in-situ soil suction measurements.

Soil-Only Section

The values collected from two of the probes for the soil suction within the soil-only section are questionable and have reported values that are unreasonable. These two probes, S2 and S3, were reported to need repair at the beginning of the monitoring period. A preliminary investigation was conducted to determine the cause of the inconsistent readings, but the findings were inconclusive and the probes were not repaired. Figure 5-23 shows that the soil suction values measured at S2 and S3 were significantly greater than the suction measured at S1. In Figure 71 and subsequent figures of the soil suction measurements the scales range from about -4 psi to +4 psi. The positive values indicate soil suction or negative pore water pressures and negative values indicate positive pore water pressures. In Figure 71 it is important to note that the y-axis on the left-hand side is for the soil suction measured at S2 and S3 and the y-axis scale on the right-hand side is for the soil suction values measured at the deepest location, S1.

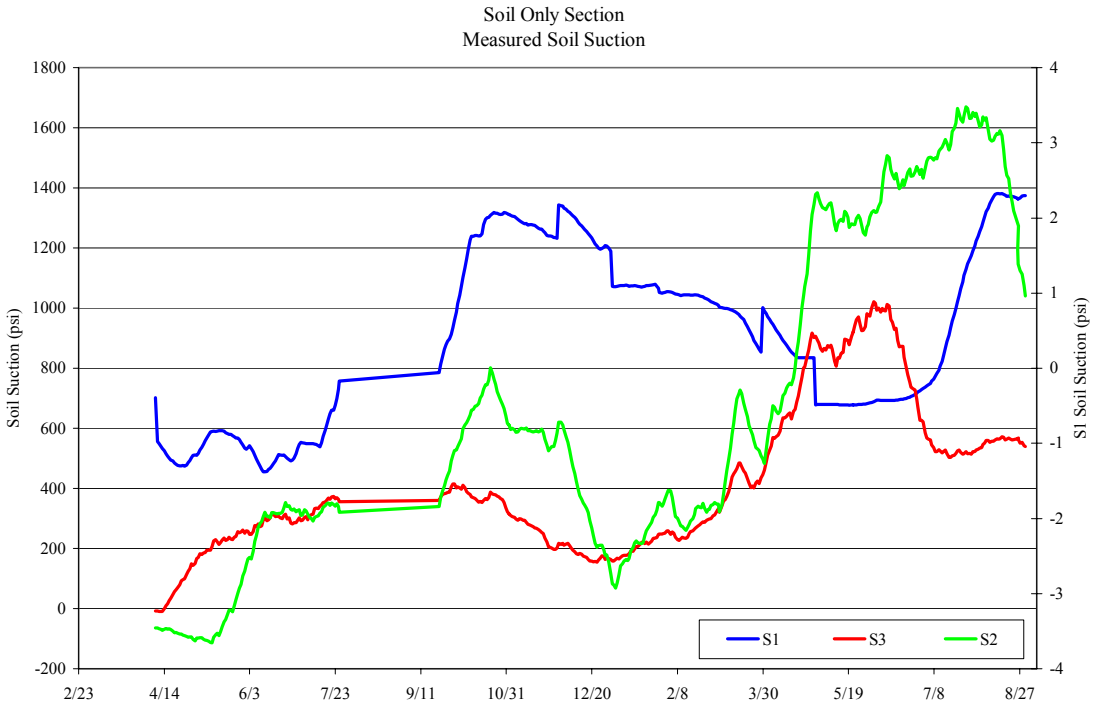

Figure 71: Soil-Only Section Soil Suction

S1 is the only probe in the soil-only section that reported reasonable values, shown in Figure 71. Therefore, only the trends observed for this probe will be considered. It appears that the trend in soil suction is opposite that of temperature, with the greater values occurring over the winter and the lower values in the summer, which would suggest that the higher temperatures within the embankment during the summer reduces the internal soil suction, indicating an increase in the moisture content.

As with the temperature, the soil suction does vary daily as shown in Figure 72. The diurnal response is only shown with the probe at S1 because of the questionable values reported using probes located at S2 and S3.

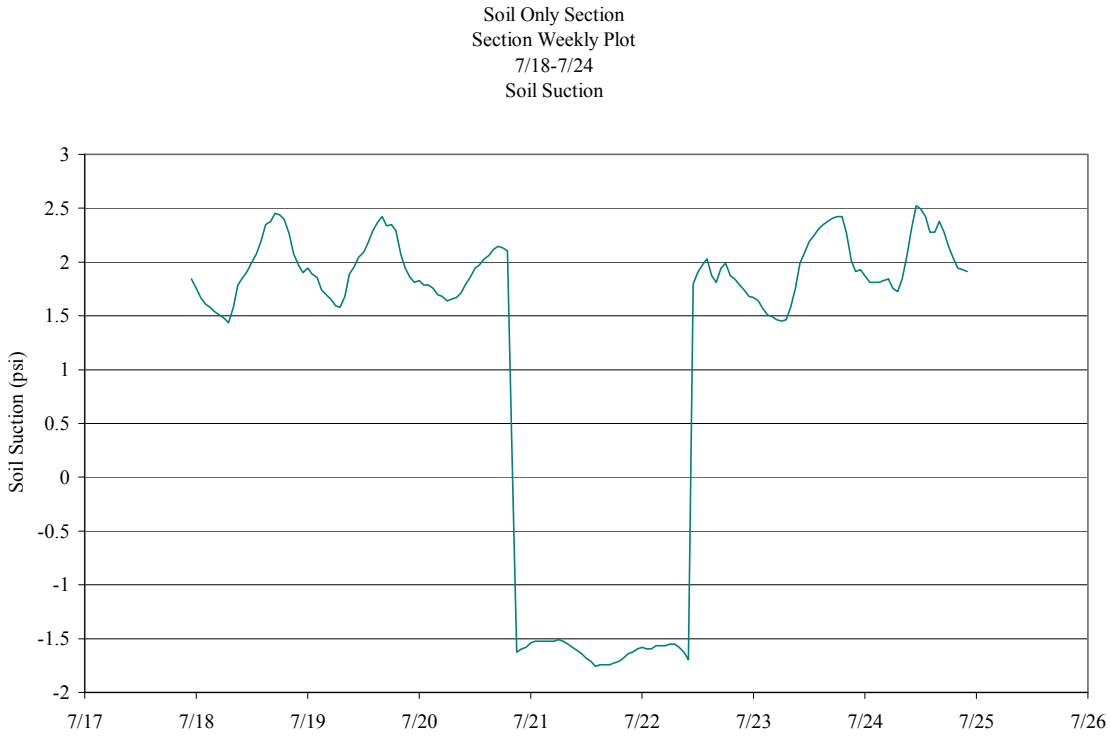

Figure 72: Soil-Only Section Weekly Soil Suction at S1

5.2.2 Mixed Section

The mixed section showed similar trends in regards to soil suction as the soil-only section: The higher values of soil suction were reported over the winter months and the lower values over the summer months. The mixed section probes reported values that correspond well with the values reported by the soil-only section probe S1. Figure 73 shows the soil suction over the monitoring period.

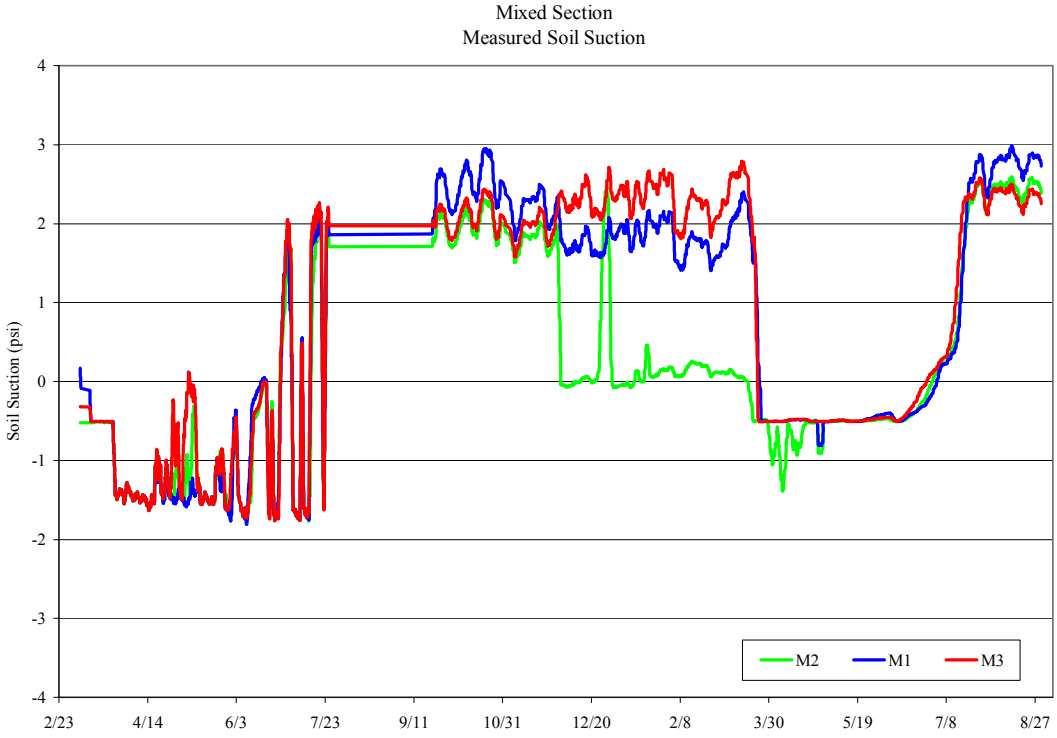

Figure 73: Mixed Section Soil Suction

As seen in Figure 73, the range of values was relatively consistent between the depths. The probe at the shallowest depth, M3 had values ranging from -2.0 psi to 3.1 psi; M2, from -2.0 psi to 3.0 psi; and, M1 from -2.0 psi to 3.3 psi. Figure 73 also indicates that the variations of soil suction over time were relatively similar for each of the probes, except for the middle probe during the winter.

Layered Section

The measured soil suction within the layered section of the embankment is shown in Figure 74. The values of the soil suction follow the same trend as within the mixed and soil-only sections: the higher values occurred during the winter and the lower values in the summer. It is interesting to note in this figure that the soil suction measured at L1, the deeper probe depth, did not vary as greatly as the other probes, which is different than what was observed in the other two sections.

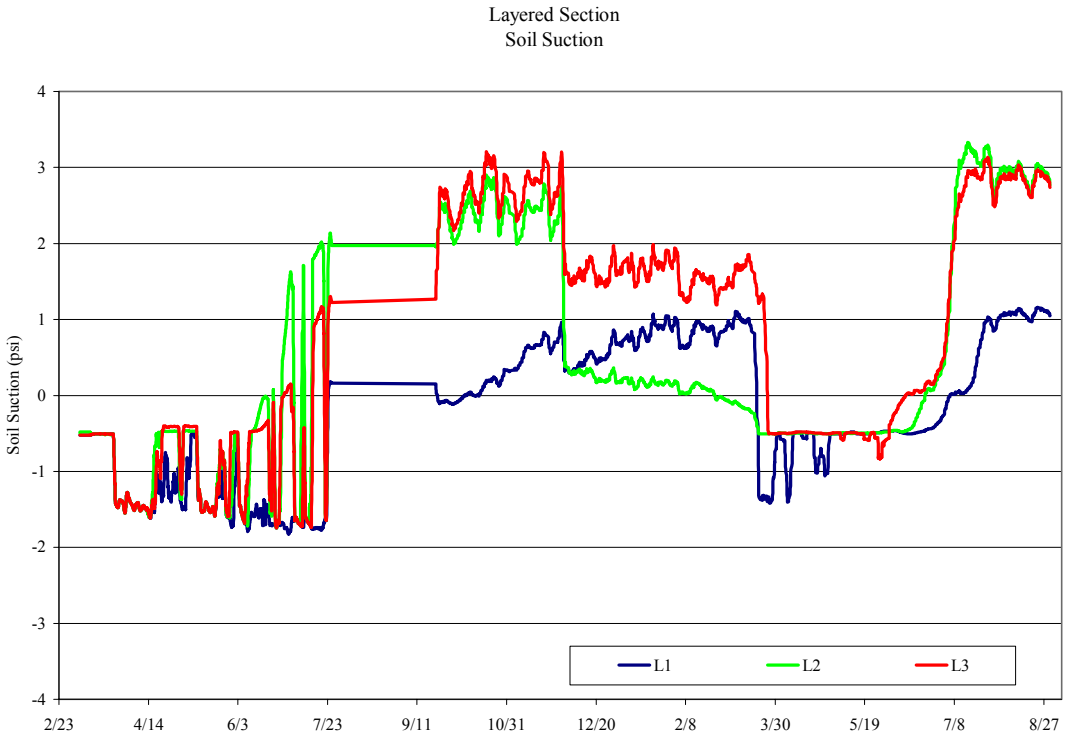

Figure 74: Layered Section Soil Suction

The range of values of the soil suction in the layered section is slightly greater than the range seen in the mixed section. For the probe at the shallow depth, L3, the range is from -2.0 psi to 3.8 psi; at L2, -2.0 psi to 3.9 psi; and at L1, -2.1 psi to 1.3 psi.

Water Content

The water content for the tire shred-soil embankment sections was determined from the soil suction measurements presented above. The soil water characteristic curve that was generated from the calibration of the soil moisture probes was used to determine the volumetric water content. The van Genuchten model was used to find the water content from the measured soil suction and from the relative humidity measured in the layered section (van Genuchten, 1980).

Figure 75 shows the soil moisture characteristic curve that was generated from the calibration of the probes using the soil collected at the site.

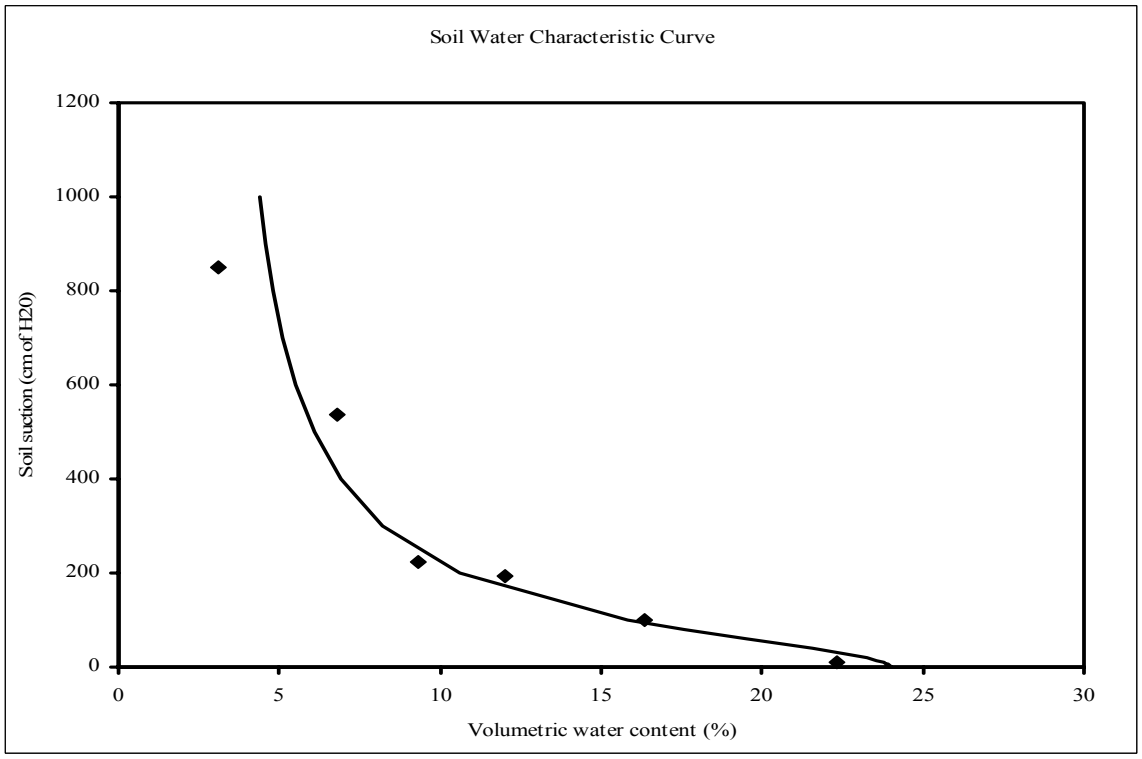

Figure 75: Soil Water Characteristic Curve

From this soil water characteristic curve the parameters to use in the van Genuchten model were determined. The van Genuchten model describes a relationship between the pressure head or relative humidity and the volumetric water content. This relationship is shown in the following equations (van Genuchten, 1980):

$$\theta = \theta_r + (\theta_s - \theta_r)\left[1 + (\alpha\Psi)^N\right]^{-\left(1-\frac{1}{N}\right)} \tag{25}$$

$$RH = \frac{\theta - \theta_r}{\theta_s - \theta_r} = \left[1 + (\alpha\Psi)^N\right]^{-\left(1-\frac{1}{N}\right)} \tag{26}$$

$$\Psi = \left[\left[\frac{RH}{100}^{-\left(\frac{1}{1-\frac{1}{N}}\right)} - 1\right]^{\frac{1}{N}}\right]\frac{1}{\alpha} \tag{27}$$

Where: $\alpha = 0.013$ = van Genuchten soil parameter (1/psi)

ψ = Measured soil suction (psi)

RH = Measured Relative Humidity (%)

N = 1.95 = van Genuchten soil parameter

θ = Volumetric water content (%)

θ_r = 0.025 = Residual volumetric water content (%)

θ_s = 0.24 = Saturated volumetric water content (%)

The volumetric water content that was found through these equations was then converted into the gravimetric water content, using the dry unit weight:

$$w = \frac{\theta \gamma_w}{\gamma_d} = \frac{62.43\theta}{\gamma_d} \tag{28}$$

Where: w = gravimetric water content (%)

θ = Volumetric water content (%) determined from van Genuchten's model

γ_w = 62.43 = Unit weight of water (pcf)

γ_d = Dry unit weight of soil (pcf)

Figures 76, 79, 72 and 83 show the moisture content results obtained by applying this procedure to the measured soil suction in each of the three tire shred-soil embankment sections.

Soil-Only Section

The collected soil suction data from only S1, was used to determine the water content of the soil-only section due to the erroneous data reported by the probes at S2 and S3.

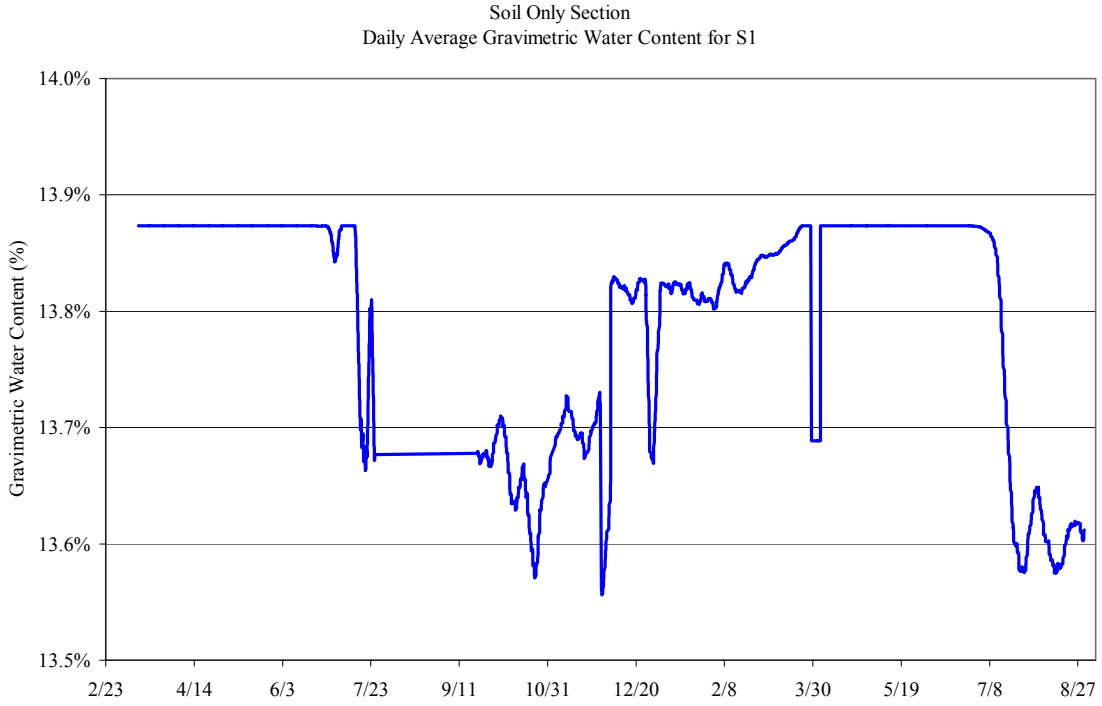

Figure 76: Soil-only section Gravimetric Water Content at S1

Figure 76 shows that the water content ranges between 13.5% and 13.9%, with the lower values over the early winter months. The water content rose in the early spring with a relatively constant value during the summer. The rainfall at the site was generally greater over the summer months and late fall, than over the winter when the water content was seen to be lower, suggesting a correlation of the tire shred-soil embankment moisture content with precipitation.

The water content, similar to the soil suction and temperature, had a diurnal tendency, as demonstrated in the Figure 77.

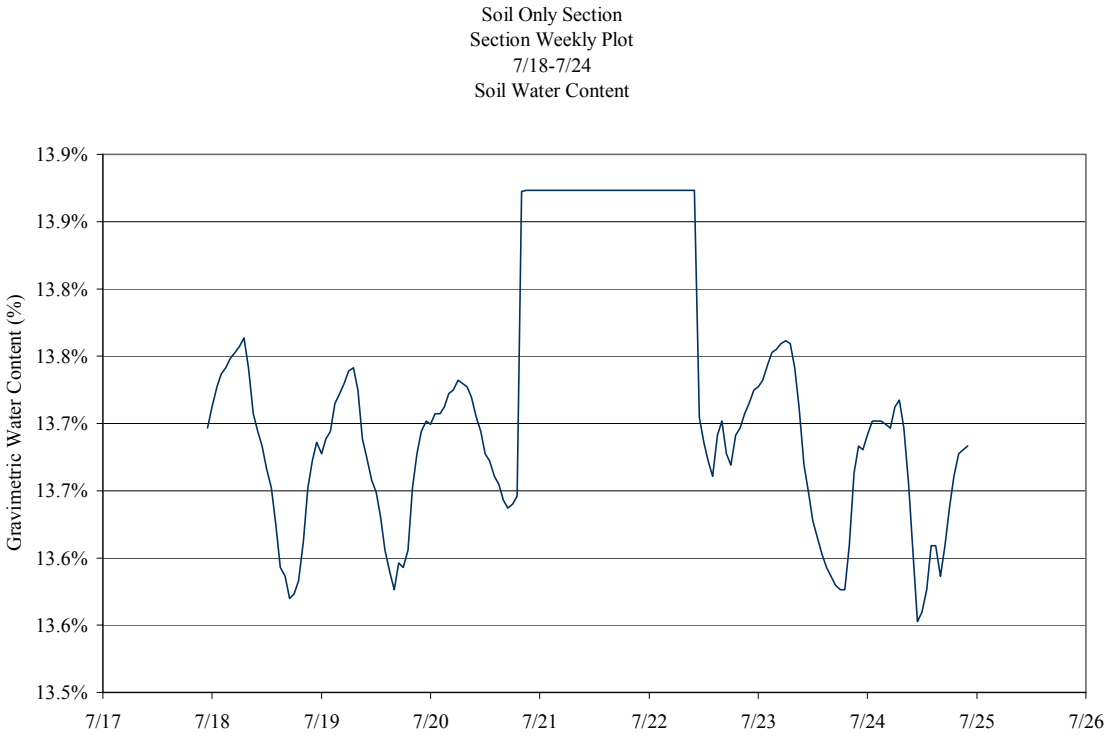

Figure 77: Soil-only section Weekly Water Content

The diurnal response of the water content illustrated in Figure 77 and of the temperature in Figure 51 suggests that there may be a correlation between the two parameters. Figure 78 shows the internal temperature plotted against the gravimetric water content at S1.

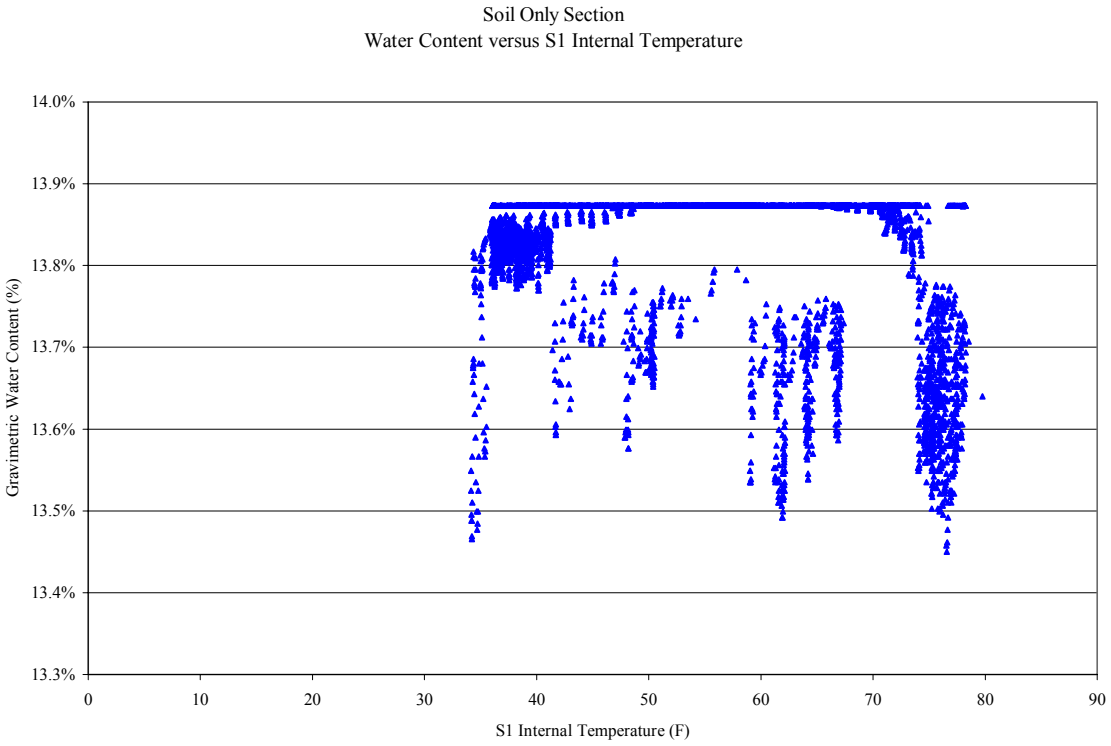

Figure 78: Soil-only section Only Water Content versus Temperature

It appears from Figure 78 that there is no distinct correlation between the internal temperature and the water content for the soil-only section. There seems to be a wide range of scatter, indicating that the two variables are independent of each other.

Mixed Section

The gravimetric water content in the mixed section over the monitoring period demonstrated similar results as those presented for S1 in the soil-only section. The range of values for the water content was generally 0.5% with the values at M3 and M2 both ranging from 14.5% to 15.0%; and at M1 ranging from 14.4% to 15.0%. Figure 79 shows these ranges and the seasonal trends.

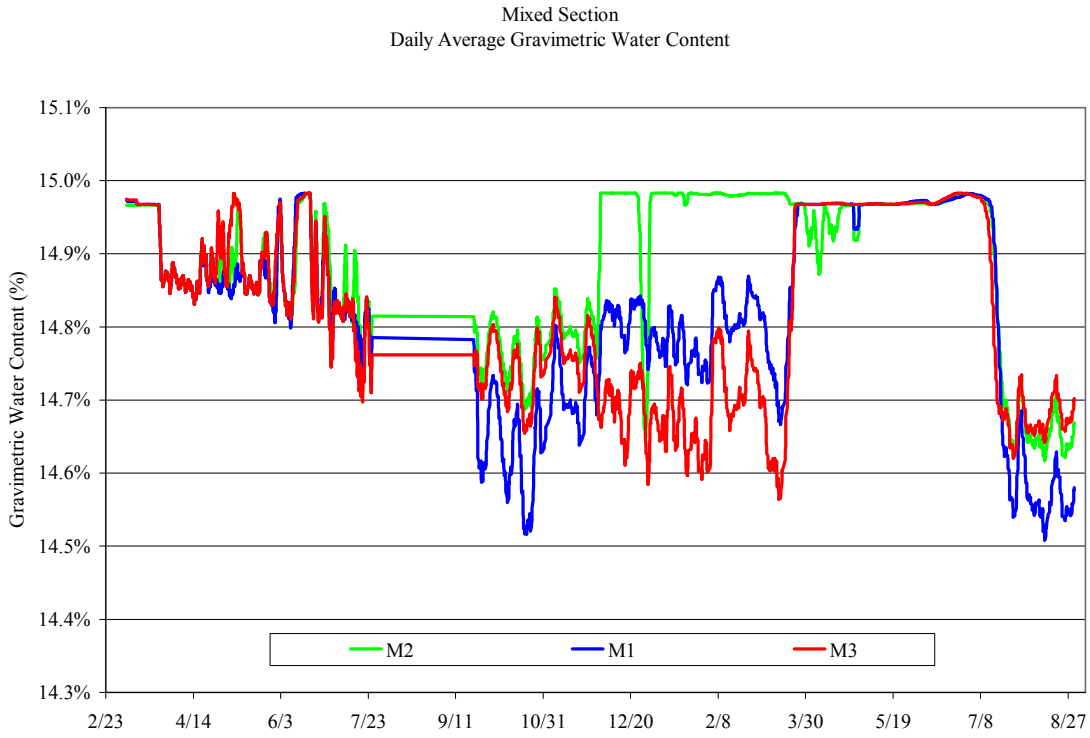

Figure 79: Mixed Section Gravimetric Water Content

The water content reached lower values in the late summer and over the winter for the monitoring probes at the shallowest, M3, and deepest, M1, locations. The middle depth, M2, showed a slightly different trend with the water content rising and reaching a relatively constant value over the winter. This may possibly have been due to a variety of factors including water seepage along the monitoring PVC pipe, influencing only this probe.

Similar to the plot of the soil-only section, Figure 80 clearly shows that there is no correlation between the internal temperature and the water content in the mixed section of the embankment.

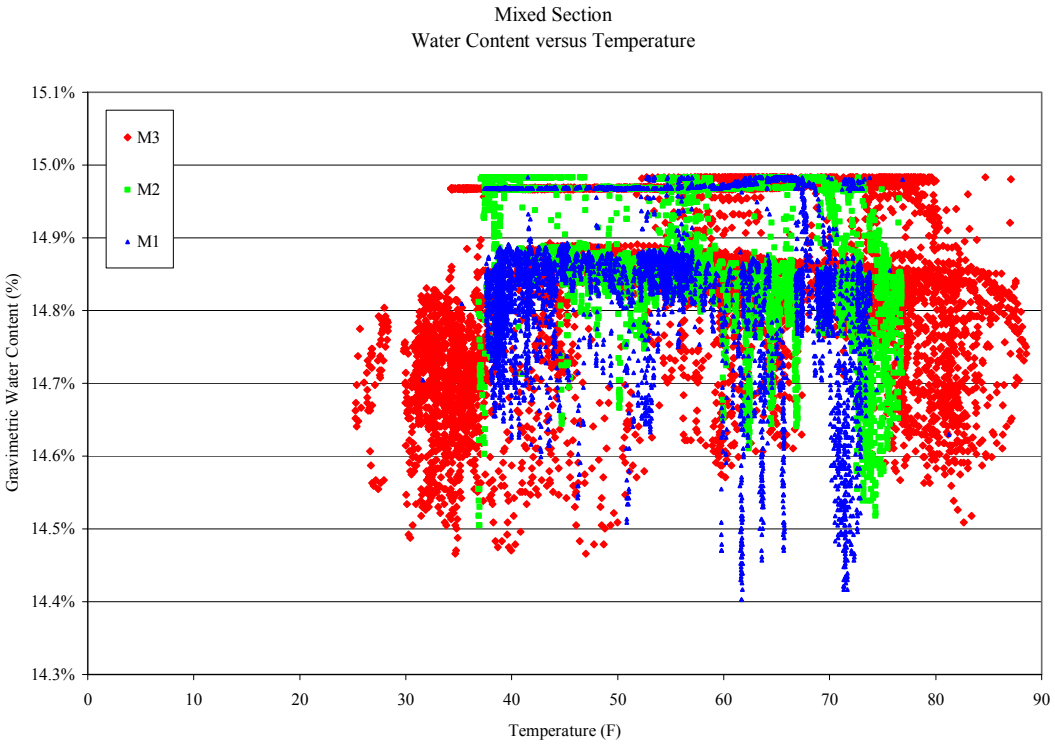

Figure 80: Mixed Section Water Content versus Internal Temperature

Layered Section

At each of the monitoring depths within the layered section, the soil suction and relative humidity were measured and used in the van Genuchten model to determine the water content changes over time. The relative humidity is the ratio of the measured amount of water vapor in the air at a specific temperature to the maximum amount of water vapor that the air can hold at that temperature. The soil suction measurements and trends were previously. Figure 81 shows the relative humidity trends over the monitoring period.

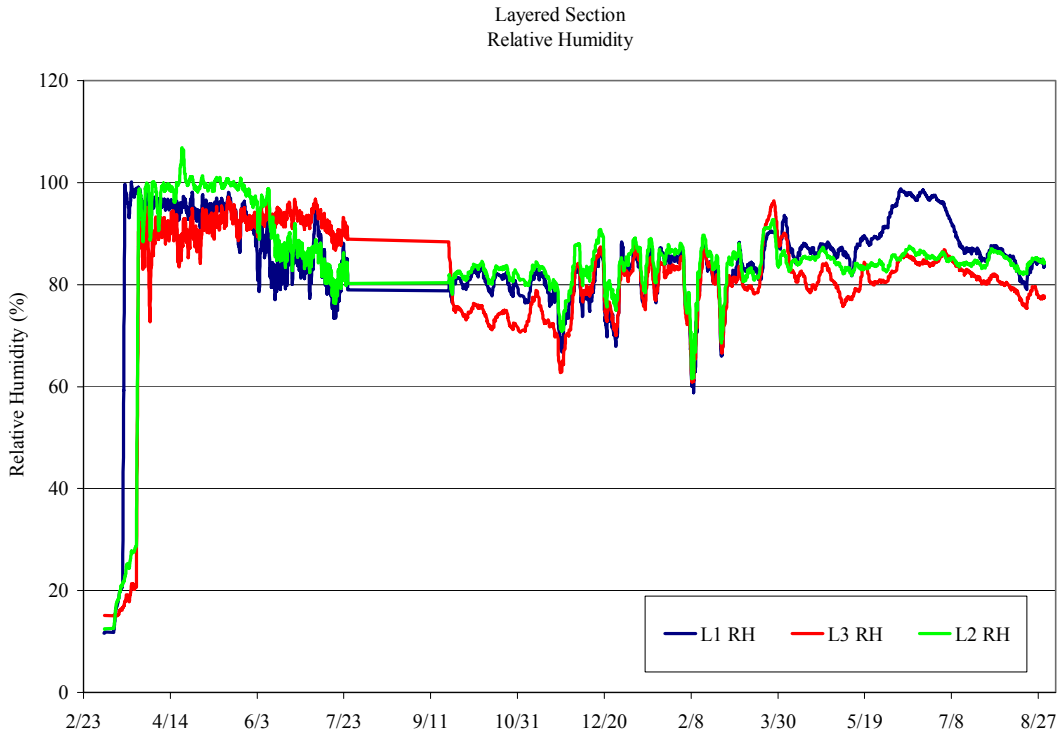

Figure 81: Layered Section Relative Humidity

Figure 81 shows that the relative humidity generally ranges between 60% and 100%. There is not a significant difference between the three depths, except for the values of L1, the deeper probe.

Both the relative humidity and the soil suction can be used to determine the moisture content based on the van Genucthen model. Figure 82 illustrates the difference in the water content found from these two measured values.

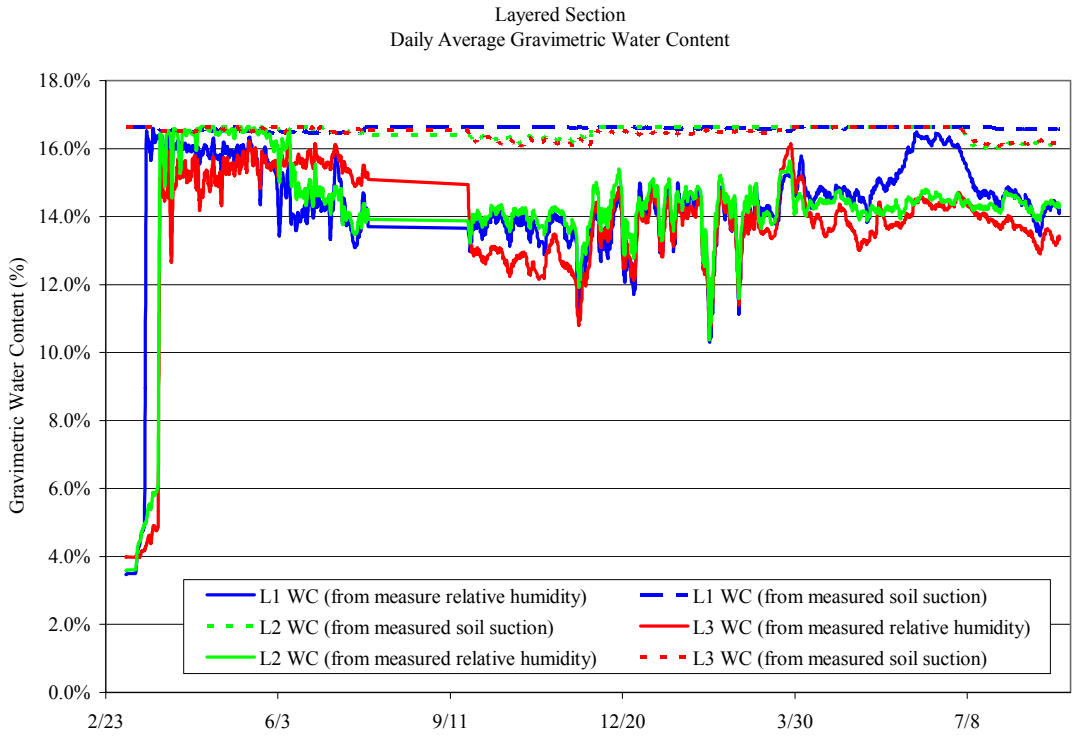

Figure 82: Layered Section Gravimetric Water Content Comparison

In Figure 82 the dashed lines show the moisture content determined from the measured soil suction values and the solid lines show the moisture content determined from the measured relative humidity. The values of water content determined from the relative humidity have a greater range, but similar trends to those obtained in the plot of the relative humidity (Figure 81). The range in values for both methods had a maximum gravimetric water content of 16.6%, but the minimum was significantly different. The relative humidity values ranged from 3.4%; whereas, the soil suction determined water content values ranged from 15.8%. Figure 83 shows the values determined only from the measured soil suction, which shows values that can be compared with the other tire shred-soil embankment sections.

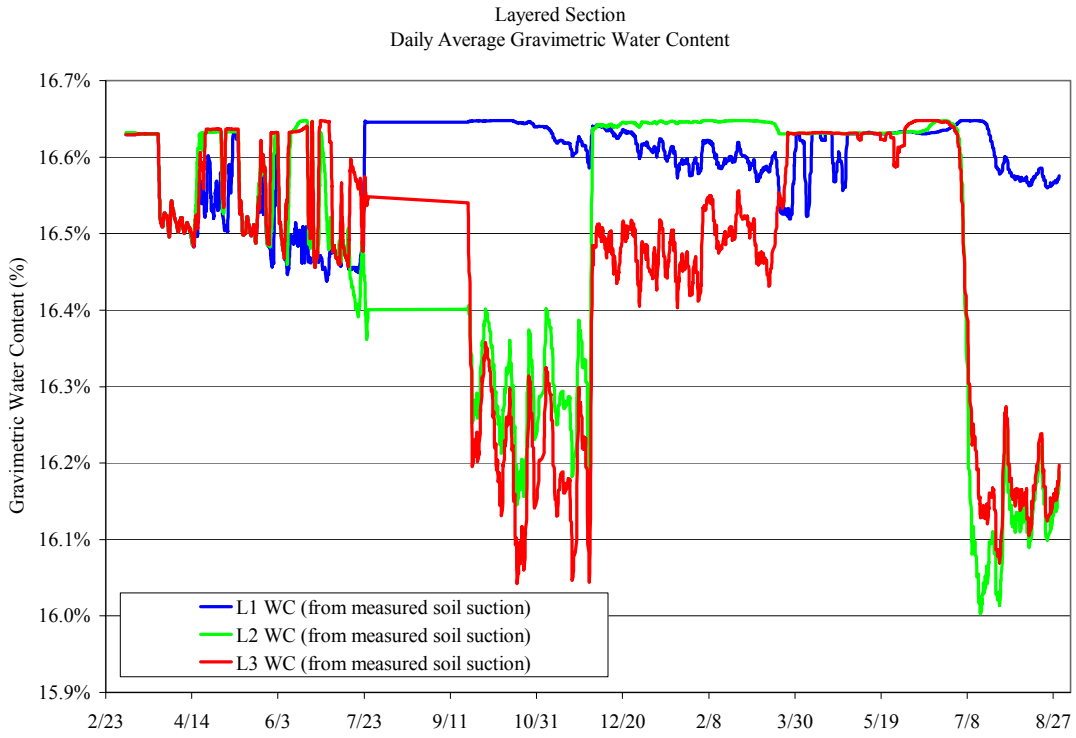

Figure 83: Layered Section Gravimetric Water Content

Figure 83 shows a slightly different trend than that seen in either the soil-only or mixed section. The lower values did occur over the early winter, but rose to a higher value in the middle of December, versus the early spring for the other sections. The middle probe, L2, has a trend similar to that seen in the mixed section; however, L1 shows a relatively small range in values over the entire monitoring period, which is not seen in either of the other embankment sections. The drop in water contents near the end of the monitoring period is consistent with the trends observed in the other two sections.

Figure 84 shows that there is no correlation between the internal temperature and the water content, which is consistent with the results from the mixed and soil-only sections.

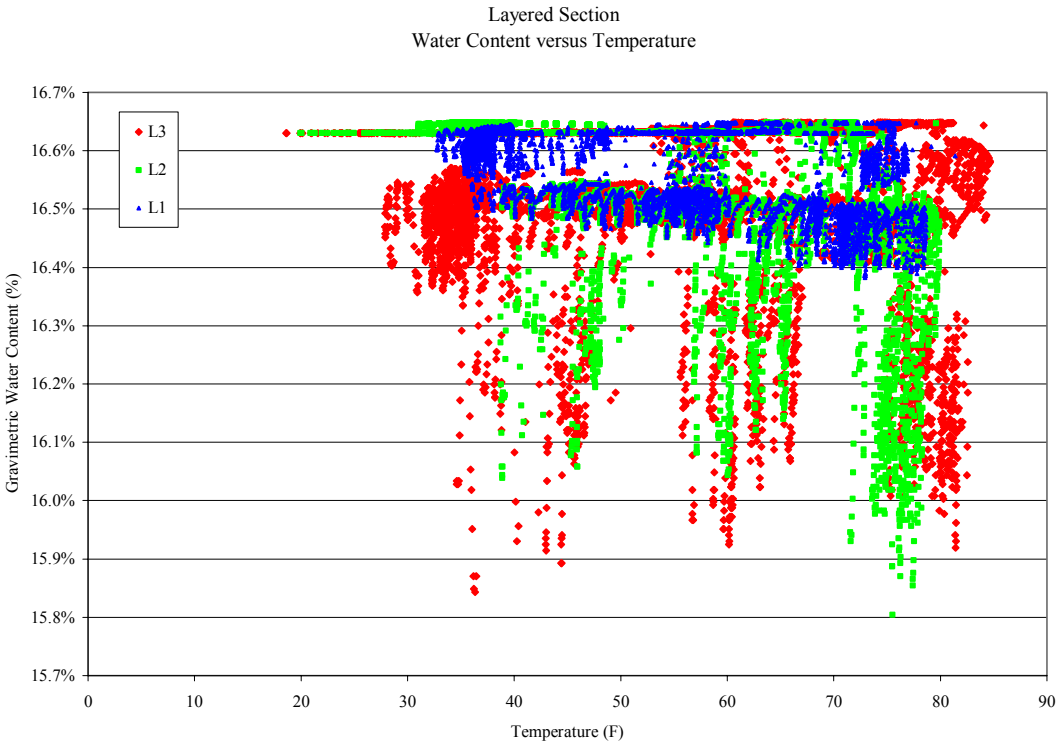

Figure 84: Layered Section Water Content versus Internal Temperature

The water content for each of the embankment sections demonstrates similar trends; however, the values are the lowest for the soil-only section and greatest for the layered section.

Remarks on the Results

The results for the three different tire shred-soil embankment sections and the large tire shred-only stockpile for temperature, soil suction, relative humidity, and water content over the monitoring period show similar trends. The temperature, soil suction and water content show diurnal fluctuations, in addition to seasonal fluctuations. No correlation can be identified between the water content and temperature. The next chapter discusses the different measured parameters in relation to the heat generation within the tire shred-soil embankment and the large tire shred-only stockpile.

Analysis

This chapter presents the analysis of the temperature, soil suction, water content, and relative humidity data collected over the 18 month monitoring period. As part of this analysis, a methodology for determining specific time periods to analyze the possible heat sources and heat flow mechanisms is proposed. The thermal conductivity of the three tire shred-soil embankment sections can also be obtained as part of this evaluation. With the thermal conductivity values determined for some representative time periods, the heat generation in other time periods can be evaluated. The results are also useful to compare other measured variables: relative humidity, soil suction, water content and precipitation.

Analytical Predictions

The potential causes of exothermic reactions within tire shred-soil embankments discussed earlier suggest that moisture within the tire shred-soil embankment plays a role in the development of conditions conducive to heat generation. The heat generation analysis presented in this chapter aims at determining the potential relationship between moisture and internal heat generation. This analysis evaluates the heat generation within each tire shred-soil embankment section, as well as within the large tire shred-only stockpile. Temperature data collected within the large tire shred-only stockpile pile will be used to evaluate any potential increase in heat generation that may occur following precipitation. The tire shred-soil embankment sections will also be evaluated to assess any relationship between rainfall and heat generation. The comparison of the thermal responses of the tire shred-soil embankment sections is expected to provide insight into the effects of precipitation and moisture on the internal heat generation within tire shred-soil embankment sections and highlight the ability of the soil to dissipate heat at a greater rate than pure tire shreds.

Time Period Determination

In order to determine specific time periods to be analyzed the daily average temperature was plotted versus time to remove any diurnal trends. Time periods were identified where the daily average ambient and internal temperatures over a span of several days remained relatively constant. There were also time periods identified where the daily average ambient and internal temperatures did show an increase. Six time periods were chosen that demonstrated both of these trends. These time periods were selected based specifically on the range of internal temperatures.

Three of the selected time periods were during a period of no rainfall, considered the "dry" time periods for this analysis. The other three time periods were following a period of rainfall, and are considered "wet" time periods. For the three dry time periods it is assumed that the effect of moisture on the heat transfer within the embankment was negligible and therefore convection and radiation due to the presence of water is negligible. Thus, the heat transfer through the embankment during the dry time periods was assumed to be through pure conduction. The wet time periods were used to compare the response of the tire shred-soil embankment sections and the large tire shred-only stockpile following a rainfall with a period of no rainfall to determine the effect of rain on the internal temperature and heat generation.

The three time periods selected over dry periods of no rainfall were used to determine the thermal conductivity values for the three tire shred-soil embankment sections and the large tire shred-only stockpile. These time periods were selected based on the assumption that the effect of moisture is negligible and other variables that could possibly affect the thermal conductivity, such as moisture content and temperature, were relatively constant. The determined thermal conductivity values were then used in the heat generation analysis of the three wet time periods that were selected. Table 5 shows the time periods that were selected and the rainfall received prior to the period evaluated.

Table 5: Time Periods

Time Period	Length (hours)	Precipitation received during previous 72 hours (inches)
Dry 1: 12/13 - 12/17	117	0
Dry 2: 5/1 - 5/7	154	0
Dry 3: 1/26 - 1/31	138	0
Wet 1: 6/8 - 6/11	80	0.73
Wet 2: 4/25 - 4/28	81	1.3
Wet 3: 5/11 - 5/14	81	0.37

Figures 85 through 90 show the daily average temperature trends during these time periods in the tire shred-soil embankment and large tire shred-only stockpile and the precipitation received prior to the selected wet time periods. These plots can be used to demonstrate qualitatively the effect of precipitation on the internal temperature.

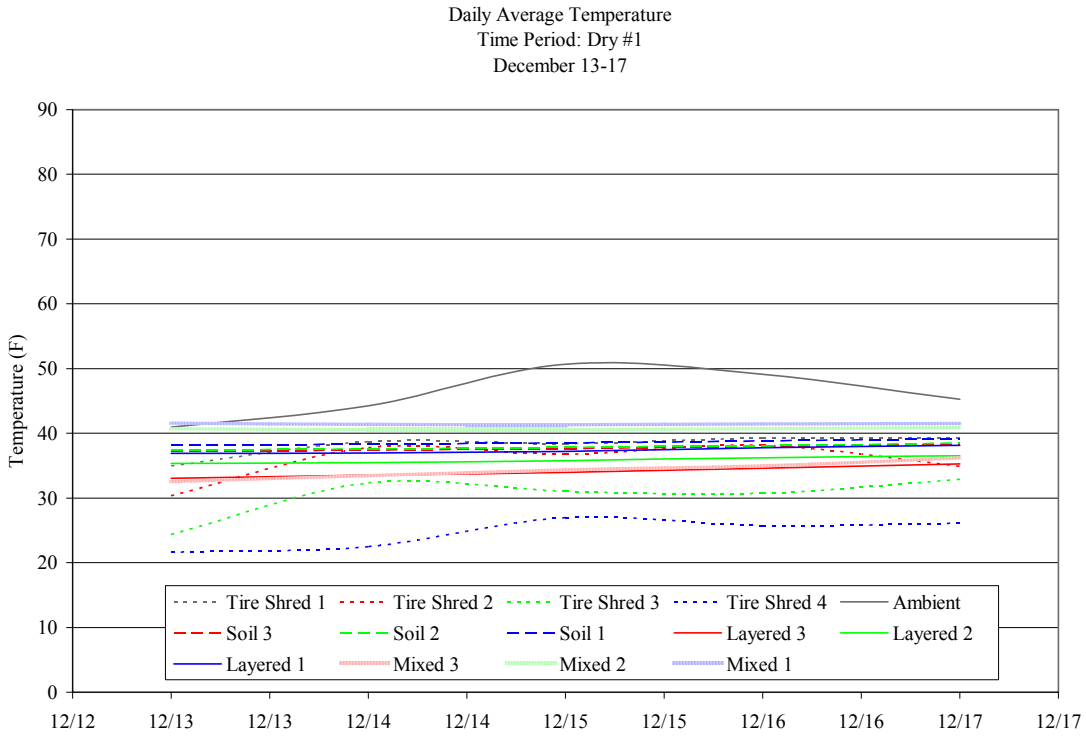

Figure 85: Time Period Dry #1: Daily Average Temperature

Time period Dry #1 shows only minor fluctuations in temperature. The average difference between the maximum and minimum temperatures for all the monitoring

probes is approximately about 1.4°F, a relatively minor change in temperature over the five day period.

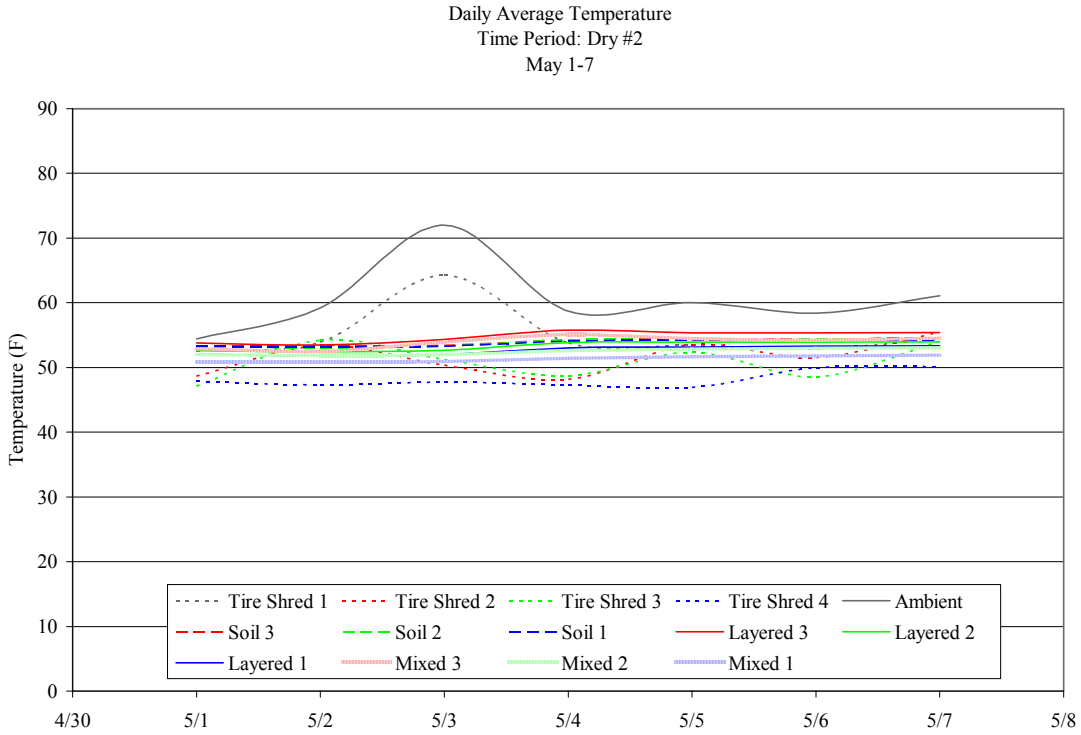

Figure 86: Time Period Dry #2: Daily Average Temperature

Dry Time Period #2, shown in Figure 86, also shows relatively minor changes in the temperature profile over the seven day monitoring period. The average change in temperature between the maximum and minimum for the internal temperature probes is 1.6°F, similar to the first dry time period. Time periods that do not experience significant changes in average temperature suggest a steady state condition.

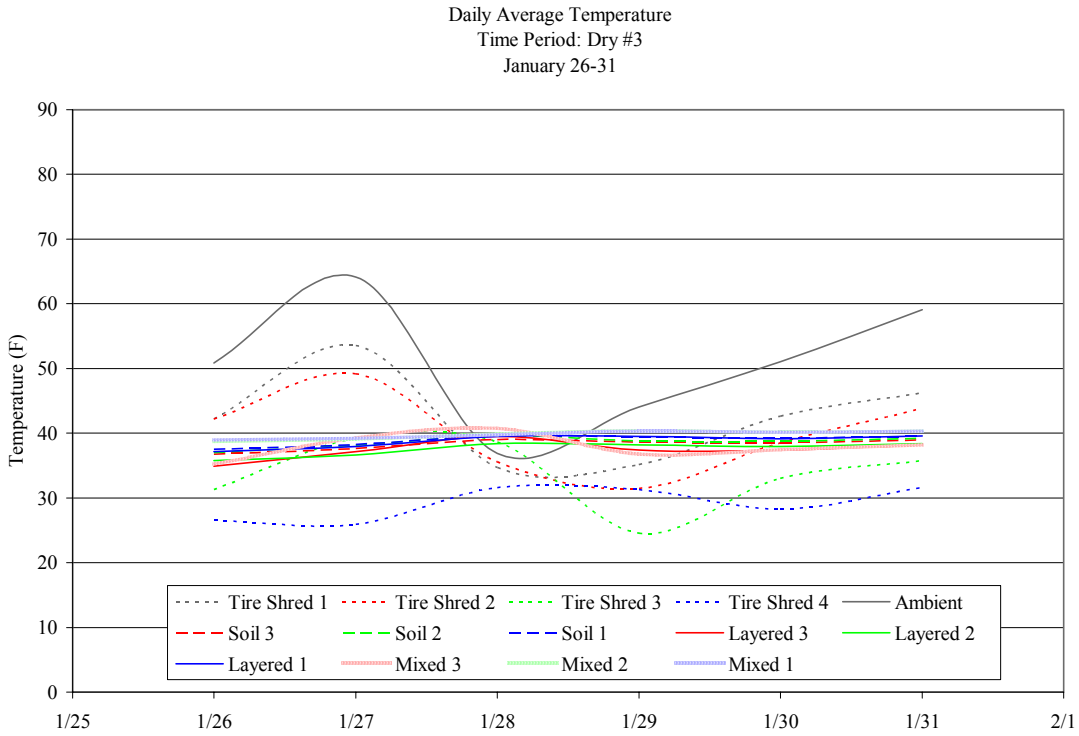

Figure 87: Time Period Dry #3: Daily Average Temperature

Dry Time Period #3 shows minor changes in the tire shred-soil embankment internal temperatures, but does show slightly more variation within the large tire shred-only stockpile. However, the difference between the maximum and minimum temperatures is an average of 2.8°F, which is slightly higher than the first two time periods, but not significant.

Figures 88, 89 and 90, show the "wet" time periods and the period of rainfall preceding the time analyzed. The temperature trends are different than the dry time periods, especially within the large tire shred-only stockpile. The large tire shred-only stockpile temperatures show an increasing trend, which may be indicative of heat generation occurring internally within this stockpile. The magnitude of the heat generated will be analyzed in the next section, but it is of interest to note the difference between the large tire shred-only stockpile temperature changes and the only slight temperature changes within the tire shred-soil embankment sections.

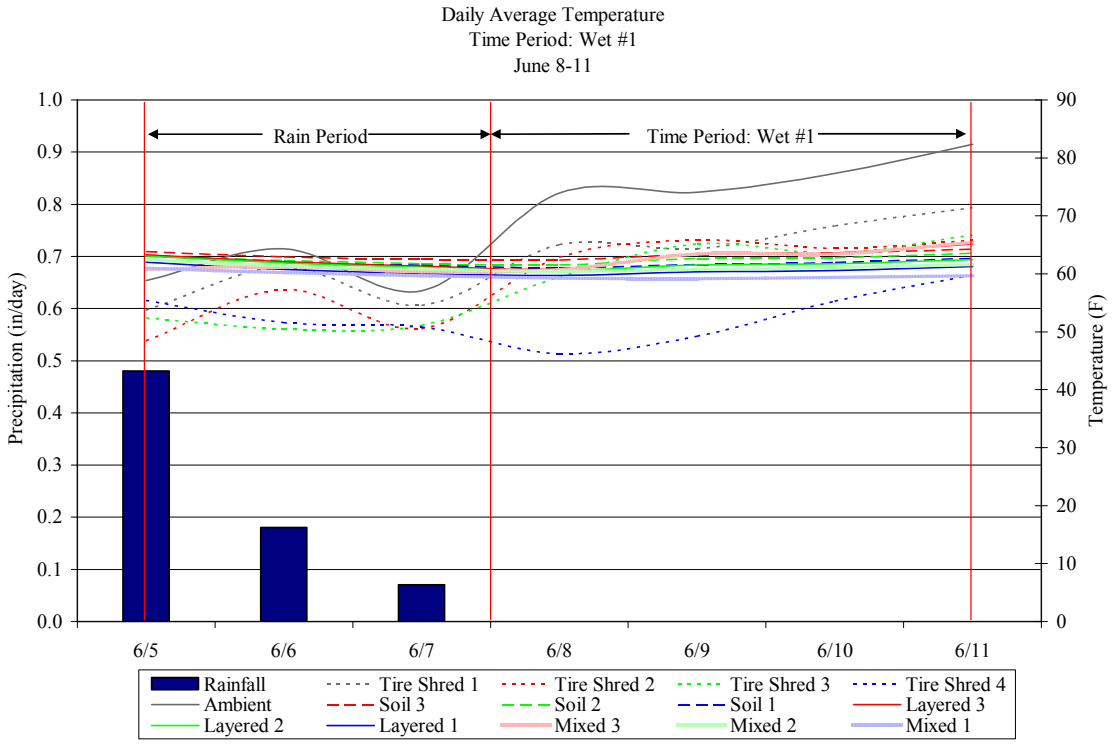

Figure 88: Time Period Wet #1: Daily Average Temperature and Precipitation

During Time Period Wet #1, shown in Figure 88, the tire shred-only stockpile temperature increases an average of 7.5°F; whereas, the tire shred-soil embankment sections experienced an increase of approximately 2.1°F. The temperature increase within the tire shred-soil embankment sections was similar in magnitude to that experienced in Time Period Dry #3, but greater than the first two dry periods. The large tire shred-only stockpile temperature increase for Time Period Wet #1 is greater than the temperature increases observed in the dry time periods: 5.5°F for Dry #1, 4.4°F for Dry #2; and 3.8°F for Dry #3.

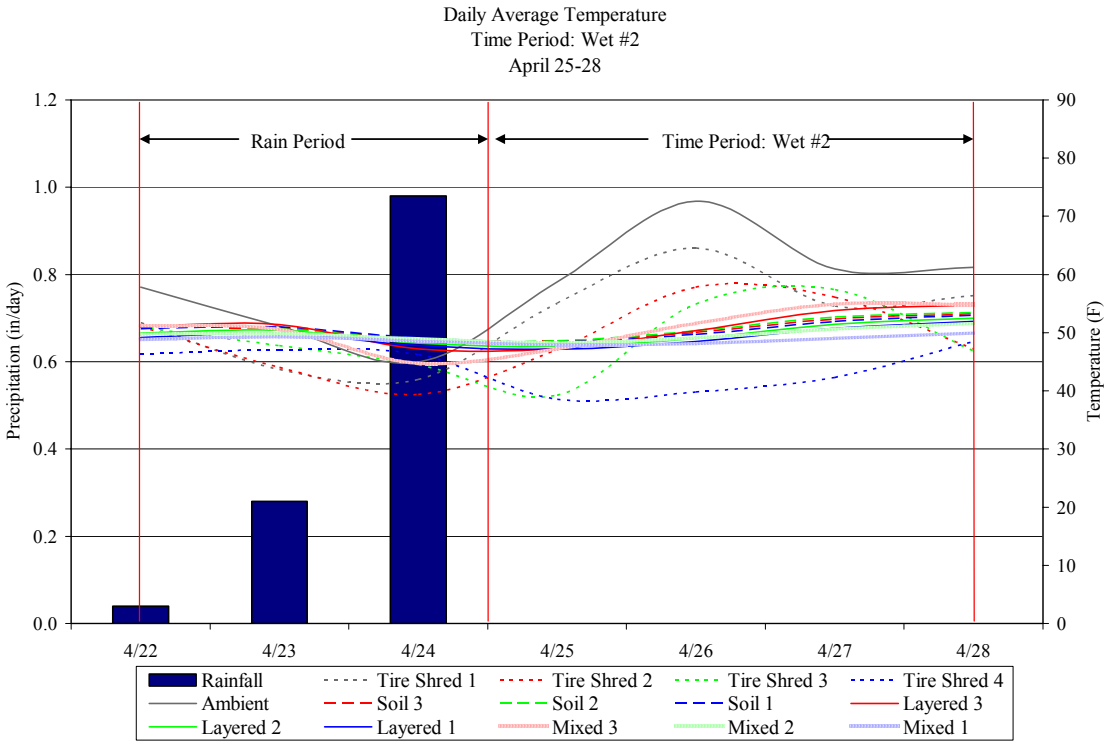

Figure 89: Time Period Wet #2: Daily Average Temperature and Precipitation

For Time Period Wet #2 the internal temperature increases for the large tire shred-only stockpile and the tire shred-soil embankment are greater than those observed in Time Period Wet #1. The average range from the minimum temperatures (which occurred at the beginning of the monitoring period) and maximum temperatures (typically at the end of the monitoring period) in the large tire shred-only stockpile is 12.2°F and the average temperature increase from the minimum to the maximum for the internal temperature of the tire shred-soil embankment sections is 4.3°F. These values are over twice the increase observed in any of the other time periods. It is anticipated that this time period will have greater heat generation than the others, due to this relatively substantial increase in temperature following the rainfall event.

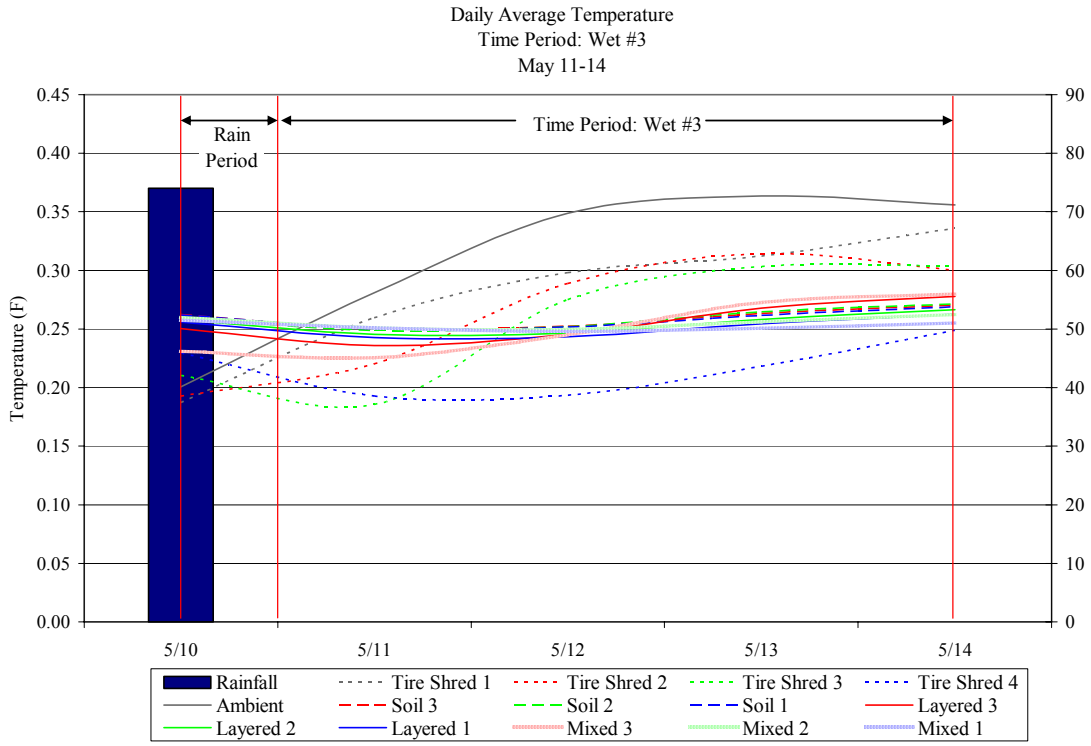

Figure 90: Time Period Wet #3: Daily Average Temperature and Precipitation

Figure 90 illustrates the general increase in temperature during Time Period Wet #3. The large tire shred-only stockpile shows an average increase of 17.2°F, a significantly greater increase than any other time period; and the tire shred-soil embankment sections show an increase of 4.9°F, which is comparable with that observed in Time Period Wet #2.

These six time periods were chosen based upon their temperature trends over the course of the time period and their relation with rainfall events. The first three time periods showed an average increase in temperature less than the average increase seen in the time periods following precipitation. These increases in temperature provide further proof of the relation between rainfall and an increase in the heat generated within the tire shred-soil embankment and large tire shred-only stockpile. It is also important to note that the increase in temperature within the tire shred-soil embankment during the wet time periods was less significant than that in the large tire shred-only stockpile. This supports the hypothesis that the mixing of soil with tire shreds (i.e. mixed and layered

systems) is an effective means of minimizing the potential for exothermic reactions within the tire shred reinforcement.

Determination of Thermal Conductivity

The thermal conductivity of the tire shred-soil embankment is a function of the soil constituents, density, water content, and of the properties of the tire shreds mixed with the soil backfill. This section presents the implementation of the method presented in Chapter 4 to determine the thermal conductivity from the data collected from the tire shred-soil embankment and the large tire shred-only stockpile.

For this analysis, the tire shred-soil embankment and the large tire shred-only stockpile have been assumed to be semi-infinite solids with a periodic surface temperature. The thermal conductivity of a semi-infinite solid heat is transferred through conduction can be expressed as (Carslaw and Jaeger, 1959):

$$k = K\rho C \tag{29}$$

Where: k = thermal conductivity (Btu/hr·ft·°F)

K = (k/ρC) = thermal diffusivity (ft^2/hr)

ρ = density (lb/ft^3)

C = mass heat capacity (Btu/lb·F)

The periodic surface temperatures are shown as diurnal trends, illustrated in the figures depicting the temperatures.. Equation (29) was only used for the temperatures collected during the dry time periods because only these time periods were assumed to have pure conduction heat transfer.

Equation (29) is used to describe the thermal conductivity (k) if the density (ρ), mass heat capacity (C) and thermal diffusivity (K) are known. These thermal properties are assumed to be constant with depth and time for this analysis based on the assumption of homogeneity through the soil mass. The density for the three tire shred-soil embankment sections is a known value from in-situ sand cone tests conducted at the site.

The heat capacity was determined from knowing the dry density and average water content of the soil used as backfill. These values are inputted into the following equation, (Zarling, 1988):

$$C = \gamma_d \left(0.17 + \frac{w}{100} \right) \tag{30}$$

Where: C = heat capacity (Btu/lb·°F)

γ_D = dry density (lb/ft^3)

w = gravimetric water content

The value determined from this equation was 0.2054 Btu/ lb·F, which is comparable to the value reported in literature for a dry soil of 0.19 Btu/ lb·F (Zarling, 1988). The value of the heat capacity for tires comes from previous research (Fitzgerald, 2003). The heat capacity for each section was then determined as the weighted average of the soil and tire heat capacities, based on the percentage of tires by weight in each section. Table 6 outlines the values used for the density and heat capacity in the determination of the thermal conductivity values.

Table 6: General Thermal Properties of Tire Shred-Soil Embankment

Tire Shred-Soil Embankment Section	Total Unit Weight (pcf)	Dry Unit Weight (pcf)	% Tires by Weight	Heat Capacity (C) (Btu/lb·F)
Soil	122	108	0	0.2054
Mixed	112.4	100	10%	0.1970
Layered	100.4	90	15.4%	0.1924

To determine the thermal diffusivity, K, the internal temperatures of the tire shred-soil embankment sections with depth were analyzed. The following equation expresses the internal temperature of a semi-infinite solid as a function of depth and time for steady state, pure conductive heat transfer conditions (Carslaw and Jaeger, 1959):

$$T(z,t) = Ae^{-\alpha \cdot z} \cos(\omega \cdot t - \alpha \cdot z) \tag{31}$$

Where: $\alpha = (\omega/2K)^{1/2}$

K = thermal diffusivity (ft^2/hr)

ω =1 cycle/time period = $(24 \text{ hours})^{-1}$

A = measurement of the curvature of the temperature profile

e = base of log 10

z = depth (ft)

t = time (hr)

This equation can be simplified by recognizing that the trigonometric value, $\cos(\omega t-\alpha z)$, is approximately equal to 1 for the depths (zero to 6 feet) and times being analyzed. Equation 31 becomes the following equation:

$$A'(z) = Ae^{-\alpha \cdot z} \tag{32}$$

Where: A'(z) = range of temperatures for time period at depth "z"

In order to apply equation (32) a plot of the temperature over the selected time periods is required to find A'(z) or the curvature of the temperature profile. Figure 91 shows the temperature profile for the soil-only section during Time Period Dry #1. As shown in this figure the values of A'(0), A'(-1.25), A'(-2.75) and A'(-4.25) are shown as the range of temperatures at each depth.

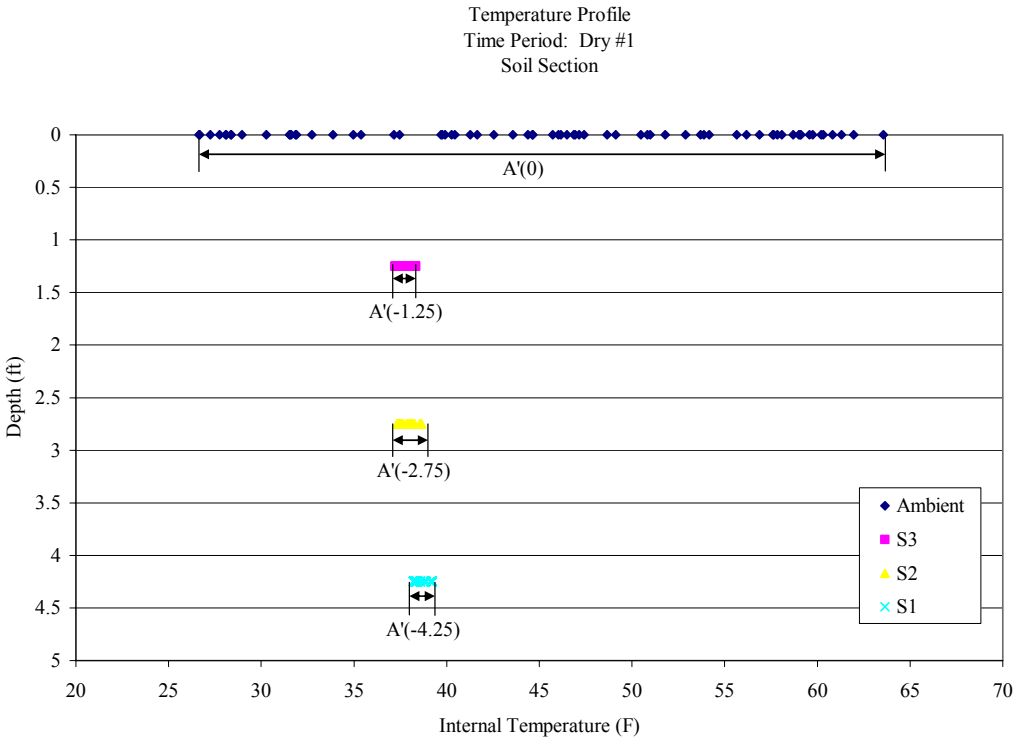

Figure 91: Temperature Profile for Soil-Only Section for Time Period Dry #1

The value of A'(z) at the surface, z = 0, is used to find the value of the constant "A" in equation (6-4). For the soil-only section during Time Period Dry #1 the value of the range of temperatures over the time period at the surface equals "A" which equals 36.93°F. It was assumed that the surface temperature was equal to the ambient temperature. From the value of "A" calculated from A'(0) the following equations were solved to find the value of α at each depth:

$$A'(-1.25) = 36.93 \cdot e^{-\alpha \cdot 1.25} \qquad \alpha = 2.80 \qquad (33)$$

$$A'(-2.75) = 36.93 \cdot e^{-\alpha \cdot 2.75} \qquad \alpha = 1.21 \qquad (34)$$

$$A'(-4.25) = 36.93 \cdot e^{-\alpha \cdot 4.25} \qquad \alpha = 0.85 \qquad (35)$$

The average of these α values (1.62) was used to find the thermal diffusivity (K) according to the following equation (Carslaw and Jaeger, 1959):

$$K = \frac{\omega}{2 \cdot \alpha_{ave}^{\ 2}} \qquad (36)$$

Where: ω = 1 cycle/time period

K = thermal diffusivity (ft^2/hr)

The value for the thermal diffusivity for the soil-only section during Time Period Dry #1 was determined to be 0.0391 ft^2/hr using α_{ave} of 1.62 and an ω of 1/(24 hours). Knowing the heat capacity (C), thermal diffusivity (K) and density (ρ), the thermal conductivity (k) can be calculated using Equation (29). The value of the thermal conductivity of the soil-only section during Time Period Dry #1 was determined to be 0.981 Btu/hr·ft·°F.

This same method outlined for the soil-only section for Time Period Dry #1 was applied to the two other tire shred-soil embankment sections and the large tire shred-only stockpile for this time period and for the other two dry time periods. Table 7 summarizes the thermal conductivity values that were determined for each of the three dry time periods.

Table 7: Calculated Thermal Conductivity Values

	Soil Only	**Layered**	**Mixed**	**Tire Shred**
Heat Capacity (Btu/lb·F)	0.2054	0.1924	0.1970	0.1211
Density (pcf)	122	100.4	112.4	40
Thermal Diffusivity	**(ft^2/hr)**	**(ft^2/hr)**	**(ft^2/hr)**	**(ft^2/hr)**
Dry 1: 12/13 - 12/17	0.0392	0.0560	0.0520	0.1069
Dry 2: 5/1 - 5/7	0.0477	0.0651	0.0710	0.0312
Dry 3: 1/26 - 1/31	0.0500	0.0700	0.0721	0.0640
Average	0.0456	0.0637	0.0650	0.0673
Thermal Conductivity	**(Btu/hr·ft·°F)**	**(Btu/hr·ft·°F)**	**(Btu/hr·ft·°F)**	**(Btu/hr·ft·°F)**
Dry 1: 12/13 - 12/17	0.981	1.082	1.152	0.518
Dry 2: 5/1 - 5/7	1.196	1.258	1.573	0.151
Dry 3: 1/26 - 1/31	1.252	1.353	1.596	0.310
Average (used in analysis)	***1.143***	***1.231***	***1.440***	***0.326***

Table 7 shows that the thermal conductivity in the soil-only section (1.14 Btu/hr·ft·°F), is smaller than the value obtained in the layered section (1.23 Btu/hr·ft·°F), which is, in turn, lower than the value obtained in the mixed section (1.44 Btu/hr·ft·°F). The values of thermal conductivity for soil reported in the literature have a wide range

due to the many different variables affecting heat transfer within soil. Nonetheless, the accepted range of thermal conductivity for a sandy coarse soil is 0.97 Btu/hr·ft·F to 1.81 Btu/hr·ft·F (Jumikis, 1977). The thermal conductivity for tire shreds has been reported to range from 0.11 Btu/hr·ft·F to 0.18 Btu/hr·ft·F (Humphrey, 1996). The average values of the thermal conductivity reported in Table 7 from the three dry time periods were used in the analysis of all time periods to determine the heat generation within the tire shred-soil embankment sections and large tire shred-only stockpile.

Heat Generation Analysis

The heat generation within each of the tire shred-soil embankments and the large tire shred-only stockpile was determined by a finite difference evaluation. The governing differential equation for heat transfer within a solid can be expressed as (Carslaw and Jaeger, 1959):

$$k\frac{\delta^2 T}{\delta z^2} = \rho \cdot C\frac{\delta T}{\delta t} \tag{37}$$

Where: k = thermal conductivity (Btu/hr·ft·°F)

ρ = density (lb/ft^3)

C = heat capacity (Btu/lb·°F)

T = temperature (°F)

t = time (hours)

z = depth (ft)

If there is any heat generation that cannot be described by conductive heat transfer, an additional heat generation variable needs to be incorporated. Equation (38) incorporates "q," which represents the heat generation that cannot be accounted for solely by conduction (Carslaw and Jaeger, 1959):

$$q + k\frac{\delta^2 T}{\delta z^2} = \rho C\frac{\delta T}{\delta t} \tag{38}$$

Where: q = generated heat (Btu/ft^3·hr)

This equation is rearranged to isolate the heat generation term:

$$q = \rho \cdot C \frac{\delta T}{\delta t} - k \frac{\delta^2 T}{\delta z^2} \tag{39}$$

The heat generation for the dry time periods used to determine the thermal conductivity, where the heat transfer was assumed to be pure conduction, the heat generation should be equal to zero (i.e. Equation (39)). For the wet time periods if the heat generation, "q", is positive, additional heat generation mechanisms occur within the tire shred-soil embankment and/or large tire shred-only stockpile that cannot be accounted for by pure conduction.

The value of "q" is determined through using the finite difference method to determine the values of the partial differential terms in Equation (39). This method was applied to two different ranges of depth within the tire shred-soil embankment sections and the large tire shred-only stockpile. The first range of depths analyzed by these equations to find the heat generation was between the surface and -2.75 feet deep in the tire shred-soil embankment and between the surface and -3 feet in the large tire shred-only stockpile. The second application of the finite difference method was used to determine the heat generated between the depths of -1.25 feet and -4.25 feet in the tire shred-soil embankment and between the depths of -1.5 feet and -6 feet in the tire shred-only stockpile. The input variables for the heat generation at the shallower depths are shown below Equation (6-12), with the second set of input variables for the heat generation at the lower depths in parenthesis. The equations used for both depth ranges in the tire shred-soil embankment, as well as the deeper range in the large tire shred-only stockpile, are expressed for unevenly spaced temperature sensors as (Dow, 1999):

$$\frac{\delta^2 T}{\delta z^2} = \frac{\dfrac{T_4 - T_3}{z_4 - z_3} - \dfrac{T_3 - T_2}{z_3 - z_2}}{\dfrac{z_3 + z_4}{2} - \dfrac{z_2 + z_3}{2}} \tag{40}$$

$$\frac{\delta T}{\delta t} = \frac{T_3^{\,p+1} - T_3^{\,p}}{\Delta t} \tag{41}$$

Where: T_4 = internal temperature at S2, M2, L2

(S1, M1, L1 and TS 4)

T_3 = internal temperature at S3, M3, L3

(S2, M2, L2 and TS3)

T_2 = internal temperature at ambient

(S3, M3, L3 and TS2)

z_4 = depth at S2, M2, L2 (-2.75 feet)

(S1, M1, L1 (-4.25 feet) and TS4 (-6 feet))

z_3 = depth at S3, M3, L3 (-1.25 feet)

(S2, M2, L2 (-2.75 feet)

z_2 = depth at surface (ambient)

(S3, M3, L3 (-1.25 feet) and TS2 (-1.5 feet))

p = current time

p+1 = one time step into the future

For the determination of the heat generation for the shallower depth of the large tire shred-only stockpile, between the surface and -3 feet, was determined using the following equations for equally spaced temperature sensors (Dow, 1999):

$$\frac{\delta^2 T}{\delta z^2} = \frac{1}{\Delta z^2} T_{n+1} + T_{n-1} - 2T_n \tag{42}$$

$$\frac{\delta T}{\delta t} = \frac{T_n{}^{p+1} - T_n{}^{p}}{\Delta t} \tag{43}$$

Where: Δt = time step = 0.5 hour

n +1 = Temperature sensor TS1

n = Temperature sensor TS 2

n -1 = Temperature sensor TS3

Δz = distance between temperature probes = 1.5 feet

p = current time

p+1 = one time step into the future

Once the values of heat generated in both depth ranges for each time step were calculated using equations (40) to (43), the two values of "q" were added together to determine the total heat generation rate within that embankment section. Figure 92 shows the heat generation rate over Time Period Dry #1 for the soil-only section. Similar figures for the other tire shred-soil embankment sections and the large tire shred-only stockpile are included in Appendix C.

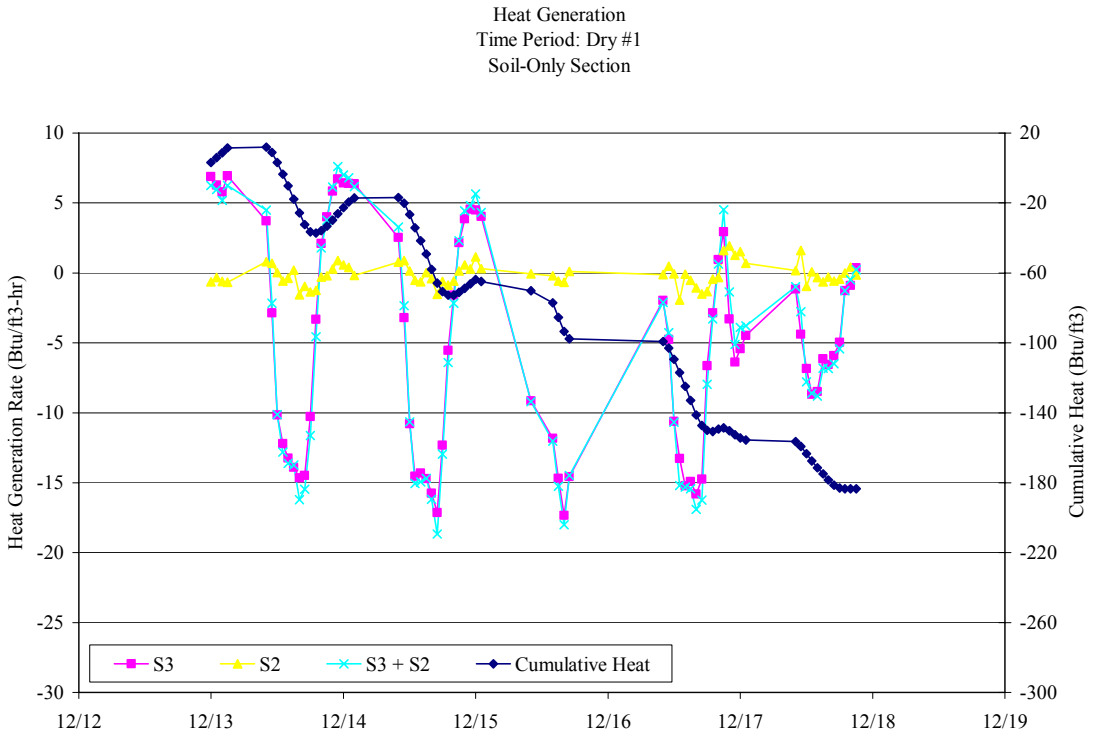

Figure 92: Time Period Dry #1 Heat Generation for the Soil-Only Section

Figure 92 reports the heat generation rate in values of Btu/ft^3·hr. In order to determine the heat generated during the time period the area under the total heat curve was calculated. For Figure 92, the area under the curve is approximately equal to -37.6 Btu/ft^3/day. The negative values indicate an endothermic or heat absorbing reaction rather than an exothermic or heat generating reaction. Several examples of endothermic reactions are evaporation, melting ice, photosynthesis and boiling water. The negative value may also be suggestive of heat dissipation at a faster rate than heat generation.

Table 8 summarizes the heat generation determined through the same finite difference method outlined above and shown with the soil-only section for Time Period Dry #1. The values reported are in Btu/ft^3/day, which allows for a comparison between the various the tire shred-soil embankment sections and large tire shred-only stockpile for all six selected time periods.

Table 8: Heat Generation (Btu/ft^3/day)

Cumulative Heat Generation Time Period	Soil Only (Btu/ft3/day)	Layered (Btu/ft3/day)	Mixed (Btu/ft3/day)	Tire Shred (Btu/ft3/day)
Dry 1: 12/13 - 12/17	-37.6	-53.7	-57.9	18.2
Dry 2: 5/1 - 5/7	-33.4	-25.8	-4.3	23.1
Dry 3: 1/26 - 1/31	-47.4	-55.0	-45.5	34.1
Wet 1: 6/8 - 6/11	-53.7	-50.6	-22.5	51.8
Wet 2: 4/25 - 4/28	-53.2	-46.4	-8.1	32.9
Wet 3: 5/11 - 5/14	-70.2	-65.8	-118.9	103.1
Dry Average	-49.3	-49.6	-42.9	43.9
Wet Average	-59.0	-54.3	-49.8	62.6

Table 8 presents the average value of heat generation within the tire shred-soil embankment sections for both the dry time periods and the wet time periods. It is important to notice that the heat generation within the three tire shred-soil embankment sections is negative, indicating an endothermic reaction, whereas within the large tire shred-only stockpile the reactions were generally exothermic (i.e. positive). The mixed section had typically less of an endothermic reaction, but the values for the three sections were fairly comparable. The difference between the wet and dry time periods is more significant in the large tire shred-only stockpile. The wet time period shows more heat generation, 62.6 Btu/ft^3/day versus 43.9 Btu/ft^3/day for the dry time periods. The tire shred-soil embankment sections actually show an opposite trend, with a more endothermic reaction occurring over the time periods following a rainfall event than the dry time periods. These results provide evidence that when tire shreds are either layered or mixed with soil they are less likely to experience an exothermic reaction in either dry

or wet conditions than a large stockpile of pure tire shreds. These results also show that there appears to be a correlation between the rainfall and the heat generation within the large tire shred-only stockpile.

Figure 93 and Figure 94 graphically portray the results shown in the Table 8 Figure 93 shows the heat generation rate over Time Period Dry #1 in Btu/ft^3·hr for the four different sections. The diurnal trends in heat generation are seen to be consistent in all the sections, plots of which are included in Appendix C.

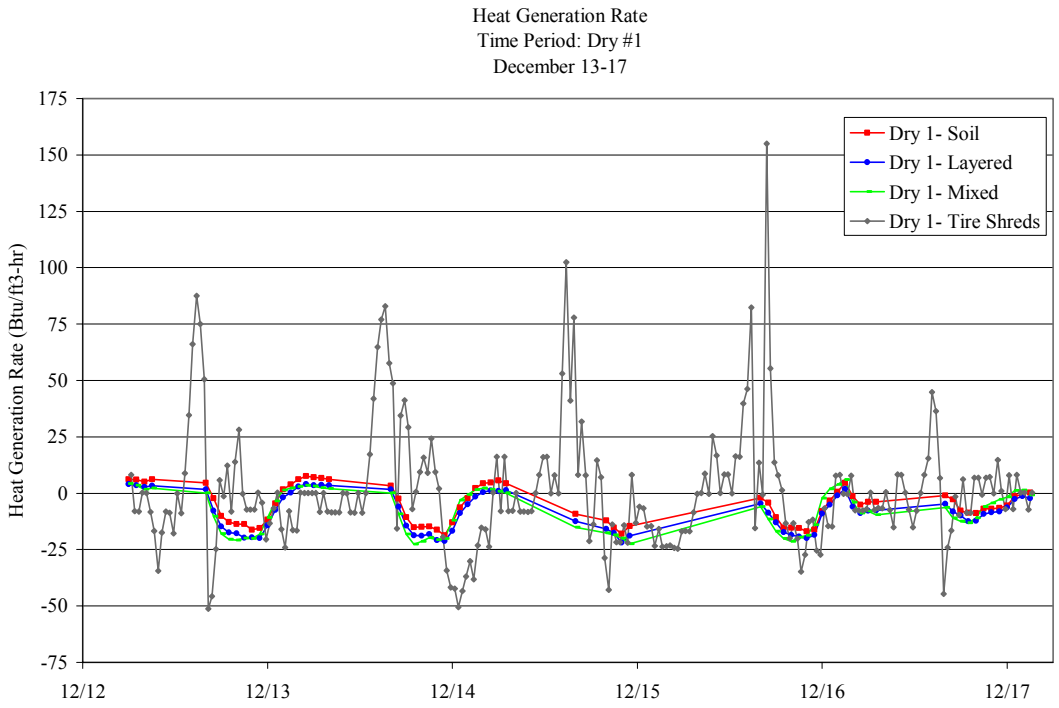

Figure 93: Time Period Dry #1: Heat Generation Rate

Figure 94 shows the general accumulation of heat or the cumulative heat generated in Btu/ft^3 for Time Period Dry #1. It is clear from Figure 93 that the large tire shred-only stockpile undergoes a greater magnitude of heat generation each hour than the tire shred-soil embankment sections, and subsequently the cumulative heat also shows a greater value as shown in Figure 94.

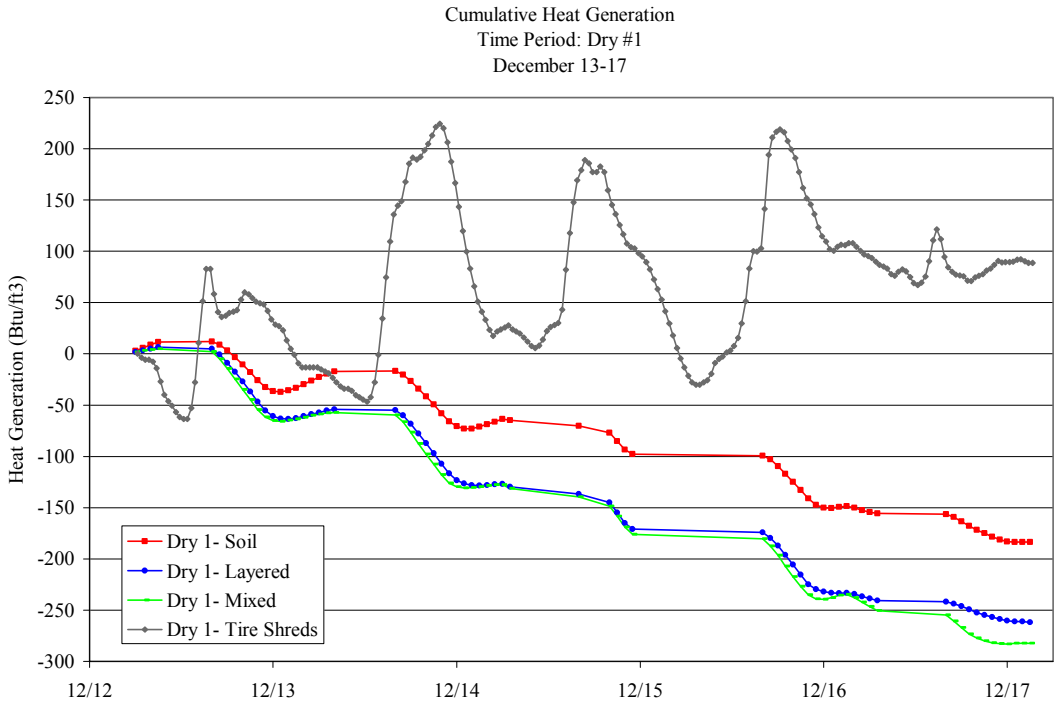

Figure 94: Time Period Dry #1: Cumulative Heat Generation

Figures 93 and 94 are representative of the results for Time Periods Dry #2, Dry #3, Wet #1, Wet #2 and Wet #3, which show similar trends. The tire shred-soil embankment sections typically show a lesser heat generation rate than the large tire shred-only stockpile and a decreasing trend in the cumulative heat generation. In contrast, the large tire shred-only stockpile shows a significant daily variation in the heat generation rate and cumulative heat generation. The cumulative heat generation at the end of each time period is greater in the large tire shred-only stockpile than those reported for the tire shred-soil embankment section, as shown in the values presented in Table 8 and graphically shown in the figures for the other five time periods included in Appendix C.

Figure 95 through Figure 96 show the cumulative heat generation for the different time periods for each of the tire shred-soil embankment sections and the large tire shred-only stockpile. These figures graphically show the comparison between the different thermal responses during each time period. The red lines correspond to the Time Period

Wet #1, Wet #2, and Wet #3 and the blue lines correspond to Time Period Dry #1, Dry #2 and Dry #3. The wet time periods generally show less of an endothermic trend than the dry time periods, which is illustrated by these figures.

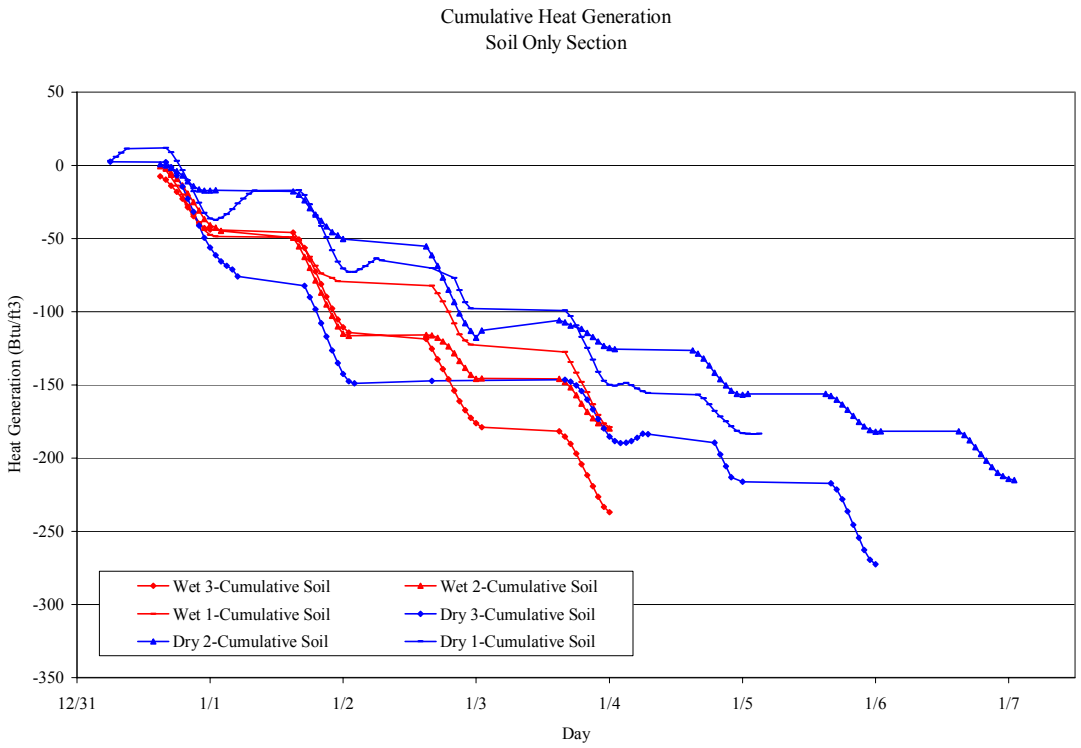

Figure 95: Soil-Only Section Cumulative Heat Generation

Figure 95 shows the thermal reaction in the soil-only section for the six time periods. The wet time periods show an opposite trend than anticipated: The generation of heat seems to be more endothermic following a rainfall event (wet time periods) than during the dry time periods.

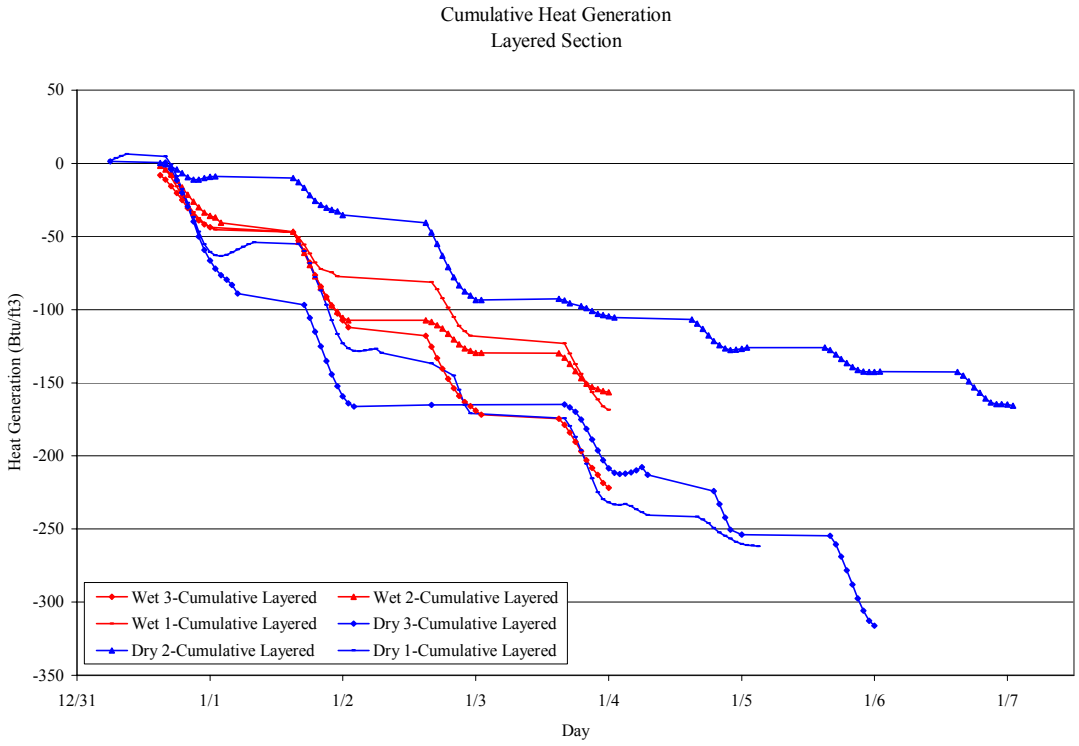

Figure 96: Layered Section Cumulative Heat Generation

The results obtained in the layered section, shown in 96, illustrate a trend slightly different than that observed in the soil-only section. The wet time periods have a less pronounced endothermic reaction than seen during the dry time periods. Time Period Dry #2 does show the least of all the endothermic reactions. The general trend for each dry time period is a negative cumulative heat generation, which corresponds to an endothermic reaction rather than an exothermic reaction.

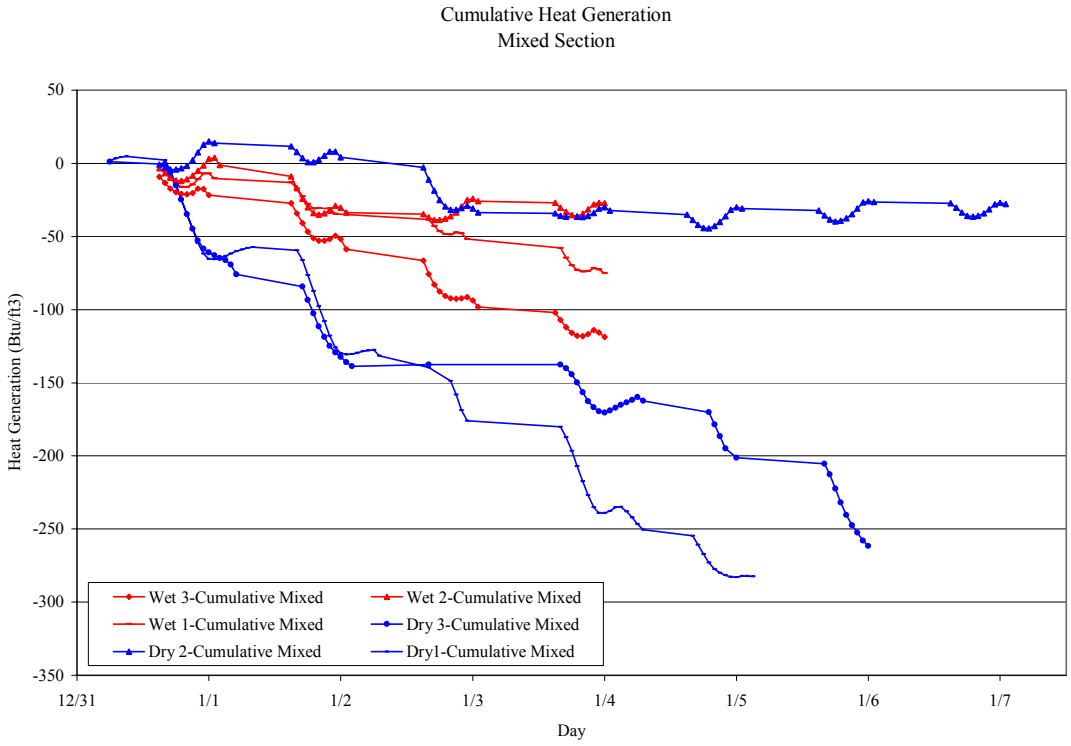

Figure 97: Mixed Section Cumulative Heat Generation

The mixed section showed a greater spread among the results obtained for the six time periods. Yet, the results show decreasing heat generation (or an increasing endothermic reaction). The wet time periods, similar to the layered section, show a slightly higher (less negative) value of cumulative heat generation than the dry periods. Time Period Dry #2 does show the least pronounced endothermic reaction.

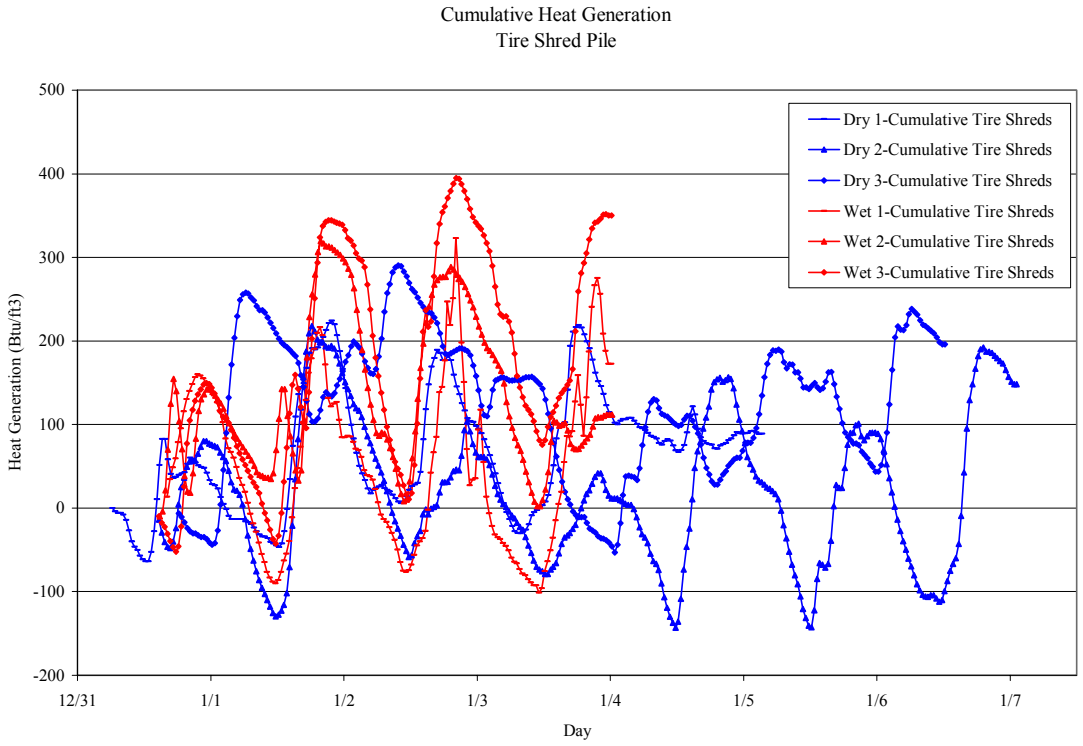

Figure 98: Tire Shred Pile Cumulative Heat Generation

Unlike the results obtained for the tires shred-soil embankment sections (Figures 96 through 98), the results obtained for the large tire shred-only stockpile show a greater daily variation and higher cumulative heat generation values. For each of the time periods, the final cumulative heat was exothermic, being greater than zero, which is a result not seen in any of the tire shred-soil embankment sections. The wet time periods show greater values of heat generation than the dry time periods. The daily trends indicate that that the wet time periods have greater peaks and generally have greater values of heat generation than the dry time periods.

Figure 96 through Figure 98 show that the use of soil mixed with tire shreds (layered or mixed) does minimize the internal heating caused by rainfall, which can be observed in the results within the large tire shred-only stockpile. The results of this analysis also provide evidence that the tire shred-soil embankment sections, layered and

mixed, minimize the possibilities of experiencing exothermic reactions that may occur in tire shred-only stockpiles.

Heat Generation Correlations

The heat generated within the tire shred-soil embankment may be related not only to the precipitation and external moisture but also to the moisture within the soil and tire shreds. Accordingly, correlations between heat generation and other measured variables were evaluated. Specifically, the heat generation rate (Btu/ft^3·hr) was compared with temperature, water content, soil suction and relative humidity.

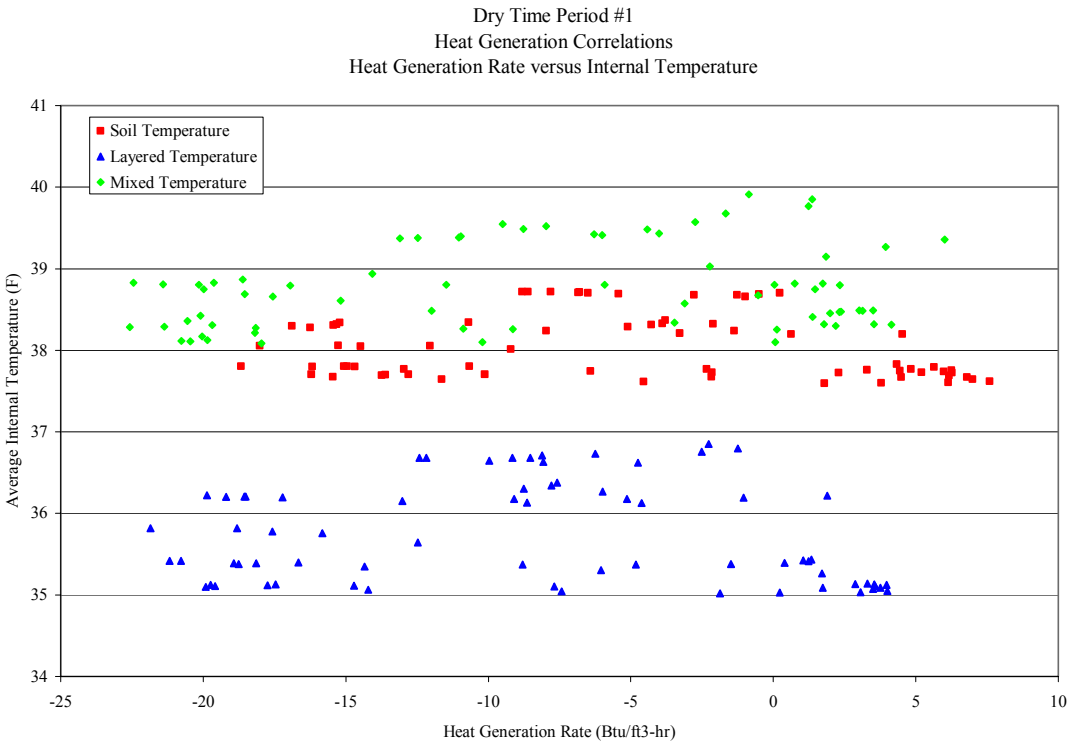

Figure 99: Time Period Dry #1 Heat Generation Rate versus Average Internal Temperature

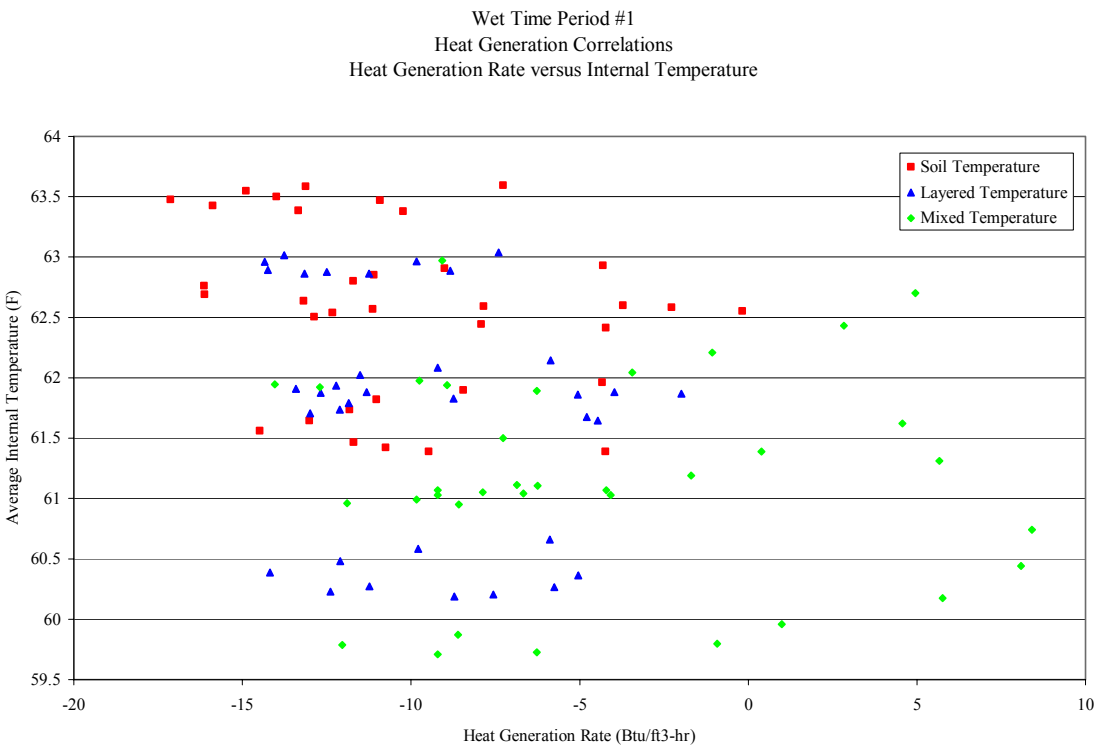

Figure 100: Time Period Wet #1 Heat Generation Rate versus Average Internal Temperature

Figures 99 and 100 show the average internal temperature (in degrees Fahrenheit) versus the heat generation rate (Btu/ft^3·hr) during the Time Period Dry #1 and Time Period Wet #1. There is significant scatter in the points indicating a lack of a distinct correlation between the temperature and heat generation. The other time period plots show a similar scatter of the data and are included in Appendix C.

The gravimetric water content, determined from the measured soil suction, was also plotted against the heat generation rate. Figures 101 and 102 illustrate that as the heat generation rate increases, the water content remains relatively constant. These two figures are representative of the other four time periods, plots of which are included in Appendix C.

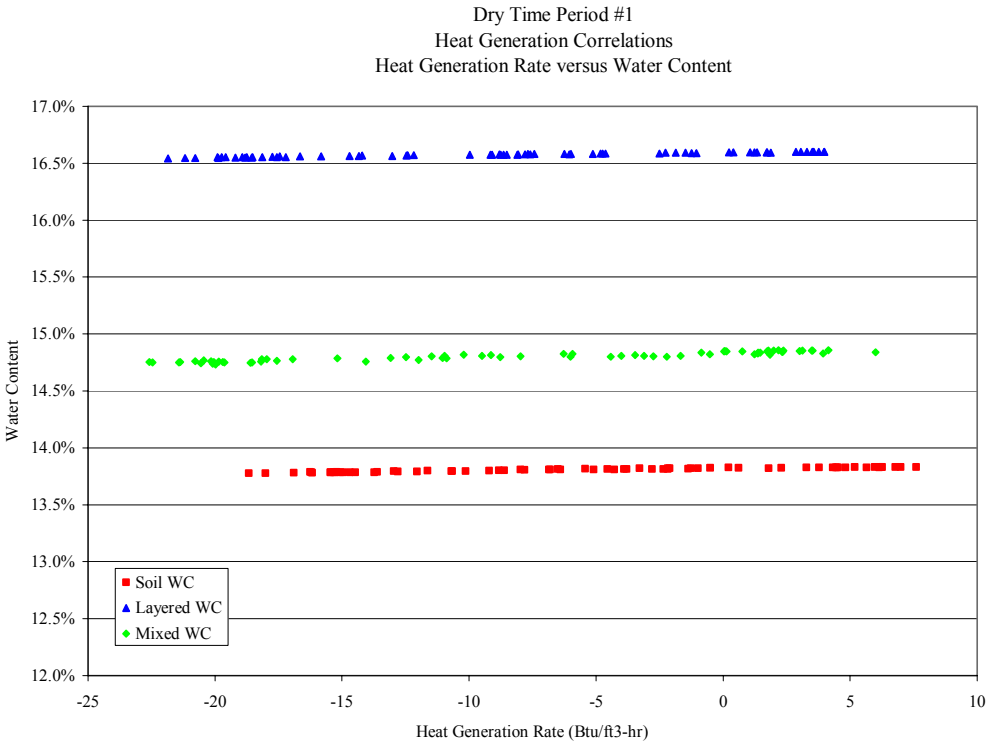

Figure 101: Time Period Dry #1 Heat Generation Rate versus Water Content

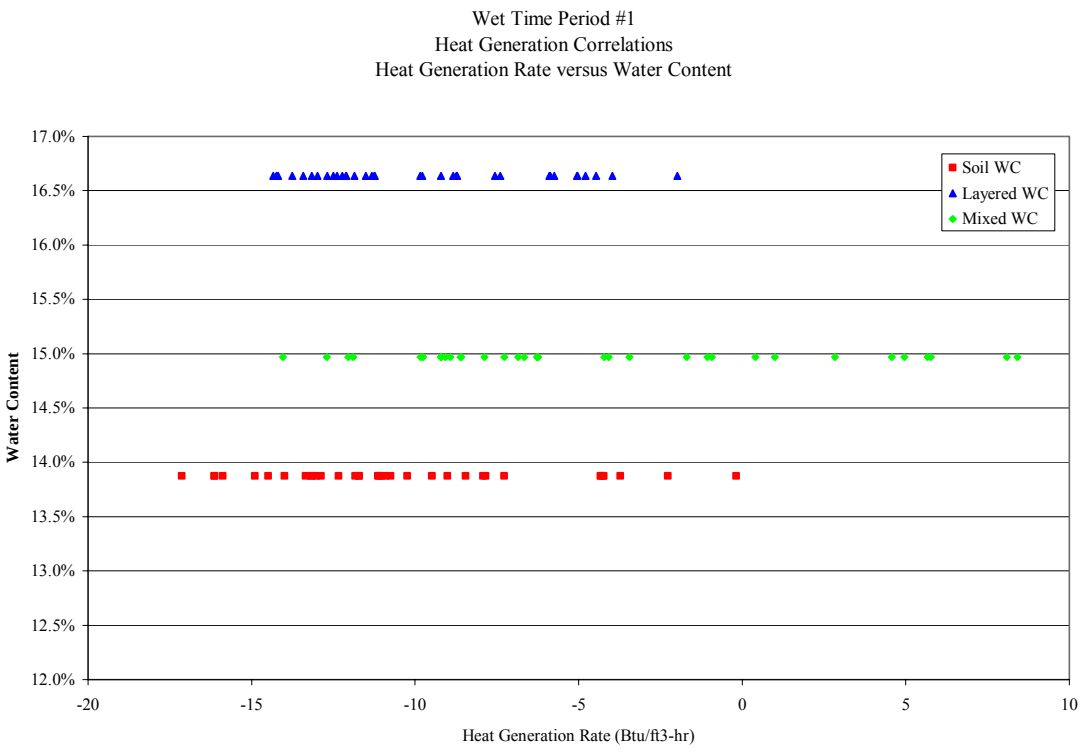

Figure 102: Time Period Wet #1 Heat Generation Rate versus Water Content

Although the water content was defined from measurements of soil suction, assumptions made in the conversion from soil suction to water content could possibly negate any correlation with the heat generation rate. Therefore, the soil suction was also plotted against the heat generation rate. As observed in Figure 103 and 104, for the measurements indicating positive soil suction (negative pore water pressures), there appears to be a decreasing trend as the heat generation values increases. This trend was observed for the Time Period Dry #1 and Time Period Dry #3. A linear regression was used to identify any similarity in values between the two time periods presented in Figures 103 and 104. The equations defining the trends are shown in Table 9. These equations indicate that with no heat generation there would still be soil suction, shown by the value of the intercept (≈ 0.8 to 1.4 psi). The negative slopes (≈ -.02) correspond to the observation that as the heat rate increases, the soil suction decreases.

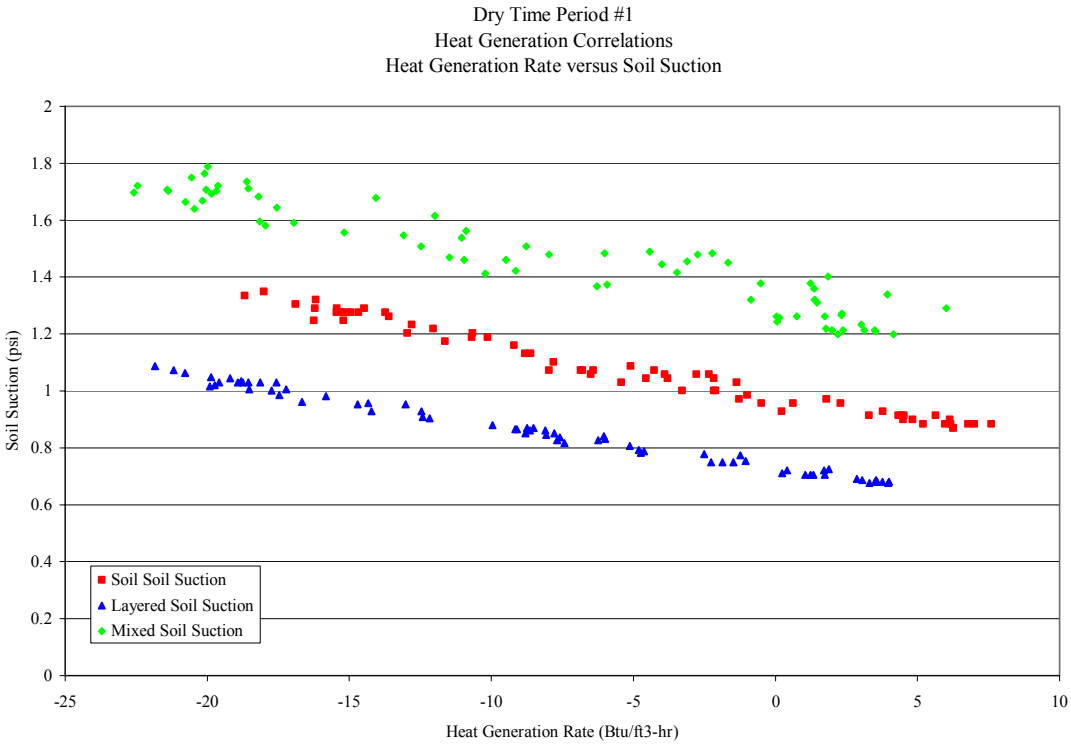

Figure 103: Time Period Dry #1 Heat Generation Rate versus Soil Suction

Table 9: Linear Trend of Heat Generation Rate versus Soil Suction

Embankment Section	Linear Fit Trend-Line Equation
Dry Time Period #1: Soil Only	Soil Suction (psi) = -0.0184(heat)+0.9852
Dry Time Period #3: Soil Only	Soil Suction (psi) = -0.0207(heat)+0.9056
Soil Only Average	Soil Suction (psi) = -0.020(heat)+0.945
Dry Time Period #1: Layered	Soil Suction (psi) = -0.0155(heat)+0.731
Dry Time Period #3: Layered	Soil Suction (psi) = -0.0173(heat)+0.7803
Layered Average	Soil Suction (psi) = -0.020(heat)+0.756
Dry Time Period #1: Mixed	Soil Suction (psi) = -0.0185(heat)+1.322
Dry Time Period #3: Mixed	Soil Suction (psi) = -0.0209(heat)+1.419
Mixed Average	Soil Suction (psi) = -0.020(heat)+1.371

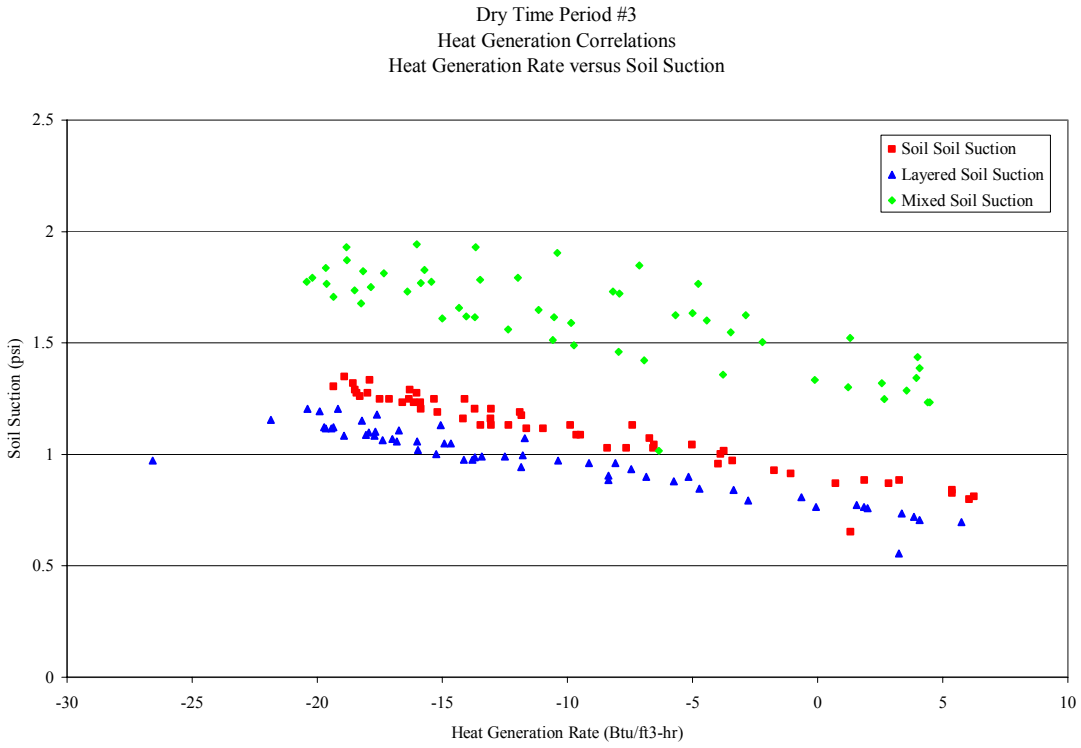

Figure 104: Time Period Dry #3 Heat Generation Rate versus Soil Suction

Figures 103 and 104, and the equations shown in Table 9 show that the slope for all three embankment sections and both time periods are similar, which identifies a distinct correlation between the soil suction (and moisture) and the heat generation rate. In addition, the y-intercept values for each of the embankment sections were relatively close in value for the different time periods.

Despite the trend shown in Figure 103 and 104, for soil suction measurements that were negative (indicating positive pore pressure), the same correlation does not exist, as shown for Time Period Wet #1 in the Figure 105. For these measurements of soil suction there is no apparent correlation with the heat generation rate. This plot is representative of the other three time periods showing negative soil suction, plots of which are included in Appendix C. The negative values that were measured were questioned, due to the fact that a measurement less than zero would indicate a saturated soil, which is not possible for the weather conditions at the site.

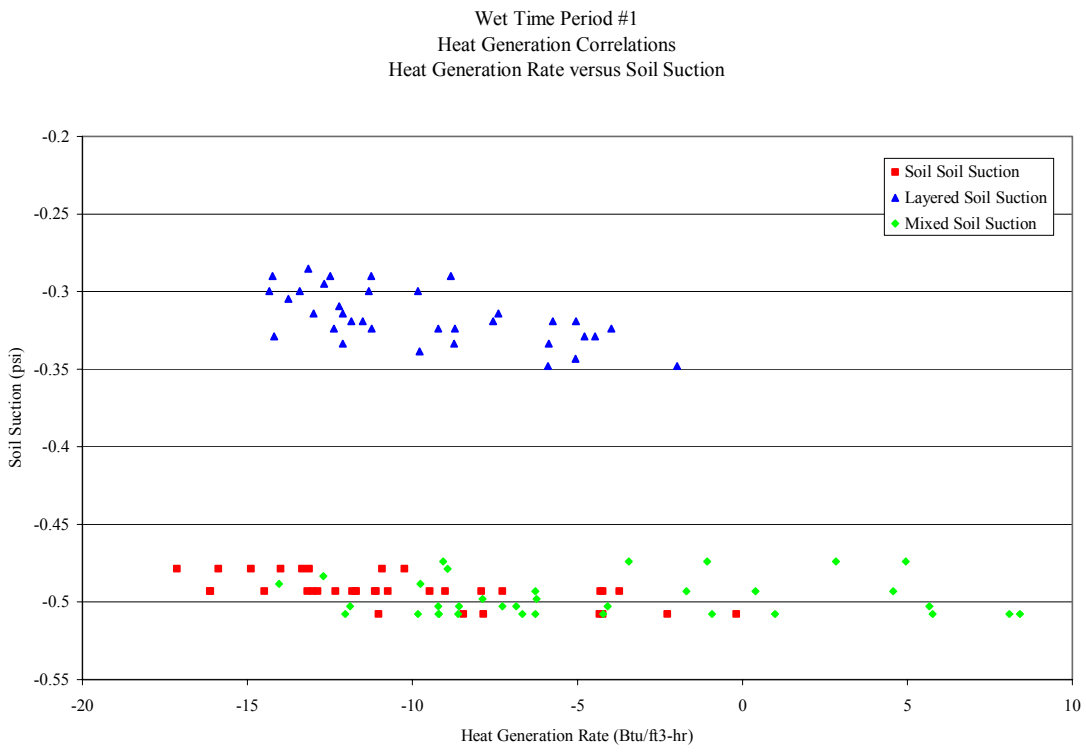

Figure 105: Time Period Wet #1 Heat Generation Rate versus Soil Suction

The relative humidity, which was only measured in the layered section of the tire shred-soil embankment, was also plotted against the total heat generation rate. Figure 106 shows the plot for the Time Period Dry #1. Significant scatter is evident in this Figure, as well as in the other five time periods, indicating that there is no correlation. Figures of the other time periods are presented in Appendix C.

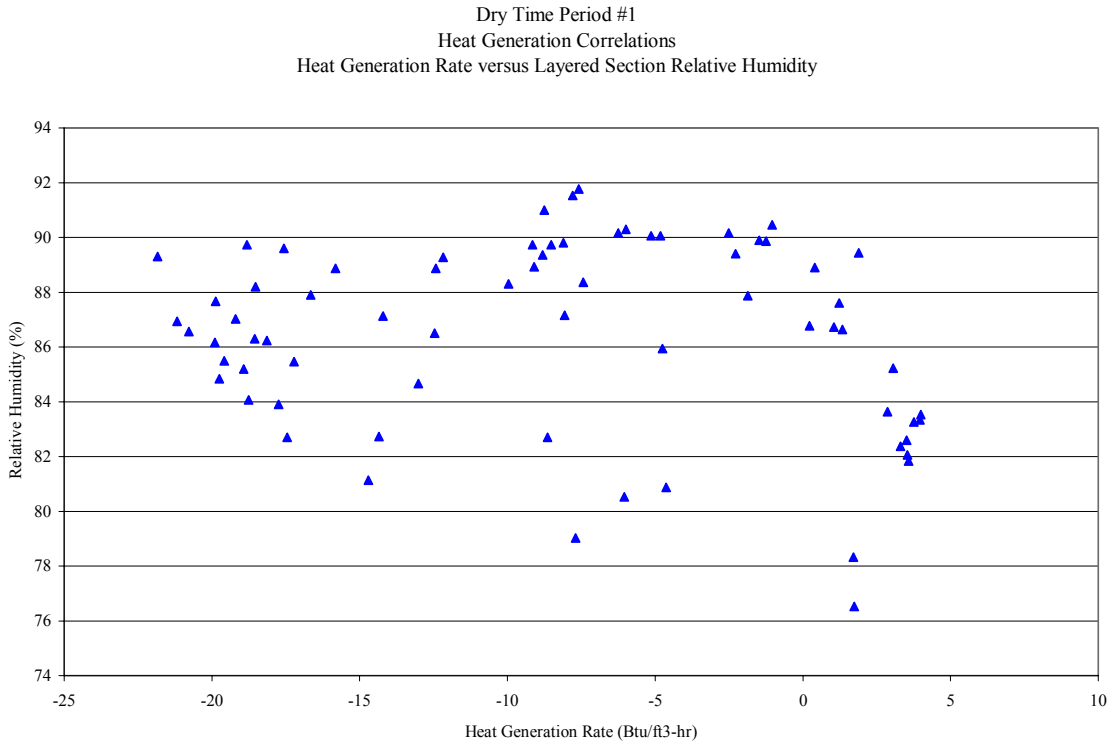

Figure 106: Time Period Dry #1 Heat Generation Rate versus Relative Humidity

It appears from the results presented in Figures 99 through 106 that the heat generation rate correlates only with the soil suction if the measured values are positive (indicating negative pore water pressures). The water content, temperature and relative humidity showed significant scatter, indicating the lack of relevant correlations. The soil suction is related to the moisture within the embankment, with the higher values indicating a drier tire shred-soil embankment section. Figure 103 and Figure 104 illustrate the trend that as the soil suction decreases (i.e. as moisture increases), the heat generation increases. This correlation is consistent with potential causes of exothermic reactions, such as oxidation of the steel belts, which are expected to be facilitated by the presence of moisture. As an environment conducive to exothermic reactions is created through an increase in soil moisture, heat generation also increases.

Remarks on the Analysis

The heat generation analysis presented above quantitatively compare the heat generation within the tire shred-soil embankment sections and the large tire shred-only stockpile. The correlation between precipitation and the increase in both internal temperature and heat generation within the large tire shred-only stockpile validate the assumption that moisture affects the internal heat generation of a tire shred stockpile. Additionally, the lack of substantial increases in internal temperature within the tire shred-soil embankment and the observed endothermic reactions provide evidence that through either mixing or layering tire shreds with soil minimizes the potential for an exothermic reaction. The analysis also showed that there was no correlation between the internal temperature or relative humidity and the heat generation rate within any of the tire shred-soil embankment sections as shown in Figures 99, 100, and 106. The only correlation determined was between the measured soil suction and heat generation within the tire shred-soil embankment, shown in Figures 103 and 104; consistent with the hypothesis that heat generation increases with increases in the moisture content.

Implications of Analysis

The results and analysis presented as part of this research project provide valuable insight into the mechanisms at play with a tire shred reinforced soil embankment. The findings from this analysis may also impact the currently recommended design guidelines and the methods currently adopted for construction of embankments reinforced with tire shreds. This section will provide a brief overview of the significance and implications of the results presented in the previous chapter.

Significance of Results

The significance of the results is mainly the confirmation that tire shreds can be used in civil engineering applications without having major concerns of exothermic reactions. The comparison of a large tire shred-only stockpile with the soil-only section showed a significant difference in their thermal responses. Further comparison between the layered and mixed sections showed that these layouts dramatically changed the thermal response of the tire shreds. The dramatic difference in the thermal response, exothermic for the large tire shred-only stockpile and endothermic for all the tire shred-soil embankment sections, demonstrate that tire shreds can be used beneficially within a soil reinforced structure without failure concerns associated with exothermic reactions.

Exothermic reactions, manifested as internal heating of the large tire shred-only stockpile were impacted by moisture more significantly than the tire shred-soil embankment. The layered and mixed sections showed endothermic reactions similar in trend and magnitude as the soil-only section, which provide additional proof that tire shreds can enhance the mechanical properties of the embankment without significantly impacting the thermal properties and responses of the structure. This finding is of importance in the future applications of tire shreds in civil engineering applications.

Implications on Design Guidelines

The current design guidelines were based upon case histories of tire shred reinforced embankment failures, specifically the three case histories discussed earlier. A committee consisting of government and industry leaders published a report, "Design Guidelines to Minimize Internal Heating of Tire Shred Fills," in 1997 that outlined recommendations for future construction of retaining structures using tire shreds as backfill material. One year later, the American Society of Testing and Materials published ASTM D6270: Standard Practice for Use of Scrap Tires in Civil Engineering Applications. The guidelines presented in ASTM D6270 will be addressed in light of the findings and results from this research which may either validate or contradict the recommendations.

ASTM D6270 addresses both the mechanical and thermal aspects of a tire shred reinforced embankment. The mechanical performance of the embankment will not be discussed in this thesis, but has been researched at this site and included in another report (Vollenweider, 2002). The thermal requirements of ASTM D6270 are summarized as follows: "The design guidelines given…have been developed to minimize the possibility for heating of tire shred fills by minimizing factors that could possibly create conditions favorable for this reaction." (ASTM, 1998) Table 10 summarizes the design guidelines included in ASTM D6270.

Table 10: Standard Practice for Use of Scrap Tires in Civil Engineering Applications

Tires should be shredded so that the largest shred is the lesser of one quarter circle in shape or 24 inches (0.6 meters) and at least one side wall should be cut from the tread.	
In applications where pavement is to be used or the tire shreds are used for drainage, the tire shred layer should be wrapped completely in either a woven or nonwoven geotextile in order to minimize the infiltration of soil particles into the voids.	
Tire shreds should be free of contaminants: oil, grease, gasoline, diesel fuel, etc.	
Tire shred fills should not include the remains of tires that have been subjected to a fire	
Class I Fill:	Maximum of 50% (by weight) passing the 1.5 in (38 mm) sieve
Height of tire shred layer: < 3.3 feet (1	Maximum of 5% (by weight) passing the 0.2 in (4.75 mm)

meter)	sieve
Class II Fill: Height of tire shred layer: 3.3 feet to 9.8 feet (1 to 3 meters)	Maximum of 25% (by weight) passing the 1.5 in (38 mm) sieve Maximum of 1% (by weight) passing the 0.2 in (4.75 mm) sieve The tire shreds should be free from fragments of wood, wood chips, and other fibrous organic matter Tire shreds should have less than 1% (by weight) of metal fragments, which are not at least partially encased in rubber. Metal fragments that are encased in rubber shall protrude no more than 1 in (25 mm) from the cut edge of the tire shred on 75% of the pieces and no more than 2 in (50 mm) on 100% of the pieces Infiltration of water shall be minimized Infiltration of air shall be minimized No direct contact between the tire shreds and soil containing organic matter, such as topsoil Tire shreds should be separated from the soil with a geotextile Drainage features at the bottom of the fill should be avoided in order to prevent free access to air

The ASTM D6270 design guidelines are overly conservative, and do not account for current research and other successful case histories. It is interesting to note that these design guidelines are based primarily on three failures as opposed to the large number of successful projects in New York, Minnesota, Washington and Oregon that have used tire shreds (WA DOT, 2003). The guidelines are complete in addressing the different potential causes of exothermic reactions, ranging from limiting the amount of exposed steel to limiting the infiltration of water or moisture into the fill. The guidelines adequately address means of limiting the potential causes of the potentially failure causing exothermic reactions, but they do not address preventive design recommendations. The guidelines attempt to limit the causes of reactions rather than suggest methods of successfully using tire shreds that would expand the applicable situations where they can be used. The findings from this research propose modifications to these guidelines to reflect the current state of knowledge.

The guidelines separate tire shred fills into two classes based on the thickness of the tire shred layers: Class I Fills with heights less than 3.3 feet (1 meter) and Class II Fills with heights between 3.3 feet and 9.8 feet (1 meter to 3 meters). The tire shred-soil embankment was 5 feet deep; however, the layers within the layered section were 6-inches thick, making this a Class I Fill. The mixed section was 4 feet thick with a 1 foot cover of soil and would be considered a Class II Fill, but because it is not entirely tire shreds, it would not be considered either a Class I or Class II Fill. The large tire shred-only stockpile was also a Class II Fill, being over 3 feet thick. The tire shreds used in this project were typically 2 inches to 6 inches long and 2 inches wide.

The most relevant impact on these design guidelines by this research include the separation of the tire shreds from the surrounding soil by a geotextile, and the control of the infiltration of water and air into the fill. The embankment layout for this research did not include a geotextile or any type of separation of the tire shreds and soil. The tire shreds were in direct contact with the layers of soil in the layered section and mixed directly with the soil in the mixed section. There were also no special measures taken to reduce the infiltration of water, such as paving the surface of the embankment or the use of a low hydraulic conductivity soils as a cover layer. This allowed precipitation to infiltrate directly into the embankment. In addition, there were no measures to minimize the infiltration of air.

Despite not following these design guidelines the reinforced embankment performed better than the tire shred pile in regards to the thermal response over the monitored time. It is significant to note that although the infiltration of water was not minimized, the reaction within the embankment was actually endothermic rather than exothermic. It was shown, however, that there was a correlation between the soil suction, hence the soil moisture, and the heat generation, which would support the requirement to minimize any additional moisture that could increase the water content. The fact that this tire shred-soil embankment did not experience an exothermic reaction indicates that the

guideline for minimization of water infiltration is a precaution rather than based on experimental validation.

In summary, the following conclusions were reached from the research presented in this thesis in relation to the existing design guidelines. The separation of the tire shreds from soil through use of a geotextile is to prevent localized sinkholes from infiltration of the soil into the voids of the tire shreds. The geotextile is required to improve the mechanical response of the embankment and has little bearing on the thermal response or internal heating of the tire shred-soil embankment. The layered and mixed sections of the tire shred-soil embankment had relatively similar thermal responses. However, a layered system would be the preferred method based upon it being the more economical design layout than mixing. The requirement to limit the infiltration of water and air into a tire shred-soil embankment should be relaxed for embankments that either layer or mix the tire shred with soil.

Conclusions

The research presented in this document addresses a technical challenge facing civil engineers involved in the beneficial reuse of waste tires within an embankment. The specific challenge involves understanding of the thermal response of tire shreds, which was evaluated in a full scale embankment over a period of 18 months. The primary objective of this research was to evaluate if tire shreds experience an exothermic reaction and subsequent internal heating when mixed or layered with soil. Other secondary objectives included evaluating design recommendations that will minimize the potential for exothermic reactions within tire shred embankments, defining the thermal properties of tire shred-soil embankments, and determining the effect of precipitation and other measured variables on the internal temperature.

Summary of Findings

The full scale embankment was constructed at Front Range Tire Recycle, Inc. in Sedalia, Colorado. The embankment consisted of three sections: a soil-only section, a section with tire shreds layered with soil, and a mixed section. The tire shred-soil embankment was instrumented to measure temperature, soil suction, and relative humidity at three different depths. In addition, a large tire shred-only stockpile located near the embankment was also instrumented to measure the temperature at four different depths. The embankment was monitored during 18 months and the large tire shred-only stockpile pile during 10 months.

The data collected from the tire shred-soil embankment and the large tire shred-only stockpile were compiled and used to determine the thermal conductivity, which was then used in a finite difference study to analyze the internal heat generation. The first step in the analysis was to determine time periods of purely conductive heat transfer, simplifying the method to determine the thermal conductivity values. The temperature

data from three time periods not experiencing rainfall was evaluated and used to determine the thermal conductivity of each tire shred-soil embankment section and of the large tire shred-only stockpile.

After the selection of the time periods, a graphical comparison of the internal daily average temperature at the different depths within the embankment and large tire shred-only stockpile with precipitation qualitatively determined the correlation between rainfall and temperature. The three dry time periods showed an average increase in temperature less than the average increase seen in the time periods following precipitation, which provides evidence that rainfall increases the heat generation within tire shred embankments. It is also important to note that the increase in temperature within the embankment during the wet time periods was less than that in the large tire shred-only stockpile. The mixed and layered sections did show an average increase in temperature greater than that observed in the soil-only section, which would correlate with the assumption that tire shreds would change the thermal properties increasing the heat generation and therefore temperature within the embankment sections. These qualitative findings support the prediction that the different embankment layouts, i.e. mixed and layered, are effective means of minimizing the potential for exothermic reactions within the tire shred reinforcement.

The thermal conductivity values determined from the dry time periods of assumed pure conductive heat transfer were determined to be 1.14 Btu/hr·ft·°F for the soil-only section, 1.23 Btu/hr·ft·°F for the layered section, 1.44 Btu/hr·ft·°F for the mixed section and 0.15 Btu/hr·ft·°F for the large tire shred-only stockpile. These values were reasonable when compared with previously published values for thermal conductivity within sandy soils and tire shreds. The higher value of the thermal conductivity of soil than tire shreds indicates that the heat is more readily dissipated within a soil than within a stockpile of only tire shreds. The higher values reported for the layered and mixed

sections indicate that heat would be more readily dissipated within the mixed section than the layered section due to the higher value reported.

The heat generation was analyzed using the finite differences method and the temperatures recorded over the time period at each depth. This analysis showed that there was greater heat generated within the large tire shred-only stockpile than in any of the three sections of the embankment. In fact, the large tire shred-only stockpile showed exothermic reactions of varying magnitudes for both the dry and wet time periods; whereas the embankment sections all showed endothermic reactions. The mixed section generally had less of an endothermic reaction than the layered and soil-only sections, which showed fairly comparable trends and values for the dry time periods. The layered section did, on average, show higher endothermic reactions than either the soil or mixed sections for the wet time periods. Each section showed a diurnal trend, with the large tire shred-only stockpile showing more pronounced differences in heat generation through a 24 hour time period.

The heat generation trends for the cumulative heat generated for both the dry and wet time periods were very similar for each of the embankment sections, with the large tire shred-only stockpile exhibiting a significant diurnal trend. The average heat generated over the wet time periods for the embankment sections showed only a slight difference between the wet and dry time periods, but with an average heat generation slightly more endothermic for the dry time periods. This trend was opposite for the tire shred embankment with the wet time periods showing more of an exothermic reaction than the dry time periods.

In summary, the heat generation analysis validated that either mixing or layering tire shreds minimizes the potential for exothermic reactions from occurring within an embankment reinforced with tire shreds. The endothermic reactions in the tire shred-soil embankment sections were in clear contrast to the exothermic reactions in the large tire shred-only stockpile. This shows that one of the most crucial elements in designing a

layout for tire shred reinforced embankments is the amount of isolated tire shreds. The difference in layout between the mixed and layered section was relatively minor, therefore there does not appear to be a distinct difference in the heat generated in either section.

These results also showed that precipitation does increase the reaction within the large tire shred-only stockpile, but does not necessarily affect the tire shred-soil embankment internal heat generation and internal temperature. This finding suggests that external moisture may contribute to increased internal heat generation. Therefore, the amount of moisture allowed within an embankment reinforced with tire shreds, specifically if there is a large quantity of tire shreds easily infiltrated by water, should be limited in order to prevent an exothermic reaction from occurring.

The results from the heat generation analysis were also compared with the other measured parameters to determine any correlation that may exist. There appeared to be no correlation between the heat generation rate and internal temperature, water content and relative humidity. The temperature and relative humidity plotted against the temperature showed a significant of scatter; whereas, the water content showed a constant value as the heat varied in magnitude. The only apparent correlation was between soil suction and the heat generation for soil suctions greater than zero. The plot of heat generated versus soil suction indicated that as the soil suction decreased, the heat generation rate increased. This correlation would indicate that as the moisture within the embankment increased, indicated by decreasing soil suction, the heat generation increases. This trend is in accordance to the hypothesis that the greater the moisture within the embankment, the more conducive the environment for the potential causes of exothermic reactions, such as oxidation of the steel belts.

The significance of the results is mainly the confirmation that tire shreds can be used in civil engineering applications without having major concerns of exothermic reactions. The comparison of a large tire shred-only stockpile with the soil-only section

showed a significant difference in their thermal responses. Further comparison between the layered and mixed sections showed that these layouts dramatically changed the thermal response of the tire shreds. The dramatic difference in the thermal response, exothermic for the large tire shred-only stockpile and endothermic for all the tire shred-soil embankment sections, demonstrate that tire shreds can be used beneficially within a soil reinforced structure without failure concerns associated with exothermic reactions.

The following conclusions were reached from the research presented in this thesis in relation to the existing design guidelines. The separation of the tire shreds from soil through use of a geotextile is to prevent localized sinkholes from infiltration of the soil into the voids of the tire shreds. The geotextile is required to improve the mechanical response of the embankment and has little bearing on the thermal response or internal heating of the tire shred-soil embankment. The layered and mixed sections of the tire shred-soil embankment had relatively similar thermal responses. However, a layered system would be the preferred method based upon it being the more economical design layout than mixing. The requirement to limit the infiltration of water and air into a tire shred-soil embankment should be relaxed for embankments that either layer or mix the tire shred with soil.

Recommendations for Future Research

The amount of data collected over the 18 month monitoring period is extensive enough to conduct further analysis of the thermal response of the different embankment sections. Additional data analysis can be conducted, though. This may involve an evaluation of the overall thermal response of the sections monitored over the entire 18 month period (rather than the select time periods that were evaluated in this research). The evaluation over the longer time period would provide greater insight into the seasonal affects, including temperature trends and moisture influx from both precipitation and infiltration from snow melt. The overall response would more clearly indicate any

correlation between all the parameters measured, due to the greater number of data points available for analysis. Of particular interest is to conduct further investigation into the correlations between the soil suction and the total heat generated in the three tire shred-soil embankment sections.

Future analysis could also focus on the time periods selected and analyzed in this research. The diurnal trends and the differences in heat generation related to the amount of precipitation received could be investigated. Additional evaluation should investigate the time dependency of the thermal conductivity values, and subsequent effect on the heat generation values. For example, the time periods used to evaluate the thermal conductivity were of different lengths, possibly numerically affecting the values reported and later used in the evaluation of the heat generated.

In regards to the thermal conductivity, it has been shown that the value of the soil thermal conductivity varies with the water content of the soil. These variations were neglected in this research; however, a sensitivity analysis would provide confirmation of this assumption. This analysis would determine the actual effects that the range in water contents determined from the soil suction measurements would have on the thermal conductivity values. A site specific relationship between water content and the thermal conductivity values of the different sections of the embankment soil in the embankment could be determined. From this relationship, the effect of the water content on the heat generated could be determined from the changes in the thermal conductivity caused by the change in moisture content.

To further confirm the findings from this research a laboratory component should be developed. A laboratory testing program would be able to more strictly control the boundary conditions and variables at play within the embankment. The ambient temperature, moisture content, and infiltration could be controlled and varied as desired to isolate variables and evaluate specific relationships between the thermal response of the tire shred-soil composite material with the measured parameters. It is recommended

that this laboratory component measure the thermal response of specimens that are similar to the embankment sections in terms of tire shred content, method of construction, (i.e. mixed or layered), and density. This testing could confirm the thermal conductivity values determined from the field data and could also validate the correlations determined in this research.

An additional topic that should be researched is the relationship of the thickness of the tire shred and soil layers in a layered system to the heat generation within the embankment. The thickness of the tire shred layer could enhance the heat dissipation, or it could prove to be detrimental to the performance of the embankment. Similarly, the percentage of tire shreds included in a mixed system could also prove to change the thermal response of the reinforced system. Research isolating these two variables, percentage of tire shreds and tire shred layer thickness, and their relationship to heat generation would prove invaluable in modifying the current design guidelines and the future of using tire shreds as inclusions in soil reinforcement technology.

References

Ad Hoc Civil Engineering Committee, 1997, "Design Guidelines to Minimize Internal Heating of Tire Shred Fills," *Scrap Tire Management Counsel*, Washington, D.C.

ASTM, 1998, "Standard Practice for Use of Scrap Tires in Civil Engineering Applications," ASTM D6270-98, *American Society for Testing and Materials*.

Ahmed, I., Lovell, C.W., 1993, "Rubber Soils as Lightweight Geomaterials," *Transportation Research Record 1422*, Transportation Research Board, Washington, D.C., pp. 61-70.

Benson, Craig H., Michael A. Olson, and Wayne R. Bergstrom, 1996, Temperatures of an Insulated Landfill Liner, Transportation Research Board, 75th annual meeting, Washington, D.C.

Biocycle, 1997, "Tire Shred Guidelines Minimize Fires," Vol. 38, No. 10, p. 56.

Bjerrum, L., 1963, "Allowable Settlement of Structures," *Proceedings, Third European Conf. Soil Mech. Found. Eng.*, Weisbaden Germany.

Bosscher, P.J., T.B. Edil, and N. Eldin, 1993, "Construction and Performance of Shredded Waste Tire Test Embankment," Transportation Research Record No. 1345, Transportation Research Board, Washington, D.C., pp. 44-52.

Bosscher, Peter J., Tuncer B. Edil, and Senro Kuraoka, 1997, "Design of Highway Embankments Using Tire Chips," Journal of Geotechnical and Geoenvironmental Engineering, Vol. 123, No. 4, April 1997, pp. 295-304.

Carslaw, H.S. and Jaeger, J.C., 1959, Conduction of Heat in Solids, 2nd ed., Oxford University Press, London, ISBN 0-19-853368-3.

Chen, L., 1996, "Laboratory Measurement of Thermal Conductivity of Tire Chips," Masters thesis, Department of Civil Engineering, University of Maine.

Devries, D.A. and Afgan, N.H., 1975, Heat and Mass Transfer in the Biosphere: Transfer Processes in Plant Environment, Washington.

Dickson, Todd H, Donald F. Dwyer, and Dana N. Humphrey, 2001, "Prototype Tire-Shred Embankment Construction," Transportation Research Record No. 1755, Transportation Research Board, Washington, D.C., pp. 160-167.

Dow, J.O., 1999, "A Unified Approach to the Finite Element Method and Error Analysis Procedures," Academic Press, ISBN 0-12-221440-4.

Eaton, R., R. Roberts, and D. Humphrey, 1994, "Gravel Road Test Sections Insulated With Scrap Tire Chips- Construction and First Year's Results," Special Report No. 94-21, USA Cold Regions Research & Engineering Laboratory, Hanover, NH.

Edil, T.B., and Bosscher, P.J., 1992, "Development of Engineering Criteria for Shredded or Whole Tires in Highway Applications," Final Report to Wisconsin Department of Transportation, GT-92-9, University of Wisconsin, Madison, Wisconsin.

Edil, T.B., and P.J. Bosscher, 1994, "Engineering Properties of Tire Chips and Soil Mixtures," Geotechnical Testing Journal, GTJODJ, Vol. 17, No. 4, December 1994, pp. 453-464.

"Emissions from Open Tire Fires," April 19, 2004, http://www.p2pays.org/ref/11/10504/html/intro/openfire.htm.

Engstrom, G. and Lamb, R., 1994, "Using Shredded Waste Tires as a Lightweight Fill Material for Road Subgrades." Minnesota Department of Transportation: Materials Research and Engineering Report 94-10.

"Environmental Problem Associated with Waste Tire," April 19, 2004, http://www.p2pays.org/ref/11/10504/html/intro/ploblems.htm.

EPA, 1991, "Summary of Markets for Scrap Tires," Report No. EPA/530-SW-90-0748B, US Environmental Protection Agency, Washington D.C., pp. 1-12.

Farouki, O.T., 1985, "Ground Thermal Properties," Thermal Design Considerations in Frozen Ground Engineering, ASCE, New York, NY, pp. 186-203.

Fitzgerald, T., December 2003, "Investigation of the Thermal Response of Tire Shred Fills," Masters Thesis, Department of Civil Engineering, University of Colorado, Boulder.

Foose, Gary J., Craig H. Benson, and Peter J. Bosscher, 1996, "Sand Reinforced with Shredded Waste Tires," Journal of Geotechnical Engineering, Vol. 122, No9, September 1996, pp. 760-767.

Fredlund, D. G., Rahardjo, H., 1993, *Soil Mechanics for Unsaturated Soils*, John Wiley & Sons, New York.

Fwa, T. F., 2003, "Highway and Airport Pavement Design," *The Civil Engineering Handbook*, second ed., CRC Press, Chen, W. F., ed., ch. 62.

Gacke, S., Lee, M., and Boyd, N., 1997, "Field Performance and Mitigation of Shredded Tire Embankment." *Transportation Research Record 1577*, pp. 81-89.

Garga, Vinod K., and Vince O'Shaughnessy, 2000, "Tire-Reinforced Earthfill. Part 1: Construction of a Test Fill, Performance, and Retaining Wall Design," Canadian Geotechnical Journal, Vol. 37, pp. 75-96.

Geisler, E., Cody, W.K., and Niemi, M.K., 1989, "Tires for Subgrade Support," Annual Conference on Forest Engineering, Coeur D'Alene, ID 5 pp.

Harr, M. E., 1966, *Foundations of Theoretical Soil Mechanics*, McGraw-Hill, New York.

Heimdahl, T.C., and Drescher, A., May 1999, "Elastic Anisotropy of Tire Shreds," *Journal of Geotechnical and Geoenvironmental Engineering*, Vol. 125, No. 5.

Holman, J.P., 1997, Heat Transfer, McGraw-Hill, International Edition, 8th Edition, ISBN 0-07-114320-3.

Hoppe, Edward J., 1998, "Field Study of Shredded-Tire Embankment," Transportation Research Record No. 1619, Transportation Research Board, Washington D.C., pp. 47-54.

Humphrey, D., and W. Manion, 1992, "Properties of Tire Chips for Lightweight Fill," Proceedings of the 1992 ASCE Specialty Conference on Grouting, Soil Improvement and Geosynthetics, Vol. 2, No. 30, ASCE, New York, N.Y., pp. 1344-1355.

Humphrey, Dana N., 1996, Investigation of Exothermic Reaction in Tire Shred Fill Located on SR100 in Ilwaco, Washington, Prepared for Federal Highway Administration, Washington, D.C.

Humphrey, D.N., 1997, "Civil Engineering Applications of Tire Shreds: A Short Course," *Organized by GeoSyntec Consultant, Inc*., June 1997.

Humphrey, Dana N., Li H. Chen, and Robert A. Eaton, 1997, Laboratory and Field Measurement of the Thermal Conductivity of Tire Chips for Use as Subgrade Insulation, Transportation Research Board, 76th annual meeting, Washington, D.C.

Humphrey, D.N., Katz, L.E., and Blumethal, M., 1997, "Water Quality Effects of Tire Chip Fills Placed Above the Groundwater Table," Testing Soil Mixed with Waste or Recycled Materials, ASTM STP 1275, ASTM, West Conshoshocken, Pa, pp. 299-313.

Humphrey, D. N., Katz, L. E. and Blumenthal, M., 1997, "Water Quality Effects of Tire Chip Fills Placed Above the Groundwater Table", Testing Soil Mixed with Waste or Recycled Materials, ASTM STP 1275, Mark A. Wasemiller, Keith B. Hoddinott,Eds, American Society for Testing and Materials.

Humphrey, D.N., Whetten, N., Weaver, J., Recker, K., and Cosgrove, T.A., 1998, "Tire Shreds as Lightweight Fill for Embankments and Retaining Walls," Proceedings of the Geo-Congress, ASCE, Reston, VA, pp. 51-65.

Humphrey, D.N., March 1999, "Civil Engineering Application of Tire Shreds," *Tire Industry Conference – Hilton Head Island, SC*.

Humphrey, D.N., and Katz, L.E., 2001, "Field Study of Water Quality Effects of Tire Shreds Placed Below the Water Table." *Proceedings of the Conference on Beneficial Use of Recycled Materials in Transportation Applications,* Air and Waste Management Association, Pittsburg, Pennsylvania.

Incropera, F.P. and DeWitt, D.P., 2002, Fundamentals of Heat and Mass Transfer, 5th ed., John Wiley and Sons, Inc., New Jersey, ISBN 0-471-38650-2.

Jumikis, A.R., 1977, Thermal Geotechnics, Rutgers University Press, New Jersy, ISBN 0-8135-0824-X.

Kersten, M.S., 1949, "Thermal Properties of Soils," Bulletin 28, Eng. Exp. Sta., University of Minnesota.

Knott Laboratory, 2000, Spontaneous Ignition Tests: Glenwood Canyon Hanging Lake Wall. Report KL 5186-1295, May 7, 1996.

Kreith, F., and Black, W.Z., 1980, Basic Heat Transfer, Hampshire & Row, Publishers, New York, ISBN 0-700-22518-8.

Lee, J.H., Salgado, R., Bernal, A., Lovell, C.W., 1999, "Shredded tires and rubber sand as lightweight backfill," *Journal of Geotechnical and Geoenvironmental Engineering*, ASCE, Vol. 125, No. 2, pp. 132-141.

Liu, H.S., Mead, J.L., Stacer, R.G., 1998, "Environmental Impacts of Recycled Rubber in Light Fill Applications: Summary and Evaluation of Existing Literature." *Chelsea Center for Recycling and Economic Development Plastics Conversion Project*.

Masad, E., R. Taha, C. Ho, and T. Papagiannakis, 1996, "Engineering Properties of Tire/Soil Mixtures as a Lightweight Fill Material," Geotechnical Testing Journal, GTODJ, Vol. 19, No. 3, September 1996, pp. 297-304.

Mitchell, James K., 1993, Fundamentals of Soil Behavior 2nd ed., New York, NY.

O'Shaughnessy, V., and Garga, V., 2000, "Tire-reinforced earthfill. Part 3: Environmental assessment." Canadian Geotechnical Journal, 37, pp. 117-131.

Papp, W.J. Jr., Maher, M.H., and Baker, R.F., 1997, "Use of Shredded Tires in the Subbase Layer of Asphalt Pavements," Testing Soil Mixed with Waste or Recycled Materials, ASTM STP 1275, *American Society for Testing and Materials*.

Poulos, H. G., Davis, E. H., 1974, *Elastic Solutions for Soils and Rock Mechanics*, John Wiley & Sons, New York.

Quian, X., Koerner, R. M., Gray, D. H., 2002, *Geotechnical Aspects of Landfill Design and Construction*, Prentice Hall, New Jersey.

Reddy, K. R., Marella, A., 2001, "Properties of Different Size Scrap Tire Shreds: Implications on Using as Drainage Material in Landfill Cover Systems," *Proceedings, 17th International Conference on Solid Waste Technology and Management*, October 2001, Philadelphia, PA.

Reddy, K. R., Saichek, R. E., 1998, "Characterization and Performance Assessment of Shredded Scrap Tires as Leachate Drainage Material in Landfills," *Proceedings, 14th International Conference on Solid Waste Technology and Manegement*, Philadelphia, PA.

Reisman, J., 1997, "Air Emissions from Scrap Tire Combustion." *EPA Project Summary*, EPA/600?SR-97/115.

"Response Strategies for Tire Fires (to reduce production of pyrolytic oil residue)." April 19, 2004, http://www.seaconsulting.com/workgroups/Pyrolytic%200il.Rev2.pdf.

RMA, 2002, "U.S. Scrap Tire Markets 2001," *Publication #ST-01*, Rubber Manufacturers Association, 37p.

Rosenbaum, David B., 2001, "California Will Use Tire Shreds as Embankment Fill in Pilot Job," Engineering News-Record, Vol. 247, No. 2, p. 18.

Rubber World, 1997, "Industry-Government Partnership Issues Design Guidelines for Tire Shred Fill Projects," Rubber World, Vol. 216, No. 5, pp. 14-15.

Sanger, F.J., 1963, "Degree-Days and Heat Conduction in Soils," Permafrost International Conference. National Academy of Science, Washington, D.C., pp. 253-262.

Tweedie, J. J., Humphrey, D. N., Sandford, T. C., 1998a, "Tire Shreds as Lightweight Retaining Wall Backfill: Active Conditions," *Journal of Geotechnical and Geoenvironmental Engineering*, ASCE, Vol. 124, No. 11, pp. 1061-1070.

Tweedie, J. J., Humphrey, D. N., Sandford, T. C., 1998b, "Full Scale Field Trials of Tire Chips as Lightweight Retaining Wall Backfill, At-Rest Conditions," *Transportation Research Record 1619*, Transportation Research Board, Washington, D.C., pp. 64-71.

Van Genuchten, M.T., 1980, Soil Science Society of America Journal, Vol. 44, pp. 892-98.

Violette, G.P., Colorado Department of Transportation. Personal Communication, July 2003.

Violette, G. P., 1995, "CDOT Rubber Retaining Wall in Glenwood Canyon: Project Summary Report and Fire Investigation Report," Colorado Department of Transportation.

Vollenweider, B., April 19, 2002, "Tire Shred Proposal: Field Study of the Thermal Behavior of Various Soil/Tire Shred Mixtures," Prepared for the Recycled Materials Resource Center, Durham, NH.

Vollenweider, B., December 15, 2002, "A Feasibility Study of the Integration of Tire-Shreds into Civil Engineering Applications: The Mechanical Performance of Two Soil/Tire-Shred Mixtures in a Prototype Road Embankment," Department of Civil Engineering, University of Colorado at Boulder.

Vollenweider, Brent, Alexandre Cabral, Tad Pfeffer, and Jorge Zornberg, 2002, Field Study of the Thermal Behavior of Various Soil/Tire Shred Mixtures, Geotechnical Research Report, University of Colorado at Boulder, Boulder, CO, pp. 1-35.

Washington State Department of Transportation, August 2003, "Evaluation of the Use of Scrap Tires Transportation Related Applications in the State of Washington," *Report to the Legislature as Required by SHB 2308*, Olympia, Washington.

Welle, Rick. Front Range Tire Recycle, Inc., Sedalia, CO. Personal Communication, October 2003.

Wu, J.T.H., Helwany, M.B., and Barret, R.K., September 1994, "Use of Shredded Tire as Backfill for a New GRS Reinforced Retaining Wall System," *Fifth International Conference on Geotextiles, Geomembranes and Related Products*, Singapore.

Wu, Wei Y., Benda, C. and Cauley, R.F., 1997, "Triaxial Determination of Shear Strength of Tire Chips," Journal of Geotechnical and Geoenvironmental Engineering, Vol. 123, No 5, pp. 479-482.

Zarling, J.P. and Braley, W.A., 1988. Geotechnical thermal analysis. Embankment Design and Construction in Cold Regions. Technical Council on Cold Regions Engineering, ASCE, New York, NY, pp. 35-92.

Zornberg, J.G. and Viratjandr, C. 2001, "Shear Strength of Tire Shred/Sand Mixtures," Geotechnical Research Report, University of Colorado at Boulder, August 2001.

Zornberg, J.G., E. Kroll, and A. Argentati, 2001, "Construction of a Prototype Embankment Using Tire Shreds." Geotechnical Research Report, University of Colorado at Boulder, August 2001.

Zornberg, J.G., Cabral, A.R., and Viratjandr, C. (2004). "Behaviour of Tire Shred-Sand Mixtures." Canadian Geotechnical Journal, April, Vol. 41, No. 2, pp. 227-241.

Zornberg, J.G., Costa, Y.D., and Vollenweider, B. (2004). "Performance of Prototype Embankment Built with Tire Shreds and Nongranular Soil." Transportation Research Record: Journal of the Transportation Research Board, December, No. 1874, TRB, National Research Council, Washington, D.C. pp. 70-77.

Appendix A: Construction Photos

Photographic Documentation of the Construction and Instrumentation of the Tire-Shred Soil Embankment, and Whole Tire, Tire Shred-Only and Large Tire Shred-Only Stockpiles

Photo A-1: Augering Holes

Photo A-2: Augering Holes (detail)

Photo A-3: Detail of PVC Hole

Photo A-4: Detail of PVC Pipe in Hole

Photo A-5: Three Augered Holes

Photo A-6: Seal Between Hole and Pipe

Photo A-7: Detail of Bentonite Seal

Photo A-8: Detail of Sealed Cap

Photo A-9: Layered Section Instruments

Photo A-10: Deployment of Instrumentation

Photo A-11: Installation of Data logger and Multiplexer

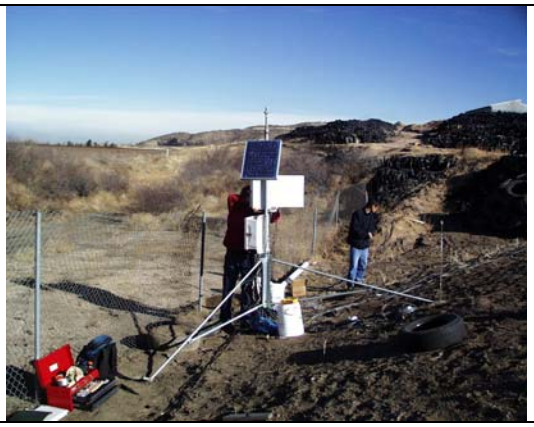

Photo A-12: View of Mount with Solar Panel, Datalogger and Multiplexer

Photo A-13: View of Layered Section

Photo A-14: Construction of Whole Tire Stockpile

Photo A-15: Construction of Tire Shred-Only Stockpile

Photo A-16: View of Tire Shred-Only and Whole Tire Stockpiles

Photo A-17: View of Tire Shred-Only Stockpile with Instrumentation

Photo A-18: View of Whole Tire Stockpile with Instrumentation

	
Photo A-19: View of Mount	Photo A-20: Sand Cone Test
	
Photo A-21: Side View of Large Tire Shred-Only Stockpile	Photo A-22: View of Large Tire Shred-Only Stockpile and Ditch Constructed for Instrumentation Installation
	
Photo A-23: Front View of Ditch in Large Tire Shred-Only Stockpile Excavated for Installation of Instrumentation	Photo A-24: Protection of Wiring of Instrumentation in the Large Tire Shred-Only Stockpile

Photo A-25: Installation of Wiring for Instrumentation of the Large Tire Shred-Only Stockpile

Photo A-26: Detail of Thermistor at the Surface of the Large Tire Shred-Only Stockpile

Photo A-27: Detail of Instrument Wiring in the Large Tire Shred-Only Stockpile

Photo A-28: Installation of Thermistor in the Large Tire Shred-Only Stockpile

Photo A-29: Closure of the Ditch Excavated for PVC Protecting Wiring of Instrumentation in the Large Tire Shred-Only Stockpile

Photo A-30: Closure of the Ditch Excavated for Installation of Instrumentation in the Large Tire Shred-Only Stockpile

	
Photo A-31: Detail of Laptop, Data logger and Wiring from the Large Tire Shred-Only Stockpile	Photo A-32: Data Acquisition Device (HOBO Data logger) for the Large Tire Shred-Only Stockpile

Appendix B: Instrumentation

Description of Instrumentation

Measured Variable	Model (Manufacturer/Distributor)	Scheme
Temperature of rubber chip and metal wire	In-house fabrication. YSI4408 0.2^{o}C interchangeable thermistor in half-bridge with 0.1 % precision resistor; resistance converted to temperature through 4th order polynomial interpolation to tabulated reference data.	N.A.
Soil and air temperature	Thermistor model 107-L (Campbell Scientific). Measures soil, air and water temperature w/ 50 ft of WIR CA 22AWG cable	
Soil moisture	Watermark 200 soil matric potential block (distributed by Campbell under model Nb 253-L) w/ 50 ft of WIR CA 22AWG cable	
Relative Humidity/Temperature	CS500 (Campbell Scientific; modified version of the Vaisala 50Y Humitter) with 50 ft of WIR CA 22AWG cable and Santoprene jacket	
Heat flux	HFT3 Soil Heat Flux Plate (Campbell Scientific) with 50 ft of CA 22AWG 2 COND BELDEN 8451 cable	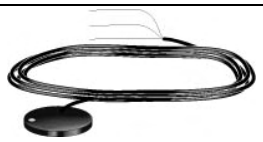
Data logger (Tire Shred-Soil Embankment)	CR10X (Campbell Scientific)	(See Appendix A)
Multiplexer	AM416 (Campbell Scientific)	(See Appendix A)

Solar radiation shield	RM Young 6 plate gill solar radiation shield (dirt. By Campbell Scientific)	
Solar Panel	MSX20R (Campbell Scientific)	(See Appendix A)
Temperature in tire shred stockpile	TMC50-HA, by Onset Computer Co. w/ 50 ft cable	
Data logger 2 (Large Tire Shred-Only Stockpile)	H08-008-04 Hobo Outdoor 4-Channel External, by Onset Computer Co.	(see Appendix A)

Computer Code Written to Control the Datalogger (Campbell Scientific CR10X)

```
;{CR10X}
;
*Table 1 Program
  01: 10          Execution Interval (seconds) NOTE: 10 sec for testing only
                                    ;planned interval is 15 minutes in field

;VERSION G 12 Feb 2002 - First version used in field


1:  Do (P86)
 1: 41          Set Port 1 High
; POWER ON Mplxr #1

2:  Beginning of Loop (P87)
 1: 0000        Delay
 2: 10          Loop Count

3:  Step Loop Index (P90)
 1: 2           Step
;Increment counter by 2 with each pass
;Result is 20 measurements into Input Locs 1-20

4:  Do (P86)
 1: 72          Pulse Port 2
;CLOCK Mplxr #1

5:  Excitation with Delay (P22)
 1: 3           Ex Channel
 2: 0           Delay W/Ex (units = 0.01 sec)
 3: 2           Delay After Ex (units = 0.01 sec)
 4: 0           mV Excitation
;Just waiting

6:  Excite-Delay (SE) (P4)
 1: 2           Reps
 2: 5           2500 mV Slow Range
 3: 3           SE Channel
 4: 1           Excite all reps w/Exchan 1
 5: 5           Delay (units 0.01 sec)
 6: 2500        mV Excitation
 7: 1       -- Loc [ th1_volt  ]
 8: 1.0         Mult
 9: 0.0         Offset
;TWO REPS - goes with increment 2

7:  End (P95)
;END OF THERMISTOR LOOP

8:  Beginning of Loop (P87)
 1: 0000        Delay
 2: 5           Loop Count
;MEASURE 10 CS500s

9:  Step Loop Index (P90)
```

```
 1: 2         Step
;10 measurements total,
;measurements go into Input locs 42-52

10:  Do (P86)
 1: 72        Pulse Port 2
;CLOCK mplxr $1. NOTE NO RESET - these come
;directly after thermistors on panel

11:  Excitation with Delay (P22)
 1: 3         Ex Channel
 2: 0         Delay W/Ex (units = 0.01 sec)
 3: 2         Delay After Ex (units = 0.01 sec)
 4: 0         mV Excitation
;just waiting

12:  Temp (107) (P11)
 1: 2         Reps
 2: 3         SE Channel
 3: 1         Excite all reps w/E1
 4: 42     -- Loc [ T107_1     ]
 5: 1.0       Mult
 6: 0.0       Offset

13:  End (P95)
;END 107 measurements

14:  Do (P86)
 1: 51        Set Port 1 Low
;POWER OFF Mplxr #1

15:  Beginning of Loop (P87)
 1: 0000      Delay
 2: 20        Loop Count
;Call Temperature calculation subroutine 20 times

16:  Do (P86)
 1: 1         Call Subroutine 1

17:  End (P95)
;End Temperature measurements

;NEXT move on to next mplxr ----------------------

18:  Do (P86)
 1: 43        Set Port 3 High
;POWER ON Mplxr 2


19:  Excitation with Delay (P22)
 1: 3         Ex Channel
 2: 0         Delay W/Ex (units = 0.01 sec)
 3: 2         Delay After Ex (units = 0.01 sec)
 4: 0         mV Excitation
;Wait

20:  Beginning of Loop (P87)
```

```
 1: 0000      Delay
 2: 5         Loop Count
;Measure 9 Soil Moistures in
;5 1/2 sets of 2


21:  Do (P86)
 1: 74        Pulse Port 4
;CLOCK Mplxr #2

22:  Step Loop Index (P90)
 1: 2         Step
;Increment counter by 2 with each pass


23:  AC Half Bridge (P5)
 1: 2         Reps
 2: 14        250 mV Fast Range
 3: 1         SE Channel
 4: 2         Excite all reps w/Exchan 2
 5: 250       mV Excitation
 6: 53     -- Loc [ SoilM_1    ]
 7: 1.0       Mult
 8: 0.0       Offset
;Inputs for 2 sensors go into 1H and 1L on logger


24:  End (P95)
;End Soil Moisture loop


25:  Do (P86)
 1: 53        Set Port 3 Low
;POWER OFF Mplxr #2


26:  BR Transform Rf[X/(1-X)] (P59)
 1: 9         Reps
 2: 53     -- Loc [ SoilM_1    ]
 3: 1.0       Multiplier (Rf)
;For soil moisture calculation 3/2 NOTE: Par 2 is incremented in
;                                        example program in manual


27:  Do (P86)
 1: 43        Set Port 3 High
;POWER ON Mplxr #2 again - this time for CS500 measurements
;NOTE DIFERENCE from Mplxr 1 - here the mplxr is reset because
;the CS500s start back at channel 1

28:  Do (P86)
 1: 45        Set Port 5 High
;POWER ON CS500s


29:  Excitation with Delay (P22)
 1: 3         Ex Channel
```

```
 2: 0         Delay W/Ex (units = 0.01 sec)
 3: 2         Delay After Ex (units = 0.01 sec)
 4: 0         mV Excitation
;Wait

30:  Beginning of Loop (P87)
 1: 0000      Delay
 2: 7         Loop Count
;Measure 7 CS500s

31:  Do (P86)
 1: 74        Pulse Port 4
;CLOCK Mplxr #2

32:  Step Loop Index (P90)
 1: 1         Step
;Increment counter by 2 with each pass - pick up
;other 2 lines on each channel


33:  Volt (SE) (P1)
 1: 1         Reps
 2: 5         2500 mV Slow Range
 3: 5         SE Channel
 4: 71     -- Loc [ CS500_T1  ]
 5: 0.1       Mult
 6: -40.      Offset
;SE5 = 3H. Mult & Offset give T in Celcius


34:  Volt (SE) (P1)
 1: 1         Reps
 2: 5         2500 mV Slow Range
 3: 6         SE Channel
 4: 78     -- Loc [ CS500_RH1 ]
 5: 0.1       Mult
 6: 0.0       Offset
;SE6 = 3L. Mult and Offset for RH in percent

35:  End (P95)
;END CS500 measurements

36:  Do (P86)
 1: 55        Set Port 5 Low
;POWER OFF CS500s

37:  Do (P86)
 1: 74        Pulse Port 4
;CLOCK Mplxr #2 ONE LAST TIME for Heat Flux

38:  Volt (SE) (P1)
 1: 1         Reps
 2: 2         7.5 mV Slow Range
 3: 5         SE Channel
 4: 87        Loc [ HeatFlx_1 ]
 5: 34.8      Mult
 6: 0.0       Offset
```

```
;Measure 1 heat flux
;UNIT s/n H013081


39:  Volt (SE) (P1)
 1: 1         Reps
 2: 2         7.5 mV Slow Range
 3: 6         SE Channel
 4: 88        Loc [ HeatFlx_2 ]
 5: 37.4      Mult
 6: 0.0       Offset
;UNIT s/n H013078

40:  Do (P86)
 1: 53        Set Port 3 Low
;POWER OFF Mplxr #2


;-------------------------------------DO Water content calculations:
;ASSUMING ONE RELEVANT TEMPERATURE for now...

;Calculate temperature correction factor
41:  Z=X+F (P34)
 1: 42        X Loc [ T107_1    ]
 2: -21       F
 3: 90        Z Loc [ WCtemp    ]

42:  Z=X*F (P37)
 1: 90        X Loc [ WCtemp
 2: 0.018     F
 3: 90        Z Loc [ WCtemp    ]

43:  Z=X+F (P34)
 1: 90        X Loc [ WCtemp    ]
 2: -1        F
 3: 90        Z Loc [ WCtemp    ]

44:  Z=X*F (P37)
 1: 90        X Loc [ WCtemp    ]
 2: -1        F
 3: 90        Z Loc [ WCtemp    ]

45:  Beginning of Loop (P87)
 1: 0         Delay
 2: 9         Loop Count
;Calculate 9 water contents ASSUMING T = WCtemp

46:  Z=X/Y (P38)
 1: 53     -- X Loc [ SoilM_1   ]
 2: 90        Y Loc [ WCtemp    ]
 3: 91     -- Z Loc [ WCont_1
;THIS CORRECTS FOR TEMPERATURE

47:  Z=X*F (P37)
 1: 91     -- X Loc [ WCont_1
 2: 0.07407   F
 3: 91     -- Z Loc [ WCont_1   ]
```

```
;SCALE FACTOR for resistance > water pressure

48:  Z=X+F (P34)
 1: 91     -- X Loc [ WCont_1   ]
 2: -.03704  F
 3: 91     -- Z Loc [ WCont_1   ]
;OFFSET for resistance > water pressure
;THIS IS THE FINAL WATER CONTENT in
;SOIL WATER POTENTIAL (bars)

49:  End (P95)
;END CALCULATION LOOP

50:  If time is (P92)
 1: 0        Minutes (Seconds --) into a
 2: 60       Interval (same units as above)
 3: 10       Set Output Flag High (Flag 0)


51:  Real Time (P77)
 1: 0220     Day,Hour/Minute (midnight = 2400)


52:  Average (P71)
 1: 20       Reps
 2: 22       Loc [ th1_temp  ]
;Average values for 20 Thermistors

53:  Average (P71)
 1: 10       Reps
 2: 42       Loc [ T107_1    ]
;Average values for 10 107s

54:  Average (P71)
 1: 7        Reps
 2: 71       Loc [ CS500_T1  ]
;Average values for 7 CS500 Temperatures

55:  Average (P71)
 1: 7        Reps
 2: 78       Loc [ CS500_RH1 ]
;Average values for 7 CS500 RH's

56:  Average (P71)
 1: 9        Reps
 2: 91       Loc [ WCont_1   ]
;Average vlaues for 7 water pressures

57:  Average (P71)
 1: 2        Reps
 2: 87       Loc [ HeatFlx_1 ]
;Average values for 2 heat fluxes

58:  Do (P86)
 1: 20       Set Output Flag Low (Flag 0)

*Table 2 Program
```

```
  02: 0.0000    Execution Interval (seconds)

*Table 3 Subroutines
1:  Beginning of Subroutine (P85)
 1: 01        Subroutine 1
;Fit thermistor output voltage to temperature
;with 5th order polynomial. Coefficients calculated
;previously in IDL. See D:\MyFiles\CSIstuff\Temperature\TcCoeffFit.pro
;Coefficients are for YSI4408 interchangeable thermistor.

2:  Z=F (P30)
 1: 2500      F
 2: 00        Exponent of 10
 3: 121       Z Loc [ Calcs     ]

3:  Z=X-Y (P35)
 1: 121       X Loc [ Calcs     ]
 2: 1      -- Y Loc [ th1_volt  ]
 3: 122       Z Loc [ _________ ]


4:  Z=X/Y (P38)
 1: 1      -- X Loc [ th1_volt  ]
 2: 122       Y Loc [ _________
 3: 123       Z Loc [ _________ ]


5:  Z=X*F (P37)
 1: 123       X Loc [ _________ ]
 2: 31.723    F
 3: 124       Z Loc [ _________ ]


6:  Z=X*F (P37)
 1: 124       X Loc [           ]
 2: 0.01      F
 3: 125       Z Loc [           ]


7:  Polynomial (P55)
 1: 1         Reps
 2: 125       X Loc [ _________ ]
 3: 22     -- F(X) Loc [ th1_temp  ]
 4: 44.713    C0
 5: -86.121   C1
 6: 57.268    C2
 7: -19.68    C3
 8: 2.5978    C4
 9: 0.0       C5


8:  End (P95)
End Program
```

CDMA Digital Cellular Modem

Models Redwing100, Redwing105

The Redwing100 and Redwing105 are full-duplex, digital cellular modems that communicate with the base station computer via a Code Division Multiple Access (CDMA) network and the Public Switched Telephone Network (PSTN). The Redwing100 and Redwing105 differ in the CDMA network used. The Redwing100 uses the Verizon Wireless network, and the Redwing105 uses the Alltel network. Both modems are manufactured by AirLink.

Features

- Supports mobile applications and datalogger sites where phone lines have not been established
- Uses IS-95 Circuit Switched CDMA
- Housed in a rugged aluminum case
- Provides lower operating costs and initial equipment investment than analog cellular
- Operates over a wide temperature range of -30° to +75°C

Typical System

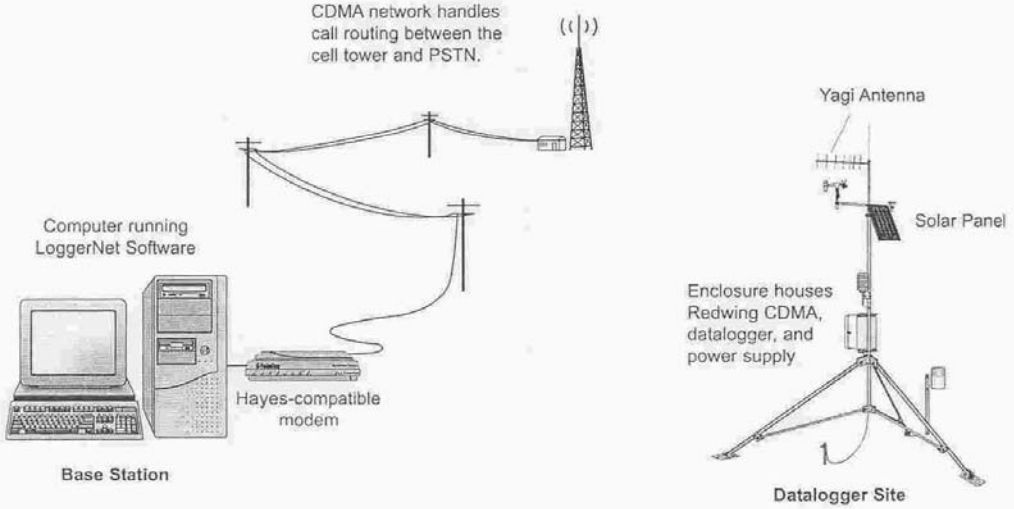

CAMPBELL SCIENTIFIC, INC.
815 W. 1800 N. • Logan, Utah 84321-1784 • (435) 753-2342 • FAX (435) 750-9540 • www.campbellsci.com

Base Station Requirements

- PC running LoggerNet software.
- Subscription to a CDMA network with coverage at the datalogger site. Prior to purchase, contact Verizon Wireless or Alltel to ensure that they provide CDMA coverage for your site.
- Hayes-compatible modem

Datalogger Site Equipment

- Redwing100 or Redwing105 Modem—includes power cable; the modem is configured using a terminal emulation program such as Microsoft® Windows HyperTerminal.
- Datalogger—CR510, CR10(X), CR23X, CR7, or CR5000
- SC105 or SC932A Interface—connects the modem to the datalogger's CS I/O port. Alternatively when using a CR23X or CR5000, a 14392 Null Modem Cable can be used to connect the modem to the datalogger's RS-232 port instead of the CS I/O port.
- 14394 Redwing Mounting Kit—includes mounting hardware for securing the modem to an environmental enclosure and a 9-pin male to 9-pin female cable.
- Antenna—the following antennas are offered from Campbell Scientific; sites near the edge of the CDMA coverage may require the Yagi antenna. Contact an Applications Engineer for help in determining the best antenna for your application.

  14453 0 dBd ½ Wave Dipole Whip Cellular Antenna

  14454 8 dBd Yagi Cellular Antenna with 10' Cable
- Power Supply (see power considerations)
- Environmental Enclosure—typically a 12" x 14" or 16" x 18" enclosure

Power Considerations

A power cable included with the modem connects to the datalogger's 12 V or switched 12 V terminal. Connection to the switched 12 V terminal allows the datalogger to switch power to the modem during scheduled transmission intervals, thereby conserving power. When using the switched 12 V terminal, the modem can be powered with a BP12 battery, CH100 charger/regulator, and MSX10 solar panel. For help on analyzing your system's power requirements, refer to our Power Supply product literature or application note.

Specifications

RF Output:	224 mW (+23.5 dBm)
Dual-band support:	800 MHz cellular, 1.9 GHz PCS bands
Data Rate:	9600 bps (CR510, CR10(X), CR7), up to 14.4 kbps (CR23X, CR5000)
IS-95B Circuit-Switched Mode:	G3 facsimile receive and transmit, Quick Net Connect (QNC) support
Short Message Service:	Send and receive, notification of new messages
Input Voltage:	10 to 28 Vdc
Input Current:	20 to 350 mA
Typical Current Drain at 12 Vdc:	20 mA dormant connection (idle for 10 to 20 seconds), 120 mA while receiving, 120 mA during transmission
Operating Temperature Range:	-30° to 75°C with transmissions limited to a 10% duty cycle above 60°C
Humidity:	5% to 95% non-condensing
Serial Interface:	RS-232, DB-9F
RF Antenna Connector:	50 Ohm TNC female
Status LEDs:	Power, Registration, Transmit, Receive
Dimensions:	3"W x 1"D x 5.1"L (5.8" w/ connector), 7.6 x 2.5 x 13 cm (14.7 cm w/connector)
Weight:	<1 lb. (<0.5 kg)

Configuring the AirLink CDMA Redwing for use with Campbell Scientific, Inc. Dataloggers

Items needed:

- Computer with a COM port.
- 9-pin cable to connect between the computer and the Redwing.
- A terminal program on the computer "HyperTerminal".
- 12 volt DC applied to the Redwing.
- CDMA account → phone #
  System Identification Number

HyperTerminal setup

HyperTerminal can be found on most Windows computers under START | PROGRAMS | ACCESSORIES | COMMUNICATIONS.

Several windows will come up one at a time to set the program up. The **Connection Description** will prompt you to enter a name for the connection. This can be any name you choose. Next you will see the **Connect To** window. On this window change the "Connect using" to COM1 or the available COM port you will be using. → the other sections will go blank.

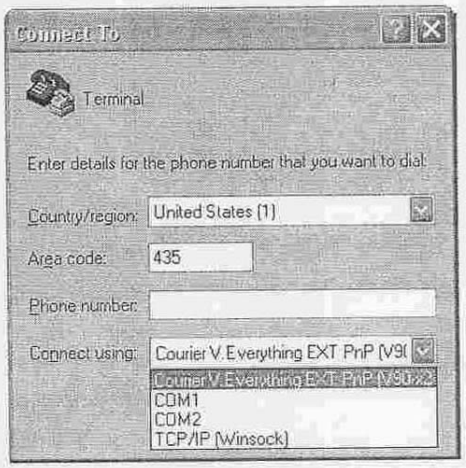

The last window is the **COM1 Properties**. Set the Bits per second to ~~115200~~ 9600, Data bits to 8, Parity to None, Stop bits to 1 and the Flow control to None.

click on OK.

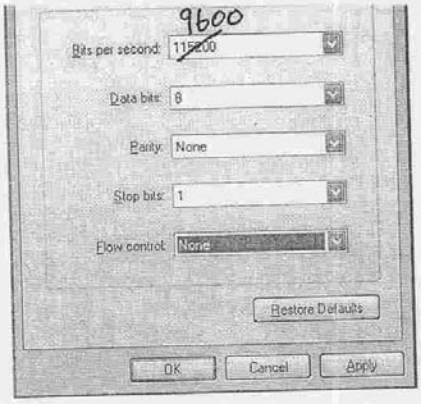

Already done

Now that HyperTerminal is setup, apply power to the Redwing and connect it to the computer via the 9-pin serial cable. → disconnect 9-Pin cable from datalo & place in connect on back of computer.

~~Enter the following AT command: at+ipr=9600 and then press Enter.~~

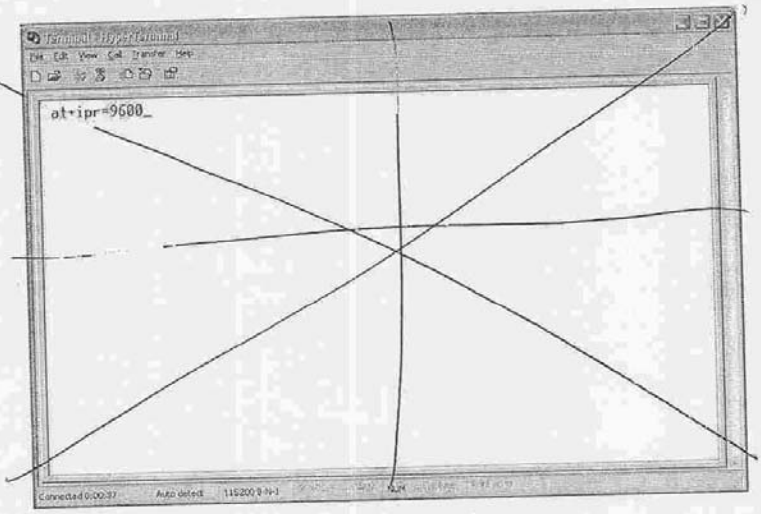

~~This has now changed the bits per second rate from 115200 to 9600. You need to change the bit per second rate in HyperTeminal to 9600 now. At the top of the~~ HyperTerminal window select **Call** ~~and then~~ **Disconnect**. Now select **File | Properties** and then the *Configure* Button. ~~Change the Bits per second rate to 9600. Once you have selected OK and are back to the terminal window select **Call | Call**.~~

Programming the Redwings Phone number

Your provider should give you a Phone number and a System Identification (SID) number to program into the Redwing.

Do the following substituting the phone number and SID with yours:
(*Example Phone number* - 4355551212, *SID* - 134)

- Type **AT~NAMLCK=000000** then press Enter. → The screen will say "OK".
- Type **AT~NAMVAL=0,4355551212,134,65535** then press Enter.

NOTE: there are no O's in the above strings, they are Zero's.

Remove the power from the Redwing and power it up again. → remove black power cord from side of modem & the re-connect.

You can type **AT~NAMVAL?0** to make sure your phone was programmed correctly.

Programming the Redwing for use with a datalogger

The Redwing needs a few settings changed in it to power-up ready to work with the datalogger.

Enter the following:

- Type **AT+ATINIT=&C1S0=1Q1V$QCVAD=4%+IFC=0^0,C,%,^** then press Enter.
- Type **AT+ATINITSTATE=1** then press Enter.

NOTE: there are no O's in the above strings, they are Zero's.

Remove the power from the Redwing and power it up again. It should be ready to use. If at all possible, test the communications before you take the equipment into the field.

MODEL 107 TEMPERATURE PROBE
INSTRUCTION MANUAL

REVISION: 6/00

Warranty and Assistance

The **MODEL 107 TEMPERATURE PROBE** is warranted by CAMPBELL SCIENTIFIC, INC. to be free from defects in materials and workmanship under normal use and service for twelve (12) months from date of shipment unless specified otherwise. Batteries have no warranty. CAMPBELL SCIENTIFIC, INC.'s obligation under this warranty is limited to repairing or replacing (at CAMPBELL SCIENTIFIC, INC.'s option) defective products. The customer shall assume all costs of removing, reinstalling, and shipping defective products to CAMPBELL SCIENTIFIC, INC. CAMPBELL SCIENTIFIC, INC. will return such products by surface carrier prepaid. This warranty shall not apply to any CAMPBELL SCIENTIFIC, INC. products which have been subjected to modification, misuse, neglect, accidents of nature, or shipping damage. This warranty is in lieu of all other warranties, expressed or implied, including warranties of merchantability or fitness for a particular purpose. CAMPBELL SCIENTIFIC, INC. is not liable for special, indirect, incidental, or consequential damages.

Products may not be returned without prior authorization. To obtain a Returned Materials Authorization (RMA), contact CAMPBELL SCIENTIFIC, INC., phone (435) 753-2342. After an applications engineer determines the nature of the problem, an RMA number will be issued. Please write this number clearly on the outside of the shipping container. CAMPBELL SCIENTIFIC's shipping address is:

CAMPBELL SCIENTIFIC, INC.
RMA#_____
815 West 1800 North
Logan, Utah 84321-1784

CAMPBELL SCIENTIFIC, INC. does not accept collect calls.

Non-warranty products returned for repair should be accompanied by a purchase order to cover the repair.

CAMPBELL SCIENTIFIC, INC.

815 W. 1800 N.
Logan, UT 84321-1784
USA
Phone (435) 753-2342
FAX (435) 750-9540
www.campbellsci.com

Campbell Scientific Canada Corp.
11564 -149th Street
Edmonton, Alberta T5M 1W7
CANADA
Phone (780) 454-2505
FAX (780) 454-2655

Campbell Scientific Ltd.
Campbell Park
80 Hathern Road
Shepshed, Loughborough
LE12 9GX, U.K.
Phone +44 (0) 1509 601141
FAX +44 (0) 1509 601091

Model 107 Temperature Probe

1. General

The 107 Temperature Probe uses a thermistor to measure temperature. Custom lead lengths are available up to 1000 ft.

The 107 Temperature Probe is designed for measuring air/soil/water temperatures. For air temperature, a 41301 radiation shield is used to mount the 107 Probe and limit solar radiation loading. The probe is designed to be buried or submerged in water to 50' (21 ps).

1.1 Specifications

Temperature Measurement Range:	-35 ° to +50°C
Thermistor Inter-changeability Error:	Typically < ±0.2°C over 0°C to 60°C; ±0.4 @ -35°C
Temperature Survival Range:	-50°C to +100°C
Polynomial Linearization Error:	<±0.5°C over -35°C to +50°C
Time Constant In Air:	Between 30 and 60 seconds in a wind speed of 5 m s^{-1}

NOTE The black outer jacket of the cable is Santoprene ® rubber. This compound was chosen for its resistance to temperature extremes, moisture, and UV degradation. However, this jacket will support combustion in air. It is rated as slow burning when tested according to U.L. 94 H.B. and will pass FMVSS302. Local fire codes may preclude its use inside buildings.

2. Accuracy

The overall probe accuracy is a combination of the thermistor's interchangeability specification, the precision of the bridge resistors, and the polynomial error. In a "worst case" all errors add to an accuracy of ±0.4°C over the range of -24 ° to 48°C and ±0.9°C over the range of -38 °C to 53 °C. The major error component is the interchangeability specification of the thermistor, tabulated in Table 2-1. For the range of 0° to 50°C the interchangeability error is predominantly offset and can be determined with a single point calibration. Compensation can then be done with an offset entered in the measurement instruction. The bridge resistors are 0.1% tolerance with a 10 ppm temperature coefficient. Polynomial errors are tabulated in Table 2-2 and plotted in Figure 2-1.

TABLE 2-1. Thermistor Interchangeability Specification	
Temperature (°C)	Temperature Tolerance (±°C)
–40	0.40
–30	0.40
–20	0.32
–10	0.25
0 to +50	0.20

TABLE 2-2. Polynomial Error	
-40 to +56	<±1.0°C
-38 to +53	<±0.5°C
-24 to +48	<±0.1°C

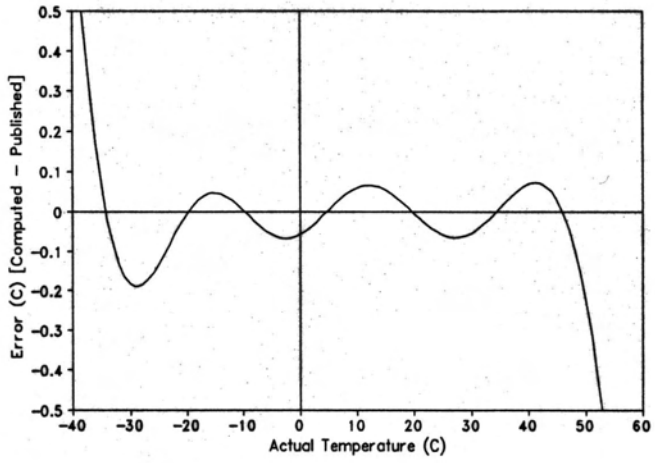

FIGURE 2-1. Error Produced by Polynomial Fit to Published Values

3. Installation and Wiring

For air temperature measurement, the 107 must be housed inside a radiation shield when used outdoors. The 41301 Radiation Shield (see Figure 3-1) mounts to a CM6 or CM10 tripod. The UT018 mounting arm and UT6 Radiation Shield mount to a UT930 tower.

The standard lead length of 6 feet and 9 feet allow the 107 to be mounted at a 2 meter height on the CM6/CM10 tripod or the UT930 tower respectively.

Connections to the datalogger for the 107 are shown in Figure 3-2 and Table 3-1.

The number of 107 probes per excitation channel is physically limited by the number of lead wires that can be inserted into a single excitation terminal (approximately 6).

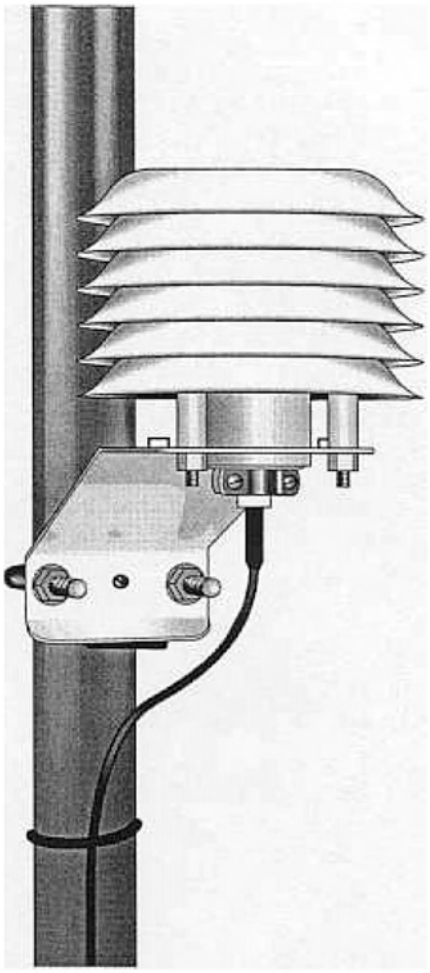

FIGURE 3-1. 107 and 41301 Radiation Shield on a CM6/CM10 Tripod Mast

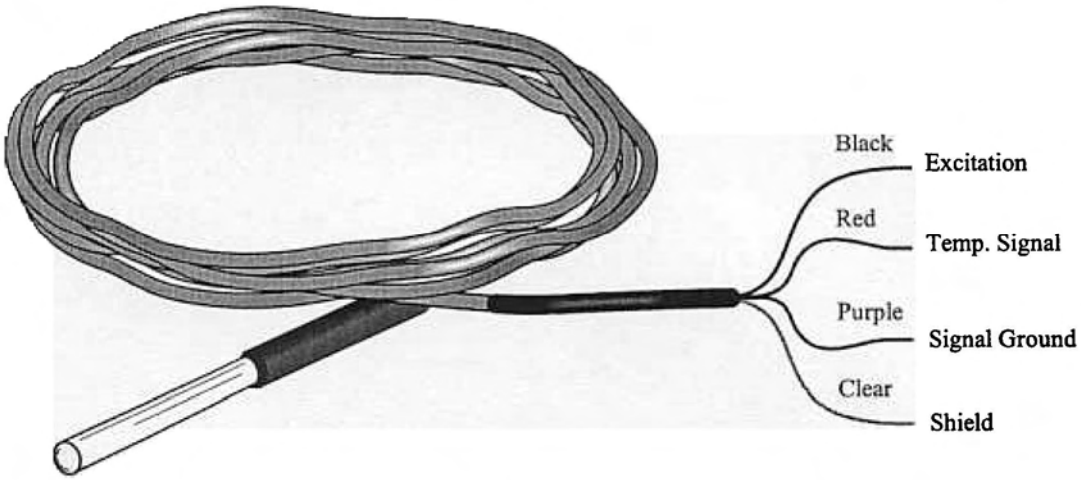

FIGURE 3-2. 107 Probe Datalogger Connections

TABLE 3-1. Sensor Wiring

Color	Function	CR10(X), CR510	21X, CR7,CR23X
Black	Excitation	Switched Excitation	Switched Excitation
Red	Signal	Single-Ended Channel	Single-Ended Channel
Purple	Signal Ground	AG	⏚
Clear	Shield	G	⏚

4. Programming

This section is for users who write their own datalogger programs. A datalogger program to measure this sensor can be created using Campbell Scientific's Short Cut Program Builder software. You do not need to read this section to use Short Cut.

Instruction 11 is used to measure temperature. Instruction 11 provides AC excitation, makes a single ended voltage measurement, and calculates temperature with a fifth order polynomial. A multiplier of 1.0 and an offset of 0.0 yields temperature in Celsius. For Fahrenheit, use a multiplier of 1.8 and an offset of 32.

TABLE 4-1. Wiring for Example Program

Color	Function	CR10(X)
Black	Excitation	Switched Ex Channel 3
Red	Signal	Single-Ended Channel 9
Purple	Signal Ground	AG
Clear	Shield	G

Example 1. Sample Program

```
1: Temp (107) (P11)
   1:        1        Reps
   2:        9        SE Channel
   3:        3        Excite all reps w/E3
   4:        1        Loc [ Air_Temp ]
   5:        1.0      Mult
   6:        0.0      Offset
```

Excitation/Integration Codes

Code	Result
0x	excite all rep with channel x
1x	increment chan x with each rep
2x	excite all reps with channel x, 60 Hz rejection, 10 ms delay
3x	excite all reps with channel x, 50 Hz rejection, 10 ms delay
4x	increment chan x with each rep, 60 Hz rejection, 10 ms delay
5x	increment chan x with each rep, 50 Hz rejection, 10 ms delay

5. Maintenance and Calibration

The 107 Probe requires minimal maintenance. Check monthly to make sure the radiation shield is free from debris.

For most applications it is unnecessary to calibrate the 107 to eliminate the thermistor offset. However, for those users that are interested, the following briefly describes calibrating the 107 probes.

A single point calibration can be performed to determine the 107 temperature offset (thermistor interchangeability). This calibration will not remove the polynomial error. The value of the offset must be chosen so that the probe outputs the temperature calculated by the polynomial, not the actual calibration temperature. For example, a 107 is placed in a calibration chamber that is at 0 °C and the probe outputs 0.1 °C. The offset is -0.16, because at 0 °C the polynomial calculates a temperature of -0.06 °C (Table 6-1).

6. Instruction 11 Details

Understanding the details in this section are not necessary for general operation of the 107 Probe with CSI's dataloggers.

Instruction 11 outputs a precise 2 VAC excitation (4 V with the 21X) and measures the voltage drop due to the sensor resistance (Figure 6-1). The thermistor resistance changes with temperature. Instruction 11 calculates the ratio of voltage measured to excitation voltage (Vs/Vx) which is related to resistance, as shown below:

$$Vs/Vx = 1000/(Rs+249000+1000)$$

where Rs is the resistance of the thermistor.

See the measurement section of the datalogger manual for more information on bridge measurements.

Instruction 11 then calculates temperature using a fifth order polynomial equation correlating Vs/Vx with temperature. The polynomial coefficients are given in Table 6-2. The polynomial input is (Vs/Vx) *800. Resistance and datalogger output at several temperatures are shown in Table 6-1.

TABLE 6-1. Temperature, Resistance, and Datalogger Output

Temperature °C	Resistance OHMS	Output °C
-40.00	4067212	-39.18
-38.00	3543286	-37.55
-36.00	3092416	-35.83
-34.00	2703671	-34.02
-32.00	2367900	-32.13
-30.00	2077394	-30.18
-28.00	1825568	-28.19
-26.00	1606911	-26.15
-24.00	1416745	-24.11
-22.00	1251079	-22.05
-20.00	1106485	-20.00
-18.00	980100	-17.97
-16.00	869458	-15.95
-14.00	772463	-13.96
-12.00	687276	-11.97
-10.00	612366	-10.00
-8.00	546376	-8.02
-6.00	488178	-6.05
-4.00	436773	-4.06
-2.00	391294	-2.07
0.00	351017	-0.06
2.00	315288	1.96
4.00	283558	3.99
6.00	255337	6.02
8.00	230210	8.04
10.00	207807	10.06
12.00	187803	12.07
14.00	169924	14.06
16.00	153923	16.05
18.00	139588	18.02
20.00	126729	19.99
22.00	115179	21.97
24.00	104796	23.95
26.00	95449	25.94
28.00	87026	27.93
30.00	79428	29.95
32.00	72567	31.97
34.00	66365	33.99
36.00	60752	36.02
38.00	55668	38.05
40.00	51058	40.07
42.00	46873	42.07
44.00	43071	44.05
46.00	39613	46.00
48.00	36465	47.91
50.00	33598	49.77
52.00	30983	51.59
54.00	28595	53.35
56.00	26413	55.05
58.00	24419	56.70
60.00	22593	58.28

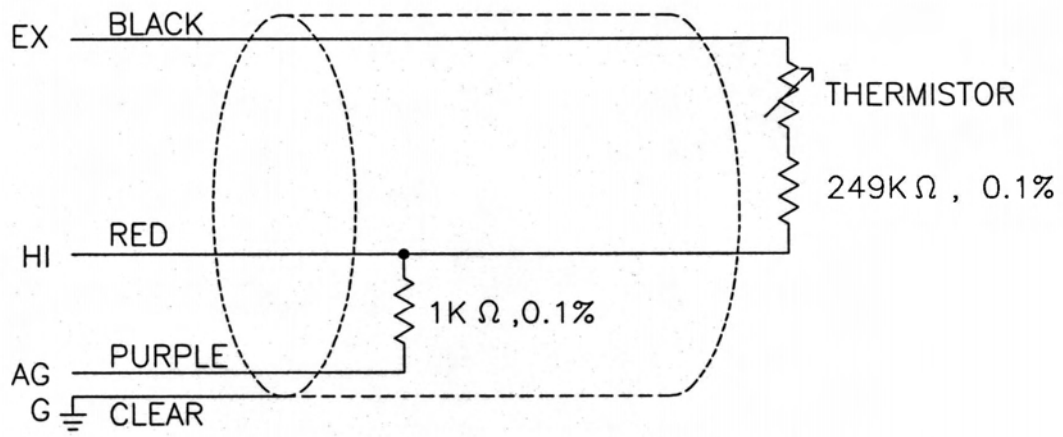

FIGURE 6-1. 107 Thermistor Probe Schematic

TABLE 6-2. Polynomial Coefficients

Coefficient	Value
C0	-53.4601
C1	90.807
C2	-83.257
C3	52.283
C4	-16.723
C5	2.211

7. Electrically Noisy Environments

AC power lines can be the source of electrical noise. If the datalogger is in an electronically noisy environment, the 107 temperature measurement should be measured with 60 Hz rejection. Sixty and 50 Hz rejection is available as an option in the Excitation Channel parameter of Instruction 11 for the CR10X, CR510, and CR23X dataloggers. For the CR10, CR21X and CR7, the 107 should be measured with the AC half bridge (Instruction 5).

Example 2. Sample CR10(X) Instructions Using AC Half Bridge

```
1: AC Half Bridge (P5)
   1:          1        Reps
   2:         22        7.5 mV 60 Hz Rejection Range
   3:          9        SE Channel
   4:          3        Excite all reps w/Exchan 3
   5:       2000        mV Excitation ;Use 4000 mV on 21X and CR7
   6:          1        Loc [ Air_Temp  ]
   7:        800        Mult
   8:          0        Offset
```

```
2: Polynomial (P55)
   1:          1        Reps
   2:          1        X Loc [ Air_Temp ]
   3:          1        F(X) Loc [ Air_Temp ]
   4:     -53.46        C0
   5:     90.807        C1
   6:    -83.257        C2
   7:     52.283        C3
   8:    -16.723        C4
   9:      2.211        C5
```

8. Long Lead Lengths

The 60 and 50 Hz rejection options for the CR10X, CR510, and CR23X include a delay to accommodate long lead lengths. For the CR10, 21X, and CR7, if the 107 has lead lengths of more than 300 feet, use the DC Half Bridge instruction (Instruction 4) with a 2 millisecond delay to measure temperature. The delay provides a longer settling time before the measurement is made. Do not use the 107 with long lead lengths in an electrically noisy environment.

Example 3. Sample Program CR10 Using DC Half Bridge with Delay

```
1: Excite-Delay (SE) (P4)
   1:          1        Reps
   2:          2        7.5 mV Slow Range
   3:          9        SE Channel
   4:          3        Excite all reps w/Exchan 3
   5:          2        Delay (units 0.01 sec)
   6:       2000        mV Excitation ;Use 4000 mV on 21X and CR7
   7:          1        Loc [ Air_Temp ]
   8:         .4        Mult ;Use 0.2 on 21X and CR7
   9:          0        Offset

2: Polynomial (P55)
   1:          1        Reps
   2:          1        X Loc [ Air_Temp ]
   3:          1        F(X) Loc [ Air_Temp ]
   4:     -53.46        C0
   5:     90.807        C1
   6:    -83.257        C2
   7:     52.283        C3
   8:    -16.723        C4
   9:      2.211        C5
```

MODEL 253 AND 253-L (WATERMARK 200)
SOIL MOISTURE SENSOR

REVISION: 6/96

WARRANTY AND ASSISTANCE

The **MODEL 253 AND 253-L (WATERMARK 200) SOIL MOISTURE SENSOR** is warranted by CAMPBELL SCIENTIFIC, INC. to be free from defects in materials and workmanship under normal use and service for twelve (12) months from date of shipment unless specified otherwise. Batteries have no warranty. CAMPBELL SCIENTIFIC, INC.'s obligation under this warranty is limited to repairing or replacing (at CAMPBELL SCIENTIFIC, INC.'s option) defective products. The customer shall assume all costs of removing, reinstalling, and shipping defective products to CAMPBELL SCIENTIFIC, INC. CAMPBELL SCIENTIFIC, INC. will return such products by surface carrier prepaid. This warranty shall not apply to any CAMPBELL SCIENTIFIC, INC. products which have been subjected to modification, misuse, neglect, accidents of nature, or shipping damage. This warranty is in lieu of all other warranties, expressed or implied, including warranties of merchantability or fitness for a particular purpose. CAMPBELL SCIENTIFIC, INC. is not liable for special, indirect, incidental, or consequential damages.

Products may not be returned without prior authorization. To obtain a Returned Materials Authorization (RMA), contact CAMPBELL SCIENTIFIC, INC., phone (435) 753-2342. After an applications engineer determines the nature of the problem, an RMA number will be issued. Please write this number clearly on the outside of the shipping container. CAMPBELL SCIENTIFIC's shipping address is:

CAMPBELL SCIENTIFIC, INC.
RMA#_____
815 West 1800 North
Logan, Utah 84321-1784

CAMPBELL SCIENTIFIC, INC. does not accept collect calls.

Non-warranty products returned for repair should be accompanied by a purchase order to cover the repair.

CAMPBELL SCIENTIFIC, INC.

815 W. 1800 N.
Logan, UT 84321-1784
USA
Phone (435) 753-2342
FAX (435) 750-9540
www.campbellsci.com

Campbell Scientific Canada Corp.
11564 -149th Street
Edmonton, Alberta T5M 1W7
CANADA
Phone (780) 454-2505
FAX (780) 454-2655

Campbell Scientific Ltd.
Campbell Park
80 Hathern Road
Shepshed, Loughborough
LE12 9GX, U.K.
Phone +44 (0) 1509 601141
FAX +44 (0) 1509 601091

MODEL 253 AND 253-L (WATERMARK 200) SOIL MOISTURE SENSOR

1 GENERAL

The Watermark 200 (CSI sensor Models 253, 253-L, 257, and 257-L) provides a convenient method of estimating water potential between 0 and 2 bars (wetter soils) with a Campbell Scientific CR10, 21X, or CR7 datalogger. CSI Models 253 and 253-L are for connection to the AM32 or AM416 Analog Multiplexers. Models 257 and 257-L connect directly to a datalogger.

The Watermark block estimates water potential. For applications requiring high accuracy, call a Campbell Scientific applications engineer for information on precision soil moisture measurement systems.

The Watermark consists of two concentric electrodes embedded in a reference matrix material. The matrix material is surrounded by a synthetic membrane for protection against deterioration. An internal gypsum tablet buffers against the salinity levels found in irrigated soils.

If cultivation practices allow, the sensor can be left in the soil all year, eliminating the need to remove the sensor during the winter months.

FIGURE 1.1 253 Soil Moisture Sensor

2. INSTALLATION AND REMOVAL

Placement of the Watermark is important. To acquire representative measurements, avoid high spots, slope changes, or depressions where water puddles. Typically, the sensor must be located in the root system of the crop.

1. Soak the sensors overnight in irrigation water. Always install a wet sensor. If time permits, allow the sensor to dry for 1 to 2 days after soaking, and repeat the soak/dry cycle twice to improve sensor response.
2. Make a sensor access hole to the depth required with a 7/8" rod. Fill the hole with water and push the sensor to the bottom of the hole. Very coarse or gravelly soils may require an oversized hole (1 to 1-1/4") to prevent abrasion damage to the sensor membrane. In this case, you will need to "grout in" the sensor with a slurry made from the sample soil to get a snug fit in the soil.

   Snug fit in the soil is most important. Lack of a snug fit is the premier problem in sensor effectiveness. In gravelly soils, and with deeper sensors, sometimes it is hard to get the sensor in without damaging the membrane. The ideal method of making the access hole is to have a "stepped" tool that makes an oversized hole for the upper portion and an exact size hole for the lower portion. In either case, the hole needs to be carefully backfilled and tamped down to prevent air pockets which could allow water to channel down to the sensor.

   A length of 1/2" class 315 PVC pipe fits snugly over the sensor collar and can be used to push in the sensor.

   You can leave the PVC in place with the wires threaded through the pipe and the open end taped shut (duct tape is adequate). This practice also makes it easy to remove sensors used in annual crops. When doing this, solvent weld the PVC pipe to the sensor collar. Use PVC/ABS cement on the stainless steel sensors with the green top. Use clear PVC cement only on the PVC sensors with the gray top.

3. When removing sensors prior to harvest in annual crops, do so just after the last irrigation when the soil is moist. Do not pull the sensor out by the wires. Careful removal prevents sensor and membrane damage.
4. When sensors are removed for winter storage, clean, dry, and place them in a plastic bag.

NOTE: The black outer jacket of the cable is Santoprene® rubber. This compound was chosen for its resistance to temperature extremes, moisture, and UV degradation. However, this jacket will support combustion in air. It is rated as slow burning when tested according to U.L. 94 H.B. and will pass FMVSS302. Local fire codes may preclude its use inside buildings.

3. WIRING

The model 253 sensor is supplied with two green leads from Watermark. The leads from the Watermark electrode are connected directly to the H and L inputs on the AM32 or AM416. The lead coming from the center of the sensor is connected to H and the lead from the outer portion of the sensor to L. The wires can be differentiated by the grooved strip in one of the leads of the green wires. On the 253-L, Campbell Scientific splices a two conductor shielded cable to the two conductor green cable supplied from Watermark. The black conductor is connected to H, the white conductor to L, and the shield wire to G or ⏚. A 1kΩ resistor at the datalogger is used to complete the half bridge measurement.

4. MEASUREMENT

Instruction 5, AC Half Bridge, is used to excite and measure the model 253. Recommended excitation voltages and input ranges are listed in Table 1.

TABLE 1. Excitation and Voltage Range

DATALOGGER	mV EX	RANGE CODE	FSR
21X	500	14	± 500 mV
CR10	250	14	± 250 mV

NOTE: Do not use a slow integration time as sensor polarization errors will occur.

4.1 CALCULATE SENSOR RESISTANCE - INSTRUCTION 59

Instruction 59, Bridge Transform, is used to output sensor resistance (R_S). The instruction takes the AC Half Bridge output (Vs/Vx) and computes the sensor resistance as follows.

$$R_S = R1(X/(1-X))$$

where, X = Vs/Vx (Output from Instruction 5)

A multiplier of 1 should be used to output sensor resistance (R_S) in terms of kΩ.

4.2 CALCULATE SOIL WATER POTENTIAL

The datalogger can calculate soil water potential (bars) from the sensor resistance (R_S) and soil temperature (T_S). See Table 2.

The need for a precise soil temperature measurement should not be over emphasized. Soil temperatures vary widely where placement is shallow and solar radiation impinges on the soil surface. A soil temperature measurement may be needed in such situations, particularly in research applications. Many applications, however, require deep placement (5 to 10 inches) in soils shaded by a crop canopy. A common practice is to assume the air temperature at sunrise will be close to what the soil temperature will be for the day.

4.2.1 Linear Relationship

For applications in the range of 0 to 2 bars, the water potential and temperature responses of the Watermark can be assumed to be linear (measurements beyond 1.25 bars have not been verified, but work in practice).

The following equation normalizes the resistance measurement to 21°C.

$$R_{21} = \frac{R_s}{1-(0.018 * dT)} \quad [1]$$

where
R_{21} = resistance at 21°C
R_s = the measured resistance
dT = (T_s-21)
T_s = soil temperature

Water potential is then calculated from R_{21} with the relationship.

$$SWP = 0.07407 * R_{21} - 0.03704 \quad [2]$$

SWP = Soil Water Potential (bars)

4.2.2 Non-Linear Relationship

For more precise work, calibration and temperature compensation in the range of 0.1 to 1.00 bar has been refined by Thompson and Armstrong (1987), as defined in the non-linear equation,

$$SWP = \frac{R_s}{0.01306[1.062(34.21 - T_s + 0.01060T_s^2) - R_s]} * .01$$

Table 2. Comparison of Estimated Soil Water Potential and Rs at 21°C

Bars (Non-Linear Equation)	Bars (Linear Equations)	(Rs)kOhms
	.037	1.00
.09	.11	2.00
.14	.18	3.00
.20	.26	4.00
.27	.33	5.00
.35	.41	6.00
.45	.48	7.00
.56	.56	8.00
.69	.63	9.00
.85	.70	10.00
1.05	.78	11.00
	.85	12.00
	.92	13.00
	.99	14.00
	1.07	15.00
	1.15	16.00
	1.22	17.00
	1.29	18.00
	1.44	20.00
	1.59	22.00
	1.74	24.00
	1.88	26.00
	1.99	27.50

5. PROGRAMMING (MEASURING BLOCK RESISTANCE)

The following examples demonstrate the connections and programming used to measure the resistances (kohms) of 32 soil moisture blocks.

5.1 AM32 AND 21X

See Figure 5.1 for wiring diagram.

```
01:     P20     Set Port (Enable AM32)
  01:     1     Set High
  02:     1     Port One
02:     P87     Beginning of Loop
  01:     0     Delay
  02:    32     Loop Count
03:     P22     Excitation with delay (clock)
  01:     1     Excitation Channel #1
  02:     1     Excite for 0.01 seconds
[3] 03:   0     0 second delay after excitation
  04:  5000     Excitation = 5000 mV
04:     P5      AC Half Bridge (Measure
                AC Conductivity)
  01:     1     Rep
  02:    14     500 mV Fast Range
  03:     1     In Channel
  04:     2     Excite All Reps w/Excite
                Channel 2
  05:   500     mV excitation
  06:    1-     Location (Indexed Location
                to Store) [:kOhms#1]
  07:     1     Multiplier
  08:     0     Offset
05:     P95     End
06:     P20     Set Port (Reset AM32)
  01:     0     Set Low
  02:     1     Port Number
07:     P59     BR Transform Rf[X/(1-X)]
                (Compute Resistances)
  01:    32     Reps
  02:     1     Location [:kOhms#1]
  03:     1     Multiplier  (Rf/1000)
```

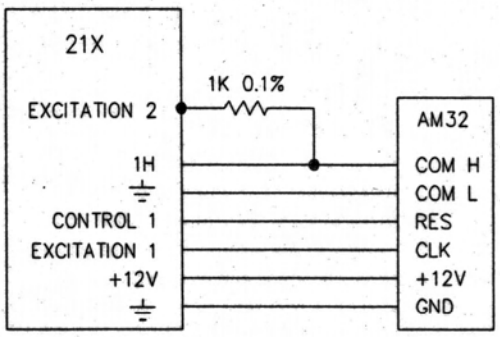

FIGURE 5.1

5.2 AM32 AND CR10

See Figure 5.2 for wiring diagram. This program can also be used with 21Xs with OSX PROMs although the clock pulse delay is 0.1 seconds (Figure 5.3).

```
01:     P86     Do
  01:    45     Set Port 5 high

02:     P87     Beginning of Loop
  01:     0     Delay
  02:    32     Loop Count

03:     P86     Do (Clock Pulse, 10 ms)
  01:    76     Pulse Port 6

04:      P5     AC Half Bridge (Measure
                AC Conductivity)
  01:     1     Rep
  02:    14     250 mV Fast Range
  03:     1     In Channel
  04:     2     Excite All Reps w/
                Excitation Channel 2
  05:   250     mV Excitation
  06:    1--    Location (Indexed Location
                to Store) [:kOhms#1]
  07:     1     Multiplier
  08:     0     Offset

05:     P95     End

06:     P86     Do (Reset AM32)
  01:    55     Set Port 5 low

07:     P59     BR Transform Rf[X/(1-X)]
                (Compute Resistances)
  01:    32     Reps
  02:     1     Location [:kOhms#1]
  03:     1     Multiplier (Rf/1000)
```

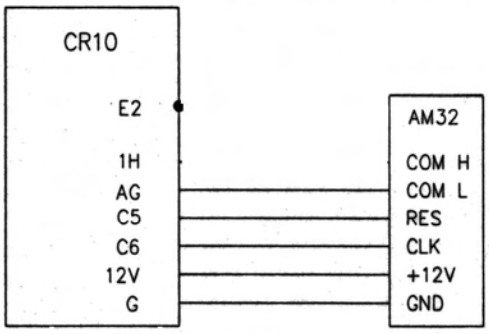

FIGURE 5.2

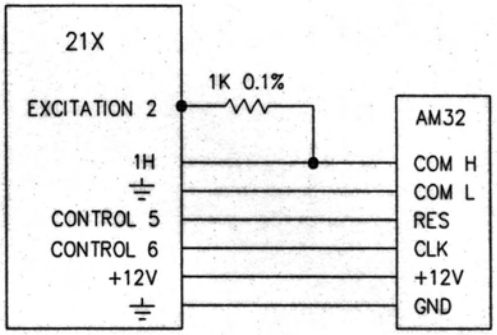

FIGURE 5.3

5.3 AM416 AND 21X

See Figure 5.4 for wiring diagram.

```
01:     P20     Port Set (Enable AM416)
  01:     1     Set High
  02:     1     Port Number

02:     P87     Beginning of Loop
  01:     0     Delay
  02:    16     Loop Count

03:     P22     Excitation with delay (clock)
  01:     1     Excitation Channel #1
  02:     1     Excite for 0.01 seconds
  03:     0     0 second delay after excitation
  04:  5000     Excitation = 5000 mV

04:     P90     Step Loop Index
  01:     2     Step

05:      P5     AC Half Bridge (Measure
                AC Conductivity)
  01:     2     Rep
  02:    14     500 mV Fast Range
  03:     1     In Channel
  04:     2     Excite All Reps w/
                Excitation Channel 2
  05:   500     mV Excitation
  06:    1--    Location (Indexed Location
                to Store) [:kOhms#1]
  07:     1     Multiplier
  08:     0     Offset

06:     P95     End

07:     P20     Set Port (Reset AM416)
  01:     0     Set Low
  02:     1     Port Number

08:     P59     BR Transform Rf[X/1(1-X)]
                Compute Resistances
  01:    32     Reps
  02:     1     Location [:kOhms#1]
  03:     1     Multiplier (Rf/1000)
```

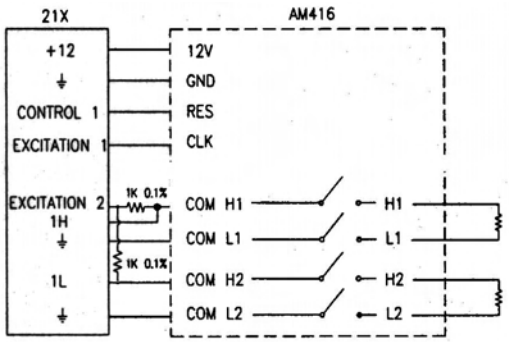

FIGURE 5.4

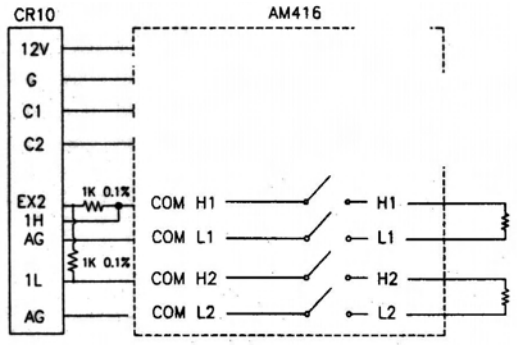

Figure 5.5

5.4 AM416 AND CR10

See Figure 5.5 for wiring diagram. This program can also be used with 21X with OSX PROMs although the clock pulse delay is 0.1 seconds (Figure 5.6).

01:	P86	Do Set Port (Enable AM416)
01:	41	Set High Port 1
02:	P87	Beginning of Loop
01:	0	Delay
02:	16	Loop Count
03:	P86	Do (Clock Pulse, 10 ms)
01:	72	Pulse Port 2
04:	P90	Step Loop Index
01:	2	Step
05:	P5	AC Half Bridge (Measure AC Conductivity)
01:	2	Rep
02:	14	250 mV Fast Range
03:	1	In Channel
04:	2	Excite All Reps w/ Excitation Channel 2
05:	250	mV Excitation
06:	1--	Location (Indexed Location to Store) [:kOhms#1]
07:	1	Multiplier
08:	0	Offset
06:	P95	End
07:	P86	Do (Reset AM416)
01:	51	Set Low Port 1
08:	P59	BR Transform Rf[X/(1-X)]
01:	32	Reps
02:	1	Location [:kOhms#1]
03:	1	Multiplier (Rf/1000)

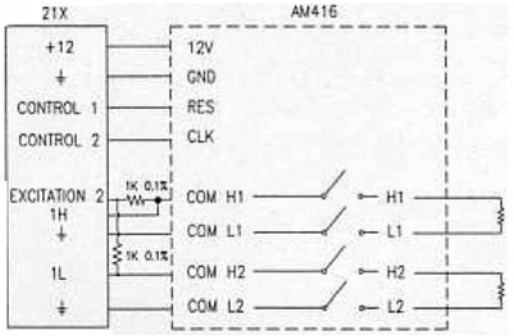

Figure 5.6

6. PROGRAMMING (CALCULATING SOIL WATER POTENTIAL)

6.1 LINEAR RESISTANCE AND TEMPERATURE RELATIONSHIP (0 TO 2 BARS)

Calculate Temperature Correction Factor. See Equation [1] in Section 4.2.1...

...Calculate dT = T - 21

04:	P34	Z=X+F
01:	34	X Loc TmpDegC
02:	-21	F
03:	36	Z Loc [:CorrFactr]

...Calculate (0.018 * dT)

05:	P37	Z=X*F
01:	36	X Loc CorrFactr
02:	.018	F
03:	36	Z Loc [:CorrFactr]

...Calculate (1 - (0.018 * dT))

```
06:     P34         Z=X+F
  01:     36        X Loc CorrFactr
  02:     -1        F
  03:     36        Z Loc [:CorrFactr]

07:     P37         Z=X*F
  01:     36        X Loc CorrFactr
  02:     -1        F
  03:     36        Z Loc [:CorrFactr]
```

Apply Temperature Correction and Sensor Calibration to Ohm Measurements. See Equation [2] in Section 4.2.1...

```
08:     P87         Beginning of Loop
  01:     0         Delay
  02:     32        Loop Count
```

...Temperature Correct Ohms:

```
09:     P38         Z=X/Y
  01:     1--       X Loc kOhms#1
  02:     36        Y Loc CorrFactr
  03:     41--      Z Loc [:Bar#1   ]
```

...Apply Calibration Slope and Offset

```
10:     P37         Z=X*F
  01:     41--      X Loc Bar#1
  02:     .07407    F
  03:     41--      Z Loc [:Bar#1   ]

11:     P34         Z=X+F
  01:     41--      X Loc Bar#1
  02:     -.03704   F
  03:     41--      Z Loc [:Bar#1   ]

12:     P95         End
```

6.2 NON-LINEAR RESISTANCE AND TEMPERATURE RELATIONSHIP (0.1 TO 1 BAR)

The following instructions convert R_S to Soil Water Potential in bars. See Equation [3] in Section 4.2.2.

```
08:     P87         Beginning of Loop
  01:     0         Delay
  02:     32        Loop Count

05:     P36         Z=X*Y  SWP = Tsoil^2
  01:     34        X Loc Tsoil C
  02:     34        Y Loc Tsoil C
  03:     41--      Z Loc [:Bars#1]
```

SWP = Tsoil^2 * 0.0106

```
06:     P37         Z=X*F
  01:     41--      X Loc Bars#1
  02:     0.0106    F
  03:     41--      Z Loc [:Bars#1]

07:     P30         Z=F
  01:     34.21     F
  02:     35        Z Loc [:Constant ]
```

SWP = 34.21-Ts

```
08:     P35         Z=X-Y
  01:     35        X Loc Constant
  02:     34        Y Loc Tsoil C
  03:     35        Z Loc [:Constant ]
```

SWPcalc.=[(34.21-Ts)+(Ts^2*0.01060)]

```
09:     P33         Z=X+Y
  01:     41--      X Loc Bars#1
  02:     3         Y Loc Constant
  03:     41--      Z Loc [:Bars#1]
```

SWP = 1.062[SWPcalc.]

```
10:     P37         Z=X*F
  01:     41--      X Loc Bars#1
  02:     1.062     F
  03:     41--      Z Loc [:Bars#1]

11:       P         35  Z=X-Y
```

SWP = SWPcalc.-Rs

```
  01:     41--      X Loc Bars#1
  02:     1--       Y Loc kOhms#1
  03:     41--      Z Loc [:Bars#1]
```

SWP = 0.01306*SWPcalc.

```
12:     P37         Z=X*F
  01:     41--      X Loc Bars#1
  02:     0.0130    F
  03:     41--      Z Loc [:Bars#1]
```

SWP = Rs/SWPcalc.

```
13:     P38         Z=X/Y
  01:     1--       X Loc kOhms#1
  02:     41--      Y Loc Bars#1
  03:     41--      Z Loc [:Bars#1]
```

SWPbars = SWP(kPa) * 0.01

```
14:     P37         Z=X*F
  01:     41--      X Loc Bars#1
  02:     0.01      F
  03:     41--      Z Loc [:Bars#1]

15:     P95         End Calculation Loop
```

7. PROGRAMMING (COMPREHENSIVE)

Follow these steps to create a complete program:

Step 1. Allocate at least 75 input locations in EDLOG.

Step 2. Set the execution interval according to need:

```
      1          Table 1 Programs
01:   3600       Sec. Execution Interval
```

Step 3. Make a temperature measurement to correct for temperature effects. Select from options 1 or 2.

Option 1. If a 107B Probe is part of your system, measure soil temperature:

```
01:     P11        Temp 107 Probe
  01:     1        Rep
  02:     3        IN Chan
  03:     3        Excite all reps w/EXchan 3
  04:    34        Loc [:TempDegC ]
  05:     1        Mult
  06:     0        Offset
```

Option 2. If a 107B Probe is not available but a 107 Probe is part of your system, measure air temperature in the early morning (6:00 A.M.) and assume that will be the soil temperature for the day:

```
02:     P92        If time is
  01:   360        minutes (seconds--) into a
  02:  1440        minute or second interval
  03:    30        Then Do

03:     P11        Temp 107 Probe
  01:     1        Rep
  02:     3        IN Chan
  03:     3        Excite all reps w/EXchan 3
  04:    34        Loc [:TempDegC ]
  05:     1        Mult
  06:     0        Offset

04:     P95        End
```

Step 4. Make the resistance measurements. It may be appropriate to make measurements only once or twice a day. This example makes measurements twice a day at 6:00 AM and 6:00 PM:

```
05:     P92        If time is
  01:   360        minutes (seconds--) into a
  02:   720        minute or second interval
  03:    30        Then Do
```

Insert one of the examples from Section 5 here.

Step 5. Calculate soil water potential using resistance and temperature:

Insert one of the examples from Section 6 here.

Step 6. Output data to final storage after each measurement and calculation:

```
06:     P86        Do
  01:    10        Set high Flag 0 (output)

07:     P77        Real Time
  01:   0220       Day,Hour-Minute

08:     P70        Sample kOhm Resistances
  01:    32        Reps
  02:     1        Loc

09:     P70        Sample Deg C Temperature
  01:     1        Reps
  02:    34        Loc

10:     P70        Sample Bar Potential
  01:    32        Reps
  02:    41        Loc

11:     P95        End 6 am and 6 pm loop
```

8. INTERPRETING RESULTS

As a general guide, Watermark 200 measurements indicate soil moisture as follows:

0 to 10 centibars =	Saturated soil.
10 to 20 centibars =	Soil is adequately wet (except coarse sands, which are beginning to lose water).
30 to 60 centibars =	Usual range for irrigation (except heavy clay).
60 to 100 centibars =	Usual range for irrigation for heavy clay soils.
100 to 200 centibars =	Soil is becoming dangerously dry for maximum production.

9. TROUBLESHOOTING

To test the sensor, submerge it in water. Measurements should be from -.03 to .03 bars. Let the sensor dry for 30 to 48 hours. You should see the reading increase from 0 to 150+. Put the sensor back in the water. The reading should run right back down to zero in 1 to 2 minutes. If the sensor passes these tests, consider the following.

Sensor may not have a snug fit in the soil. This usually happens when an oversized access hole has been used and the backfilling of the area around the sensor is not complete.

2. Sensor is not in an active portion of the root system, or the irrigation is not reaching the sensor area. This can happen if the sensor is sitting on top of a rock or below a hard pan which may impede water movement. Re-installing the sensor usually solves this problem.

3. When the soil dries out to the point where you are seeing readings higher than 80 centibars, the contact between soil and sensor can be lost because the soil may start to shrink away from the sensor. An irrigation which only results in a partial rewetting of the soil will not fully rewet the sensor, which can result in continued high readings from the Watermark. Full rewetting of the soil and sensor usually restores soil/sensor contact. This is most often seen in the heavier soils and during peak crop water demand when irrigation may not be fully adequate. The plotting of readings on a chart is most useful in getting a good picture of this sort of behavior.

Reference

Thompson, S.J. and C.F. Armstrong, Calibration of the Watermark Model 200 Soil Moisture Sensor, Applied Engineering in Agriculture, Vol. 3, No. 2, pp. 186-189, 1987.

Parts of this manual were contributed by Irrometer Company, Inc., manufacturer of the Watermark 200.

CS500 TEMPERATURE AND RELATIVE HUMIDITY PROBE

REVISION: 1/99

WARRANTY AND ASSISTANCE

The **CS500 TEMPERATURE AND RELATIVE HUMIDITY PROBE** is warranted by CAMPBELL SCIENTIFIC, INC. to be free from defects in materials and workmanship under normal use and service for twelve (12) months from date of shipment unless specified otherwise. Batteries have no warranty. CAMPBELL SCIENTIFIC, INC.'s obligation under this warranty is limited to repairing or replacing (at CAMPBELL SCIENTIFIC, INC.'s option) defective products. The customer shall assume all costs of removing, reinstalling, and shipping defective products to CAMPBELL SCIENTIFIC, INC. CAMPBELL SCIENTIFIC, INC. will return such products by surface carrier prepaid. This warranty shall not apply to any CAMPBELL SCIENTIFIC, INC. products which have been subjected to modification, misuse, neglect, accidents of nature, or shipping damage. This warranty is in lieu of all other warranties, expressed or implied, including warranties of merchantability or fitness for a particular purpose. CAMPBELL SCIENTIFIC, INC. is not liable for special, indirect, incidental, or consequential damages.

Products may not be returned without prior authorization. To obtain a Returned Materials Authorization (RMA), contact CAMPBELL SCIENTIFIC, INC., phone (435) 753-2342. After an applications engineer determines the nature of the problem, an RMA number will be issued. Please write this number clearly on the outside of the shipping container. CAMPBELL SCIENTIFIC's shipping address is:

CAMPBELL SCIENTIFIC, INC.
RMA#_____
815 West 1800 North
Logan, Utah 84321-1784

CAMPBELL SCIENTIFIC, INC. does not accept collect calls.

Non-warranty products returned for repair should be accompanied by a purchase order to cover the repair.

CAMPBELL SCIENTIFIC, INC.

815 W. 1800 N.
Logan, UT 84321-1784
USA
Phone (435) 753-2342
FAX (435) 750-9540
www.campbellsci.com

Campbell Scientific Canada Corp.
11564 -149th Street
Edmonton, Alberta T5M 1W7
CANADA
Phone (780) 454-2505
FAX (780) 454-2655

Campbell Scientific Ltd.
Campbell Park
Hathern Road
Shepshed, Leics. LE12 9RP
ENGLAND
Phone (44)-50960-1141
FAX (44)-50960-1091

CS500 TEMPERATURE AND RELATIVE HUMIDITY PROBE

1. GENERAL

The CS500 Temperature and Relative Humidity probe contains a Platinum Resistance Temperature detector (PRT) and a Vaisala INTERCAP® capacitive relative humidity sensor.

The -L option on the model CS500 Temperature and Relative Humidity probe (CS500-L) indicates that the cable length is user specified. This manual refers to the sensor as the CS500.

2. SPECIFICATIONS

Operating Temperature: -40 °C to +60°C

Storage Temperature: -40 °C to +80°C

Probe Length: 6.8 cm (2.66 in.)

Probe Body Diameter: 1.2 cm (0.47 in.)

Filter: 0.2 µm Teflon membrane

Filter Diameter: 1.2 cm (0.47 in.)

Housing Material: ABS Plastic

Power Consumption: <2 mA

Supply Voltage: 7 to 28 VDC

Settling Time after power is switched on:
1 second

2.1 TEMPERATURE SENSOR

Sensor: 1000 Ω PRT, DIN 43760B

Temperature Measurement Range:
-40°C to +60°C

Temperature Output Signal range:
0 to 1.0 VDC

Temperature Accuracy:

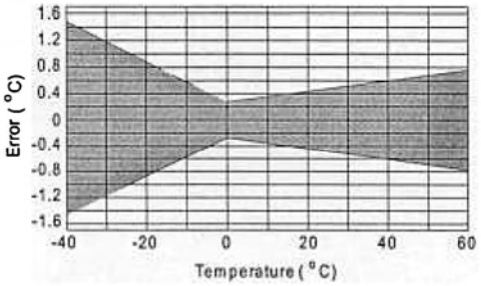

2.2 RELATIVE HUMIDITY SENSOR

Sensor: INTERCAP®

Relative Humidity Measurement Range:
0 to 100% non-condensing

RH Output Signal Range:
0 to 1.0 VDC

Accuracy at 20°C
unspecified (0 to 10% Relative Humidity)
±3% RH (10 to 90% Relative Humidity)
±6% RH (90 to 100% Relative Humidity)

Temperature Dependence of Relative Humidity Measurement:

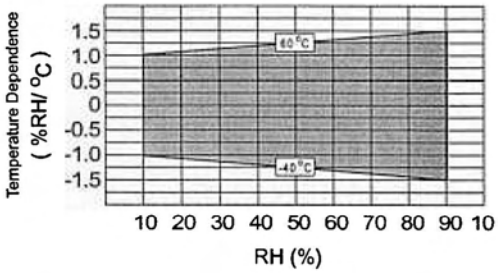

Typical Long Term Stability:
Better than 1% RH per year

Response Time (at 20°C, 90% response to a steep change in humidity):
15 seconds with membrane filter

3. INSTALLATION

The CS500 must be housed inside a solar radiation shield when used in the field. The 41301 6-Plate Radiation Shield (Figure 1) mounts to a CM6/CM10 tripod or UT10 tower. The CS500 is held within the 41301 by a mounting clamp (Figure 2).

The 41002 12-Plate Radiation Shield (Figure 3) mounts to a CM6/CM10 tripod. The UT12VA 12-Plate Radiation Shield mounts to a UT10 or UT30 tower with the UT018 horizontal mounting arm.

The CS500 is held in place, within the 41002 or UT12VA Radiation Shield, via an adapter, Model 41381. The 41381 adapter is threaded onto the bottom of the CS500 (Figure 4). The 41004 12-Plate Radiation Shield, used with 207 probes, can be converted to a 41002 with P/N 6638.

NOTE: The black outer jacket of the cable is Santoprene® rubber. This compound was chosen for its resistance to temperature extremes, moisture, and UV degradation. However, this jacket will support combustion in air. It is rated as slow burning when tested according to U.L. 94 H.B. and will pass FMVSS302. Local fire codes may preclude its use inside buildings.

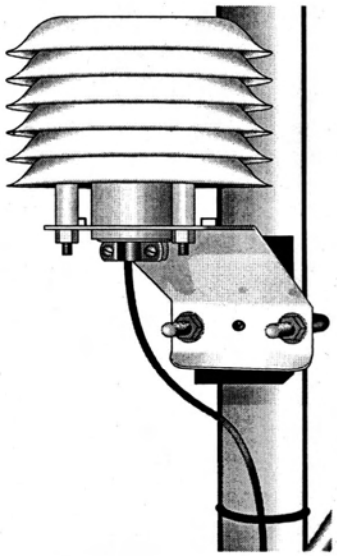

FIGURE 1. CS500 and 41301 Radiation Shield on a CM6/CM10 Tripod Mast

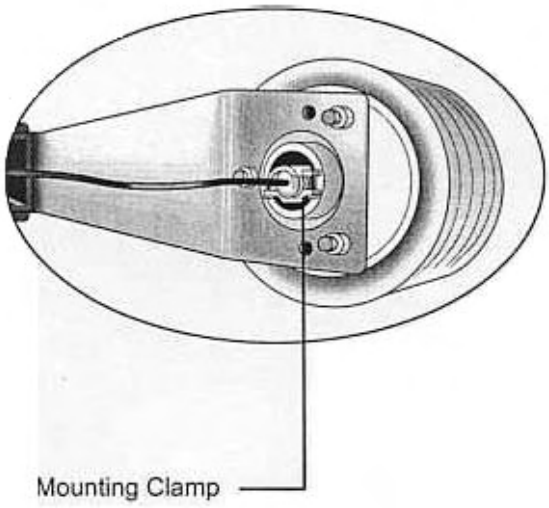

FIGURE 2. CS500 and 41301 Radiation Shield

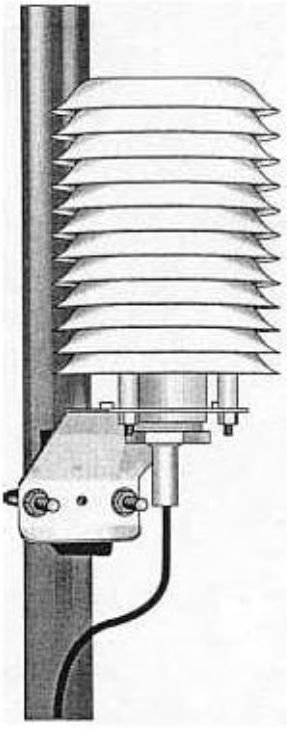

FIGURE 3. CS500 and 41002 Radiation Shield on a CM6/CM10 Tripod Mast

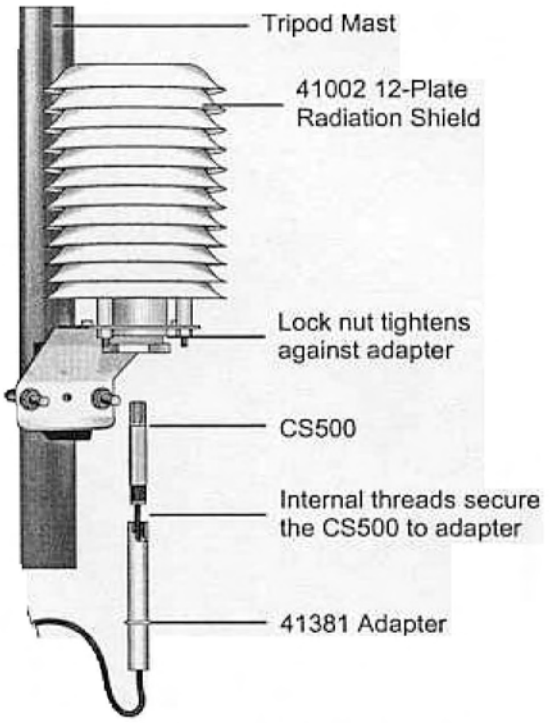

FIGURE 4. Radiation Shield, CS500, and 41381 Adapter

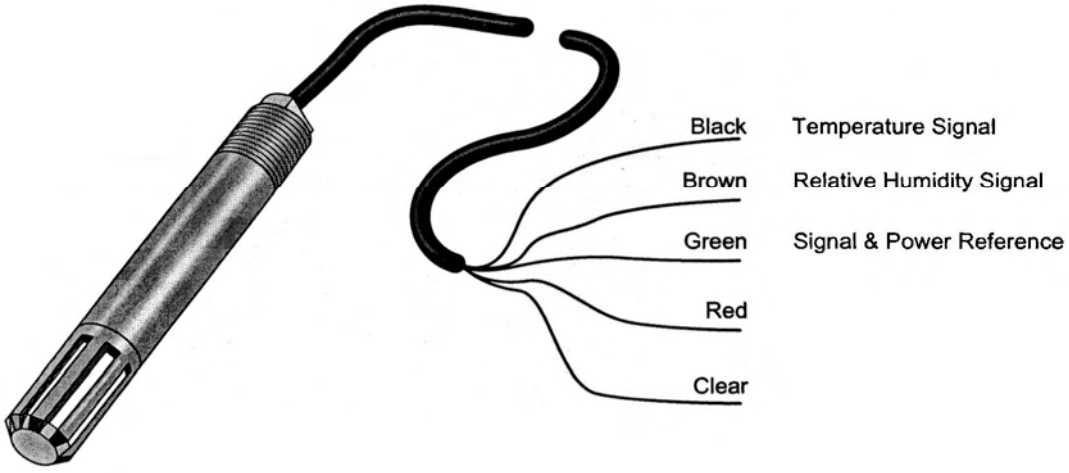

FIGURE 5. CS500 Wiring

TABLE 1. Datalogger Connections

Description	Color	CR10(X), CR500	CR23X	21X, CR7
Temperature	Black	Single-Ended Input	Single-Ended Input	Single-Ended Input
Relative Humidity	Brown	Single-Ended Input	Single-Ended Input	Single-Ended Input
Signal & Power Reference	Green	G	G	⏚
Power	Red	12 V	12 V	12 V
Shield	Clear	G	⏚	⏚

4. WIRING

Connections to Campbell Scientific dataloggers are given in Table 1. The probe is measured by two single-ended analog input channels, one for temperature and one for relative humidity.

CAUTION: Always connect the Green lead to the datalogger first, followed by the Black, Brown, and Clear leads. Connect the Red (Power) lead last.

5. EXAMPLE PROGRAMS

This section is for users who write their own datalogger programs. A datalogger program to measure this sensor can be created using Campbell Scientific's Short Cut Program Builder Software. You do not need to read this section to use Short Cut.

The temperature and relative humidity signals from the CS500 are measured using two single-ended analog measurements (Instruction 1).

The probe output scale is 0 to 1000 millivolts for the temperature range of -40 °C to +60 °C and for the relative humidity range of 0 to 100%. Tables 2 and 3 provide calibration information for temperature and relative humidity.

TABLE 2. Calibration for Temperature

Units	Multiplier (degrees mV^{-1})	Offset (degrees)
Celsius	0.1	-40
Fahrenheit	0.18	-40

TABLE 3. Calibration for Relative Humidity

Units	Multiplier (% mV^{-1})	Offset (%)
Percent	0.1	0
Fraction	0.001	0

TABLE 4. Wiring for Example 1

Description	Color	CR10(X)
Temperature	Black	SE 3 (2H)
Relative Humidity	Brown	SE 4 (2L)
Signal & Power Reference	Green	G
Power	Red	12 V
Shield	Clear	G

Example 1. Sample CR10(X) Program using Single-Ended Measurement Instructions

```
;Measure the CS500 temperature.
;
01:   Volt (SE) (P1)
        1:    1       Reps
        2:    5       2500 mV Slow Range   ;CR500 (2500 mV); CR23X (1000 mV); 21X, CR7 (5000 mV)
        3:    3       SE Channel           ;Black wire (SE 3), Green wire (G)
        4:    1       Loc [ T_C     ]
        5:    .1      Mult                 ;See Table 2 for alternate multipliers
        6:  -40       Offset               ;See Table 2 for alternate offsets

;Measure the CS500 relative humidity.
;
02:   Volt (SE) (P1)
        1:    1       Reps
        2:    5       2500 mV Slow Range   ;CR500 (2500 mV); CR23X (1000 mV); 21X, CR7 (5000 mV)
        3:    4       SE Channel           ;Brown wire (SE 4), Green wire (G)
        4:    3       Loc [ RH_pct   ]
        5:    .1      Mult                 ;See Table 3 for alternate multipliers
        6:    0       Offset

;Limit the maximum relative humidity to 100%.
;
03:   If (X<=>F) (P89)
        1:    3       X Loc [ RH_pct
        2:    3       >=
        3:  100       F
        4:   30       Then Do

04:   Z=F (P30)
        1:  100       F
        2:    0       Exponent of 10
        3:    3       Z Loc [ RH_pct

05:   End (P95)
```

6. LONG LEAD LENGTHS

Long lead lengths cause errors in the measured temperature and relative humidity. The approximate error in temperature and relative humidity is 0.35°C and 0.35% per 100 feet of cable length, respectively.

When long lead lengths are required and the above errors in temperature and relative humidity are unacceptable, use the HMP45C temperature and humidity probe.

Understanding the following details are not required for the general operation of the CS500 with Campbell Scientific's dataloggers. The signal reference and the power ground (black) are the same lead in the CS500. When the CS500 temperature and relative humidity are measured, both the signal reference and power ground are connected to ground at the datalogger. The signal reference/power ground lead serves as the return path for 12 V. There will be a voltage drop along this lead because the wire itself has resistance. The CS500 draws approximately 2 mA when it is powered. The wire used in the CS500 (P/N 9720) has resistance of 17.5 Ω/1000 feet. Using Ohm's law, the voltage drop (V_d), along the signal reference/power ground lead, is given by Eq. (1).

$$V_d = I * R$$
$$= 2\ mA * 17.5\ \Omega / 1000\ ft \quad (1)$$
$$= 35\ mV / 1000\ ft$$

This voltage drop will raise the apparent temperature and relative humidity because the difference between the signal and signal reference, at the datalogger, has increased by V_d. The approximate error in temperature and relative humidity is 0.35°C and 0.35% per 100 feet of cable length, respectively.

7. ABSOLUTE HUMIDITY

The CS500 measures the relative humidity. Relative humidity is defined by the equation below:

$$RH = \frac{e}{e_s} * 100 \quad (2)$$

where RH is the relative humidity, e is the vapor pressure in kPa , and e_s is the saturation vapor pressure in kPa. The vapor pressure, e, is an absolute measure of the amount of water vapor in the air and is related to the dew point temperature. The saturation vapor pressure is the maximum amount of water vapor that air can hold at a given air temperature. The relationship between dew point and vapor pressure, and air temperature and saturation vapor pressure are given by Goff and Gratch (1946), Lowe (1977), and Weiss (1977).

When the air temperature increases, so does the saturation vapor pressure. Conversely, a decrease in air temperature causes a corresponding decrease in saturation vapor pressure. It follows then from Eq. (2) that a change in air temperature will change the relative humidity, without causing a change in absolute humidity.

For example, for an air temperature of 20°C and a vapor pressure of 1.17 kPa, the saturation vapor pressure is 2.34 kPa and the relative humidity is 50%. If the air temperature is increased by 5°C and no moisture is added or removed from the air, the saturation vapor pressure increases to 3.17 kPa and the relative humidity decreases to 36.9%. After the increase in air temperature, the air can hold more water vapor. However, the actual amount of water vapor in the air has not changed. Thus, the amount of water vapor in the air, relative to saturation, has decreased.

Because of the inverse relationship between relative humidity and air temperature, finding the mean relative humidity is meaningless. A more useful quantity is the mean vapor pressure. The mean vapor pressure can be computed on-line by the datalogger (Example 2).

TABLE 5. CR10(X) Wiring for Example 2

Description	Color	CR10(X)
Temperature	Black	SE 3 (2H)
Relative Humidity	Brown	SE 4 (2L)
Signal & Power Reference	Green	G
Power	Red	12 V
Shield	Clear	G

Example 2. Sample CR10(X) Program that Computes Vapor Pressure and Saturation Vapor Pressure

```
;Measure the CS500 temperature.
;
01:   Volt (SE) (P1)
        1:    1       Reps
        2:    5       2500 mV Slow Range    ;CR500 (2500 mV); CR23X (1000 mV); 21X, CR7 (5000 mV)
        3:    3       SE Channel            ;Black wire (SE 3), Green wire (G)
        4:    1       Loc [ T_C     ]
        5:    .1      Mult                  ;See Table 2 for alternate multipliers
        6:   -40      Offset                ;See Table 2 for alternate offsets

;Measure the CS500 relative humidity.
;
02:   Volt (SE) (P1)
        1:    1       Reps
        2:    5       2500 mV Slow Range    ;CR500 (2500 mV); CR23X (1000 mV); 21X, CR7 (5000 mV)
        3:    4       SE Channel            ;Brown wire (SE 4), Green wire (G)
        4:    2       Loc [ RH_frac  ]
        5:    .001    Mult                  ;See Table 3 for alternate multipliers
        6:    0       Offset

;Limit the maximum value of relative humidity
;to 1 (expressed as a fraction).
;
03:   If (X<=>F) (P89)
        1:    2       X Loc [ RH_frac
        2:    3       >=
        3:    1       F
        4:   30       Then Do

04:   Z=F (P30)
        1:    1       F
  2     :     0       Exponent of 10
        3:    2       Z Loc [ RH_frac

05:   End (P95)

;Compute the saturation vapor pressure in kPa.
;The temperature must be in degrees Celsius.
;
06:   Saturation Vapor Pressure (P56)
        1:    1       Temperature Loc [ T_C     ]
        2:    3       Loc [ e_sat    ]

;Compute the vapor pressure in kPa.
;Relative humidity must be a fraction.
;
07:   Z=X*Y (P36)
        1:    3       X Loc [ e_sat    ]
        2:    2       Y Loc [ RH_frac
        3:    4       Z Loc [ e        ]
```

8. MAINTENANCE

The CS500 Probe requires minimal maintenance. Check monthly to make sure the radiation shield is free from debris. The white screen at the tip of the probe should also be checked for contaminants.

When installed in close proximity to the ocean or other bodies of salt water (e.g., Great Salt Lake), a coating of salt (mostly NaCl) may build up on the radiation shield, sensor, filter and even the chip. NaCl has an affinity for water. The humidity over a saturated NaCl solution is 75%. A buildup of salt on the filter or chip will delay or destroy the response to atmospheric humidity.

The filter can be rinsed gently in distilled water. If necessary, the chip can be removed and rinsed as well. Do not scratch the chip while cleaning.

The offset and gain on the CS500 electronics can not be adjusted as part of a recalibration. Replace the RH chip as needed.

9. REFERENCES

Goff, J. A. and S. Gratch, 1946: Low-pressure properties of water from -160° to 212°F, *Trans. Amer. Soc. Heat. Vent. Eng.*, **51**, 125-164.

Lowe, P. R., 1977: An approximating polynomial for the computation of saturation vapor pressure, *J. Appl. Meteor.*, **16**, 100-103.

Weiss, A., 1977: Algorithms for the calculation of moist air properties on a hand calculator, *Amer. Soc. Ag. Eng.*, **20**, 1133-1136.

HFT3 SOIL HEAT FLUX PLATE

REVISION: 2/99

WARRANTY AND ASSISTANCE

The **HFT3 SOIL HEAT FLUX PLATE** is warranted by CAMPBELL SCIENTIFIC, INC. to be free from defects in materials and workmanship under normal use and service for twelve (12) months from date of shipment unless specified otherwise. Batteries have no warranty. CAMPBELL SCIENTIFIC, INC.'s obligation under this warranty is limited to repairing or replacing (at CAMPBELL SCIENTIFIC, INC.'s option) defective products. The customer shall assume all costs of removing, reinstalling, and shipping defective products to CAMPBELL SCIENTIFIC, INC. CAMPBELL SCIENTIFIC, INC. will return such products by surface carrier prepaid. This warranty shall not apply to any CAMPBELL SCIENTIFIC, INC. products which have been subjected to modification, misuse, neglect, accidents of nature, or shipping damage. This warranty is in lieu of all other warranties, expressed or implied, including warranties of merchantability or fitness for a particular purpose. CAMPBELL SCIENTIFIC, INC. is not liable for special, indirect, incidental, or consequential damages.

Products may not be returned without prior authorization. To obtain a Returned Materials Authorization (RMA), contact CAMPBELL SCIENTIFIC, INC., phone (435) 753-2342. After an applications engineer determines the nature of the problem, an RMA number will be issued. Please write this number clearly on the outside of the shipping container. CAMPBELL SCIENTIFIC's shipping address is:

CAMPBELL SCIENTIFIC, INC.
RMA#_____
815 West 1800 North
Logan, Utah 84321-1784

CAMPBELL SCIENTIFIC, INC. does not accept collect calls.

Non-warranty products returned for repair should be accompanied by a purchase order to cover the repair.

CAMPBELL SCIENTIFIC, INC.

815 W. 1800 N.
Logan, UT 84321-1784
USA
Phone (435) 753-2342
FAX (435) 750-9540
www.campbellsci.com

Campbell Scientific Canada Corp.
11564 -149th Street
Edmonton, Alberta T5M 1W7
CANADA
Phone (403) 454-2505
FAX (403) 454-2655

Campbell Scientific Ltd.
Campbell Park
80 Hathern Road
Shepshed, Leics. LE12 9RP
ENGLAND
Phone (44)-50960-1141
FAX (44)-50960-1091

MODEL HFT3
SOIL HEAT FLUX PLATE

1. GENERAL DESCRIPTION

The HFT3 Soil Heat Flux plate uses a thermopile to measure temperature gradients across the plate. Each plate is individually calibrated to output flux.

In order to measure soil heat flux at the surface, several HFT3s are used to measure the soil heat flux at a depth of eight cm. A TCAV Averaging Soil Thermocouple is used to measure the temporal change in temperature of the soil layer above the HFT3. Finally, a CS615 Water Content Reflectometer is used to measure the soil water content. The temporal change in soil temperature and soil water content are used to compute the soil storage term.

The -L option on the model HFT3 Soil Heat Flux plate (HFT3-L) indicates that the cable length is user specified. This manual refers to the sensor as the HFT3.

2. SPECIFICATIONS

Operating Temperature: -40°C to +55°C

Storage Temperature: -40°C to +55°C

Plate Thickness: 3.91 mm (0.154 in.)

Plate Diameter: 38.2 mm (1.5 in.)

Sensor: thermopile

Measurement Range: ±100 W m^{-2}

Signal Range: ±2.4 mV for the above range

Accuracy: better than ±5% of reading

Thermal Conductivity: 1.22 W m^{-1} K^{-1}

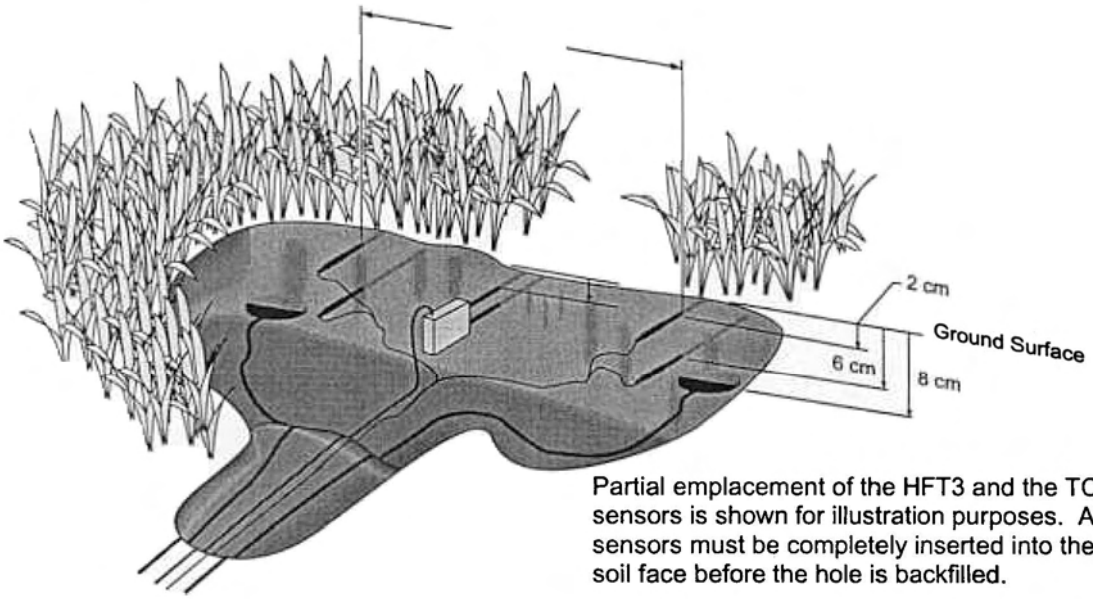

Partial emplacement of the HFT3 and the TCAV sensors is shown for illustration purposes. All sensors must be completely inserted into the soil face before the hole is backfilled.

FIGURE 1. Placement of Heat Flux Plates

3. INSTALLATION

The HFT3 Soil Heat Flux plates, the TCAV Averaging Soil Temperature probes, and the CS615 Water Content Reflectometer are installed as shown in Figure 1.

The location of the heat flux plates and thermocouples should be chosen to be representative of the area under study. If the ground cover is extremely varied, it may be necessary to have additional sensors to provide a valid average of soil heat flux.

Use a small shovel to make a vertical slice in the soil. Excavate the soil to one side of the slice. Keep this soil intact so that is can be replaced with minimal disruption.

The sensors are installed in the undisturbed face of the hole. Measure the sensor depths from the top of the hole. With a small knife, make a horizontal cut eight cm below the surface into the undisturbed face of the hole. Insert the heat flux plate into the horizontal cut.

NOTE: Install the HFT3 in the soil such that the side with the white dot is facing the sky.

CAUTION: In order for the HFT3 to make quality soil heat flux measurements, the plate must be in full contact with the soil.

Never run the sensors leads directly to the surface. Rather, bury the sensor leads a short distance back from the hole to minimized thermal conduction on the lead wire. Replace the excavated soil back into it original position after all the sensors are installed.

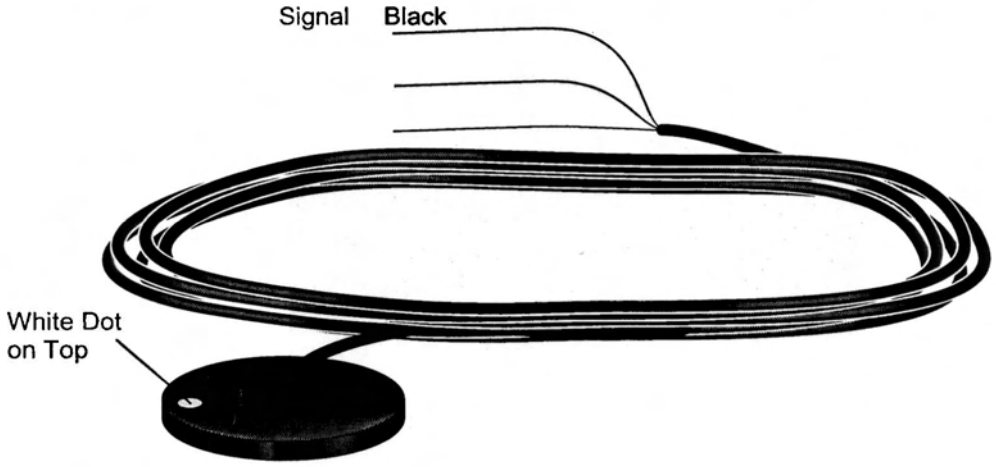

FIGURE 2. HFT3 Plate to Datalogger Connections

TABLE 1. Datalogger Connections for a Single-Ended Measurement

Description	Color	CR10(X), CR510	CR23X, 21X, CR7
Signal	Black	Single-Ended Input	Single-Ended Input
Signal Reference	White	AG	⏚
Shield	Clear	G	⏚

TABLE 2. Datalogger Connections for a Differential Measurement

Description	Color	CR10(X), CR510	CR23X, 21X, CR7
Signal	Black	Differential Input (H)	Differential Input (H)
Signal Reference	White	Differential Input (L)	Differential Input (L)
Shield	Clear	G	⏚

4. WIRING

Connections to Campbell Scientific dataloggers are given in Tables 1 and 2. The output of the HFT3 can be measured using a single-ended analog measurement (Instruction 1) or a differential analog measurement (Instruction 2).

The wiring convention is that the black wire is positive with respect to the other insulated wire, when energy is flowing through the transducer from the side with white dot to the side without the white dot.

5. EXAMPLE PROGRAMS

This section is for users who write their own dataloger programs. A datalogger program to measure the sensor can be created using Campbell Scientific's Short Cut Program Builder software. You do not need to read this section use Short Cut.

The HFT3 has a nominal calibration of 42 W m^{-2} mV^{-1}. Each sensor is accompanied with a calibration certificate. Each sensor has a unique calibration label on it. The label is located on the pigtail end of the sensor leads.

TABLE 3. Wiring for Example 1

Description	Color	CR10(X)
Signal	Black	SE 5 (3H)
Signal Reference	White	AG
Shield	Clear	G

Example 1 Sample CR10(X) Program using a Single-Ended Measurement Instruction

```
01:   Volt (SE) (P1)
        1:   1      Reps
        2:   2      7.5 mV Slow Range          ;CR510 (7.5 mV);CR23X (10 mV); 21X, CR7 (5 mV)
        3:   5      SE Channel                 ;Black wire (SE 5), White wire (AG)
        4:   1      Loc [ HFT3     ]
        5:   1      Mult                       ;Enter Calibration
        6:   0      Offset
```

TABLE 4. Wiring for Example 2

Description	Color	CR23X
Signal	Black	9H
Signal Reference	White	9L
Shield	Clear	⏚

Example 2 Sample CR23X Program using a Differential Measurement Instruction

```
;Measure the HFT3 Soil Heat Flux plate.
;
01:  Volt (Diff) (P2)
       1:  1        Reps
       2:  21       10 mV, 60 Hz Reject, Slow Range   ;CR510, CR10(X) (7.5 mV); 21X, CR7 (5 mV)
       3:  9        DIFF Channel                      ;Black wire (9H); White wire (9L)
       4:  1        Loc [ HFT3    ]
       5:  1        Mult                              ;Enter Calibration
       6:  0        Offset
```

6. SOIL HEAT FLUX AND STORAGE

The soil heat flux at the surface is calculated by adding the measured flux at a fixed depth, d, to the energy stored in the layer above the heat flux plates. The specific heat of the soil and the change in soil temperature, ΔT_s, over the output interval, t, are required to calculate the stored energy.

The heat capacity of the soil is calculated by adding the specific heat of the dry soil to that of the soil water. The values used for specific heat of dry soil and water are on a mass basis. The heat capacity of the moist is given by:

$$C_s = \rho_b (C_d + \theta_m C_w) = \rho_b C_d + \theta_v \rho_w C_w \qquad (1)$$

$$\theta_m = \frac{\rho_w}{\rho_b} \theta_v \qquad (2)$$

where C_S is the heat capacity of moist soil, ρ_b is bulk density, ρ_w is the density of water, C_d is the heat capacity of a dry mineral soil, θ_m is soil water content on a mass basis, θ_v is soil water content on a volume basis, and C_w is the heat capacity of water.

This calculation requires site specific inputs for bulk density, mass basis soil water content or volume basis soil water content, and the specific heat of the dry soil. Bulk density and mass basis soil water content can be found by sampling (Klute, 1986). The volumetric soil water content is measured by the CS615 water content reflectometer. A value of 840 J kg^{-1} K^{-1} for the heat capacity of dry soil is a reasonable value for most mineral soils (Hanks and Ashcroft, 1980).

The storage term is then given by Eq. (3) and the soil heat flux at the surface is given by Eq. (4).

$$S = \frac{\Delta T_s C_s d}{t} \qquad (3)$$

$$G_{sfc} = G_{8cm} + S \qquad (4)$$

7. MAINTENANCE

The HFT3 requires minimal maintenance. Check the sensor leads monthly for rodent damage.

Recalibrate the HFT3 every two years of continuous use. Obtain an RMA number before returning the HFT3 to Campbell Scientific for calibration.

8. REFERENCES

Hanks, R. J., and G. L. Ashcroft, 1980: *Applied Soil Physics: Soil Water and Temperature Application.* Springer-Verlag, 159 pp.

Klute, A., 1986: *Method of Soil Analysis.* No. 9, Part 1, Sections 13 and 21, American Society of Agronomy, Inc., Soil Science Society of America, Inc.

MSX10, MSX10R, MSX20R, MSX64R, AND MSX128R
SOLAR PANELS
INSTRUCTION MANUAL

REVISION: 10/01

Warranty and Assistance

The **MSX10, MSX10R, MSX20R, MSX64R, AND MSX128R SOLAR PANELS** are warranted by CAMPBELL SCIENTIFIC, INC. to be free from defects in materials and workmanship under normal use and service for twelve (12) months from date of shipment unless specified otherwise. Batteries have no warranty. CAMPBELL SCIENTIFIC, INC.'s obligation under this warranty is limited to repairing or replacing (at CAMPBELL SCIENTIFIC, INC.'s option) defective products. The customer shall assume all costs of removing, reinstalling, and shipping defective products to CAMPBELL SCIENTIFIC, INC. CAMPBELL SCIENTIFIC, INC. will return such products by surface carrier prepaid. This warranty shall not apply to any CAMPBELL SCIENTIFIC, INC. products which have been subjected to modification, misuse, neglect, accidents of nature, or shipping damage. This warranty is in lieu of all other warranties, expressed or implied, including warranties of merchantability or fitness for a particular purpose. CAMPBELL SCIENTIFIC, INC. is not liable for special, indirect, incidental, or consequential damages.

Products may not be returned without prior authorization. To obtain a Returned Materials Authorization (RMA), contact CAMPBELL SCIENTIFIC, INC., phone (435) 753-2342. After an applications engineer determines the nature of the problem, an RMA number will be issued. Please write this number clearly on the outside of the shipping container. CAMPBELL SCIENTIFIC's shipping address is:

CAMPBELL SCIENTIFIC, INC.
RMA#_____
815 West 1800 North
Logan, Utah 84321-1784

CAMPBELL SCIENTIFIC, INC. does not accept collect calls.

Non-warranty products returned for repair should be accompanied by a purchase order to cover the repair.

815 W. 1800 N.
Logan, UT 84321-1784
USA
Phone (435) 753-2342
FAX (435) 750-9540
www.campbellsci.com

Campbell Scientific Canada Corp.
11564 -149th Street
Edmonton, Alberta T5M 1W7
CANADA
Phone (780) 454-2505
FAX (780) 454-2655

Campbell Scientific Ltd.
Campbell Park
80 Hathern Road
Shepshed, Loughborough
LE12 9GX, U.K.
Phone +44 (0) 1509 601141
FAX +44 (0) 1509 601091

MSX10, MSX10R, MSX20R, MSX64R, and MSX128R Solar Panels

1. General

The solar panel is a photovoltaic power source used for charging lead acid batteries. The MSX10, MSX10R, MSX20R, MSX64R, and MSX128R are 10, 10, 20, 64, and 128-watt solar panels, respectively.

The MSX10 Solar Panels has two leads stripped and tinned to insert into the terminals labeled 'CHG' on the PS12-LA Charging Regulator. With a CR7, the two wires from the solar panel are inserted into the terminals marked SOLAR PANEL located underneath the 700X Control Module. An external lead acid battery can be connected to the CR7 at the terminals marked EXTERNAL BATTERY next to the SOLAR PANEL terminals.

The MSX10 must have a connector (Part No. 788) to plug into the 21XL Micrologger. This connector is supplied and attached if the solar panel is purchased with the 21XL. If the solar panel is not purchased with a 21XL, the connector is taped to the cable and can be discarded if not needed. See Appendix A for details.

The MSX10R, MSX20R, MSX64R, and MSX128R are regulated solar panels with two stripped and tinned leads for direct connection to an external 12-volt lead acid battery.

2. Specifications

	MSX10/MSX10R	MSX20R	MSX64R	MSX128R
Typical peak power (Pp)	10 W	20 W	64	128
Voltage @ peak power (Vpp)	17.5 V	17.1 V	17.5	17.5
Current @ peak power (Ipp)	0.57 A	1.17 A	3.66	7.32
Guaranteed minimum peak power	9 W	18 W	62	124
Approximate effect of temperature on power	-0.37%/°C	-0.38%/°C	-.38/°C	-.38/°C
Length, cm	42.0	50.1	111.3	111.3
Width, cm	26.9	42.2	50.2	100.4
Depth, cm	2.3	5.0	5	5
Weight, kg	1.50	2.95	7.2	14.4

NOTE The above solar panel characteristics assume a 1 kilowatt per square meter illumination and a solar panel temperature of 25 °C. Individual panels may vary up to 10%. The output panel voltage increases as the panel temperature decreases.

*The MSX128R includes two 64-watt solar panels. An MSX64R can be updated to an MSX128R with part number 13968.

3. Installation

3.1 Mounting

The panel should be mounted facing south if located in the Northern Hemisphere, or facing north in the Southern Hemisphere. The solar panel mounts to the mast or leg of the CM10/CM6 Tripod, or any 1 5/8" schedule 40 pipe, see Figure 1. The panel should be mounted to the pipe using the U-bolts and 5/16 NC (course) nuts provided with the solar panel. The nuts fastening the bracket to the pipe should be as tight as possible without bending the bracket.

If the MSX10 solar panel is being used, route the solar panel cable to the datalogger power supply and charging circuitry. If the MSX10R, MSX20R, MSX64R, or MSX128R is being used, attach the leads of the solar panel directly to the external battery with a user supplied connector. Figure 2 shows an example of a regulated solar panel connected to an external battery to run a radiotelemetry system.

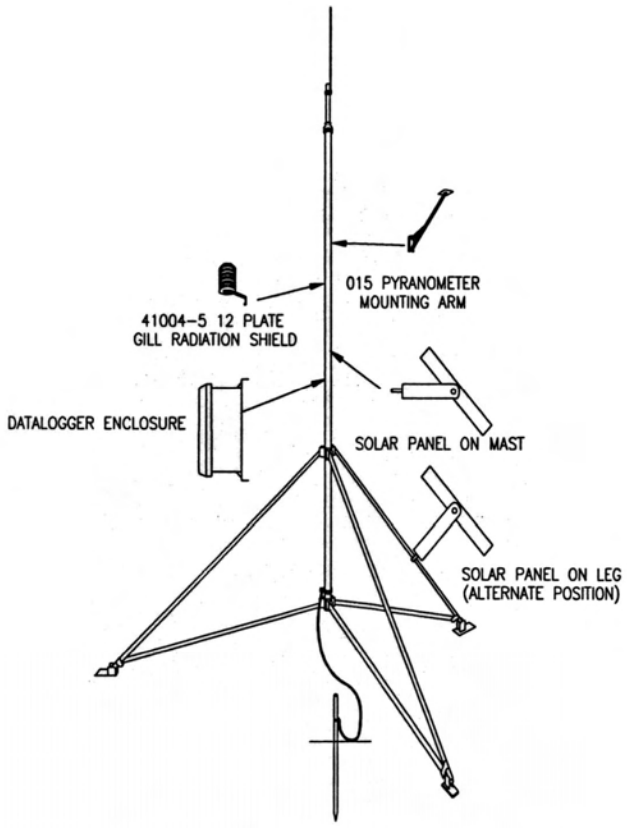

FIGURE 1. Solar Panel Mounting

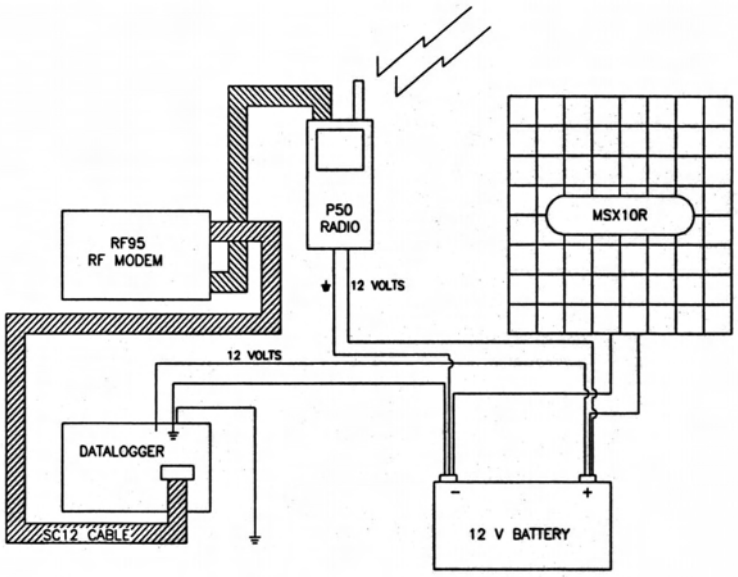

FIGURE 2. Regulated Solar Panel and External Battery

3.2 Orientation

The solar panel should be oriented to receive maximum insolation (incident solar radiation) over the course of a year. Suggested tilt angles of the solar panel are given in Table 1.

After determining the tilt angle, loosen the 5/16" nuts on each side of the solar panel, adjust the panel, and tighten the two nuts to secure the position. See Figure 3.

0 – 10°	10°
11 – 20°	Latitude +5°
21 – 45	Latitude +10°
46 – 65	Latitude +15°
> 65	80°

* From "Design Aids for Small PV Power Systems", Solorex Corp.

4. Maintenance

An occasional cleaning of the glass improves the solar panel's efficiency.

If a problem with the solar panel is suspected, the panel may be checked by measuring the voltage output. Check the voltage with a voltmeter connected

between the two leads of the solar panel. There must be solar radiation incident on the panel and there must be a load connected to the solar panel. The load can be the datalogger, other equipment, or a 75 ohm resistor capable of dissipating solar panel power between the two leads. No voltage output implies a bad solar panel, regulator, or cable. The magnitude of the voltage output depends on the incident solar radiation.

5. Power Considerations

5.1 Solar Power and Lead Acid Batteries

The solar panel converts light energy to electricity, or specifically direct current. The direct current produced is used as a charging source for lead acid batteries.

The solar panel operates in both direct and diffuse light (cloudy days), but not at night.

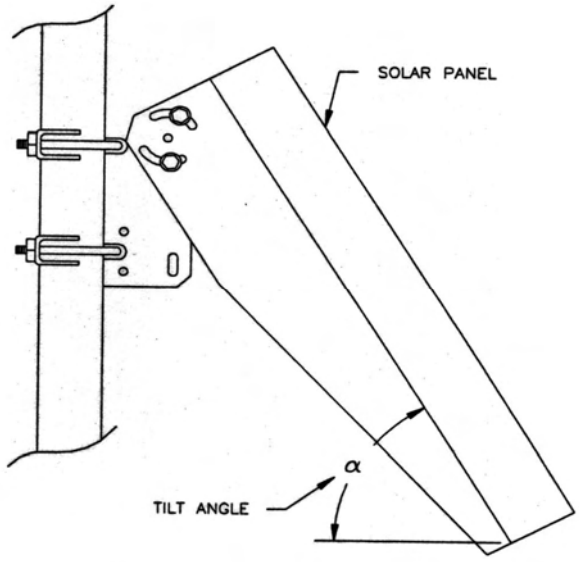

FIGURE 3. Solar Panel Orientation

The minimum battery size and solar panel output required depends on 1) the average current drain of the system, 2) the maximum time the battery must supply power to the system without being charged, and 3) the location of the site. When some batteries are discharged below a specified voltage, the battery becomes damaged and cannot be recharged.

The battery supplies power directly to the operating system, the solar panel supplies power to recharge the battery. Therefore, on the average, the solar panel must provide at least as much power to the battery as is being used by the system.

The battery must have enough capacity to power the system during times of no charging (night) or low charging (stormy winter days).

5.2 Voltage Regulator

The solar panel must be regulated either with a Campbell Scientific regulator or an attached regulator. The regulator has two basic functions: 1) blocks any current flow from the battery to the solar panel, and 2) limits the source current to the battery.

The MSX10 is unregulated and must be connected to a Campbell Scientific voltage regulator. These regulators include the PS12-LA, PS512M, CH12R, CH512R, 21XL base, and the CR7 solar panel input.

The MSX10R, MSX20R, MSX64R, and MSX128R have a voltage regulator attached. These panels are connected directly to a battery.

Appendix A. Solar Panel Connector

The MSX10 solar panel is shipped standard with the two lead wires stripped and tinned and a connector taped to the cable. This connector must be attached to use the MSX10 with the 21XL.

With the connector, the cable can be inserted directly into the 21XL Charging Port on the side of the Micrologger.

If it is necessary to solder the connector on the cable, please refer to the diagram below.

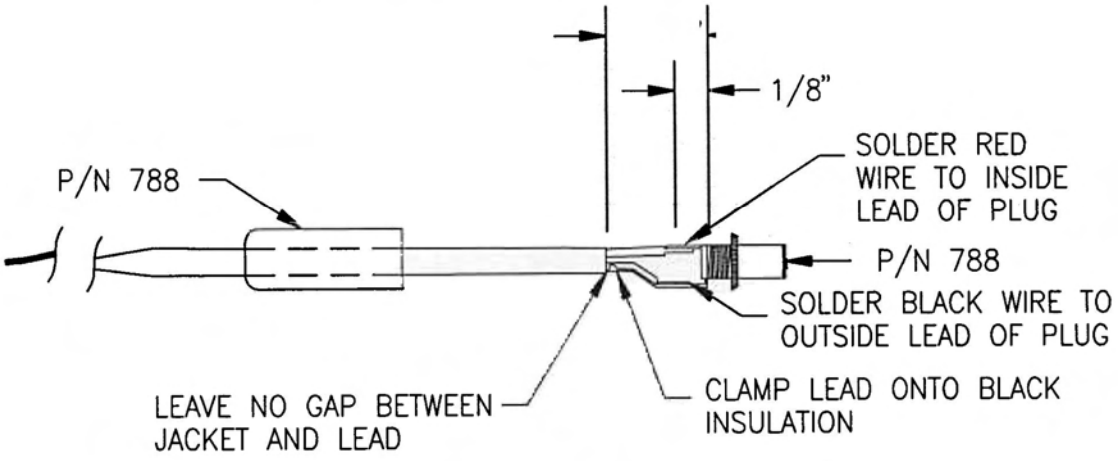

FIGURE A-1. Connector Wiring

Appendix C: Graphs

Soil Only Section
Temperature

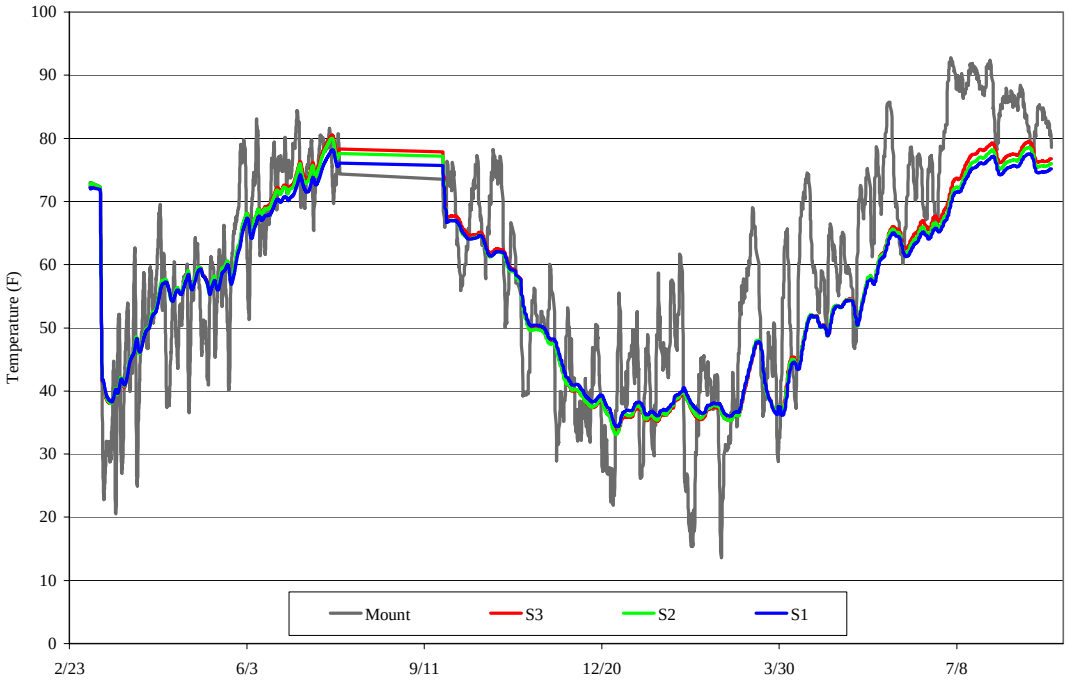

Soil Only Section
Ambient Temperature versus Internal Temperature for S1

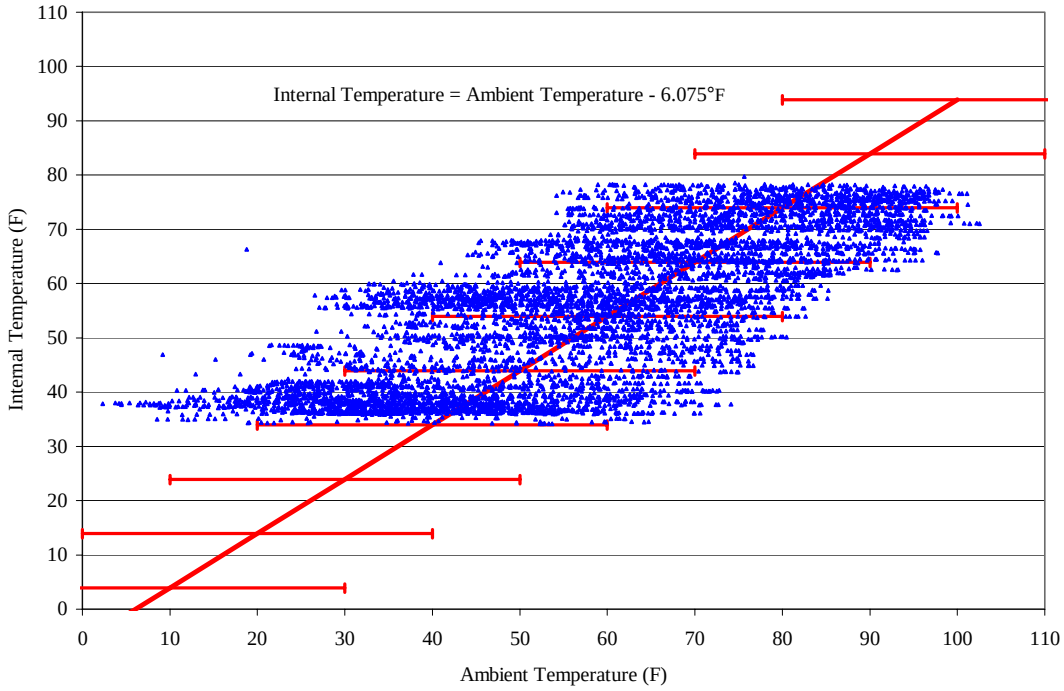

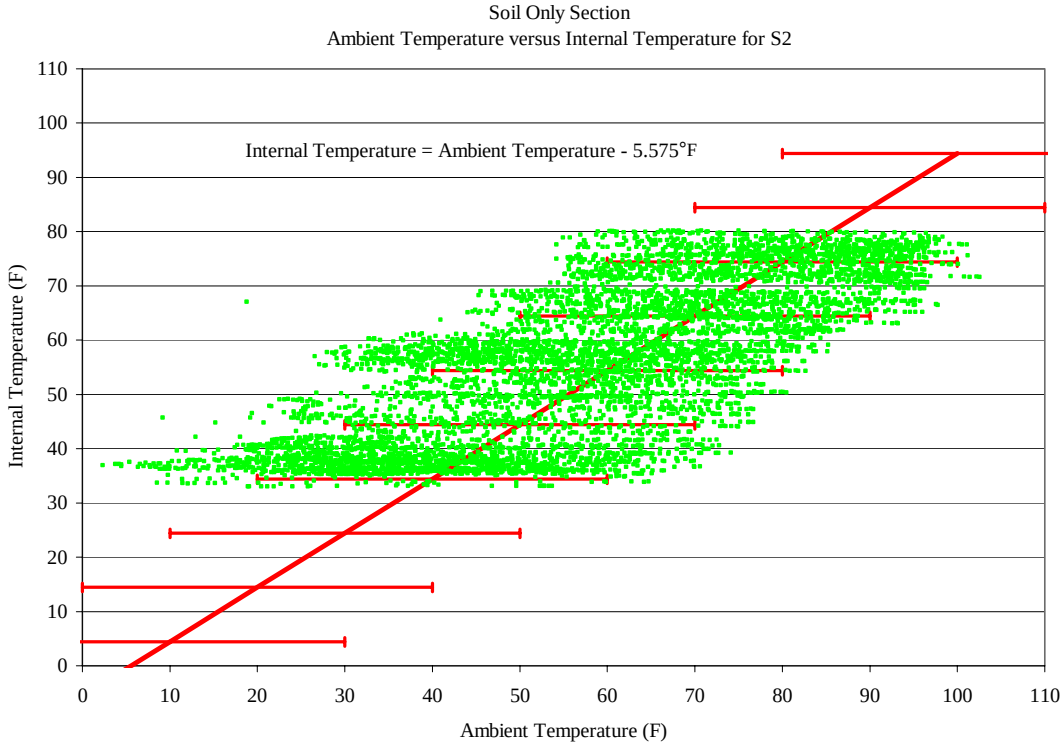
Soil Only Section
Ambient Temperature versus Internal Temperature for S2
Internal Temperature = Ambient Temperature - 5.575°F
Internal Temperature (F)
Ambient Temperature (F)
0
10
20
30
40
50
60
70
80
90
100
110

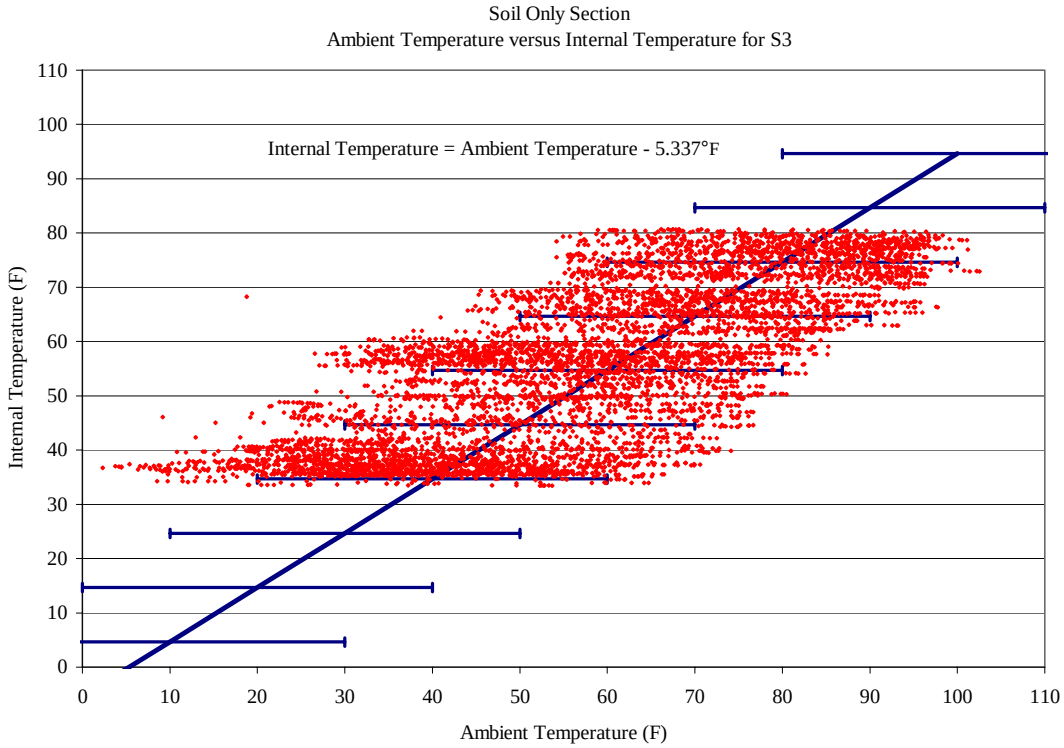
Soil Only Section
Ambient Temperature versus Internal Temperature for S3
Internal Temperature = Ambient Temperature - 5.337°F
Internal Temperature (F)
Ambient Temperature (F)
0
10
20
30
40
50
60
70
80
90
100
110

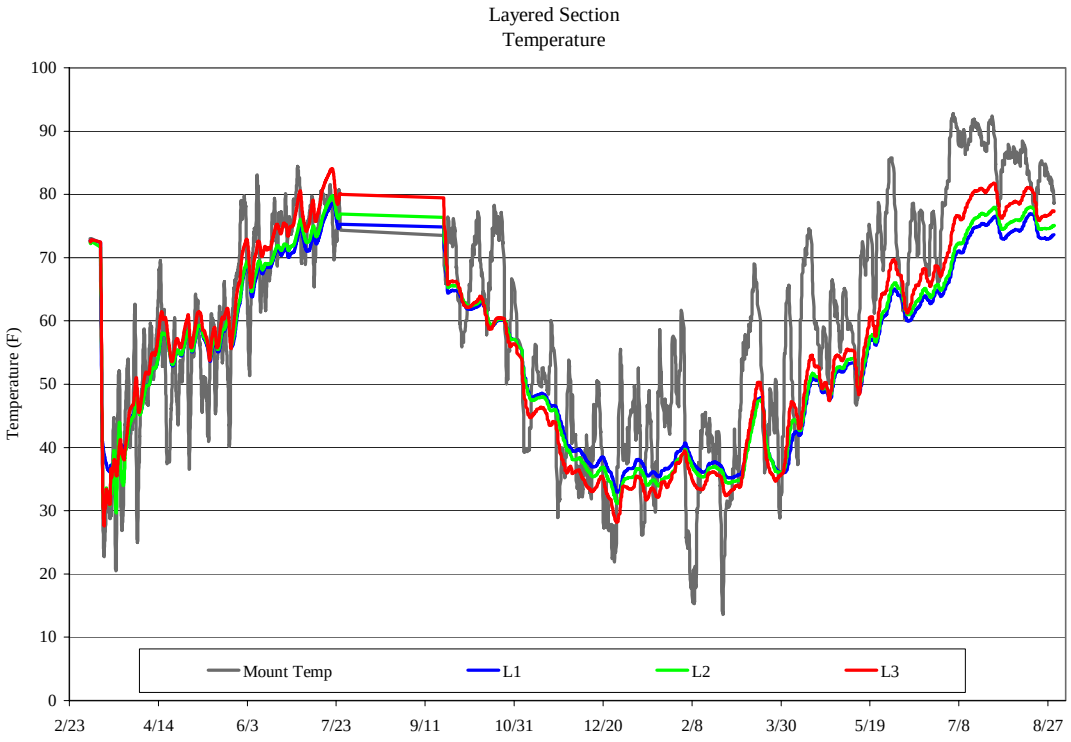
Layered Section
Temperature
Temperature (F)
100
90
80
70
60
50
40
30
20
10
0
2/23
4/14
6/3
7/23
9/11
10/31
12/20
2/8
3/30
5/19
7/8
8/27
Mount Temp
L1
L2
L3

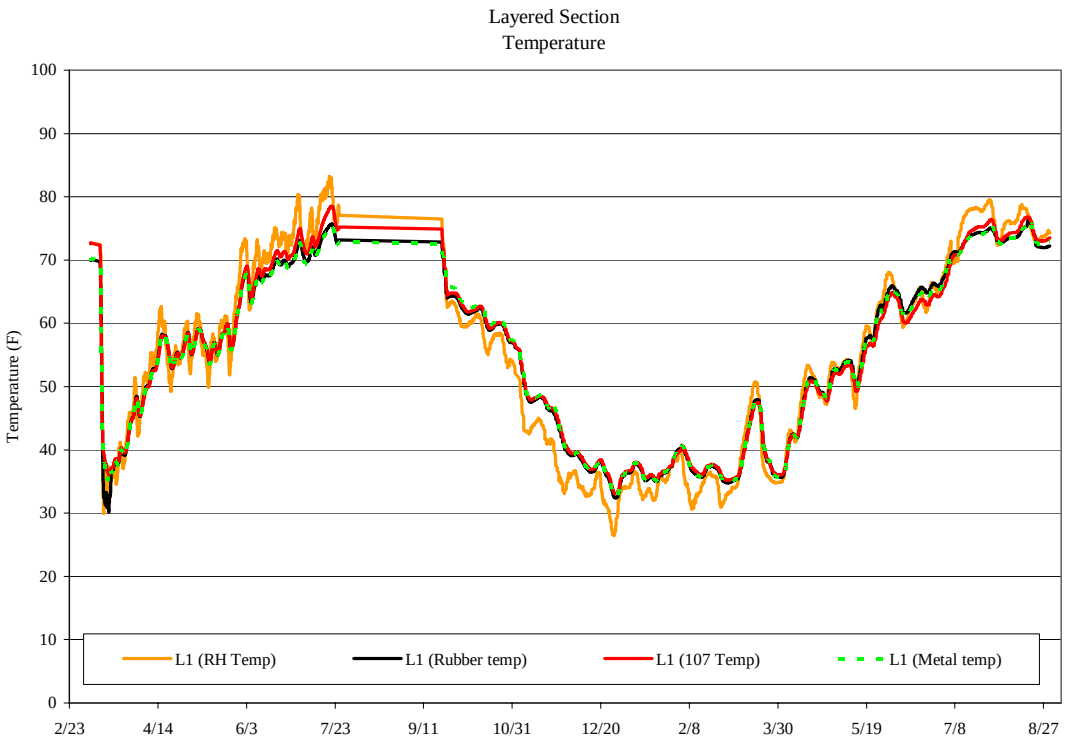
Layered Section
Temperature
Temperature (F)
100
90
80
70
60
50
40
30
20
10
0
2/23
4/14
6/3
7/23
9/11
10/31
12/20
2/8
3/30
5/19
7/8
8/27
L1 (RH Temp)
L1 (Rubber temp)
L1 (107 Temp)
L1 (Metal temp)

Layered Section
Temperature

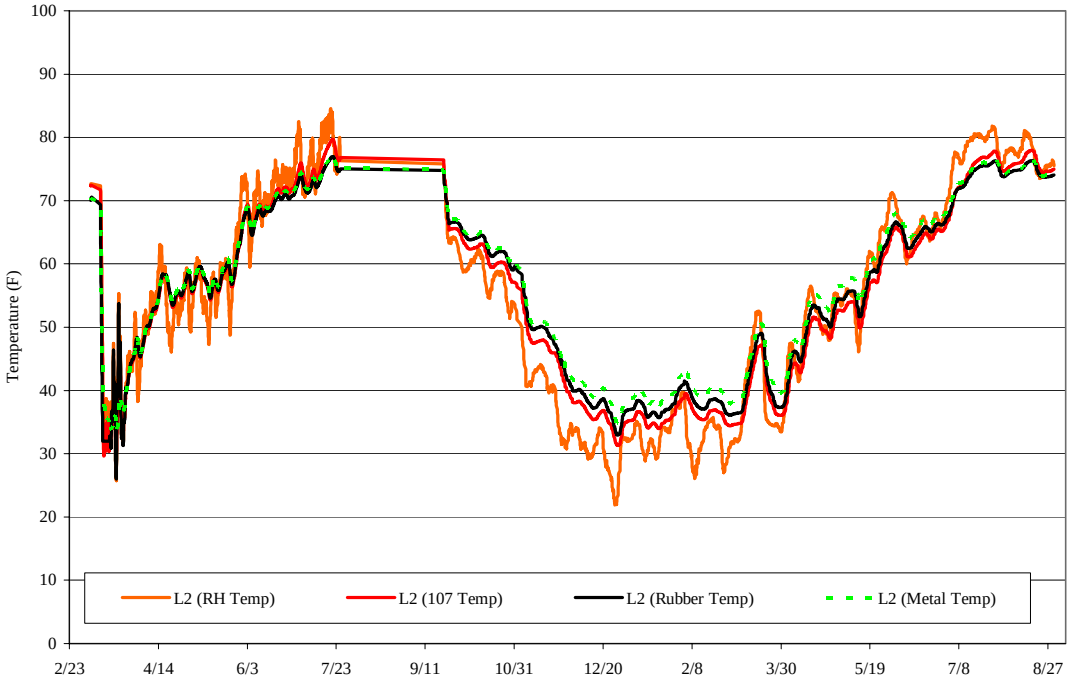

Layered Section
Temperature

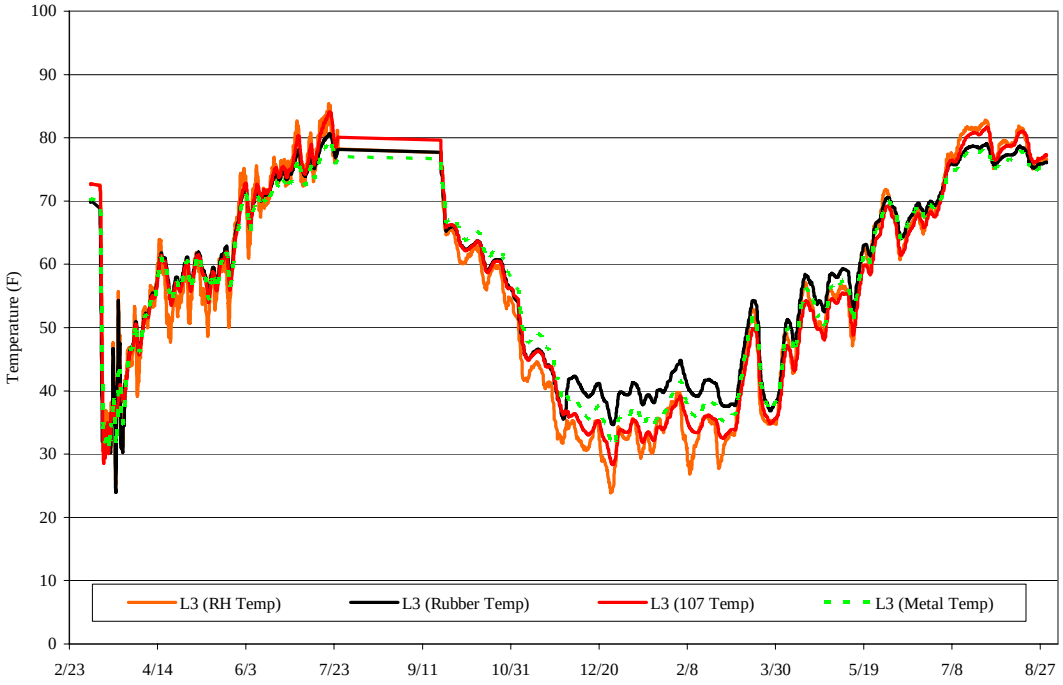

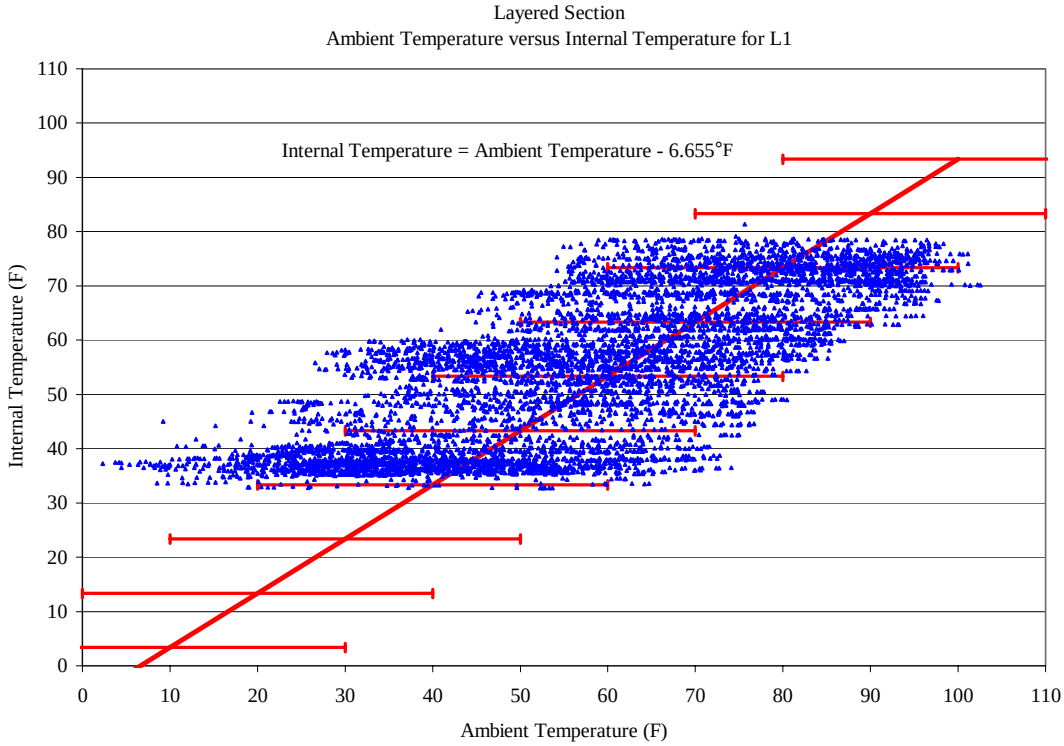
Layered Section
Ambient Temperature versus Internal Temperature for L1
Internal Temperature = Ambient Temperature - 6.655°F
Internal Temperature (F)
Ambient Temperature (F)
0
10
20
30
40
50
60
70
80
90
100
110

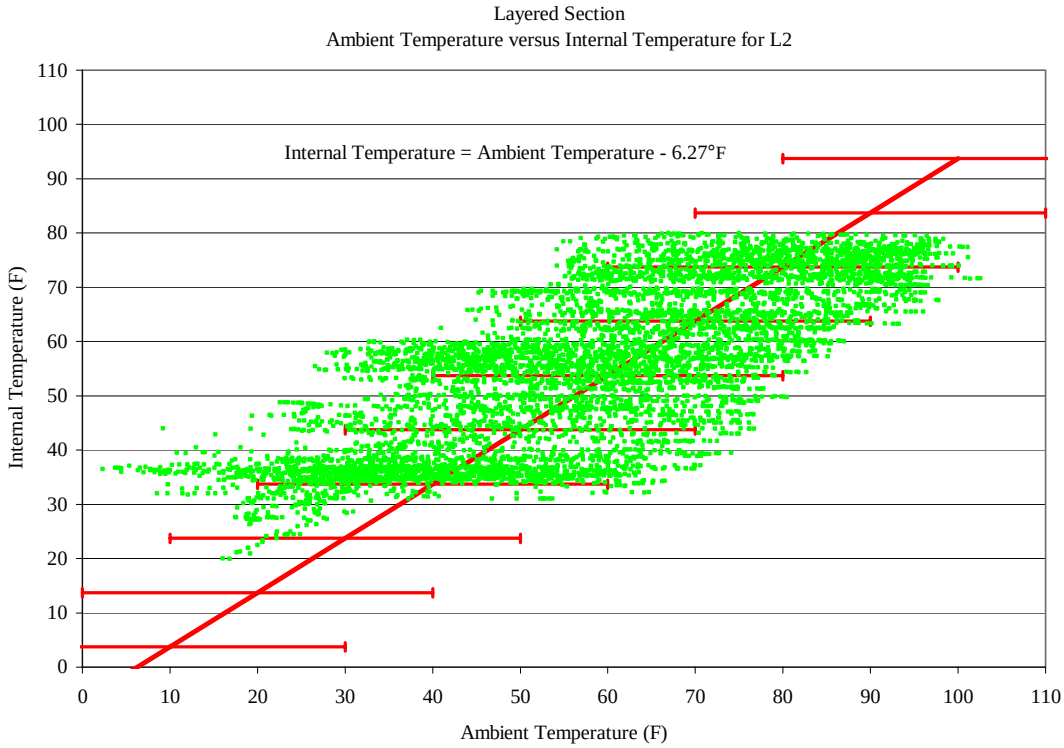
Layered Section
Ambient Temperature versus Internal Temperature for L2
Internal Temperature = Ambient Temperature - 6.27°F
Internal Temperature (F)
Ambient Temperature (F)
0
10
20
30
40
50
60
70
80
90
100
110

Layered Section
Ambient Temperature versus Internal Temperature for L3

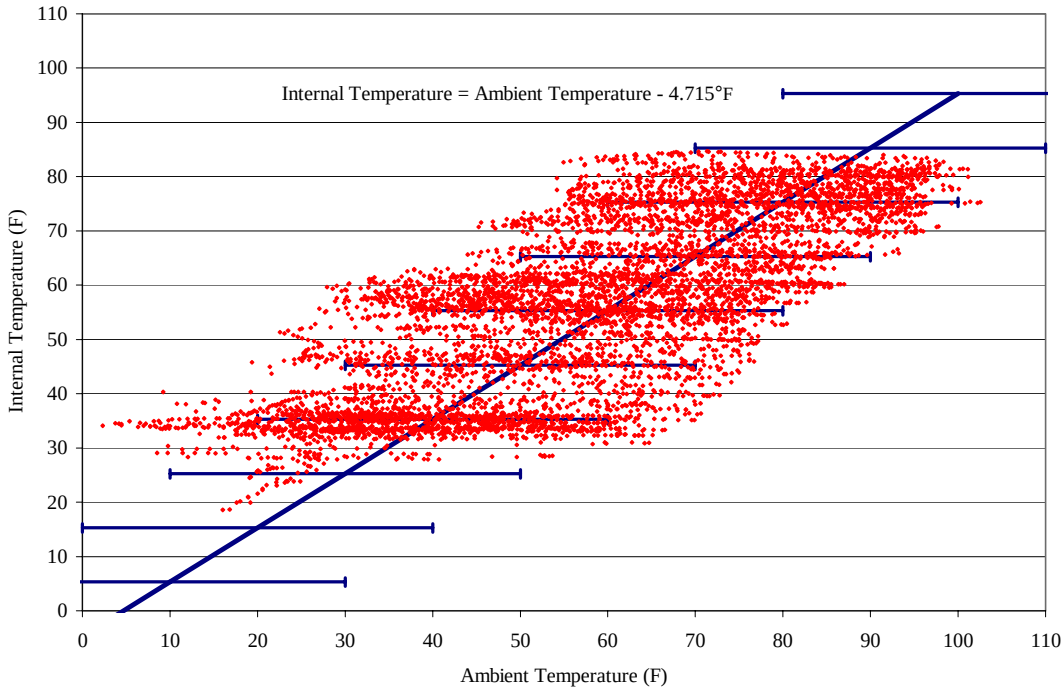

Mixed Section
Temperature

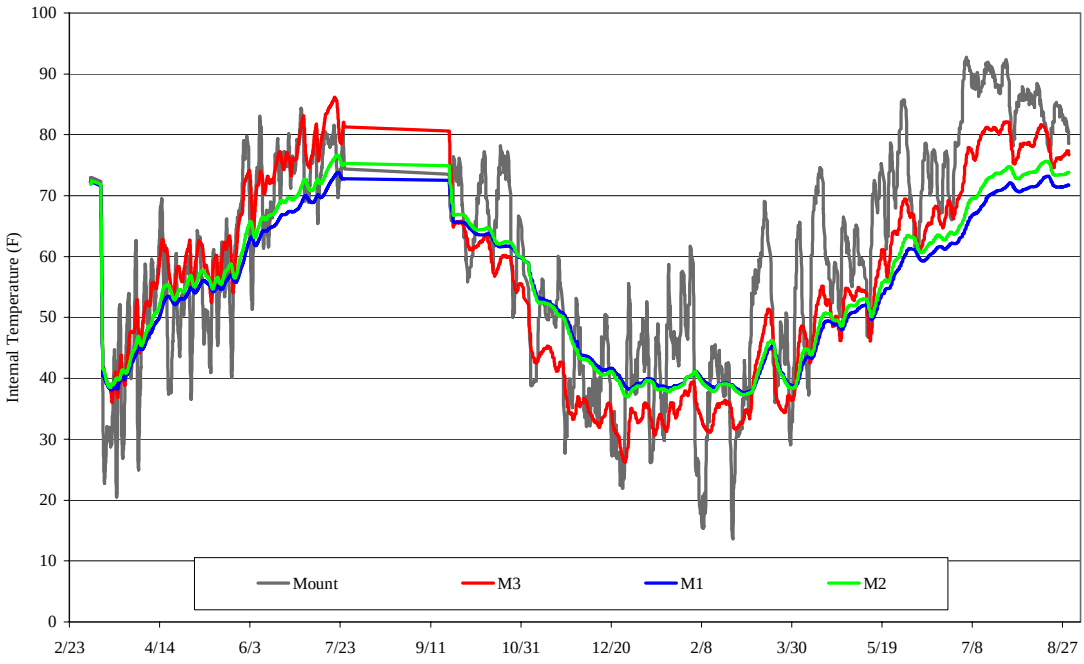

Mixed Section
M1 Temperature

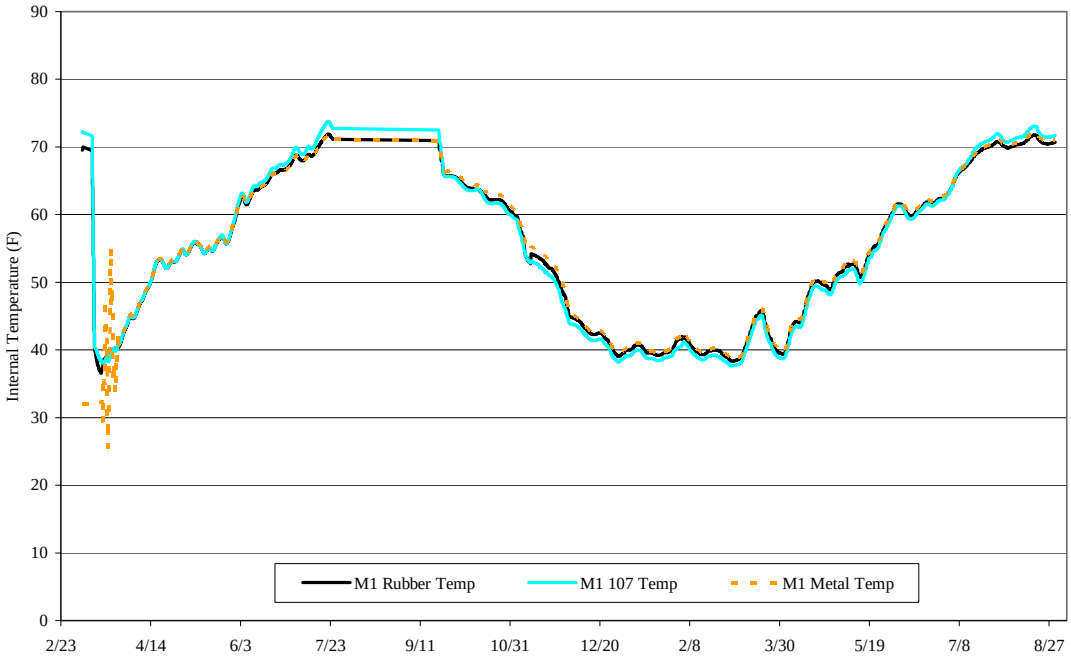

Mixed Section
M2 Temperature

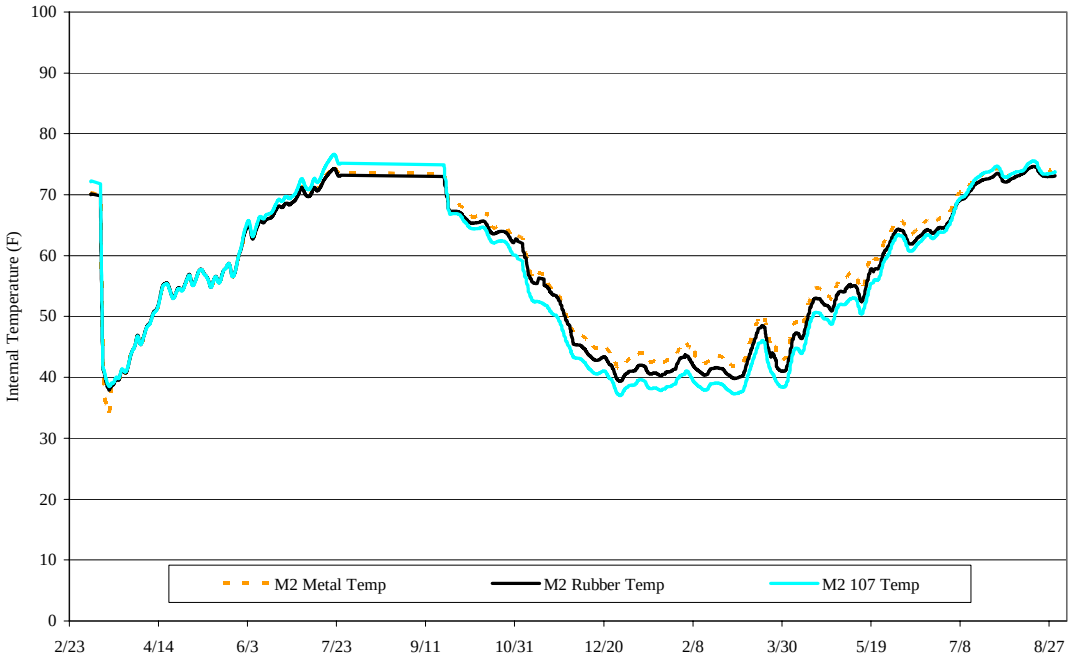

Mixed Section
M3 Temperature

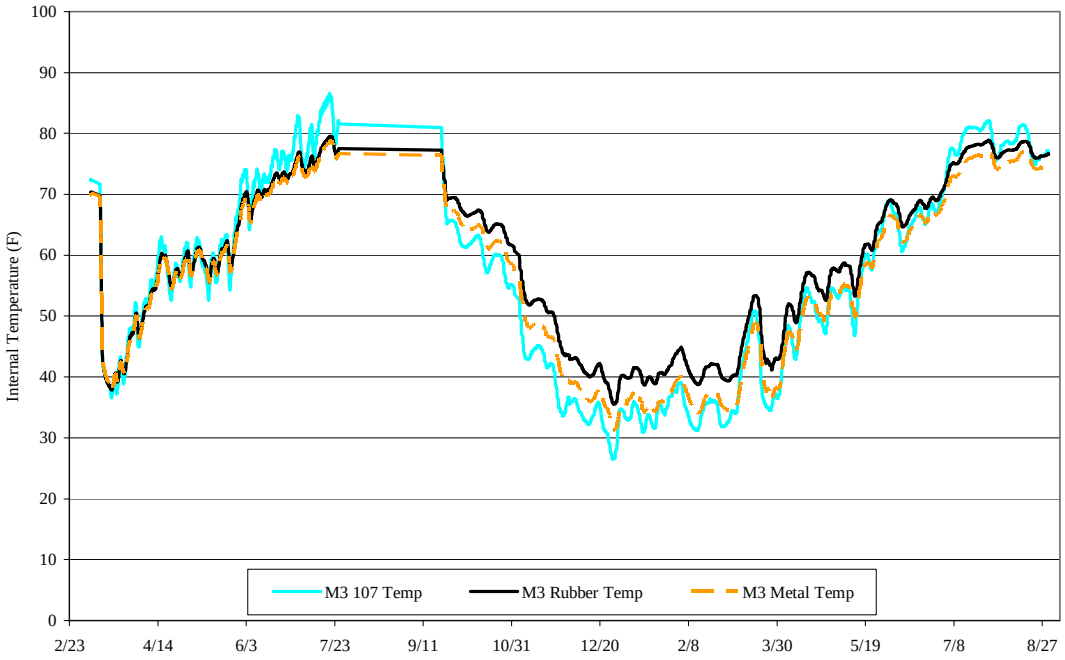

Mixed Section
Ambient Temperature versus Internal Temperature for M1

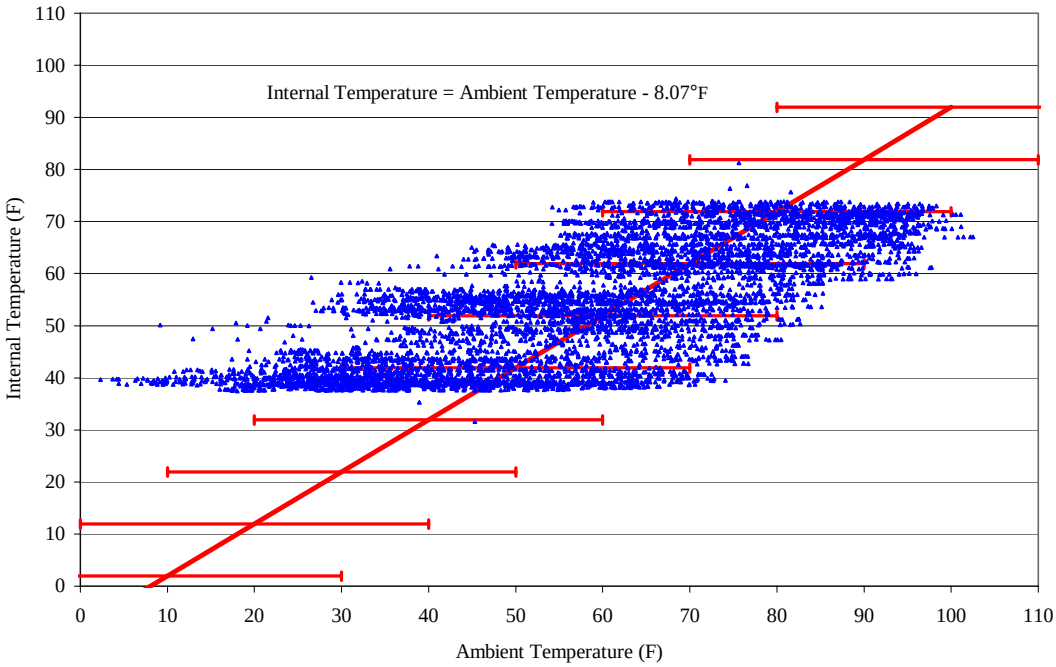

Mixed Section
Ambient Temperature versus Internal Temperature for M2

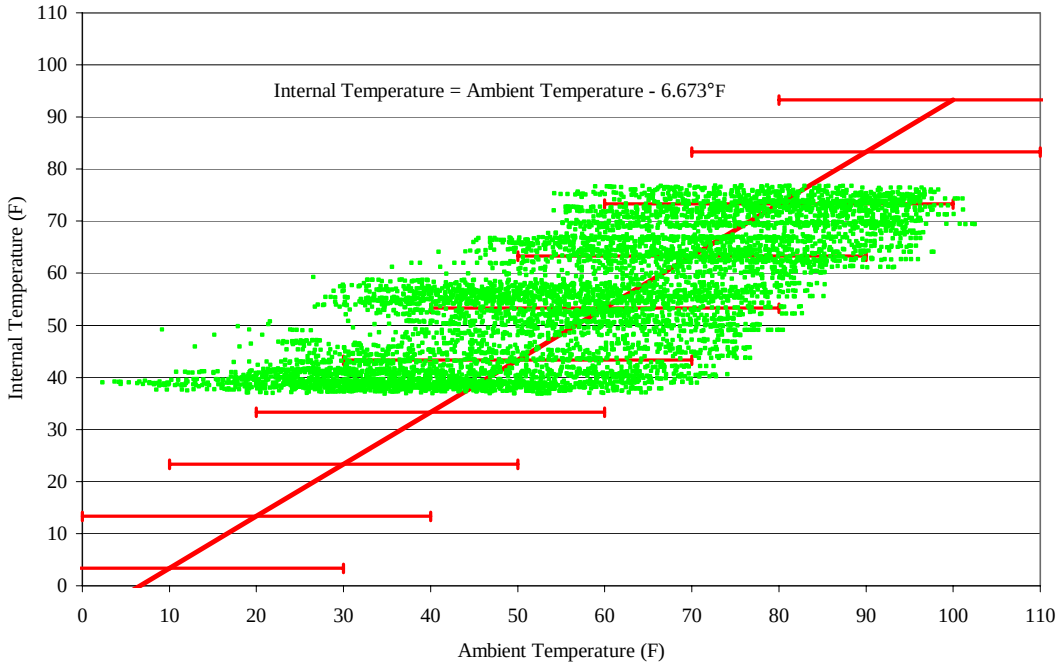

Mixed Section
Ambient Temperature versus Internal Temperature for M3

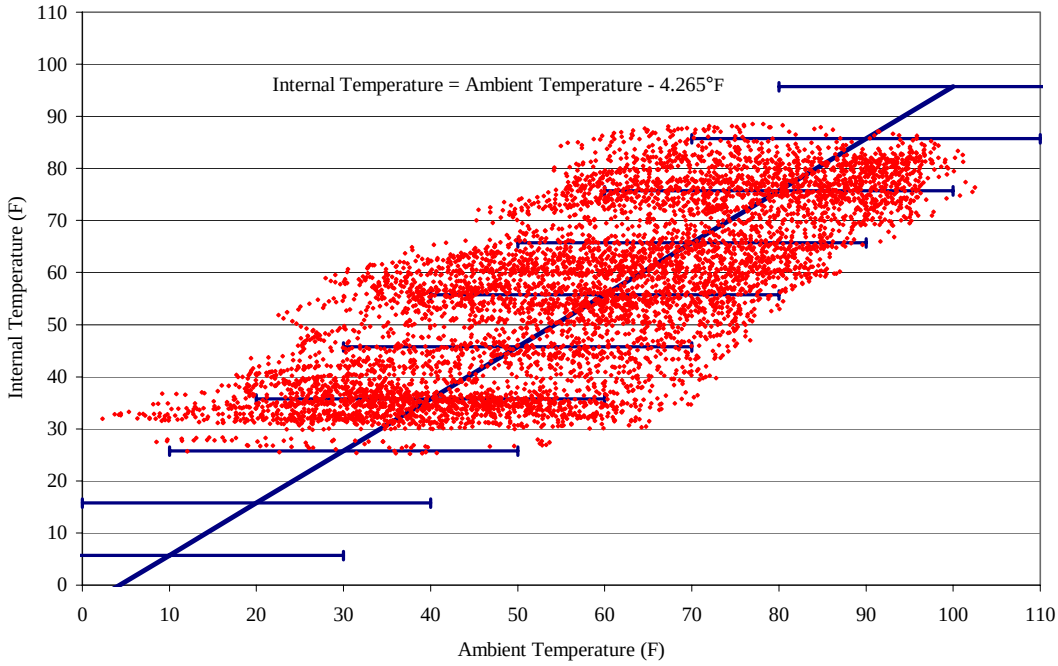

Tire Shred Pile
Temperature

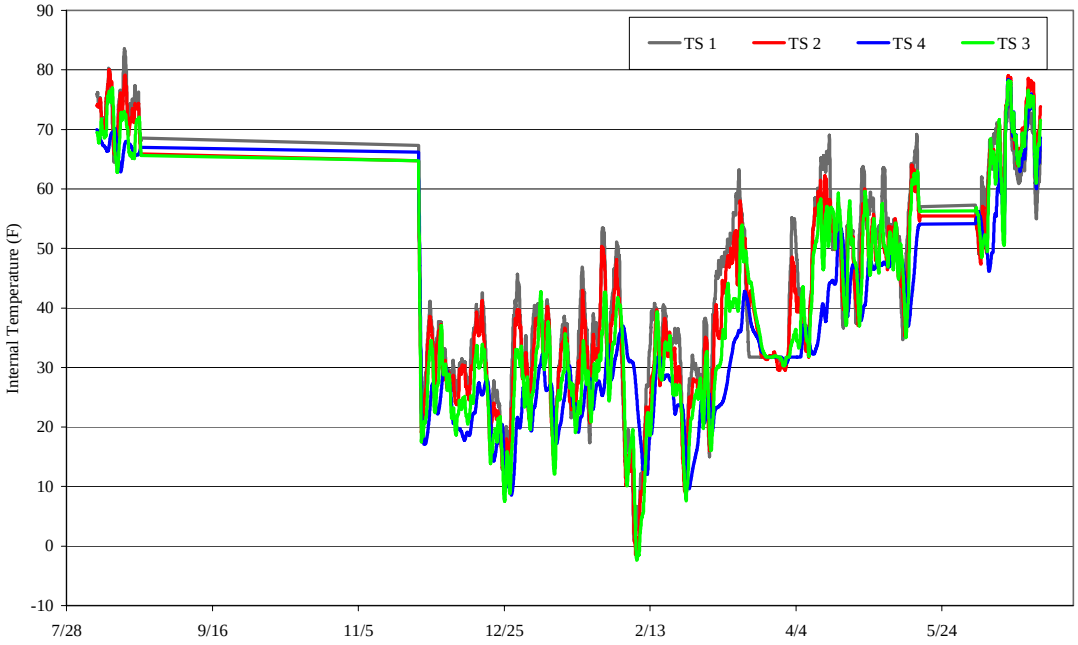

Tire Shred Pile
Ambient Temperature versus Internal Temperature
Linear Regression

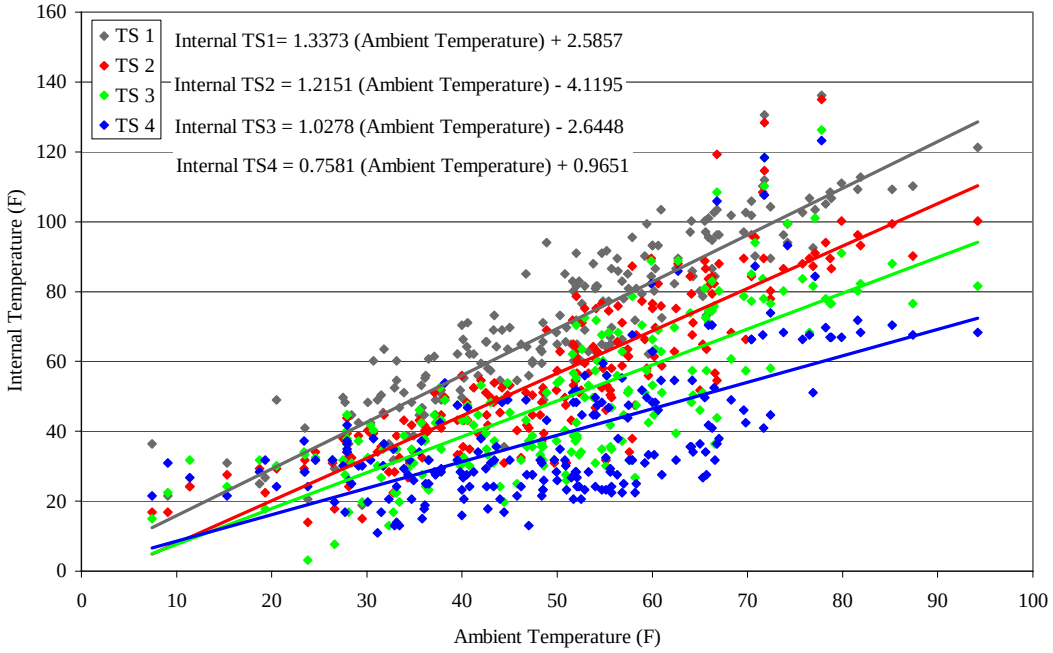

Soil Only Section
Measured Soil Suction

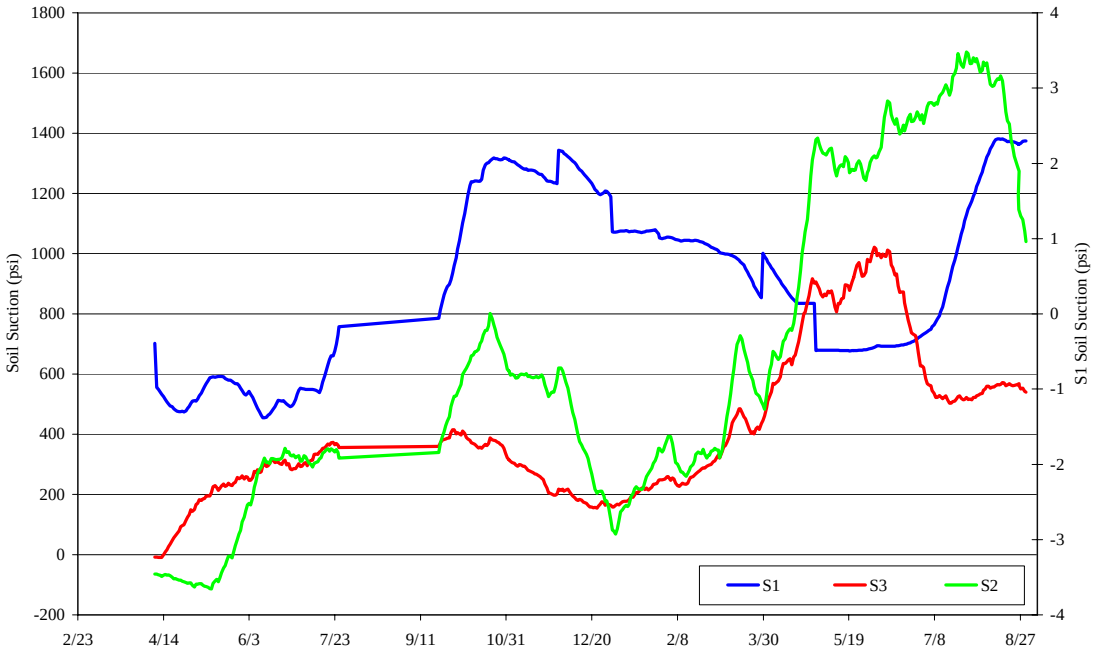

Layered Section
Soil Suction

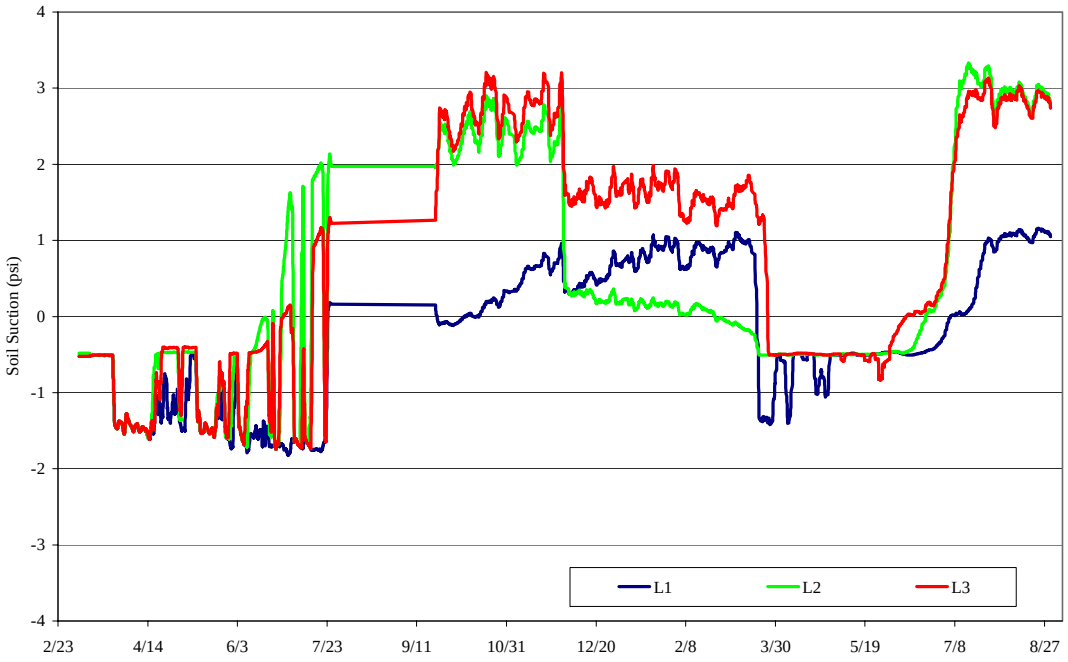

Mixed Section
Measured Soil Suction

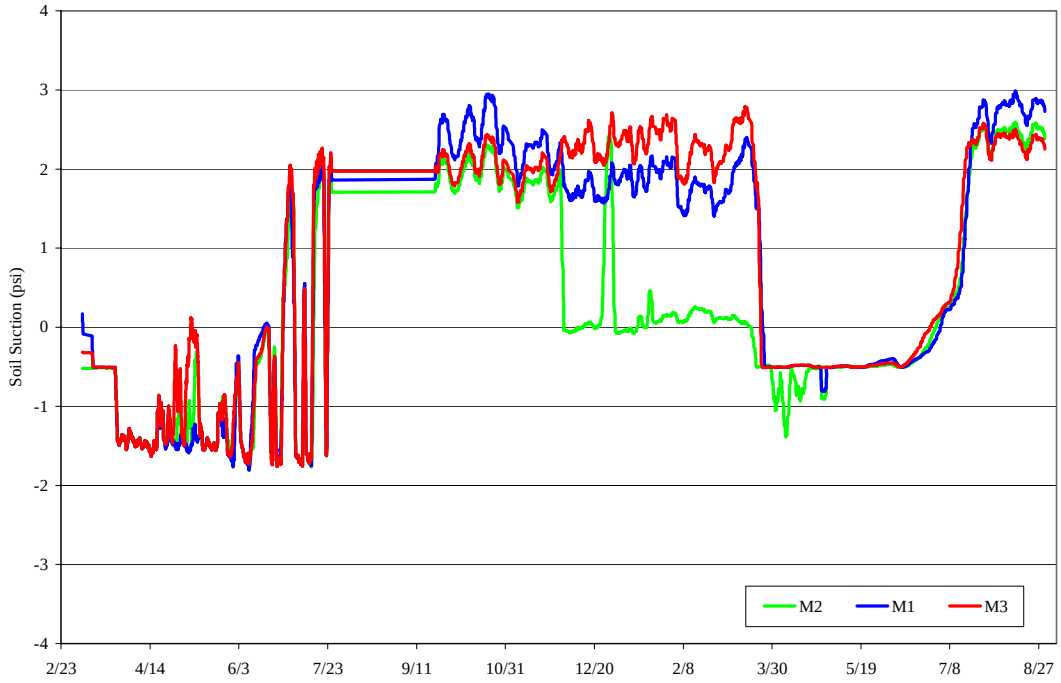

Soil Only Section
Daily Average Gravimetric Water Content for S1

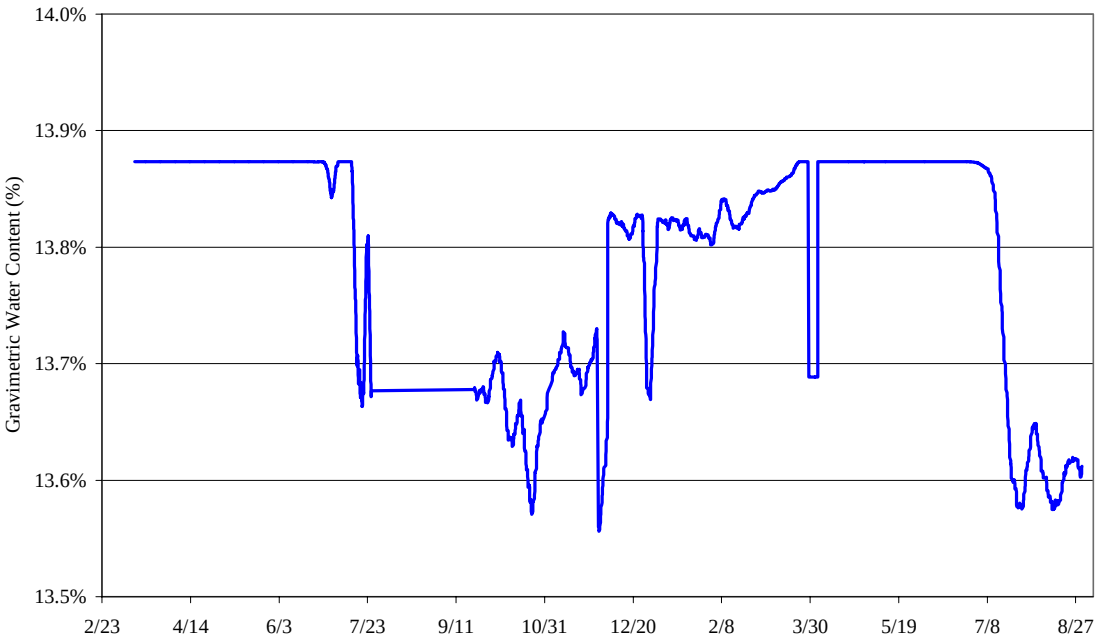

Soil-Only Section
Water Content versus S1 Internal Temperature

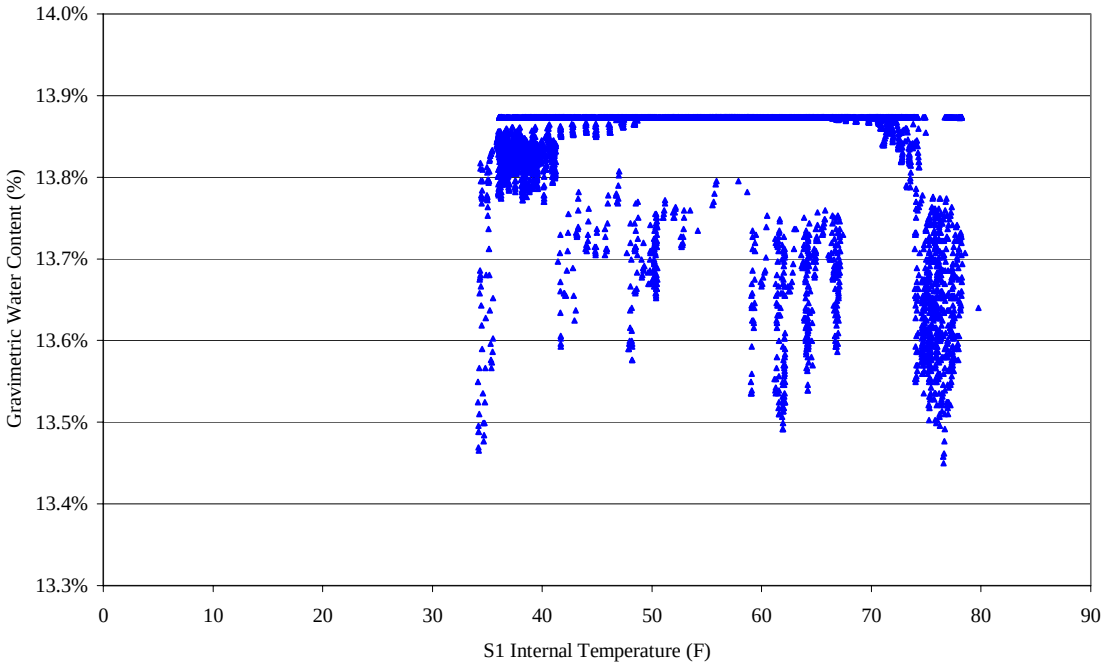

Mixed Section
Daily Average Gravimetric Water Content

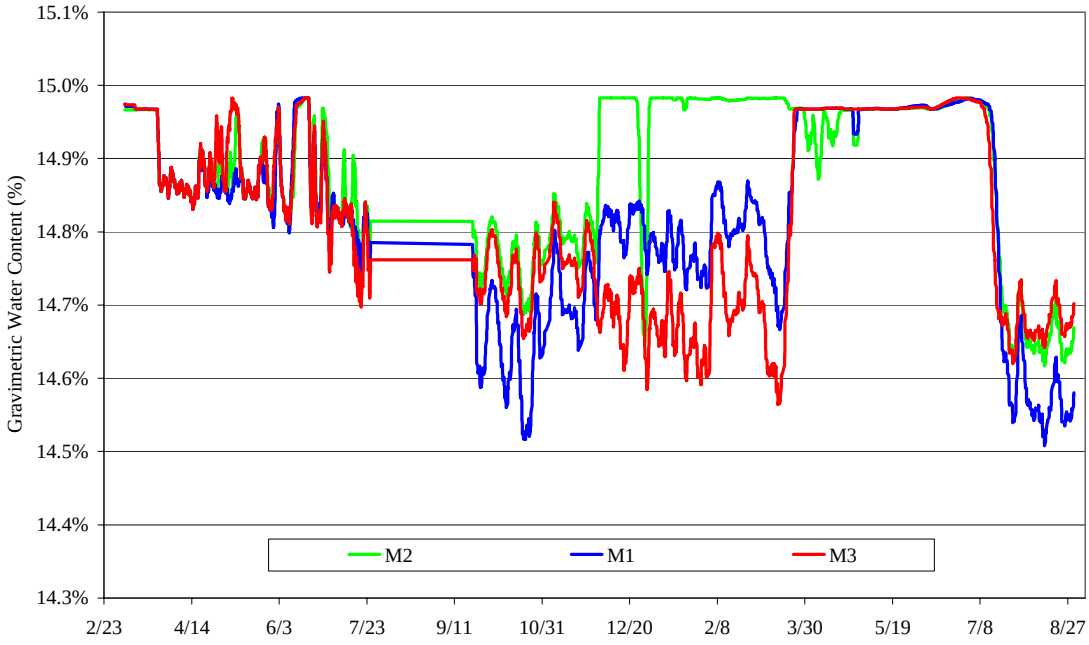

Mixed Section
Water Content versus Temperature

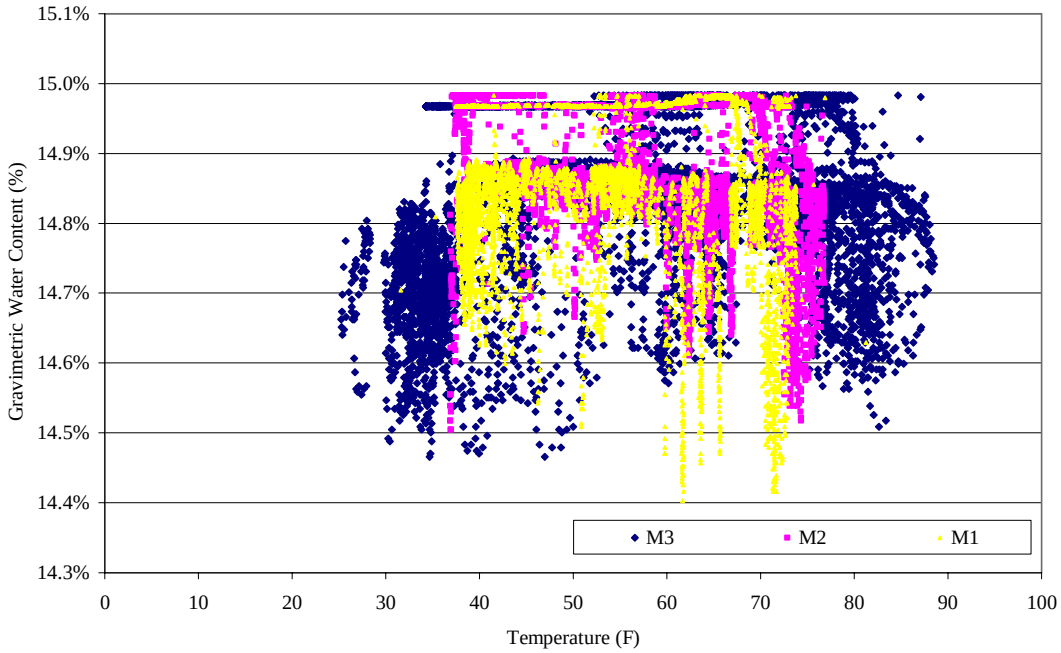

Layered Section
Daily Average Gravimetric Water Content

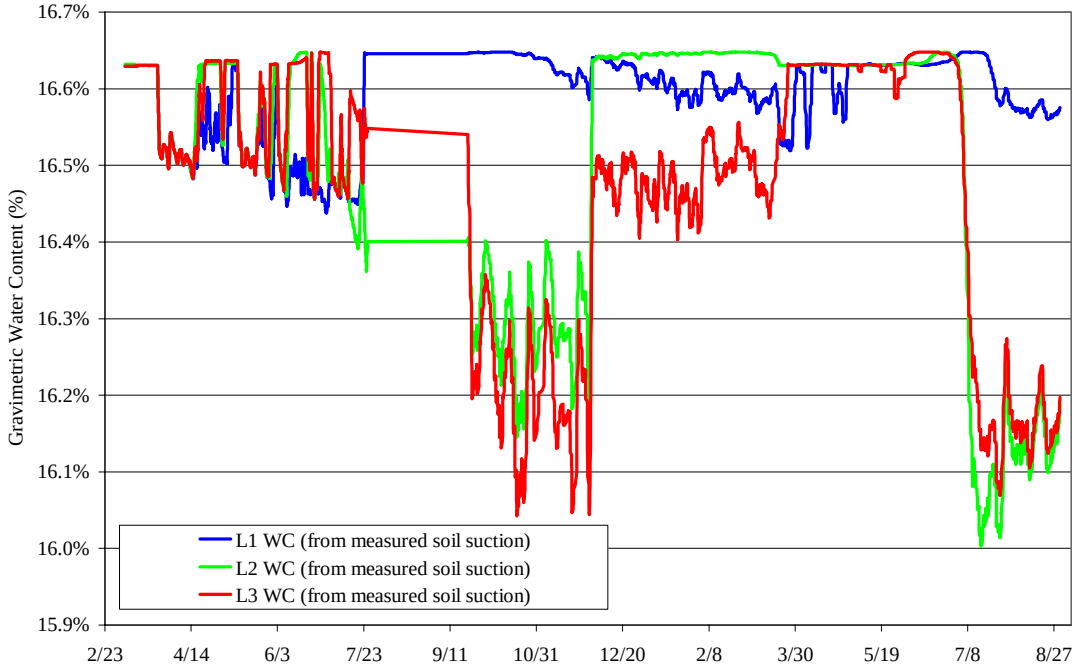

Layered Section
Daily Average Gravimetric Water Content

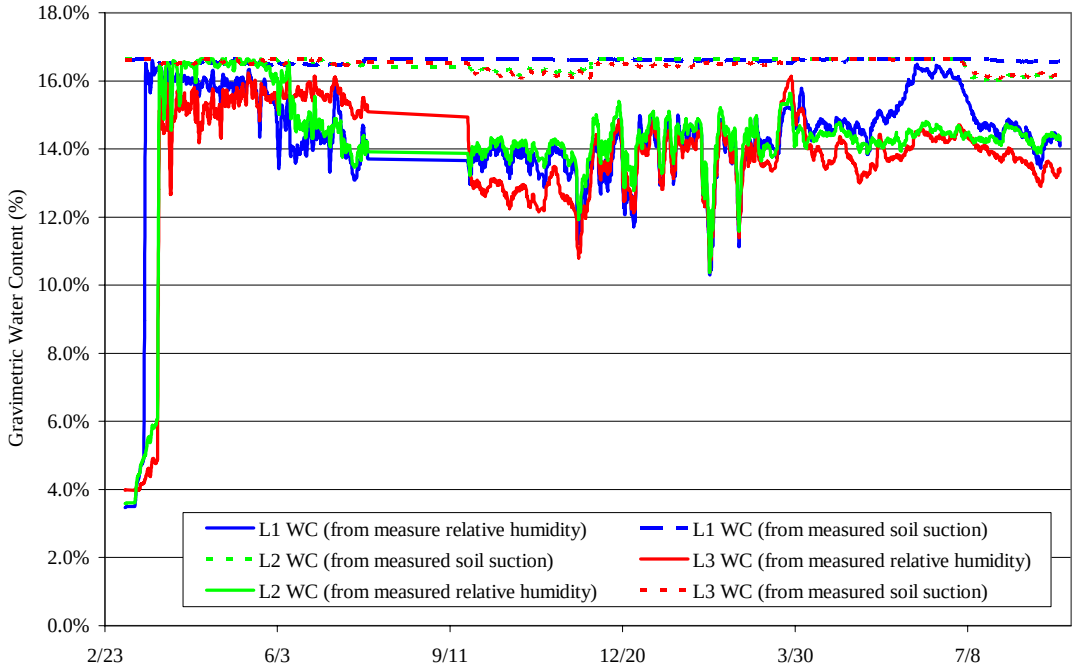

Layered Section
Relative Humidity

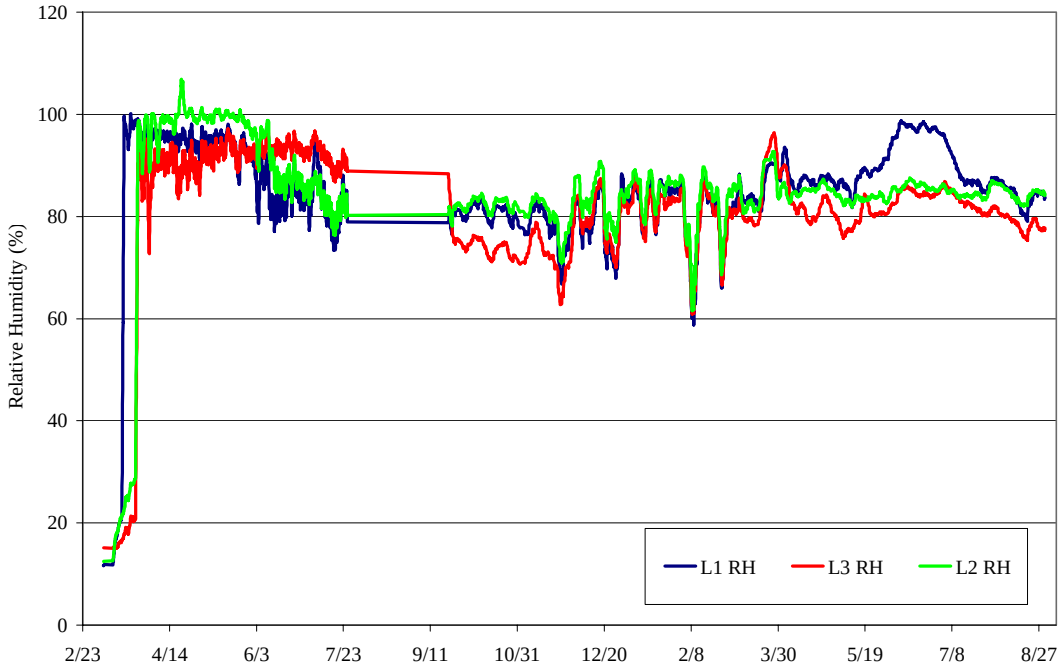

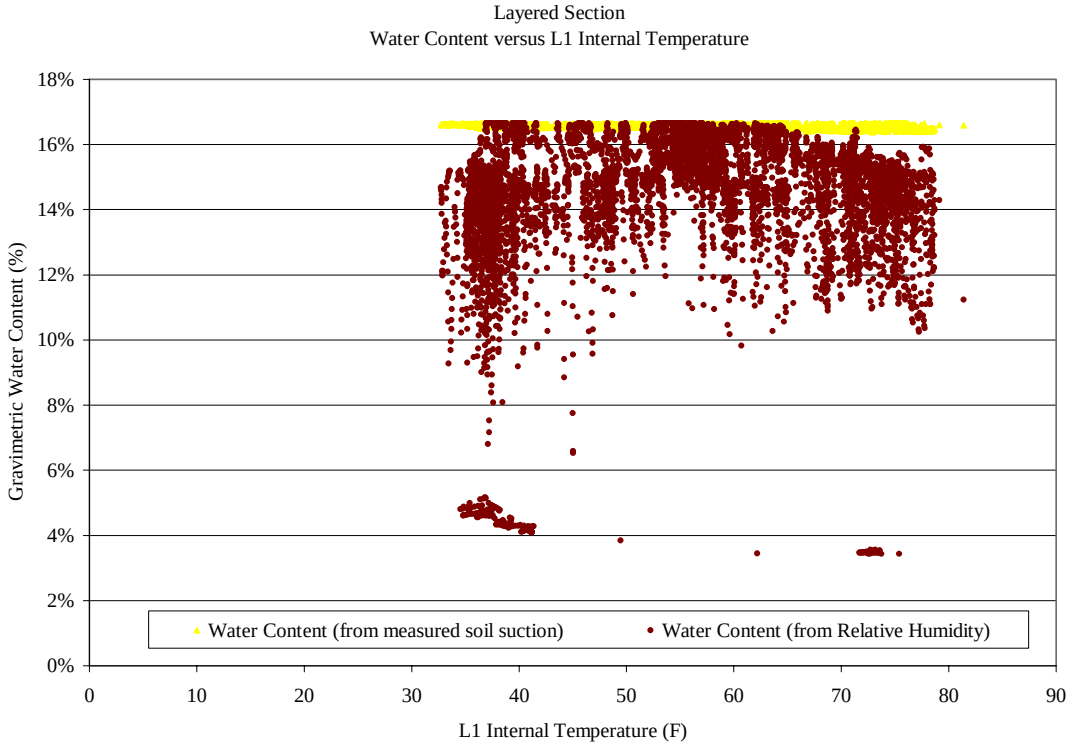
Layered Section
Water Content versus L1 Internal Temperature
Gravimetric Water Content (%)
18%
16%
14%
12%
10%
8%
6%
4%
2%
0%
0
10
20
30
40
50
60
70
80
90
L1 Internal Temperature (F)
Water Content (from measured soil suction)
Water Content (from Relative Humidity)

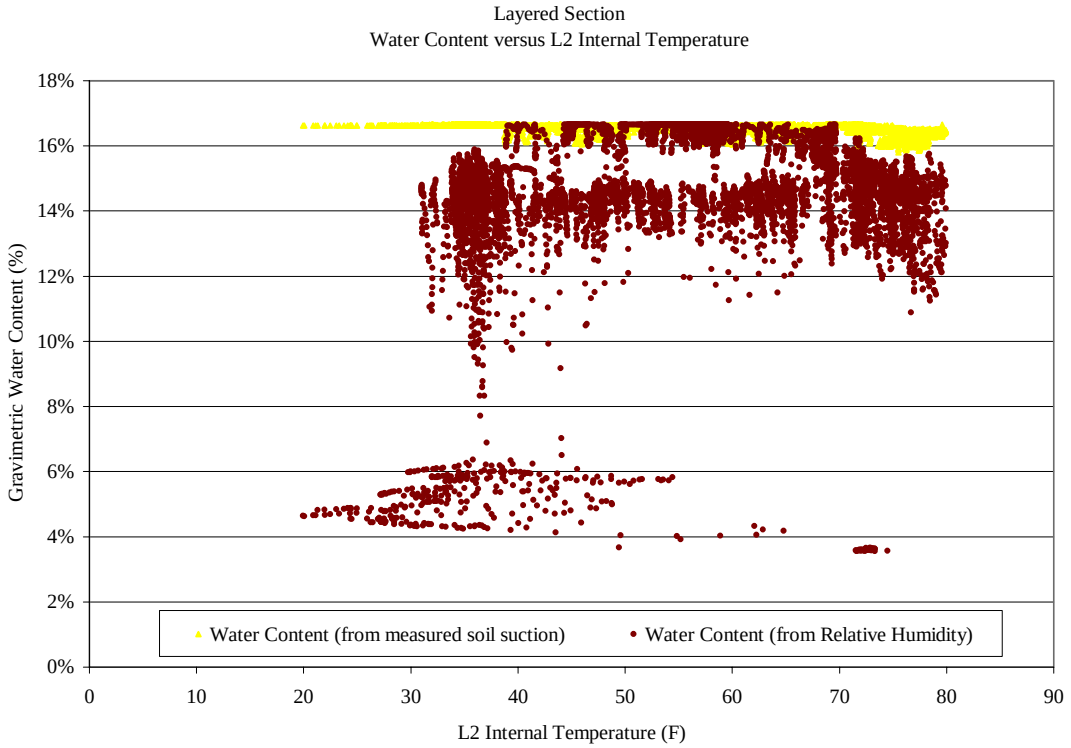
Layered Section
Water Content versus L2 Internal Temperature
Gravimetric Water Content (%)
18%
16%
14%
12%
10%
8%
6%
4%
2%
0%
0
10
20
30
40
50
60
70
80
90
L2 Internal Temperature (F)
Water Content (from measured soil suction)
Water Content (from Relative Humidity)

Layered Section
Water Content versus L3 Internal Temperature

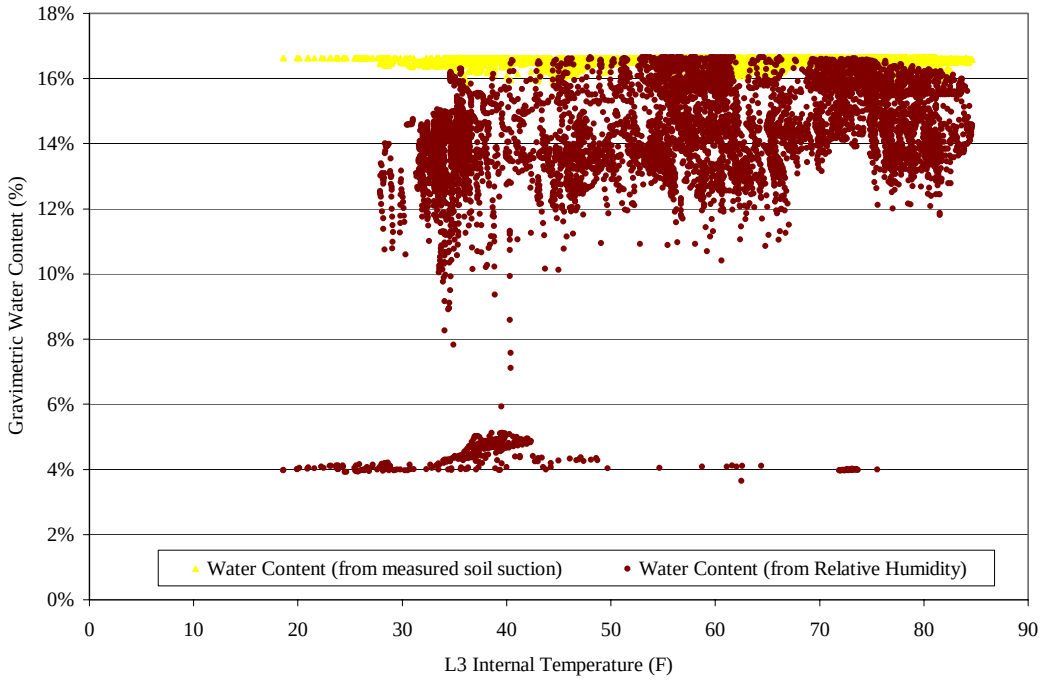

Soil Only Section
Heat Flux

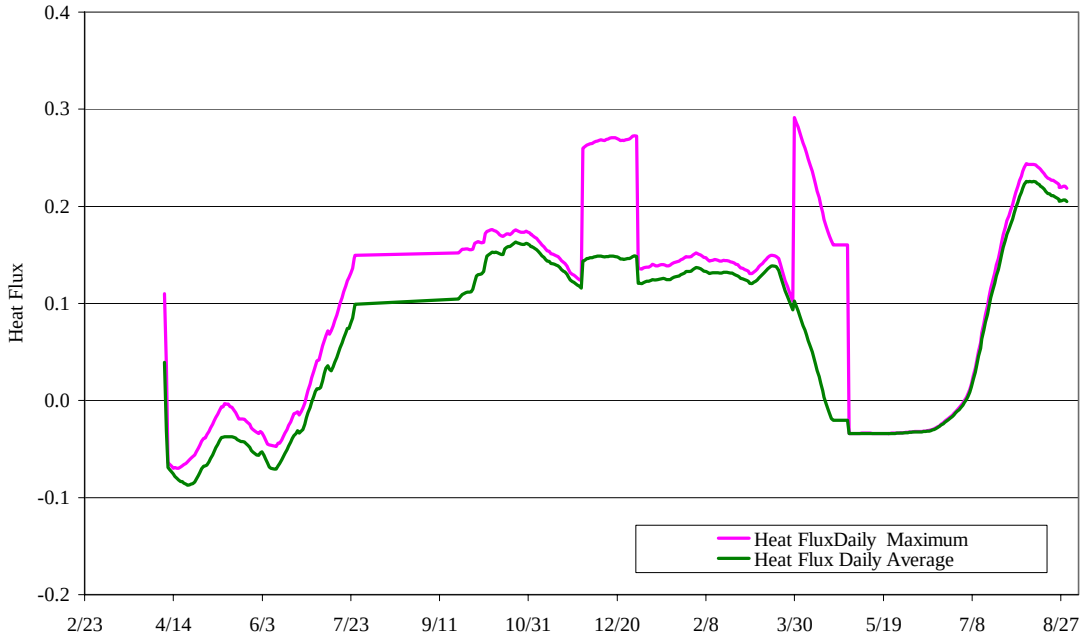

Soil-Only Section
Internal Temperature at S3 (nearest surface) versus Heat Flux

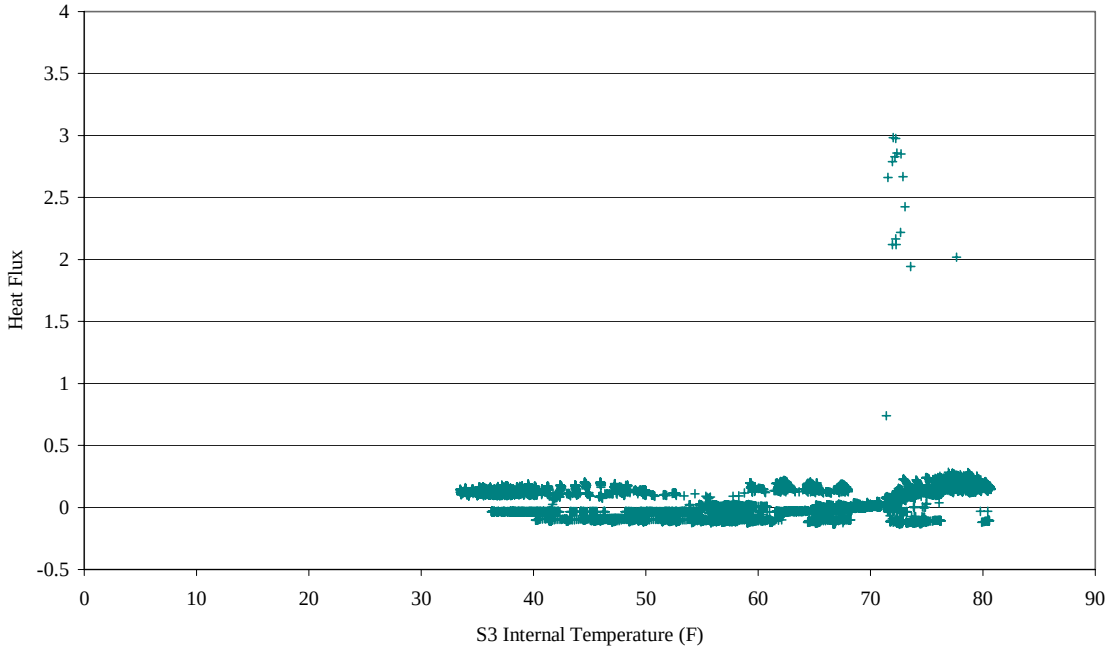

Daily Average Temperature
Time Period: Dry #1
December 13-17

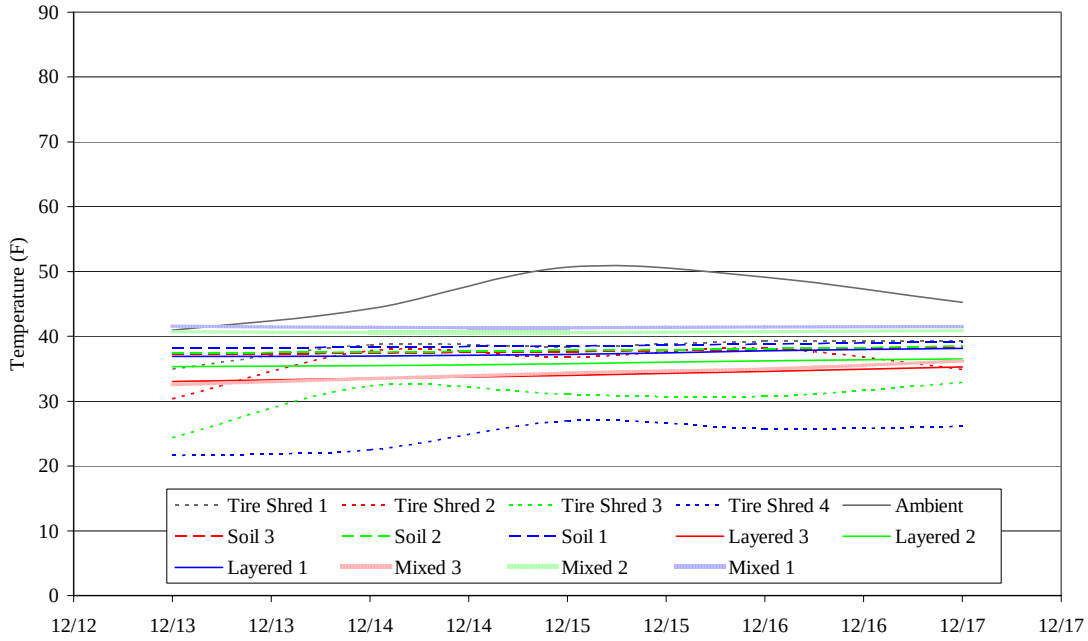

Daily Average Temperature
Time Period: Dry #2
May 1-7

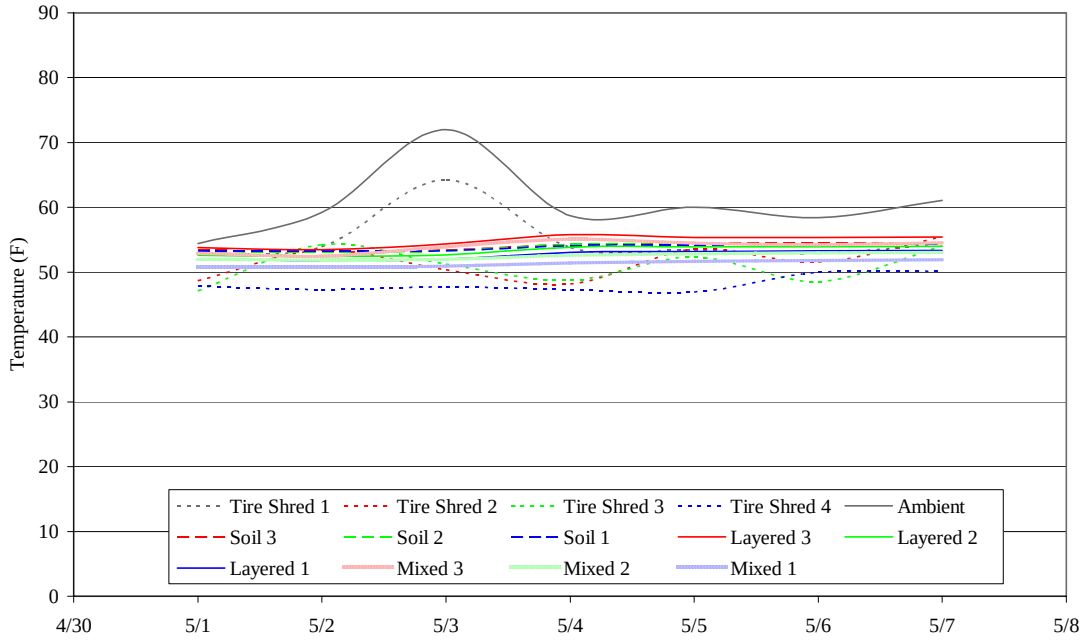

Daily Average Temperature
Time Period: Dry #3
January 26-31

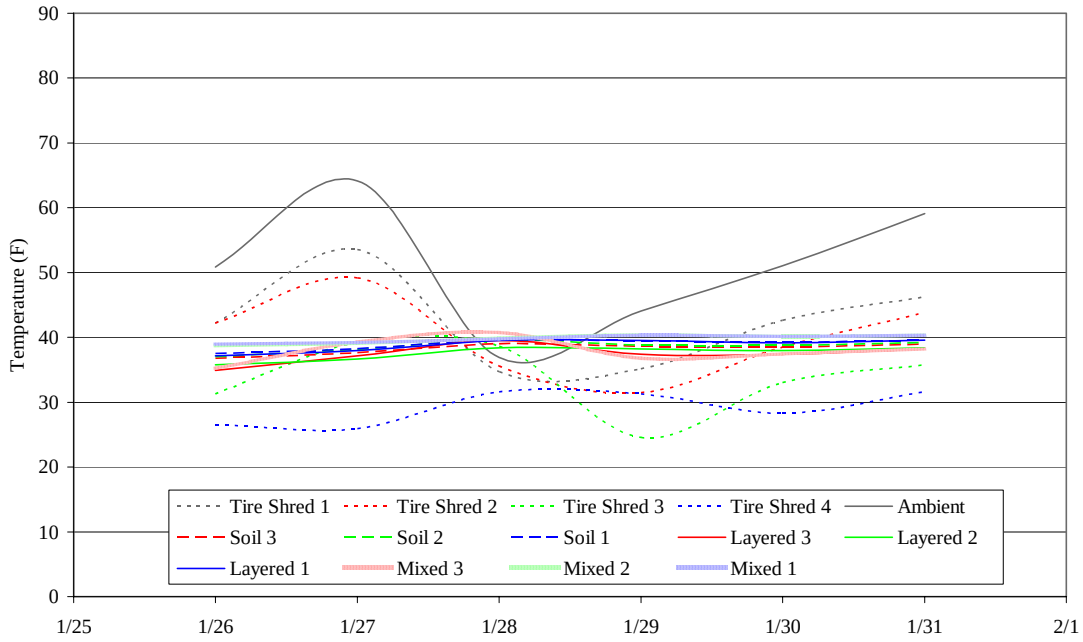

Daily Average Temperature
Time Period: Wet #1
June 8-11

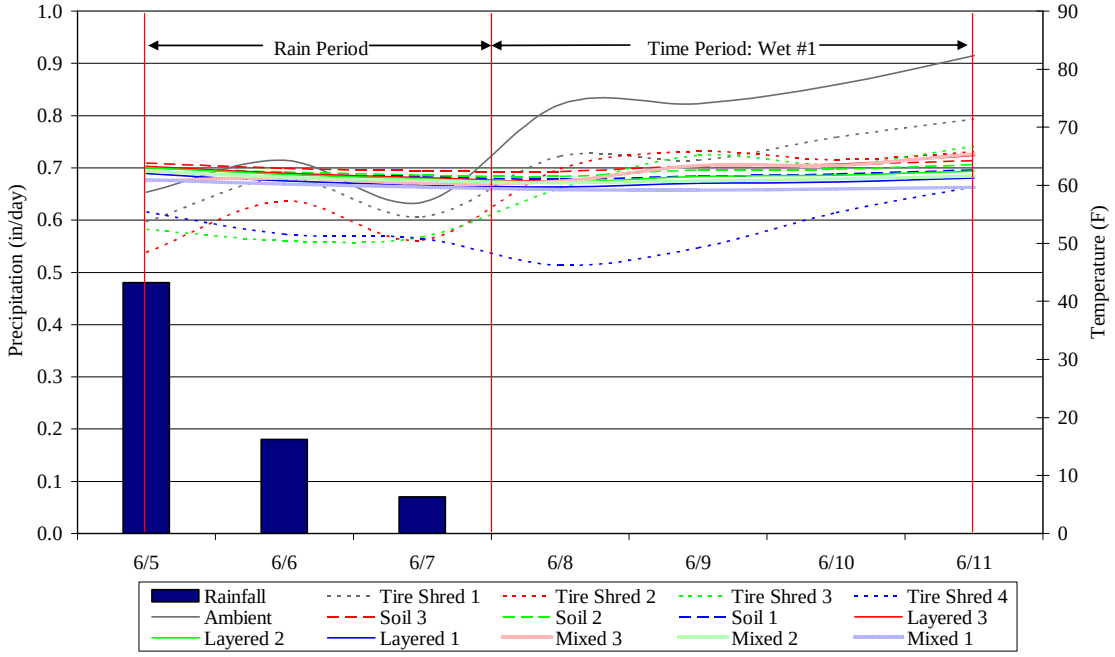

Daily Average Temperature
Time Period: Wet #2
April 25-28

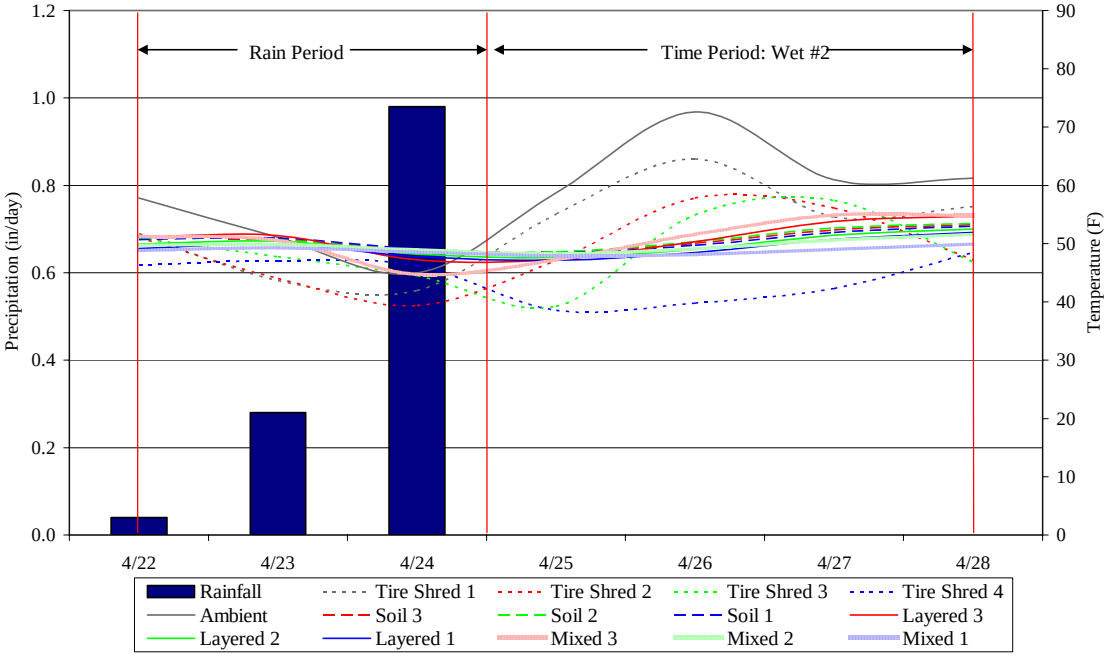

Daily Average Temperature
Time Period: Wet #3
May 11-14

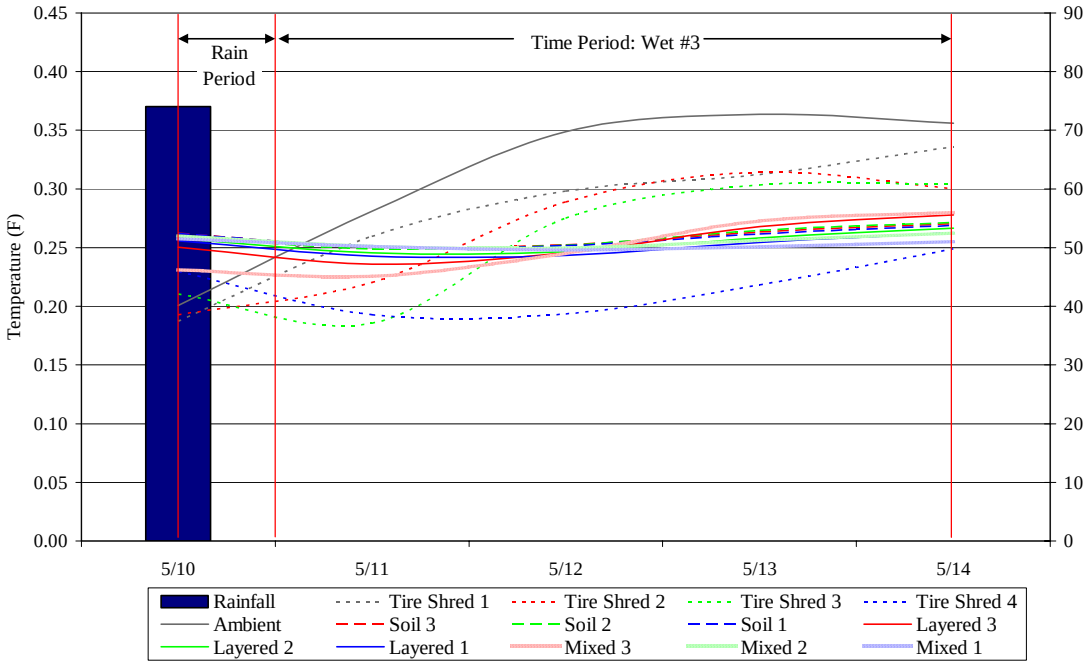

Temperature Profile
Time Period: Dry #1
Soil Section

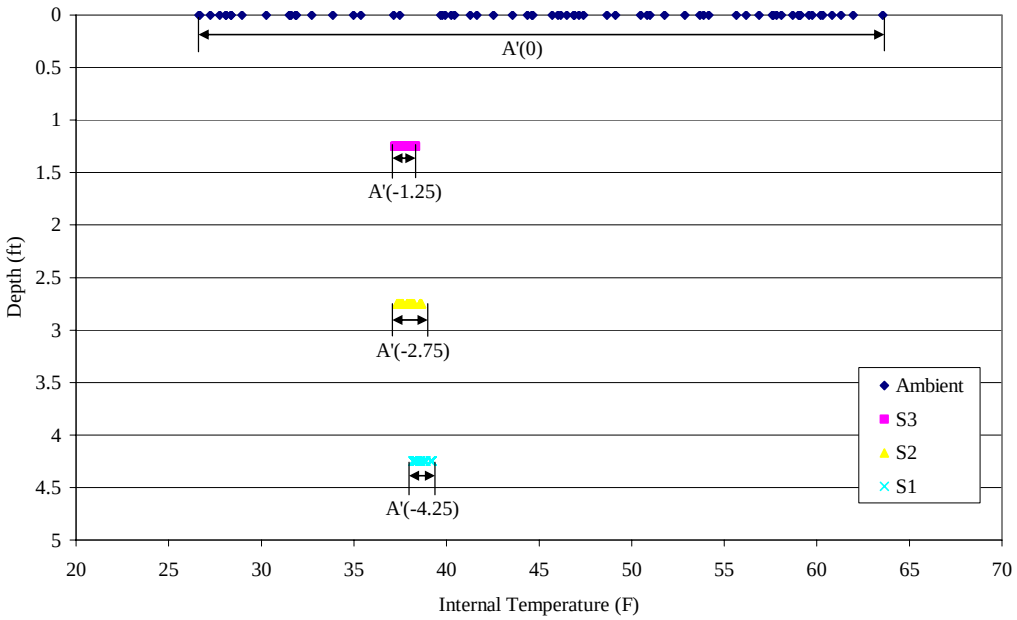

Temperature Profile
Time Period: Dry #1
Layered Section

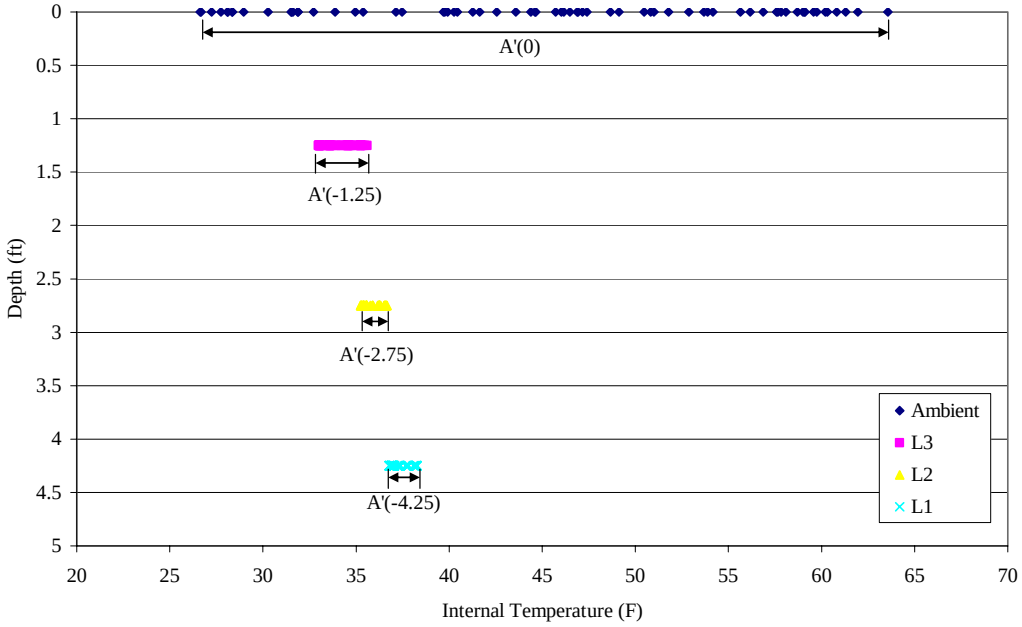

Temperature Profile
Time Period: Dry #1
Mixed Section

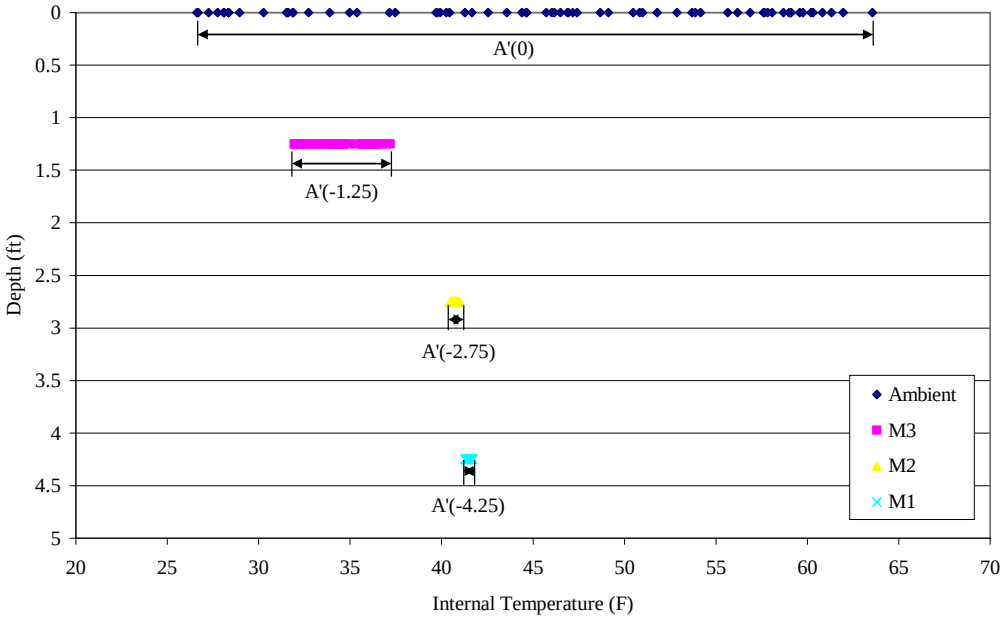

Temperature Profile
Time Period: Dry #1
Large Tire Shred-Only Stockpile

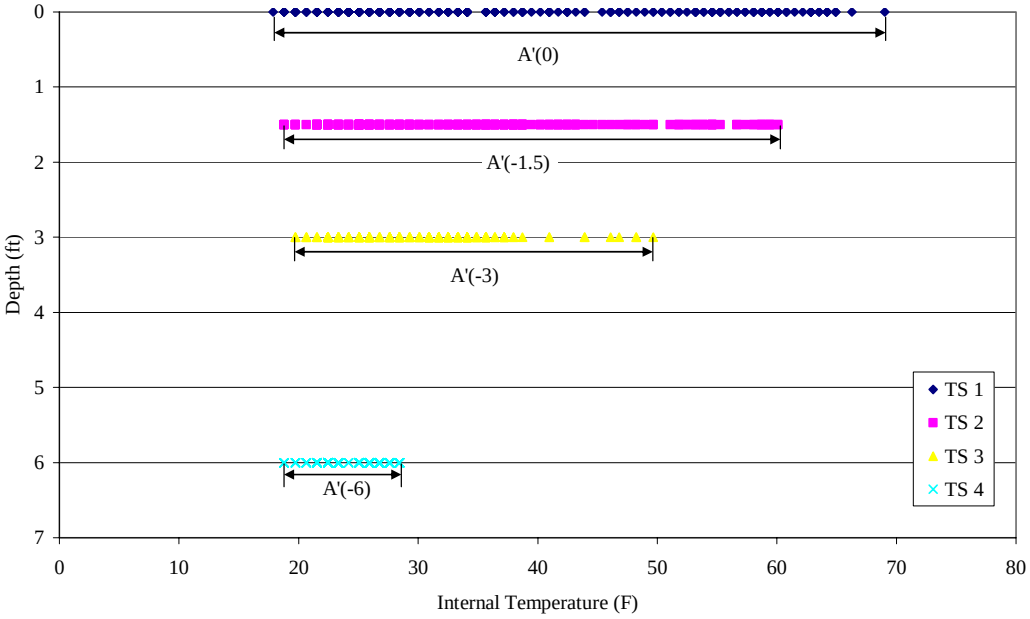

Temperature Profile
Time Period: Dry #2
Soil Section

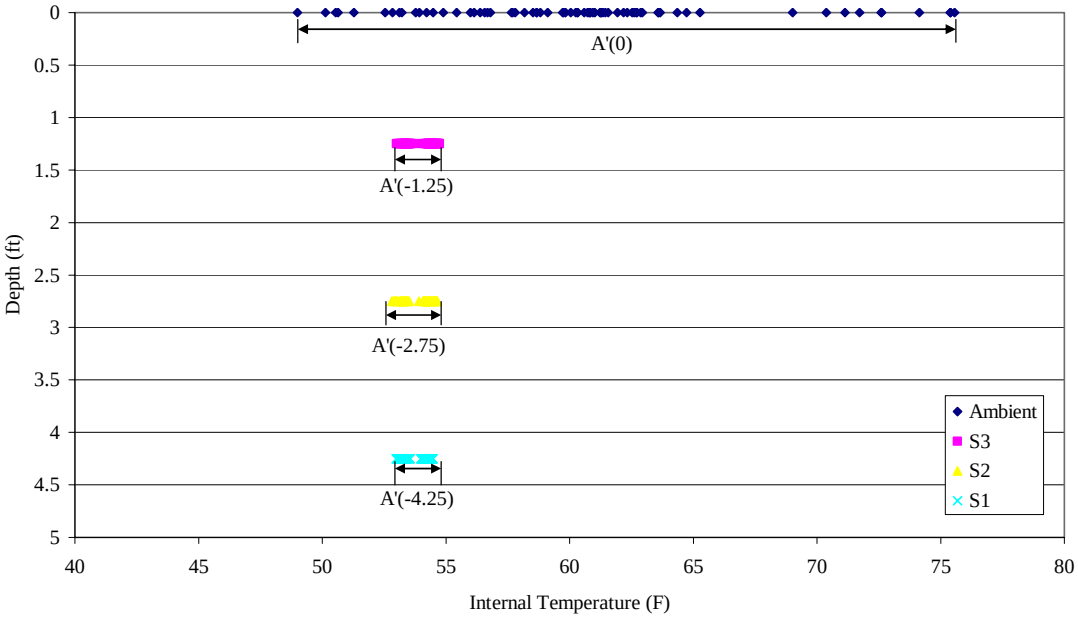

Temperature Profile
Time Period: Dry #2
Layered Section

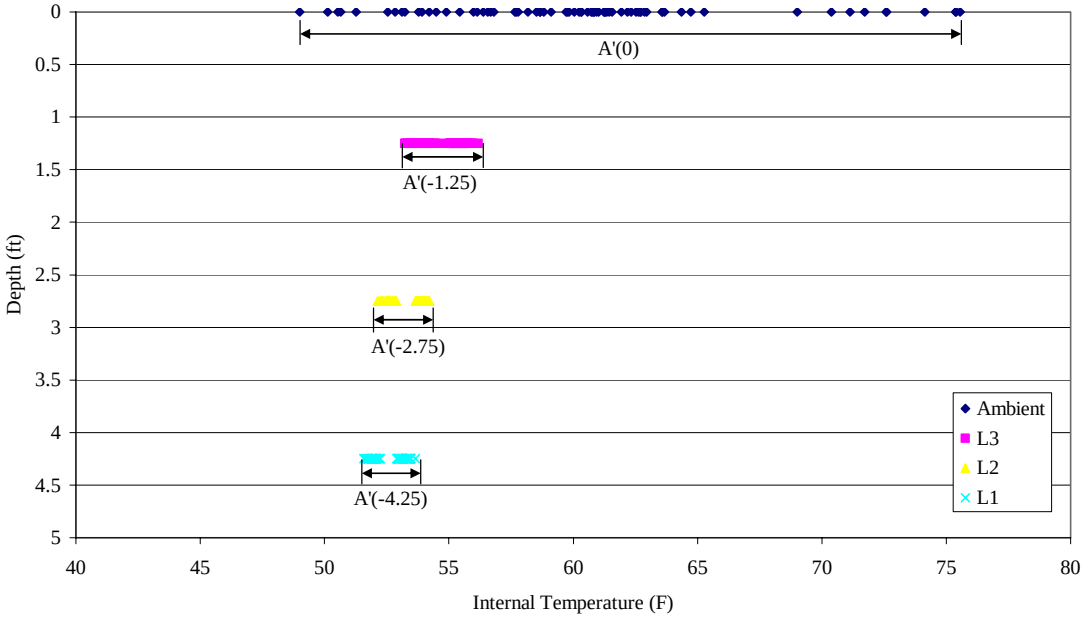

Temperature Profile
Time Period: Dry #2
Mixed Section

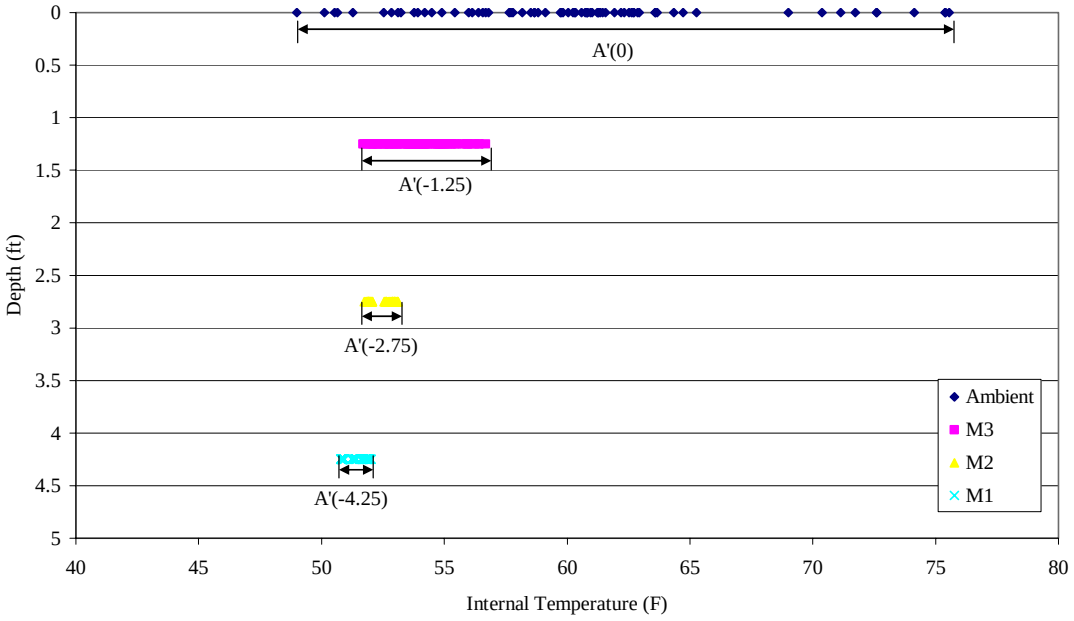

Temperature Profile
Time Period: Dry #2
Large Tire Shred-Only Stockpile

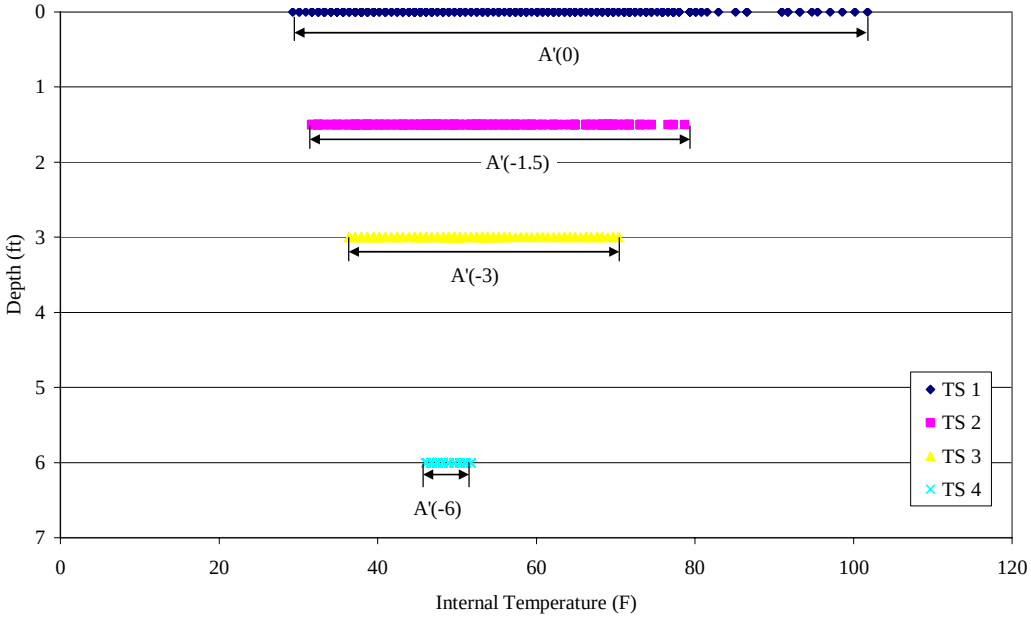

Temperature Profile
Time Period: Dry #3
Soil Section

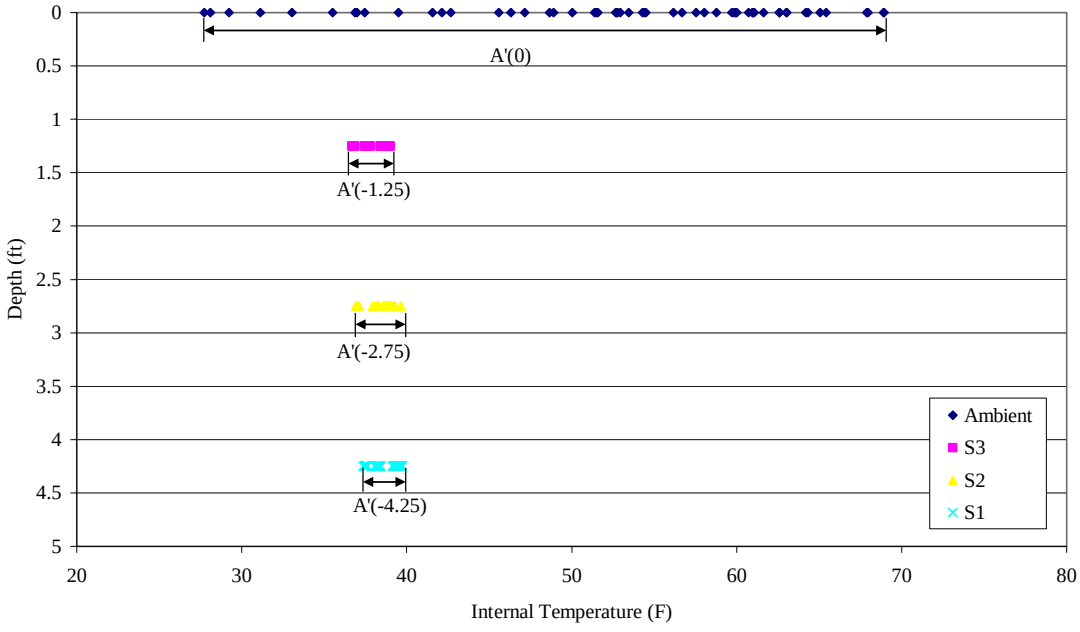

Temperature Profile
Time Period: Dry #3
Layered Section

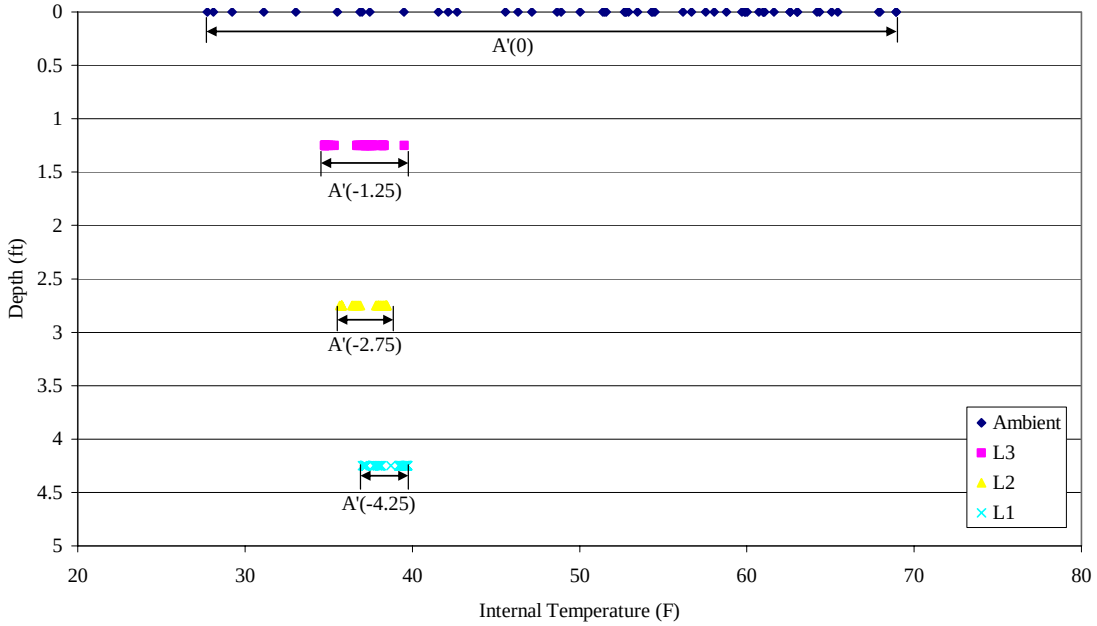

Temperature Profile
Time Period: Dry #3
Mixed Section

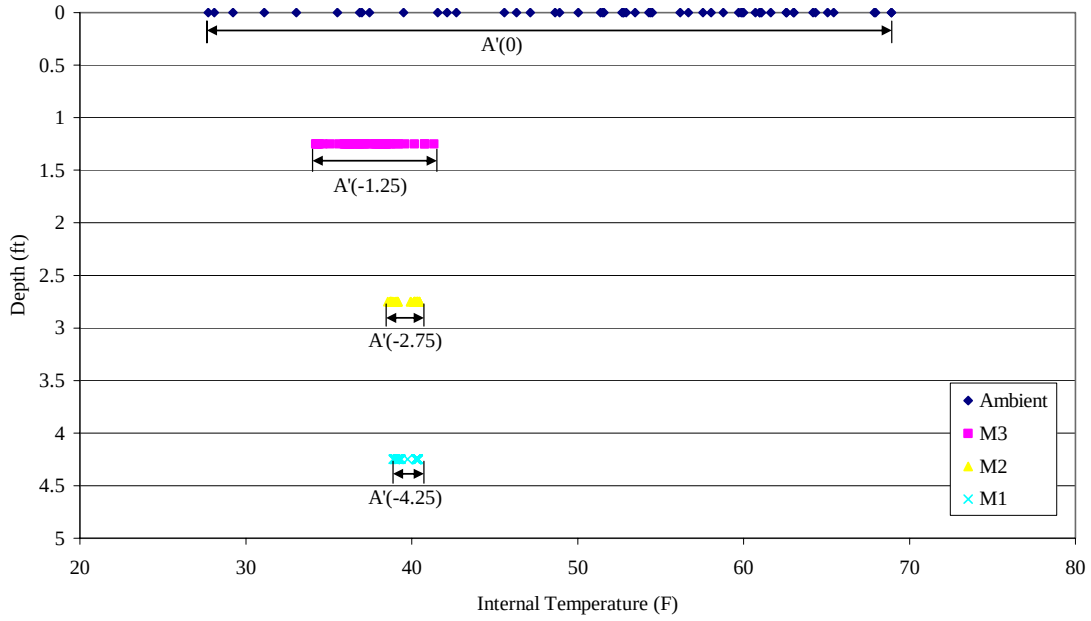

Temperature Profile
Time Period: Dry #3
Large Tire Shred-Only Stockpile

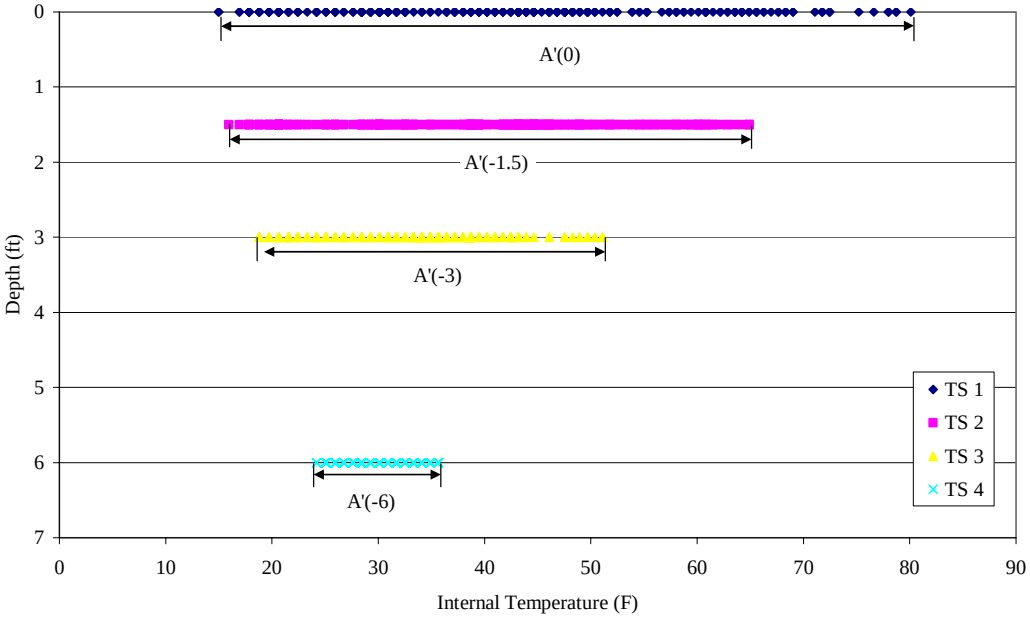

Temperature Profile
Time Period: Wet #1
Soil Section

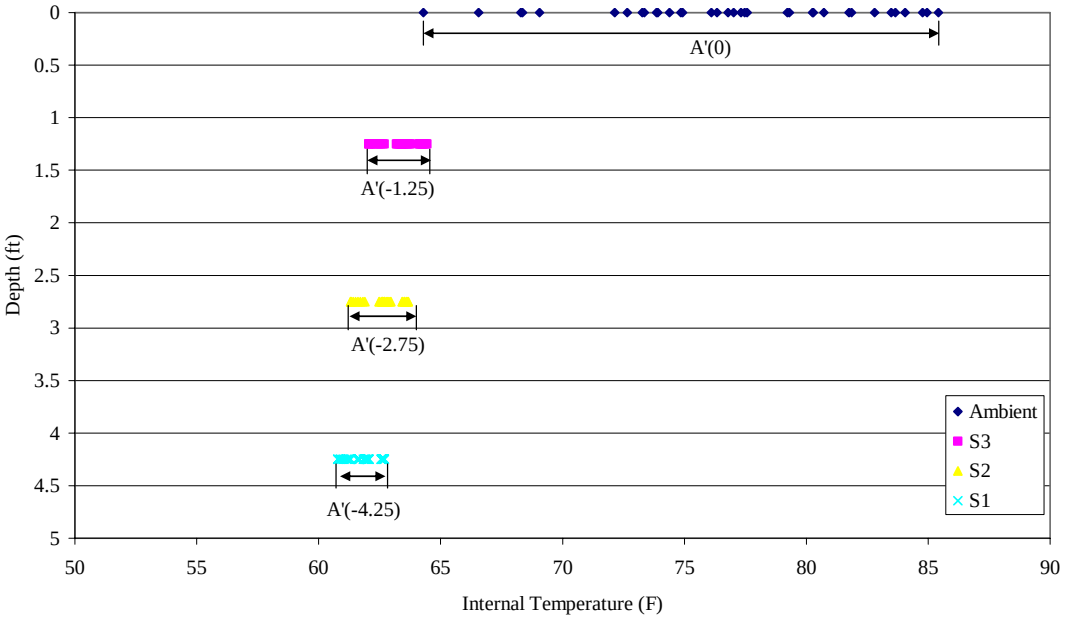

Temperature Profile
Time Period: Wet #1
Layered Section

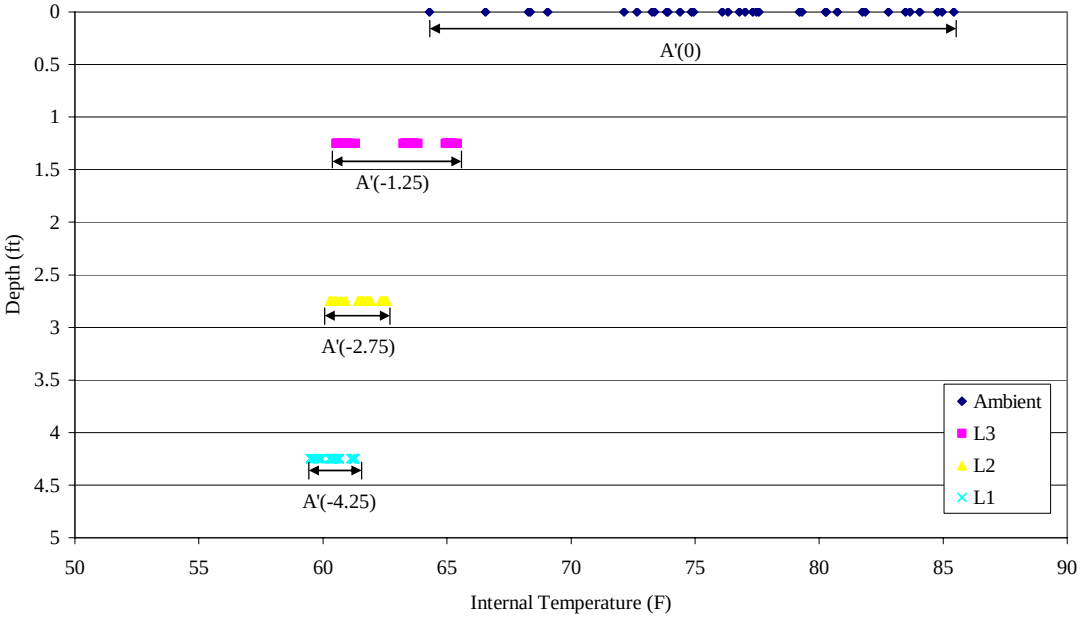

Temperature Profile
Time Period: Wet #1
Mixed Section

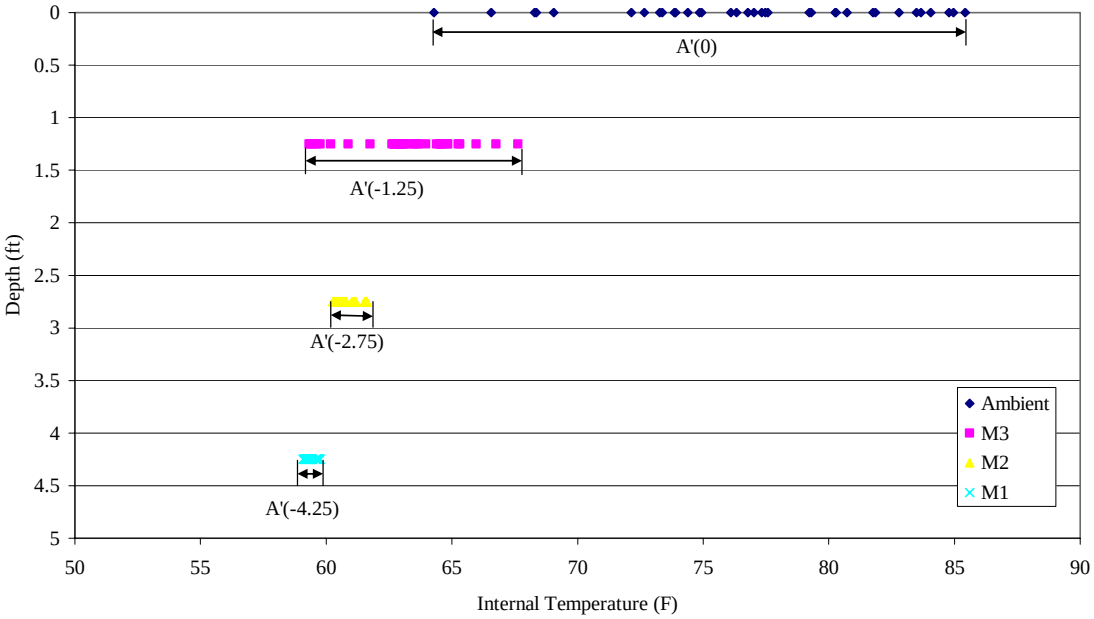

Temperature Profile
Time Period: Wet #1
Large Tire Shred-Only Stockpile

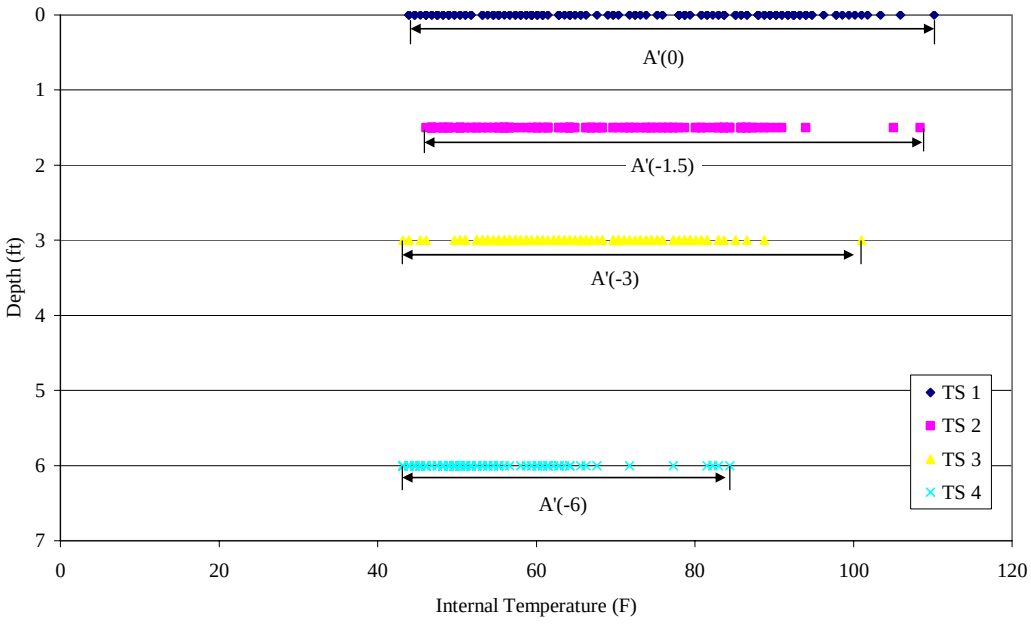

Temperature Profile
Time Period: Wet #2
Soil Section

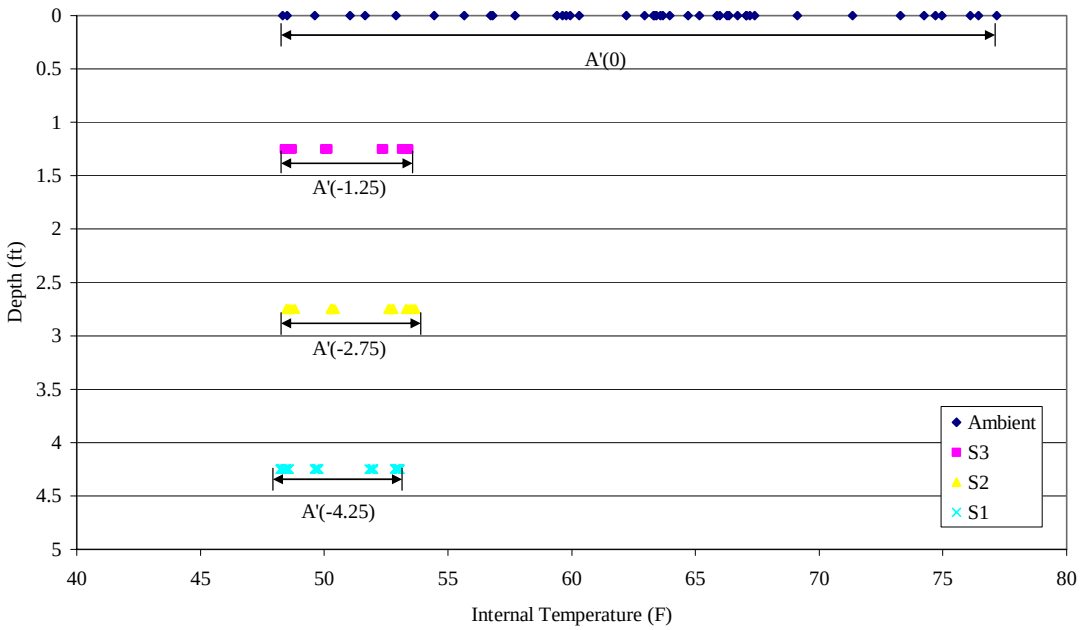

Temperature Profile
Time Period: Wet #2
Layered Section

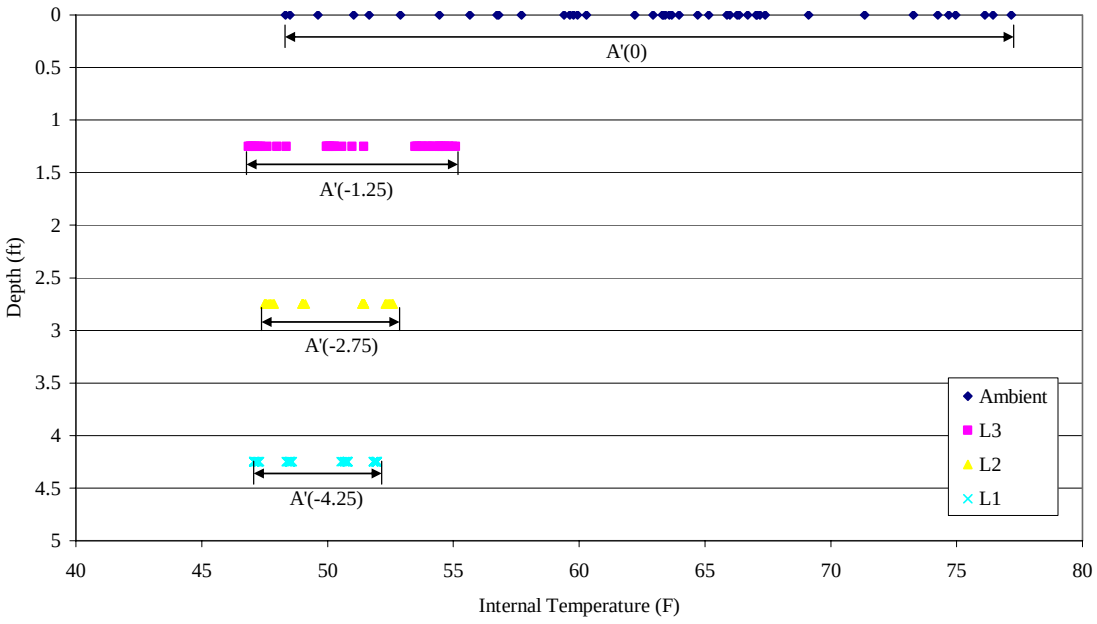

Temperature Profile
Time Period: Wet #2
Mixed Section

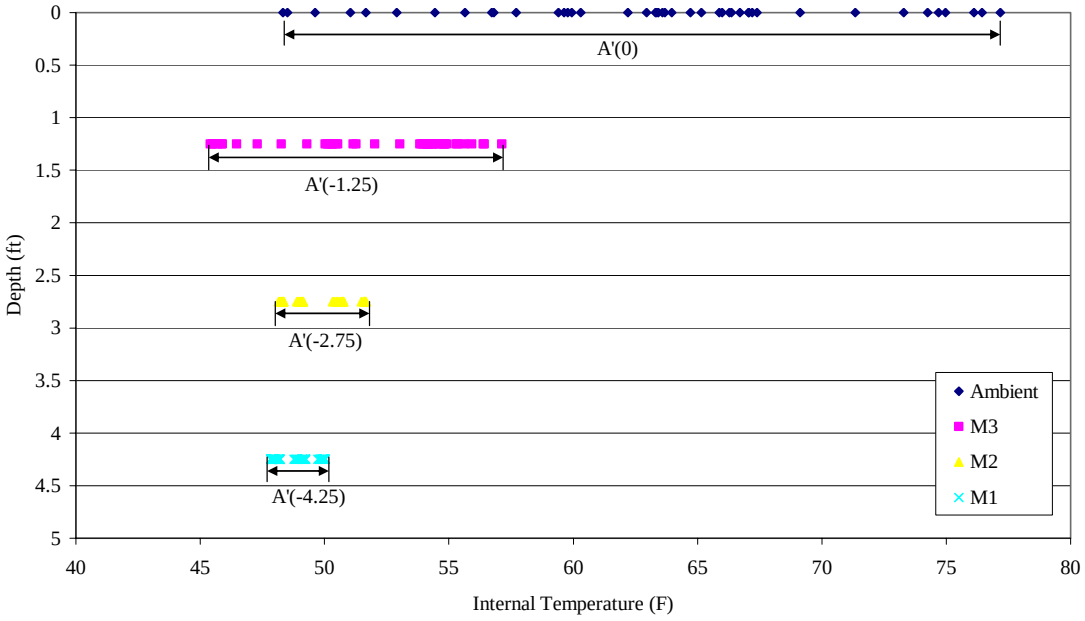

Temperature Profile
Time Period: Wet #2
Large Tire Shred-Only Stockpile

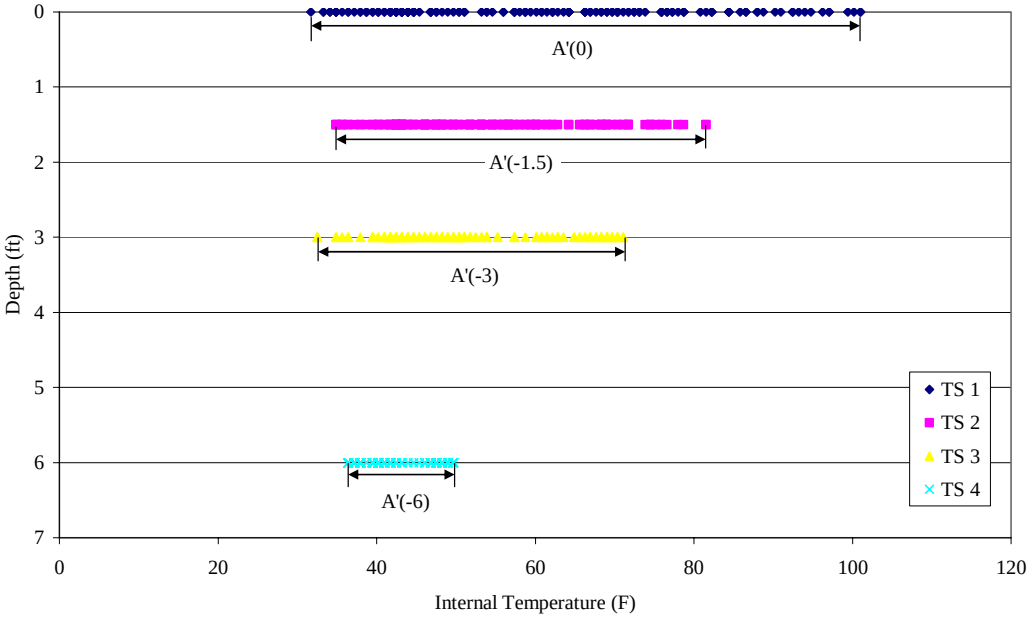

Temperature Profile
Time Period: Wet #3
Soil Section

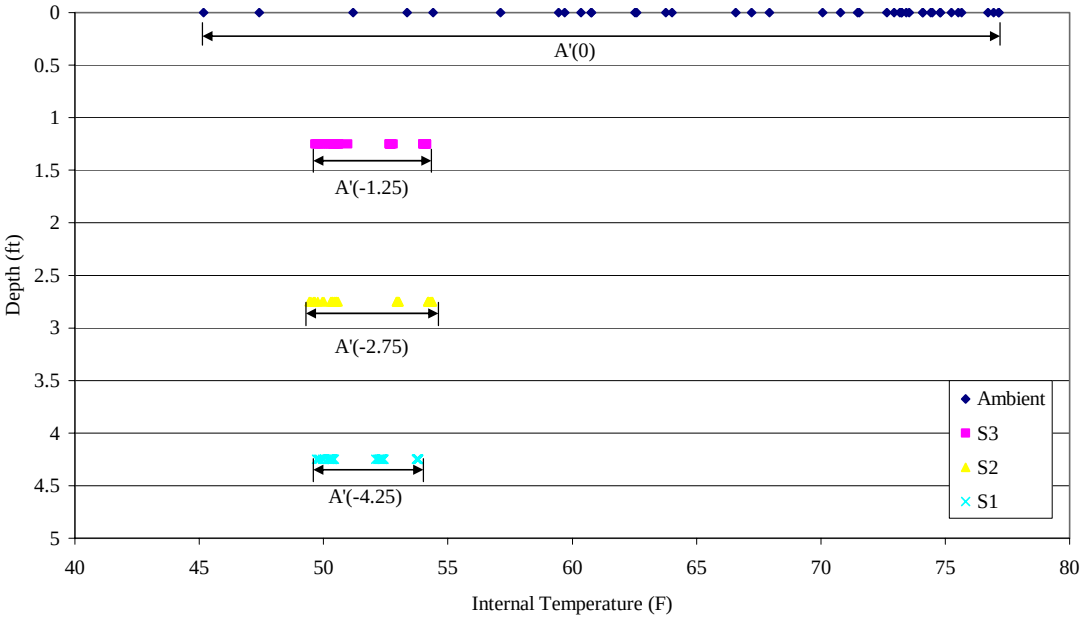

Temperature Profile
Time Period: Wet #3
Layered Section

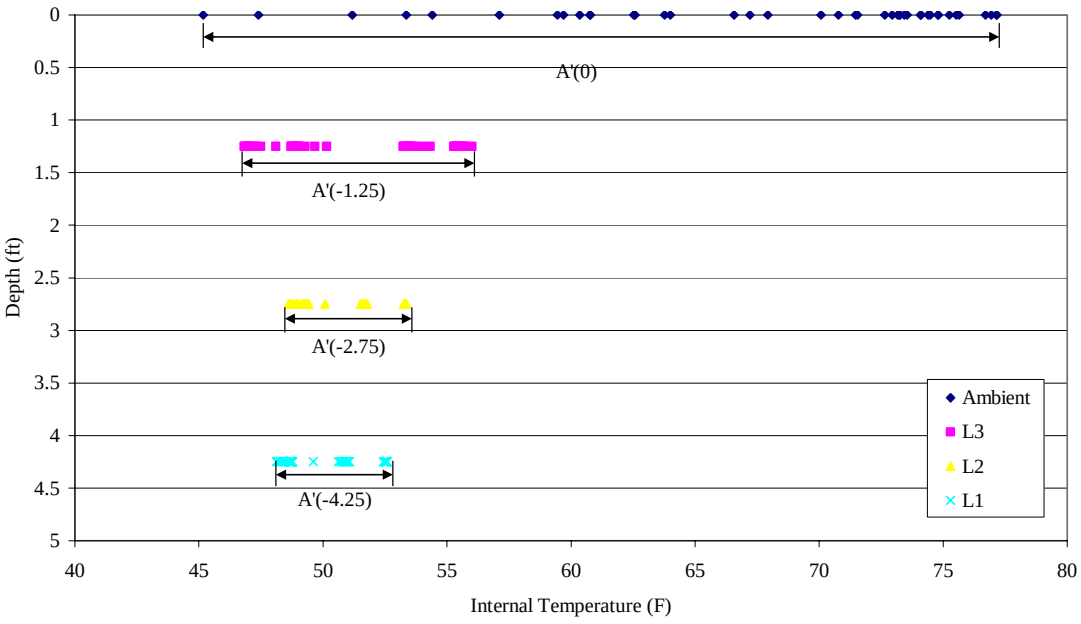

Temperature Profile
Time Period: Wet #3
Mixed Section

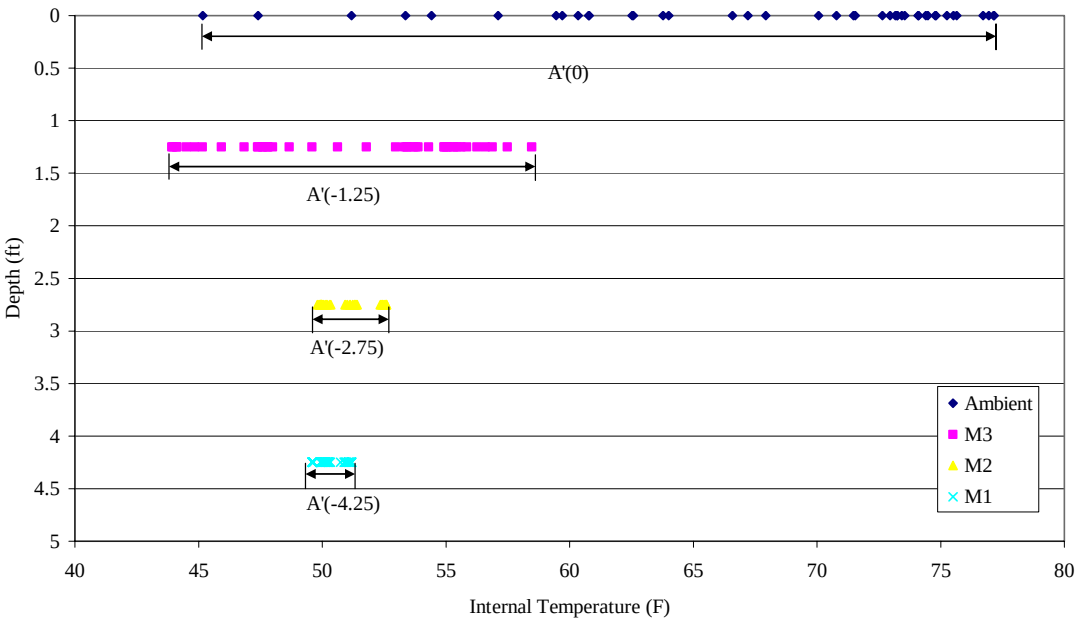

Temperature Profile
Time Period: Wet #3
Large Tire Shred-Only Stockpile

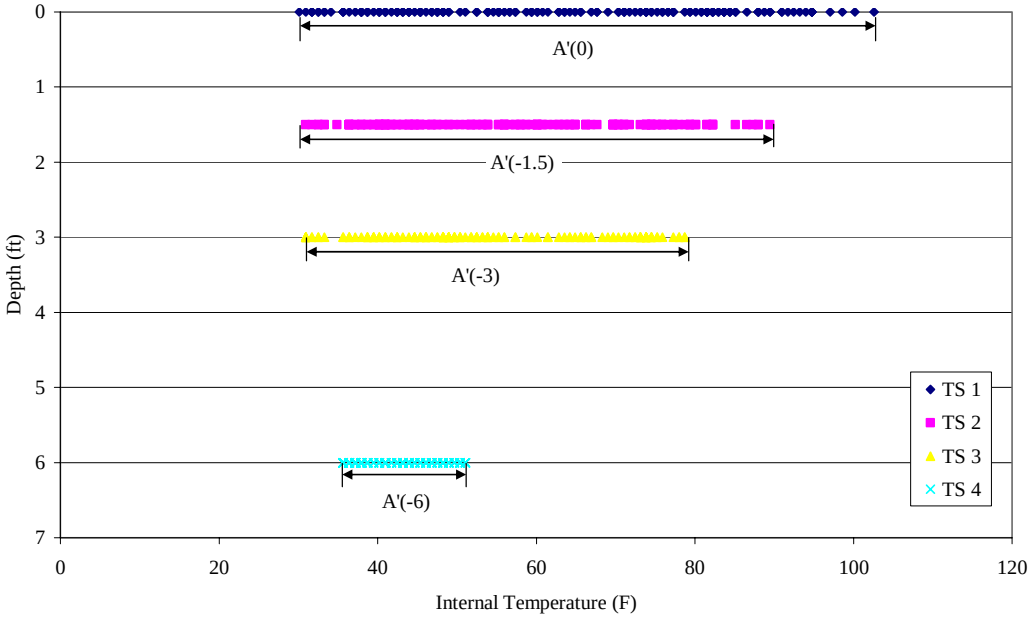

Heat Generation
Time Period: Dry #1
Soil-Only Section

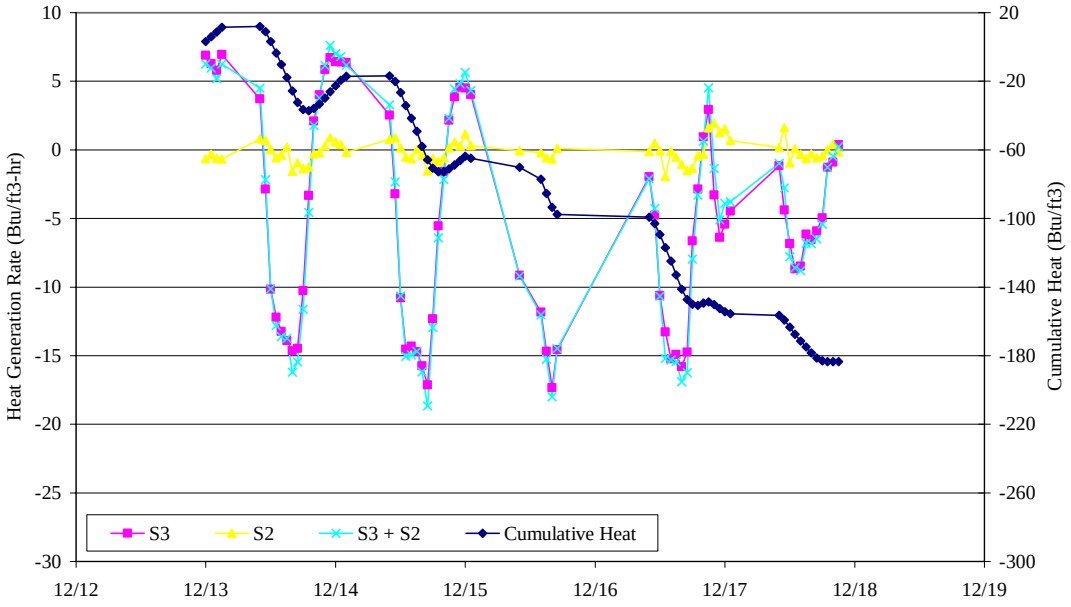

Heat Generation
Time Period: Dry #1
Layered Section

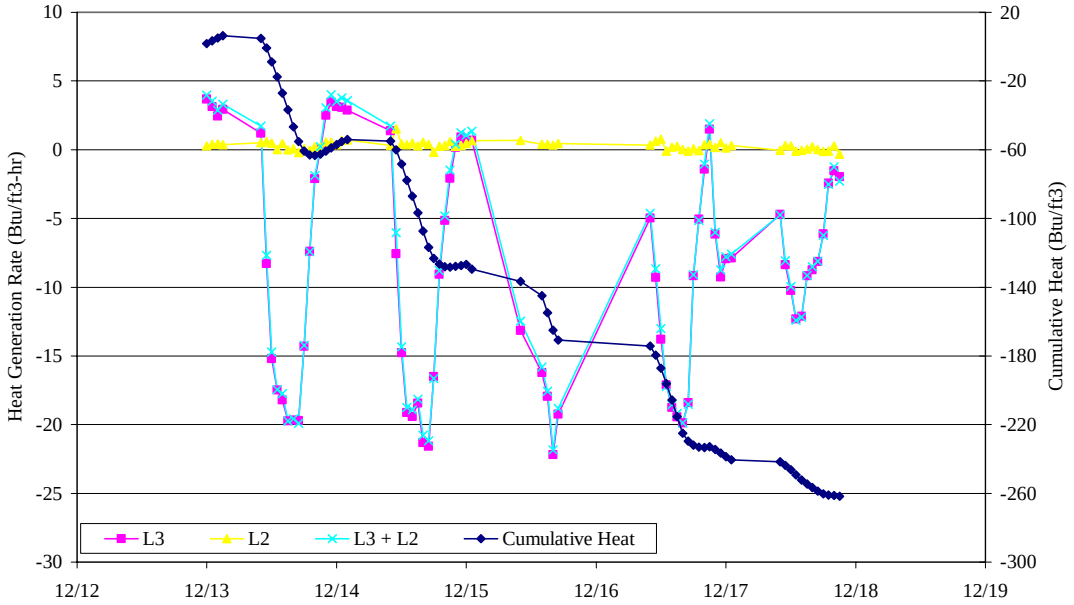

Heat Generation
Time Period: Dry #1
Mixed Section

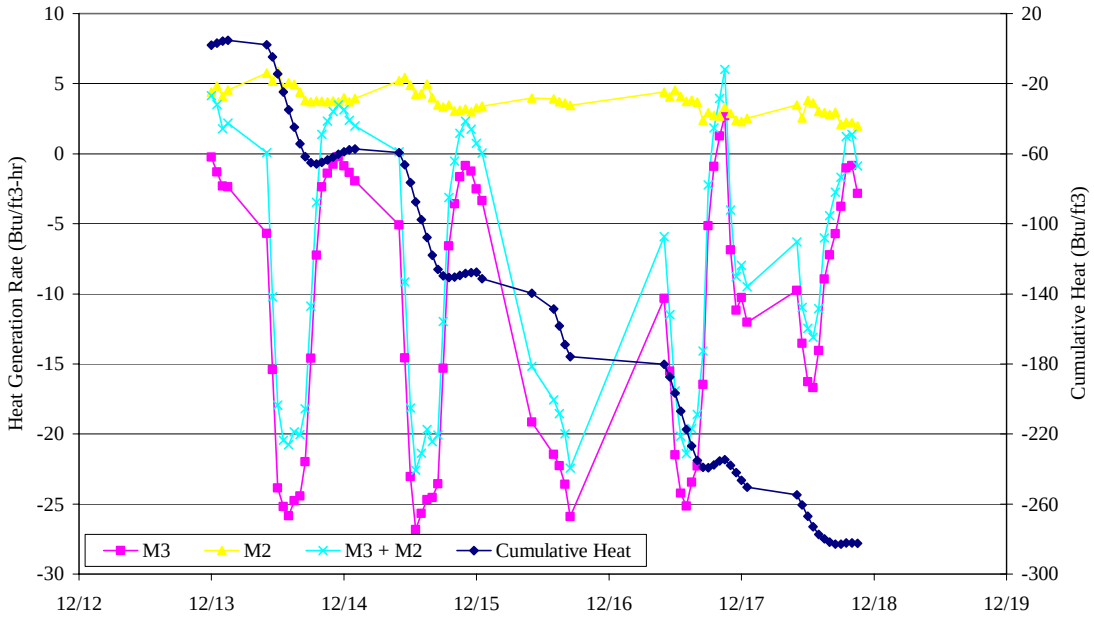

Heat Generation
Time Period: Dry #1
Large Tire Shred-Only Stockpile

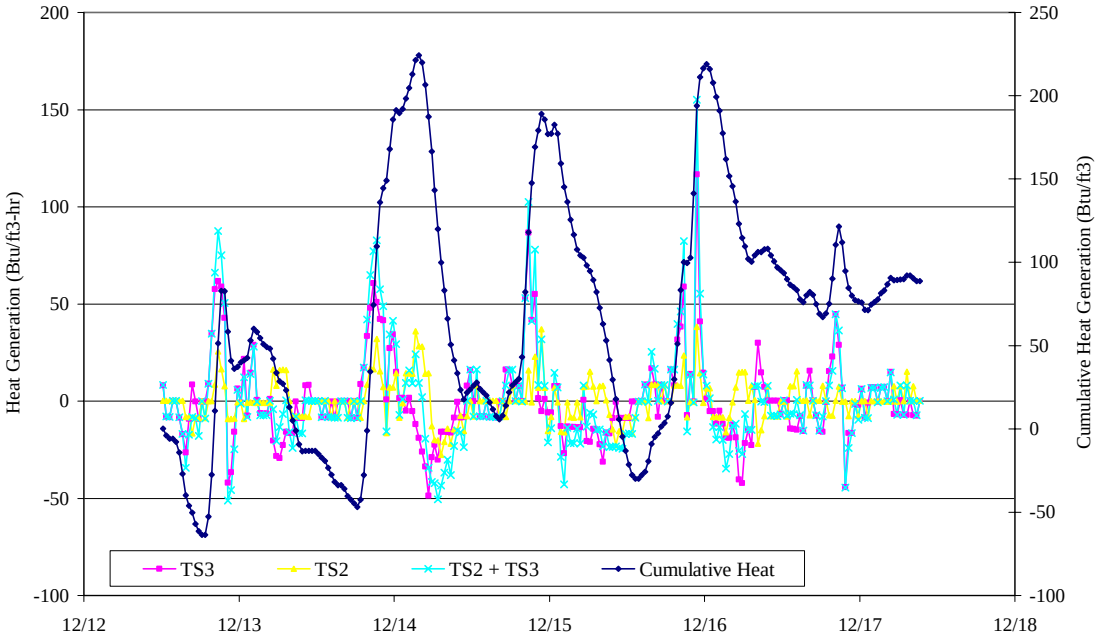

Heat Generation
Time Period: Dry #2
Soil-Only Section

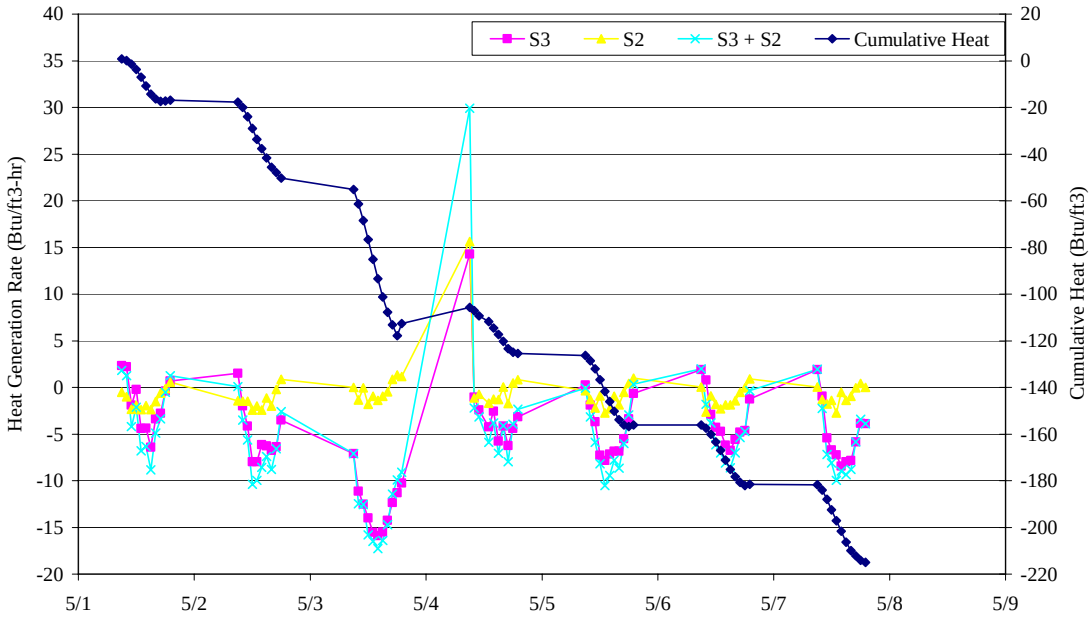

Heat Generation
Time Period: Dry #2
Layered Section

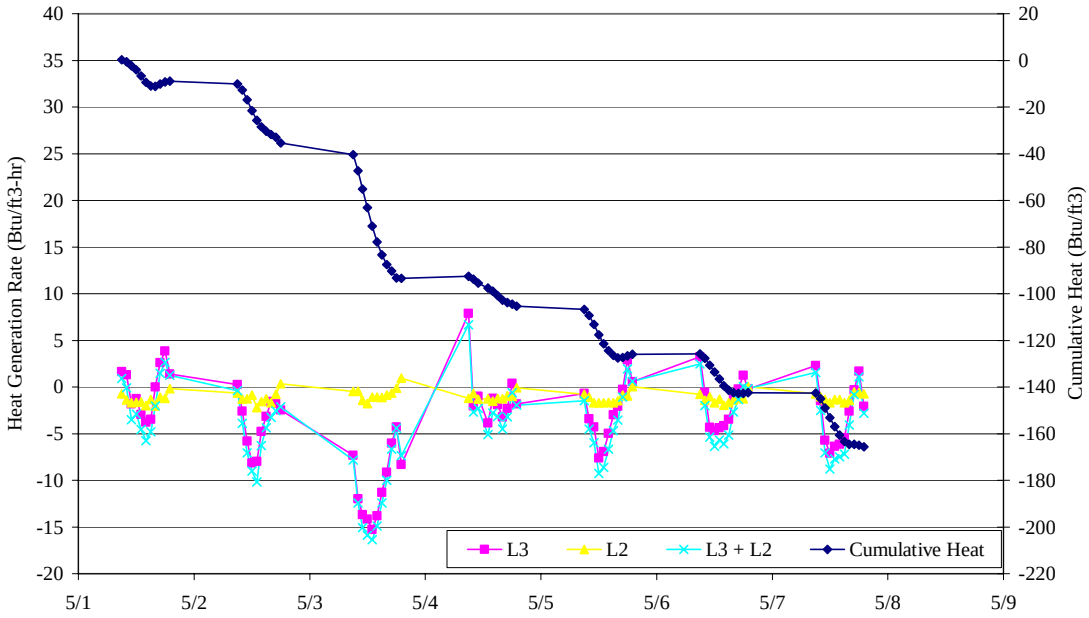

Heat Generation
Time Period: Dry #2
Mixed Section

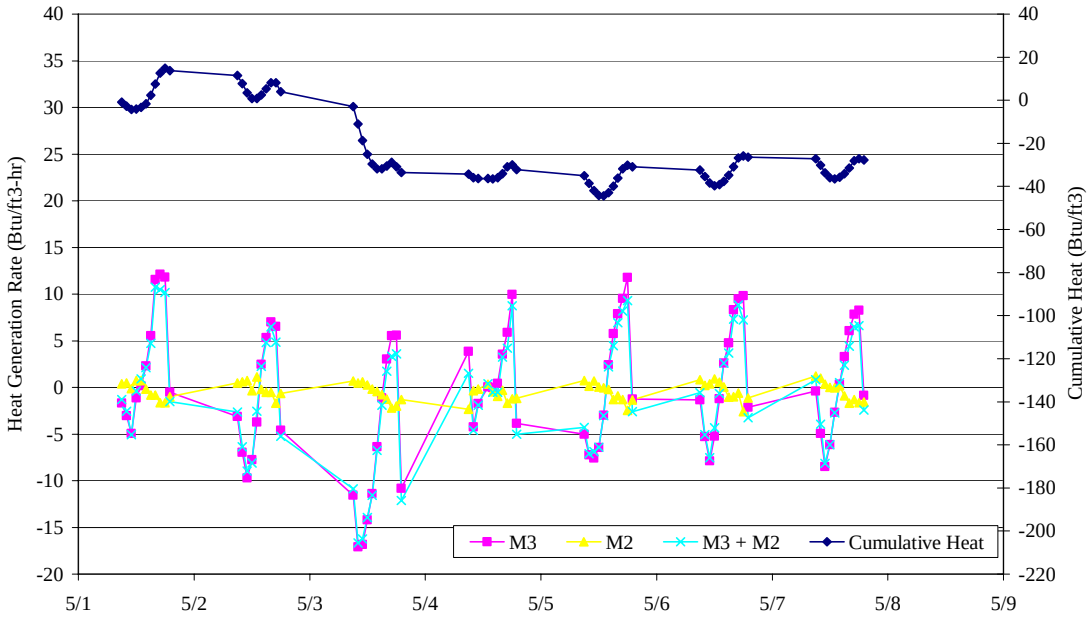

Heat Generation
Time Period: Dry #2
Large Tire Shred-Only Stockpile

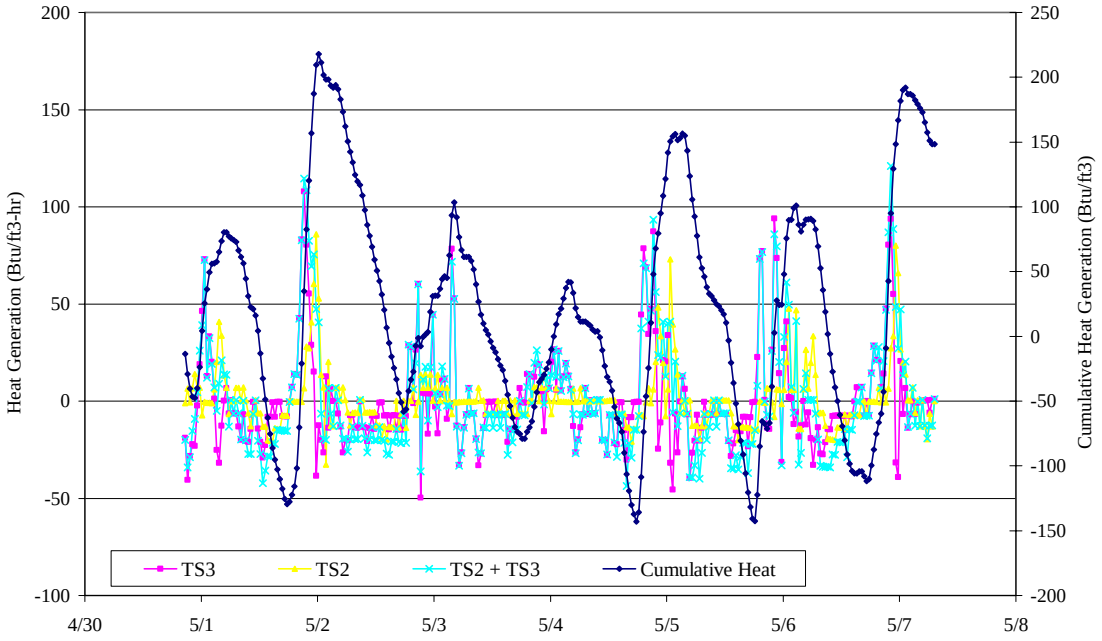

Heat Generation
Time Period: Dry #3
Soil-Only Section

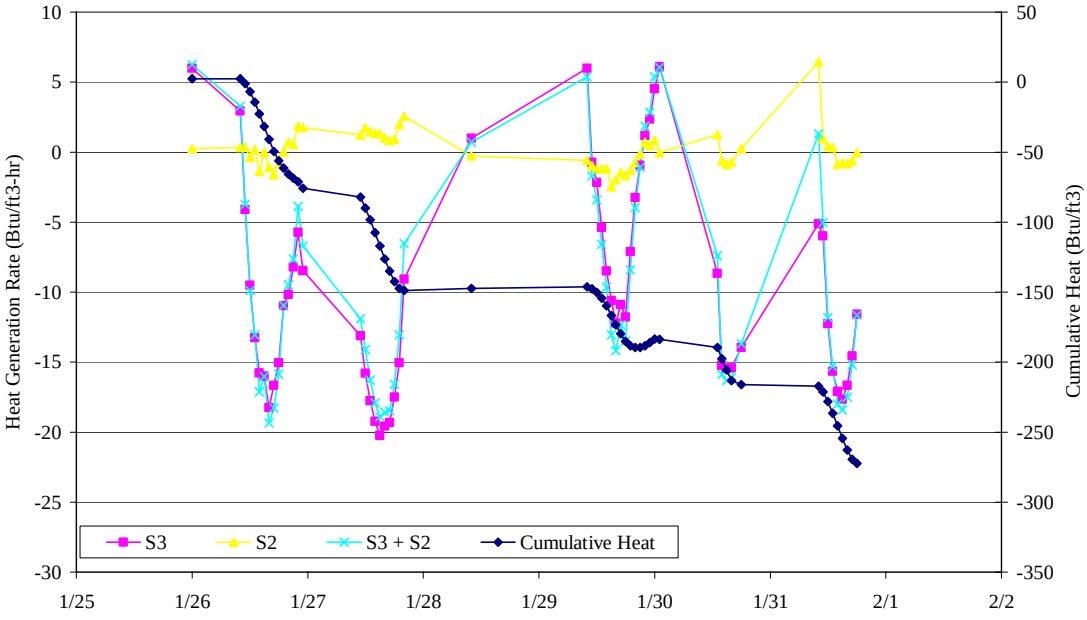

Heat Generation
Time Period: Dry #3
Layered Section

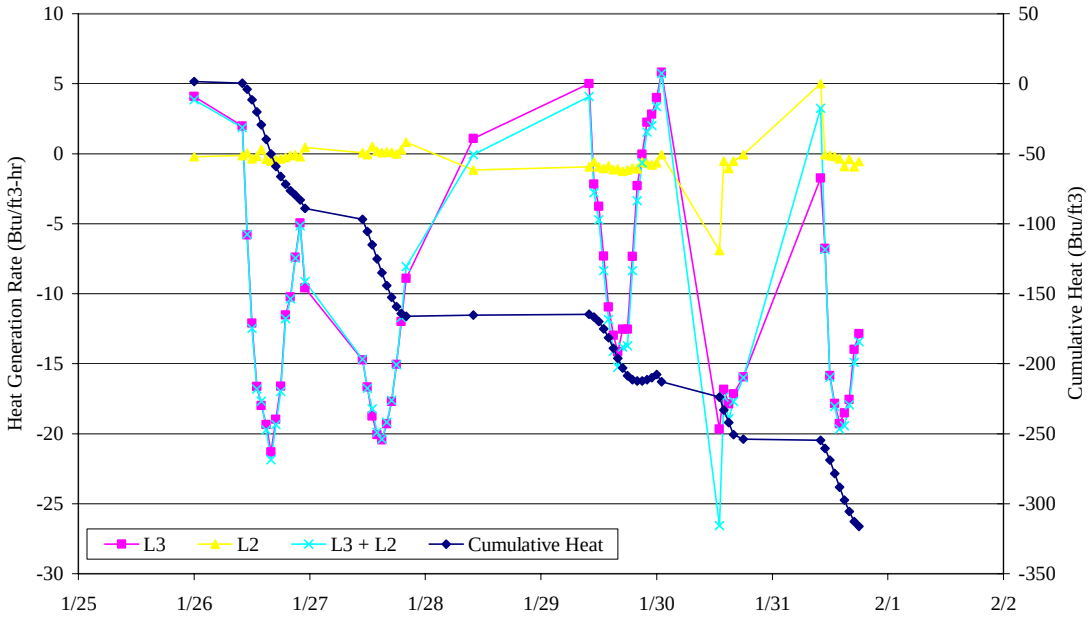

Heat Generation
Time Period: Dry #3
Mixed Section

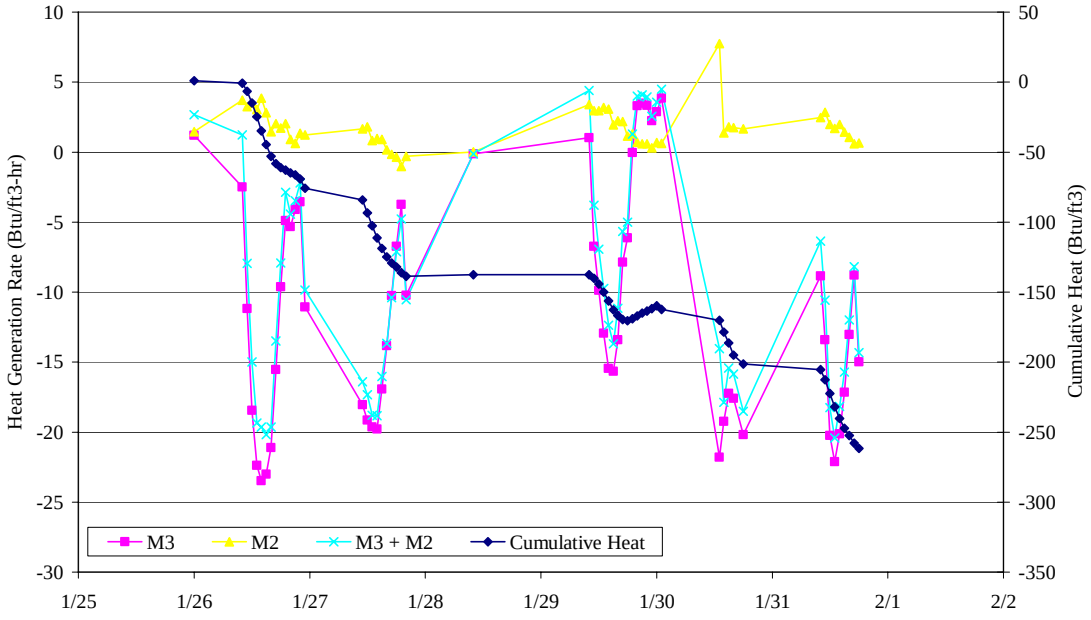

Heat Generation
Time Period: Dry #3
Large Tire Shred-Only Stockpile

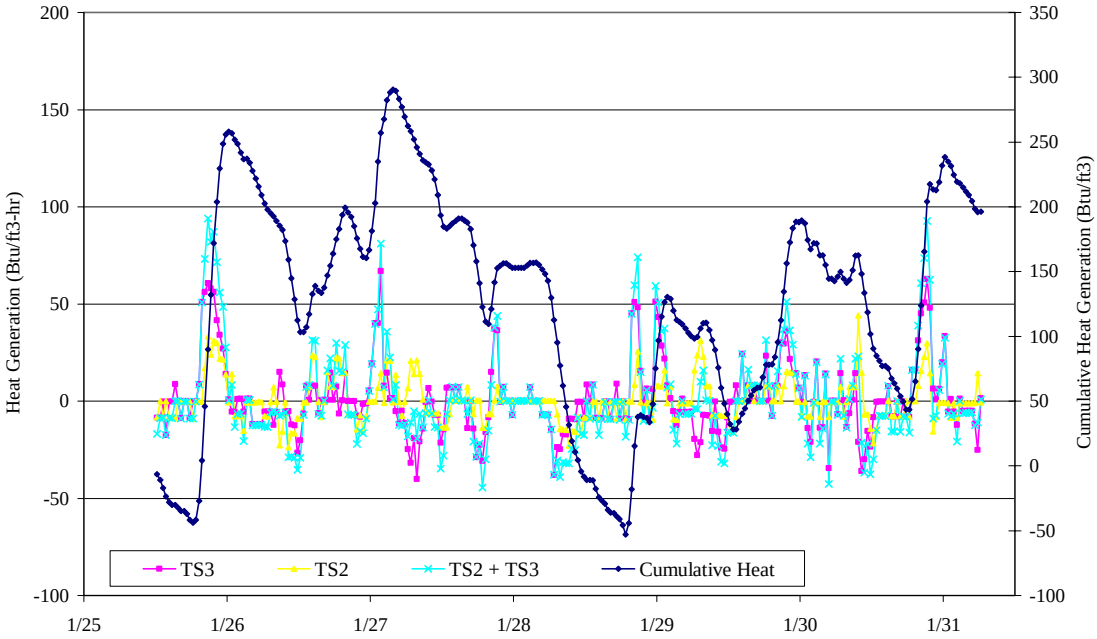

Heat Generation
Time Period: Wet #1
Soil-Only Section

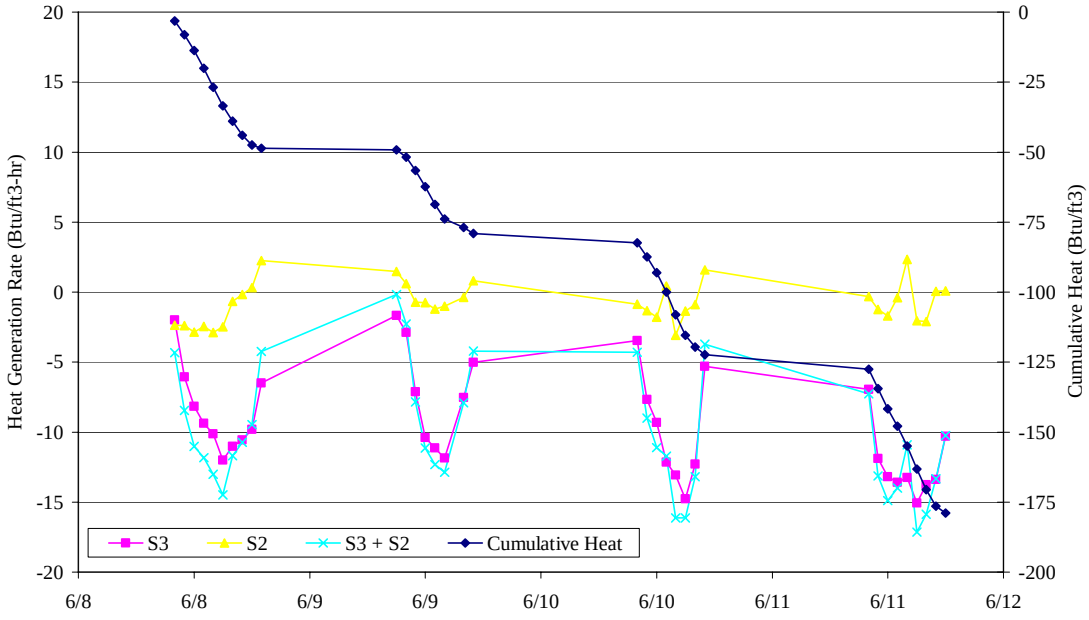

Heat Generation
Time Period: Wet #1
Layered Section

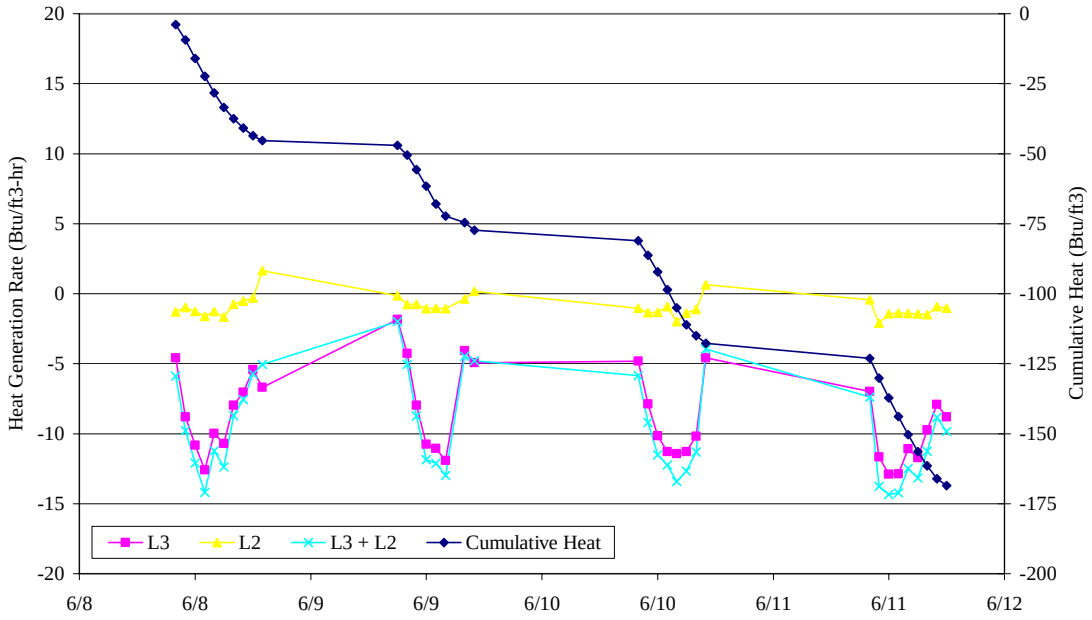

Heat Generation
Time Period: Wet #1
Mixed Section

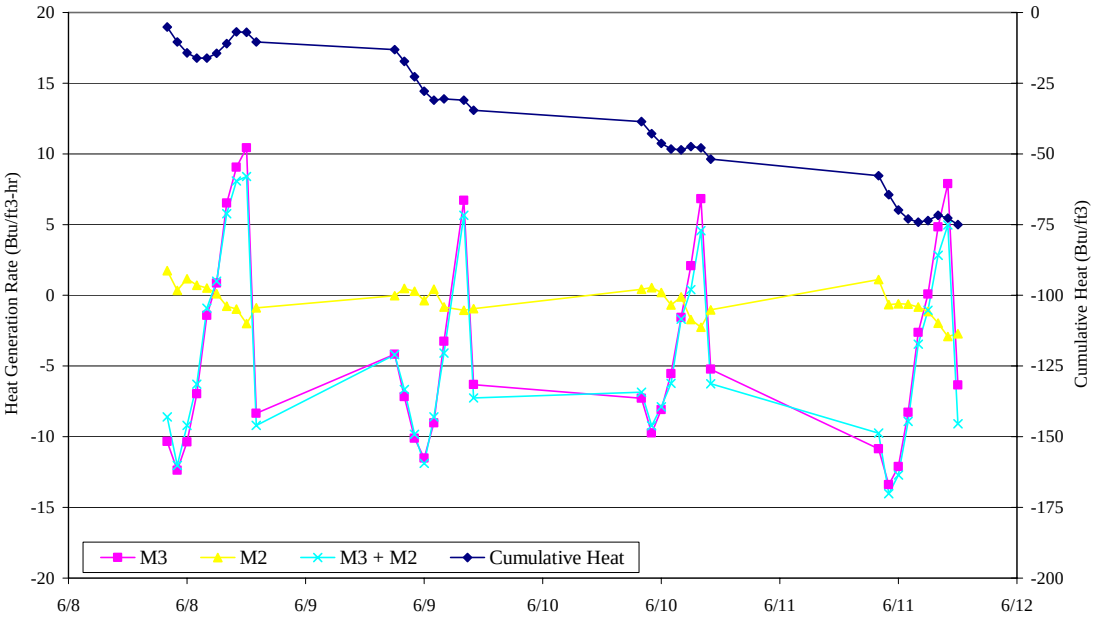

Heat Generation
Time Period: Wet #1
Large Tire Shred-Only Stockpile

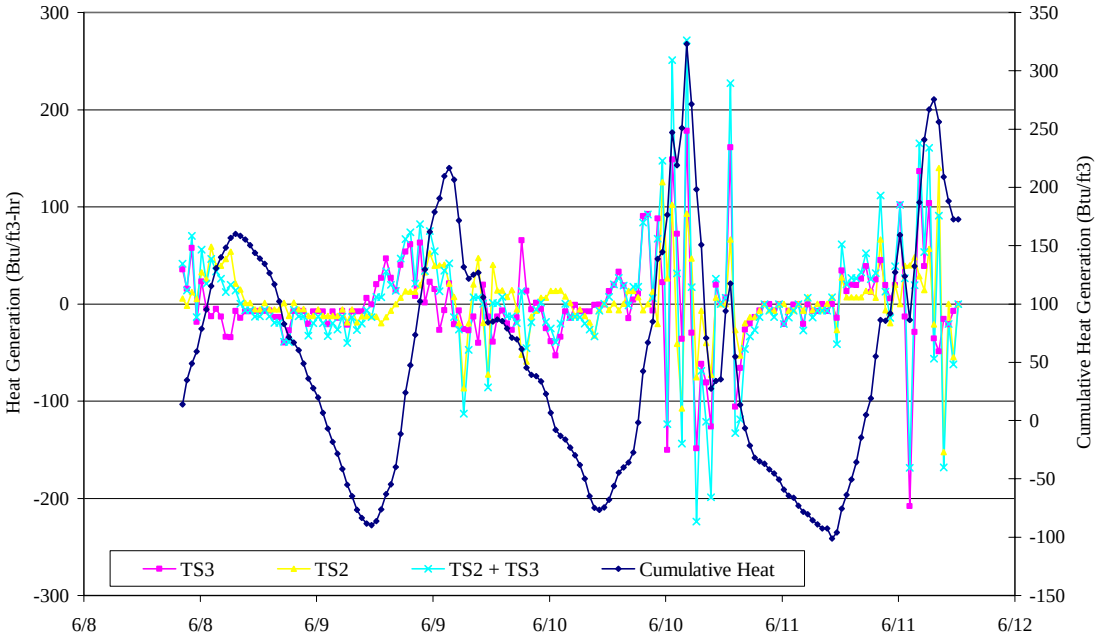

Heat Generation
Time Period: Wet #2
Soil-Only Section

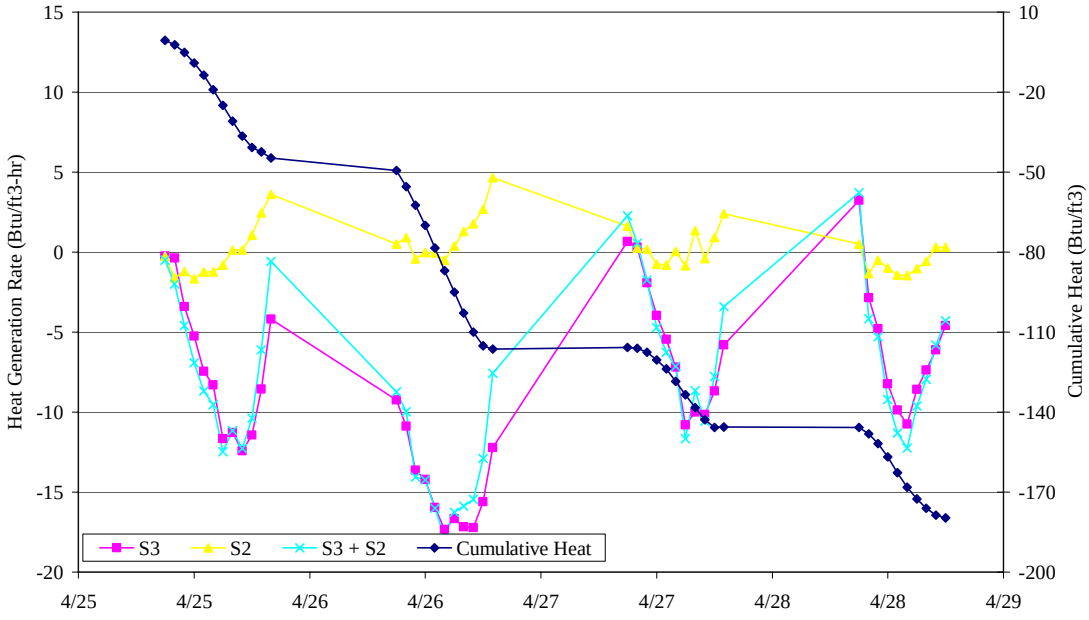

Heat Generation
Time Period: Wet #2
Layered Section

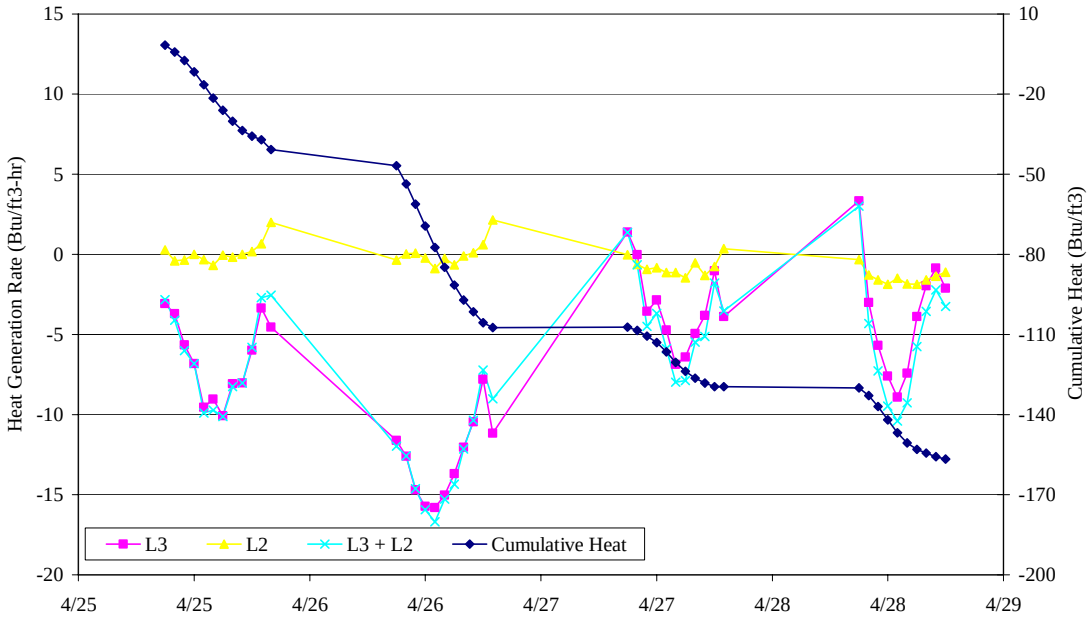

Heat Generation
Time Period: Wet #2
Mixed Section

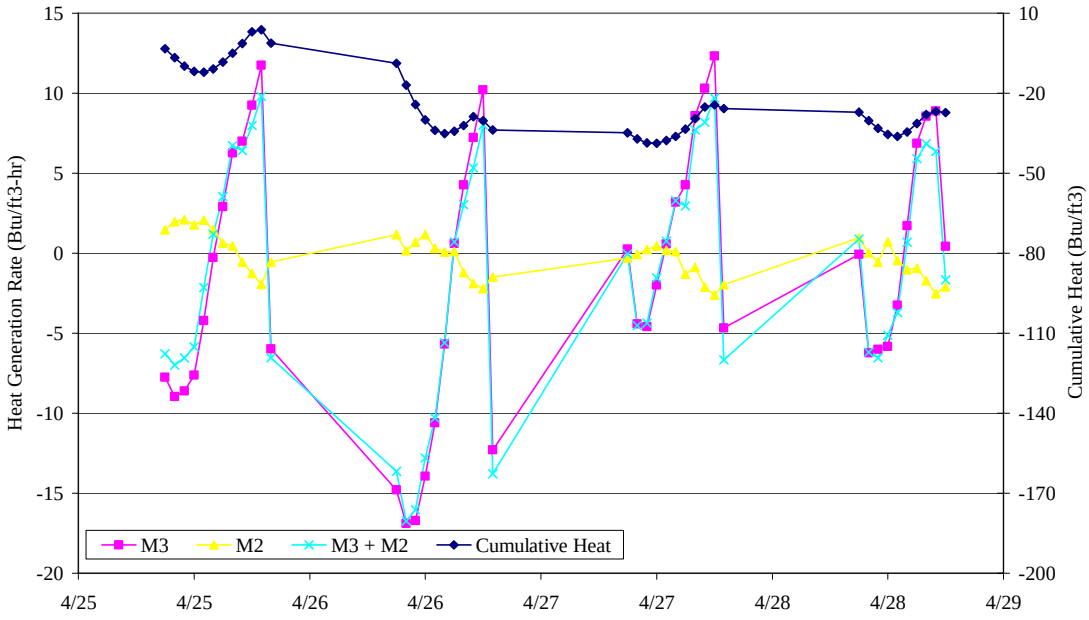

Heat Generation
Time Period: Wet #2
Large Tire Shred-Only Stockpile

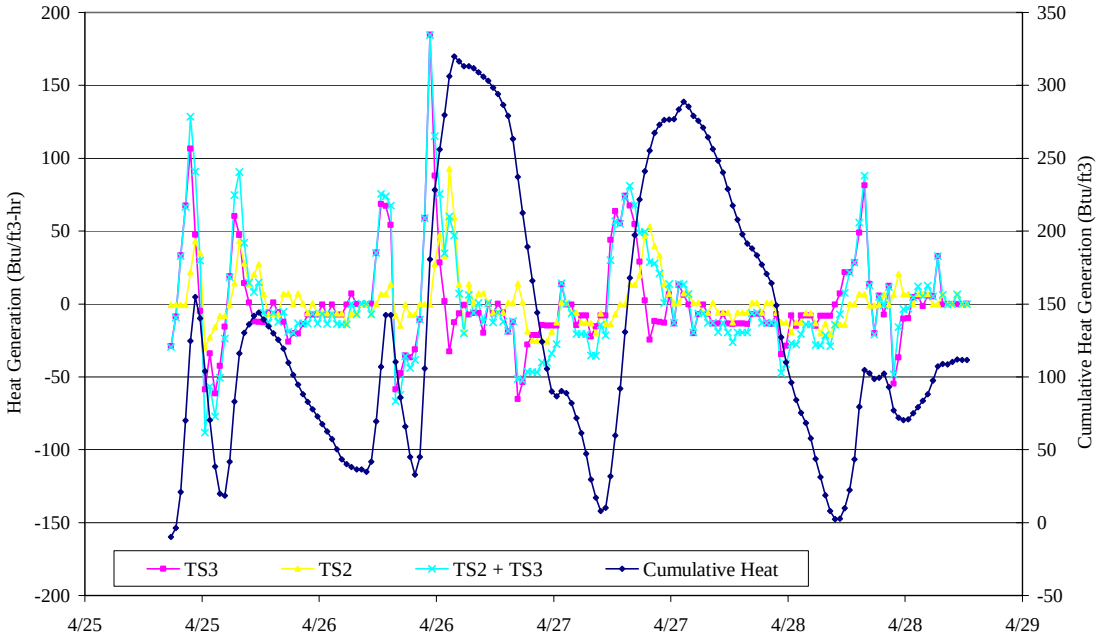

Heat Generation
Time Period: Wet #3
Soil-Only Section

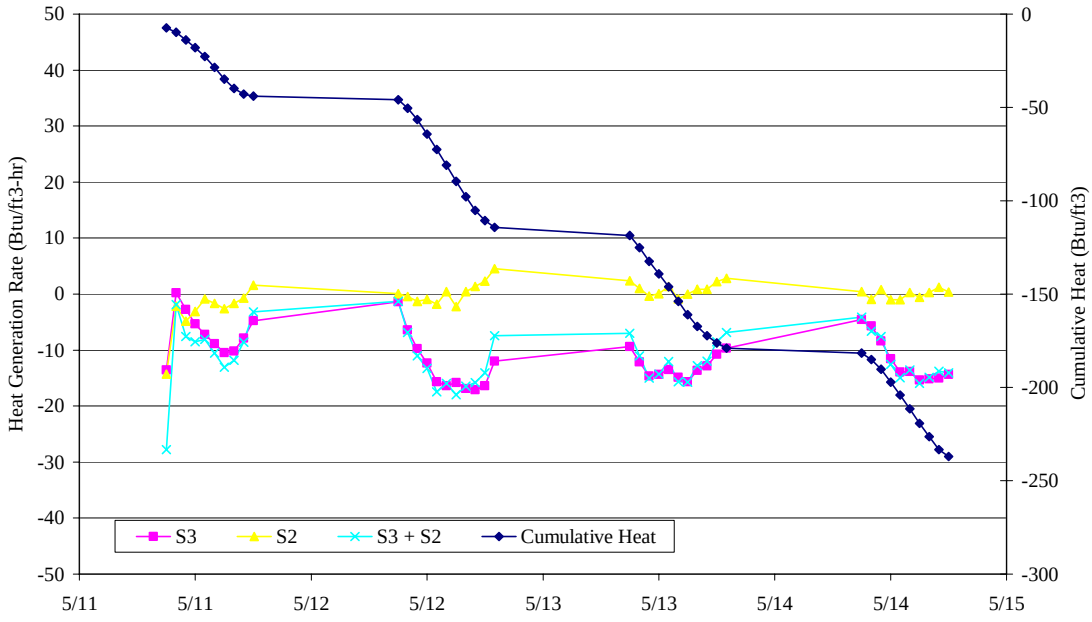

Heat Generation
Time Period: Wet #3
Layered Section

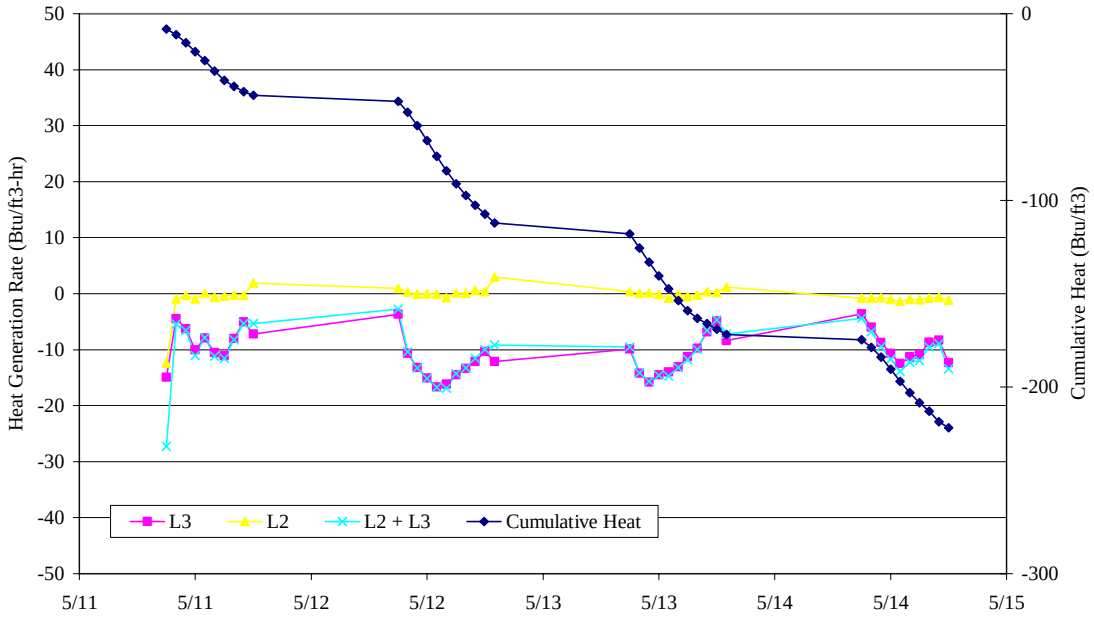

Heat Generation
Time Period: Wet #3
Mixed Section

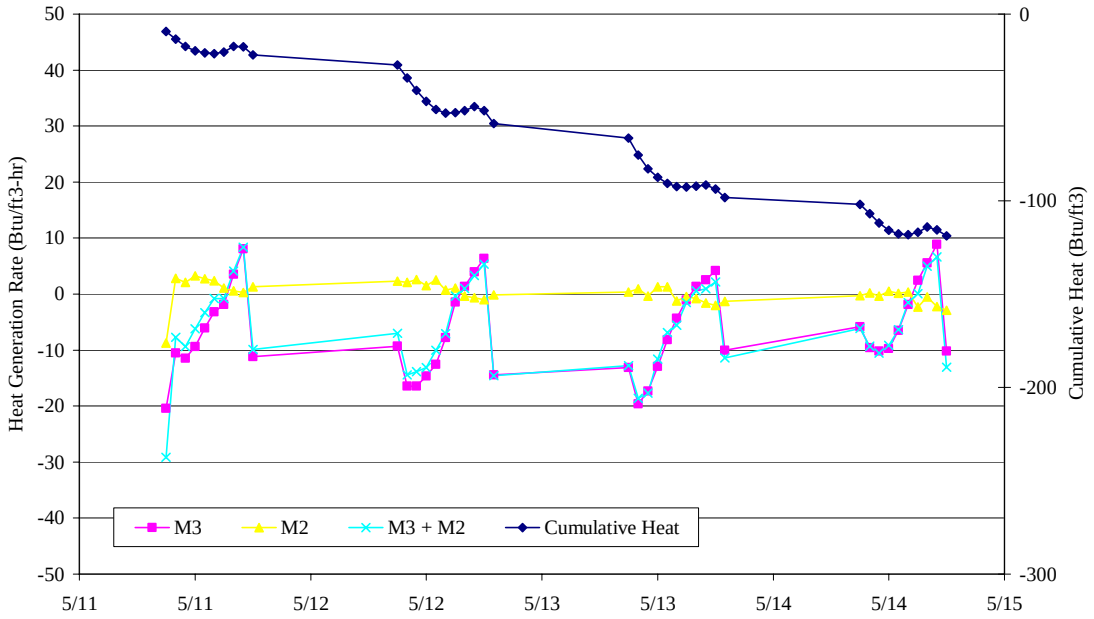

Heat Generation
Time Period: Wet #3
Large Tire Shred-Only Stockpile

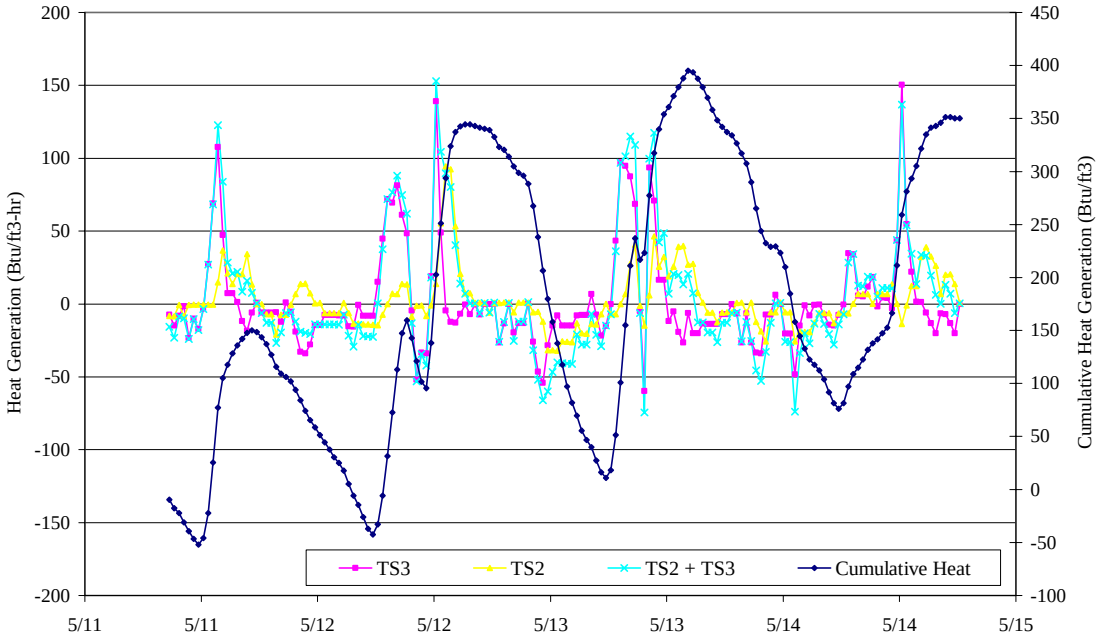

Heat Generation Rate
Time Period: Dry #1
December 13-17

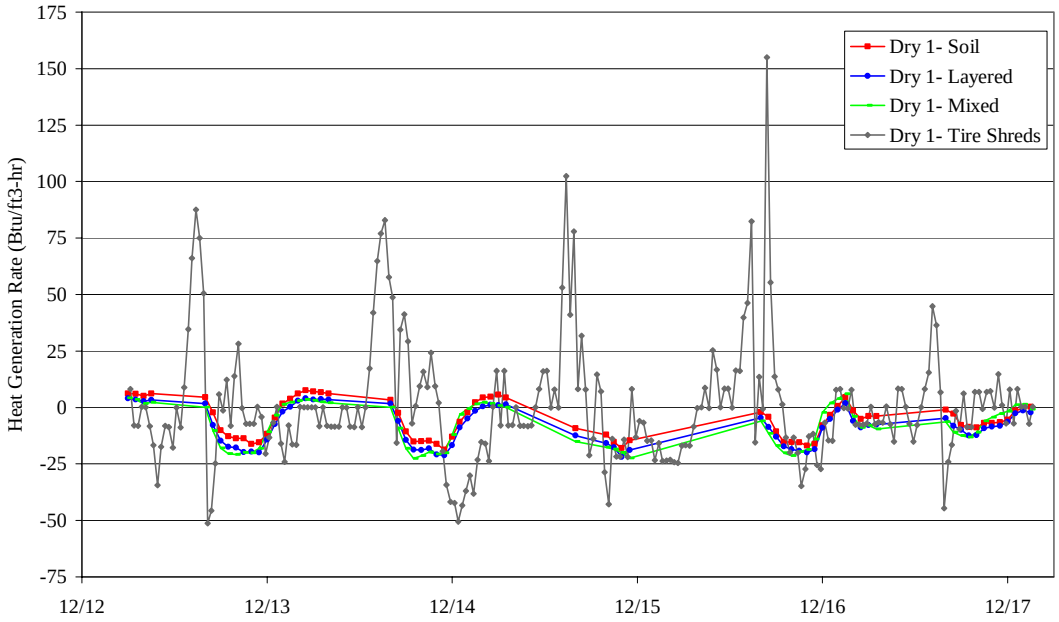

Heat Generation Rate
Time Period: Dry #2
May 1-7

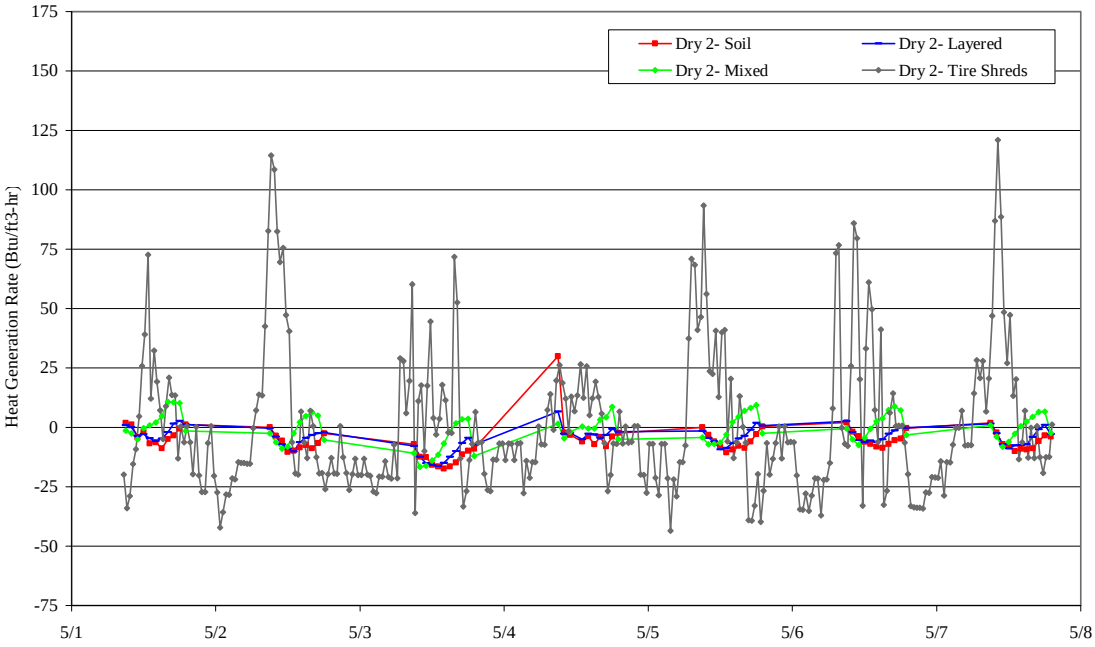

Heat Generation Rate
Time Period: Dry #3
January 26-31

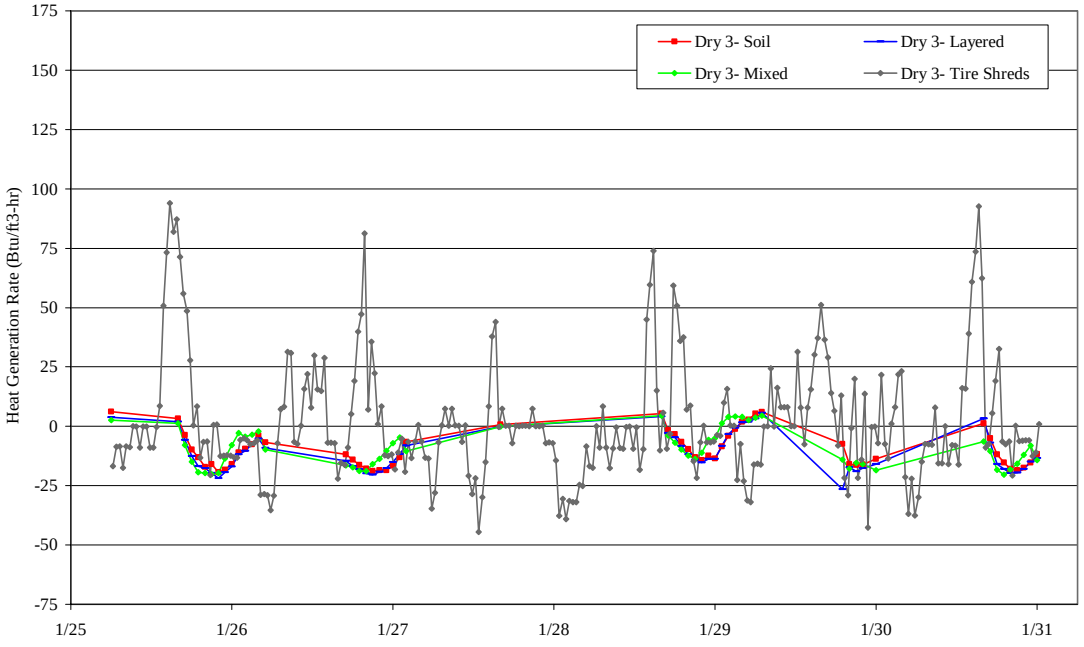

Heat Generation Rate
Time Period: Wet #1
June 8-11

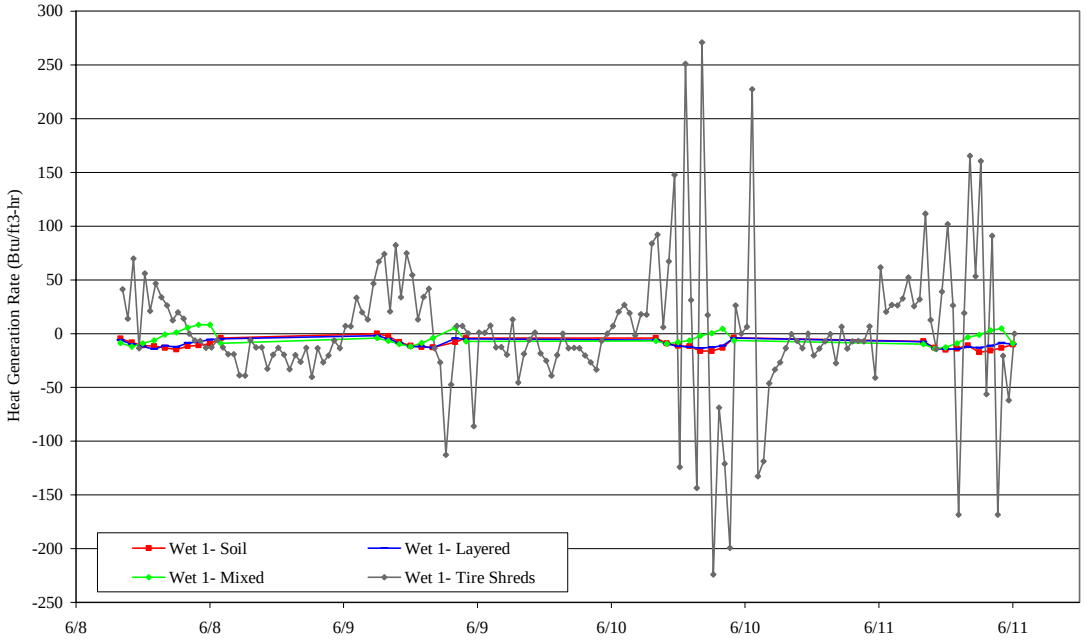

Heat Generation Rate
Time Period: Wet #2
April 25-28

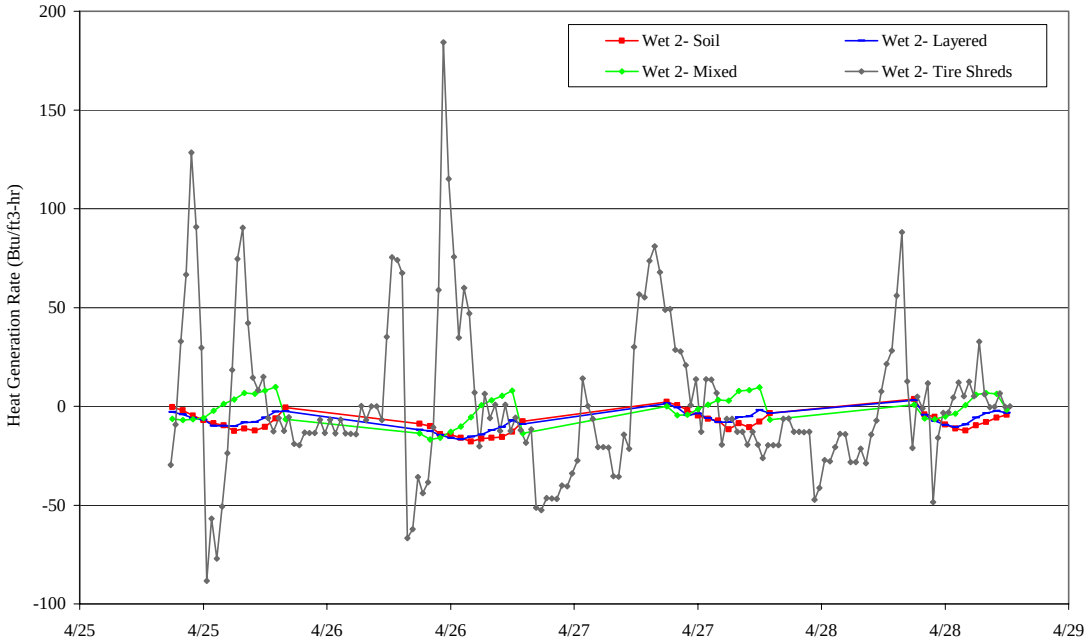

Heat Generation Rate
Time Period: Wet #3
May 11-14

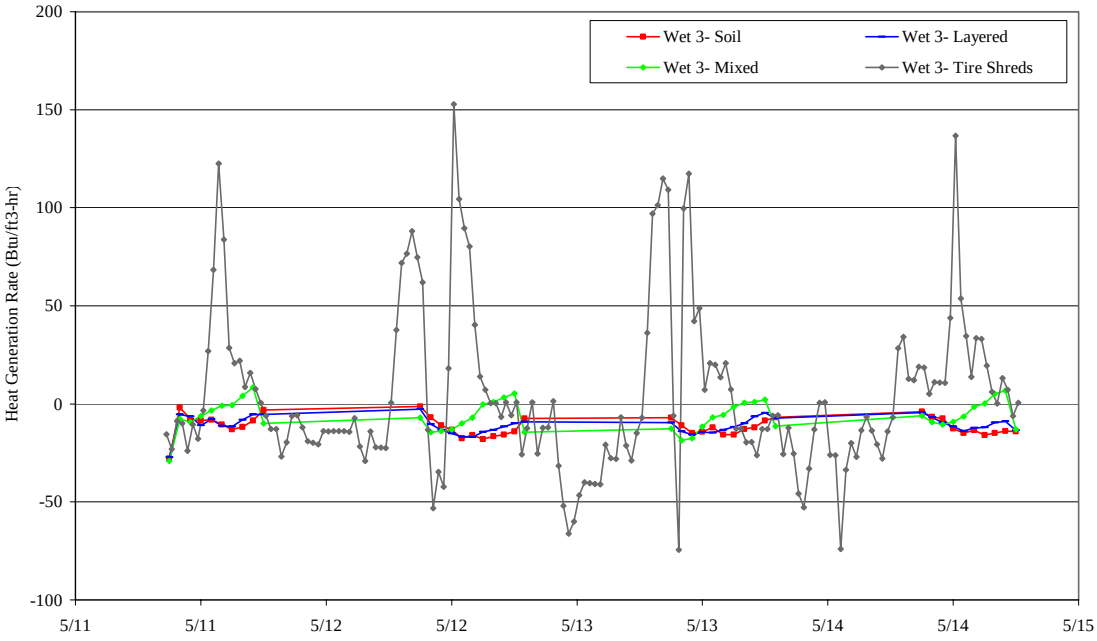

Cumulative Heat Generation
Time Period: Dry #1
December 13-17

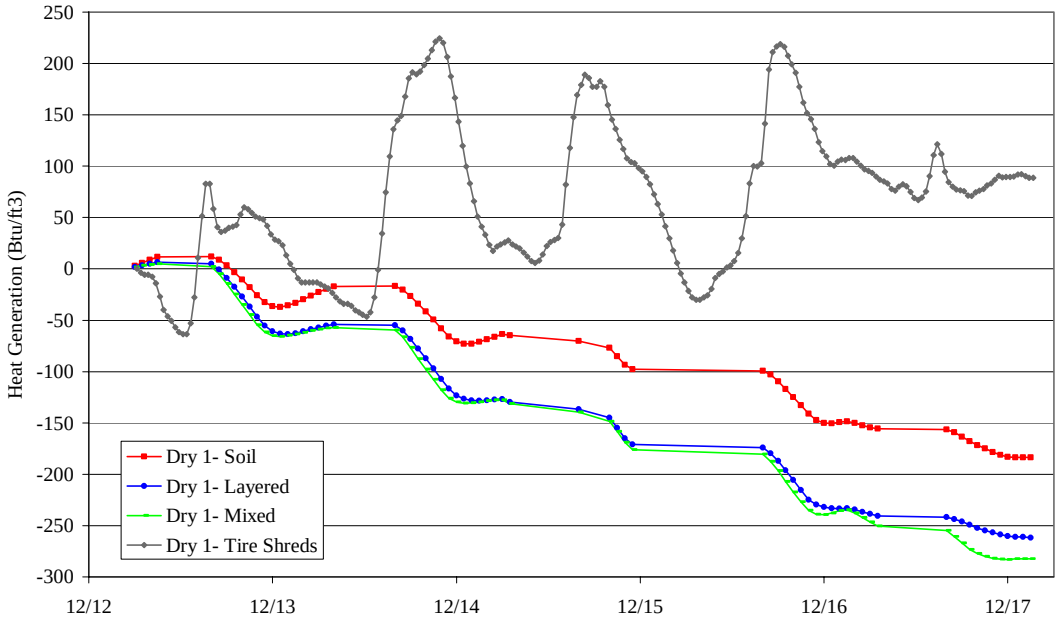

Cumulative Heat Generation
Time Period: Dry #2
May 1-7

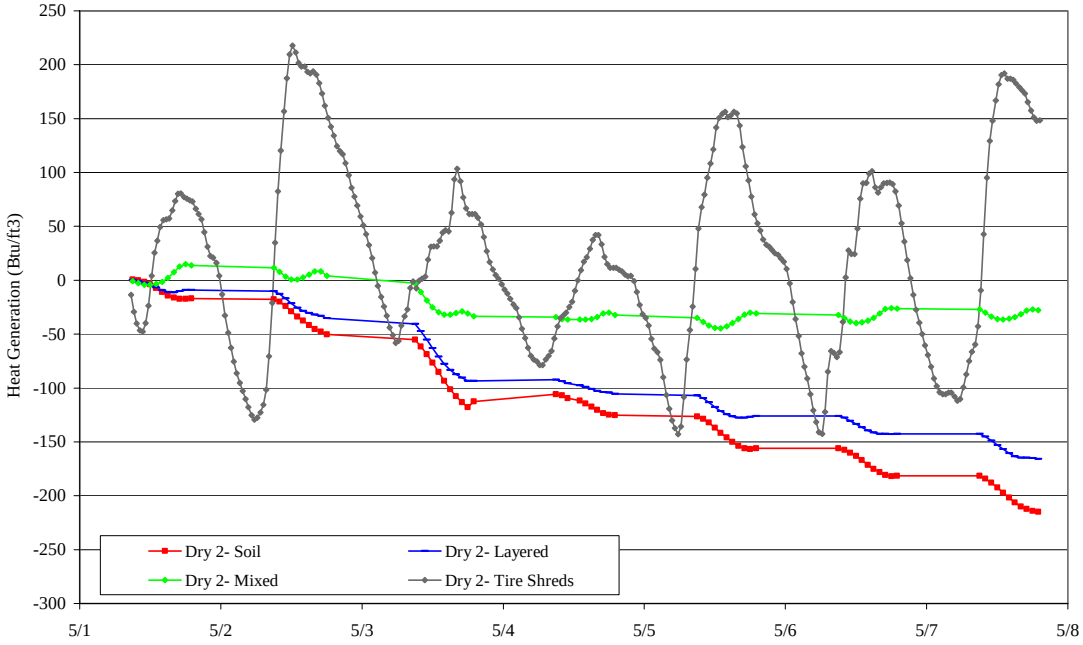

Cumulative Heat Generation
Time Period: Dry #3
January 26-31

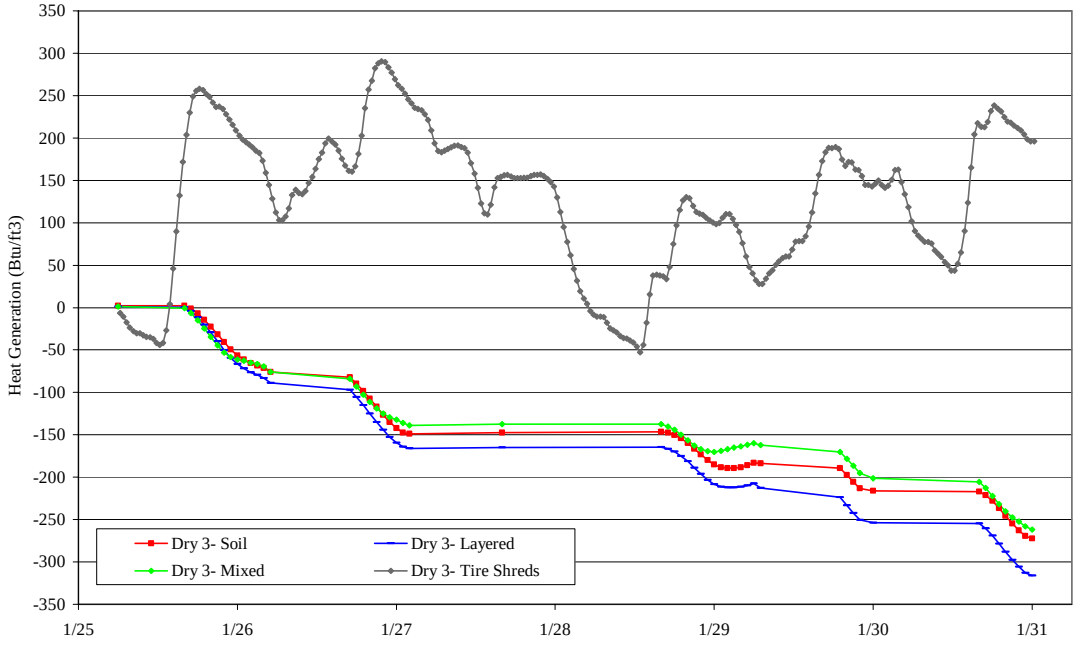

Cumulative Heat Generation
Time Period: Wet #1
June 8-11

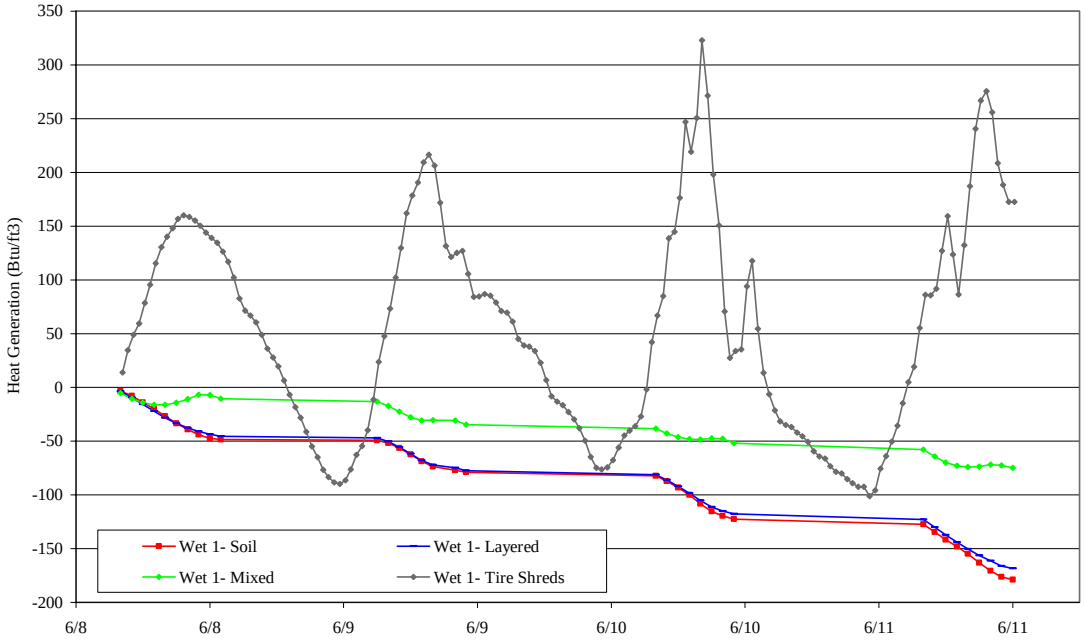

Cumulative Heat Generation
Time Period: Wet #2
April 25-28

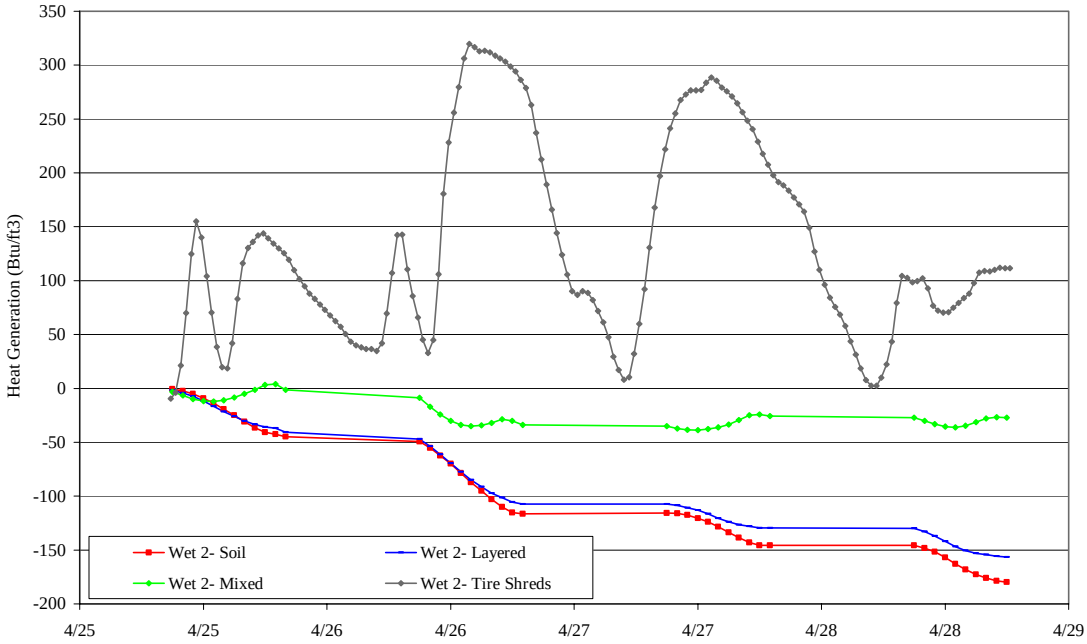

Cumulative Heat Generation
Time Period: Wet #3
May 11-14

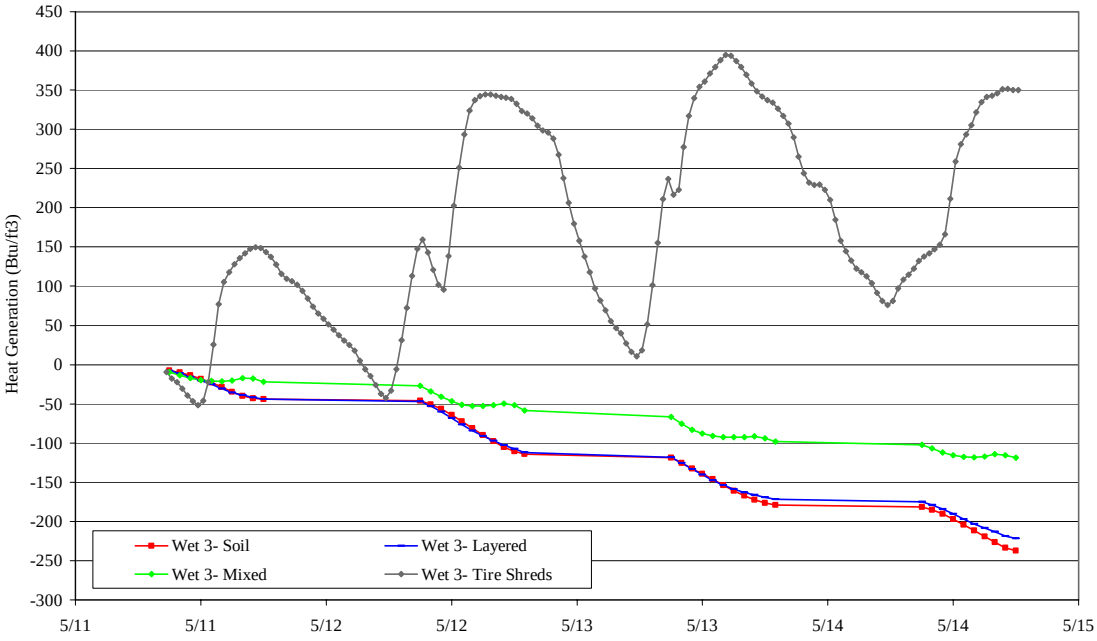

Cumulative Heat Generation
Soil-Only Section

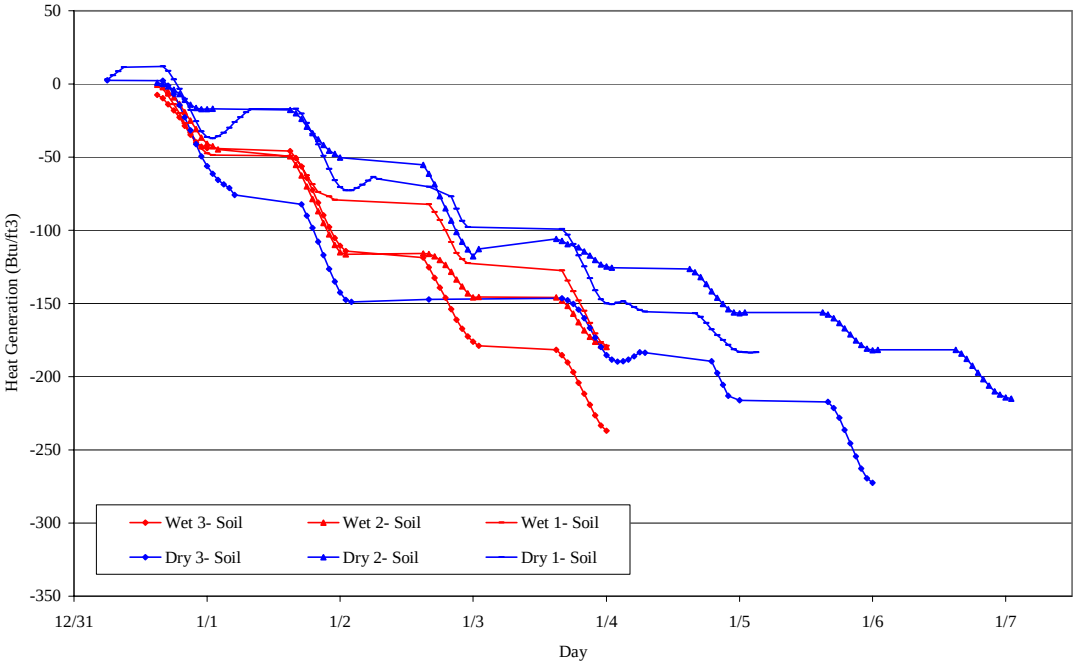

Cumulative Heat Generation
Layered Section

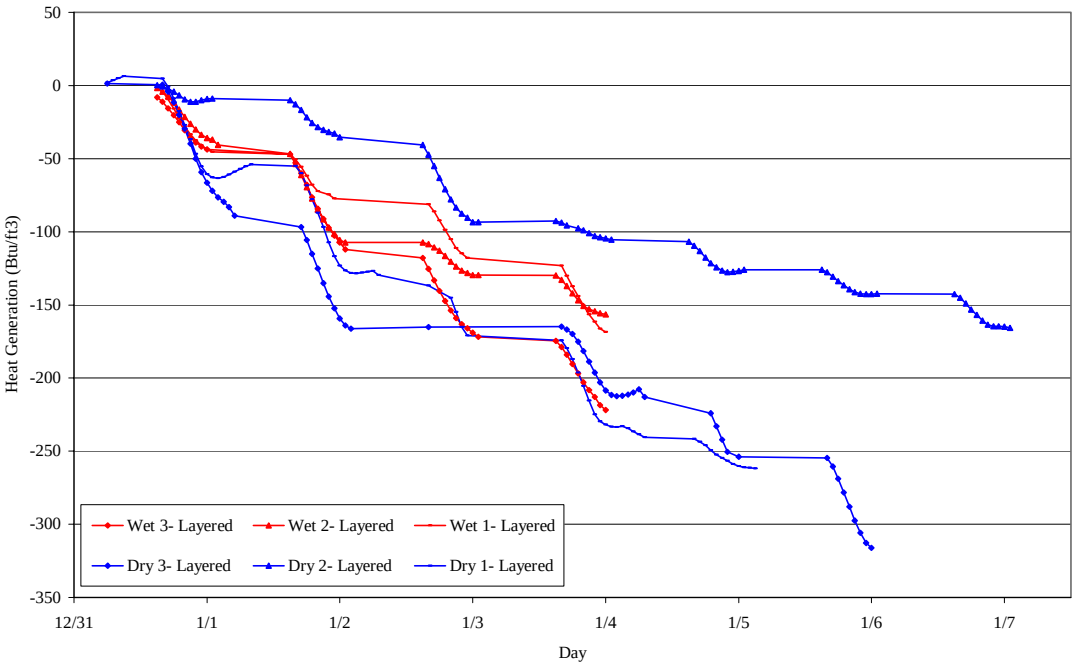

Cumulative Heat Generation
Mixed Section

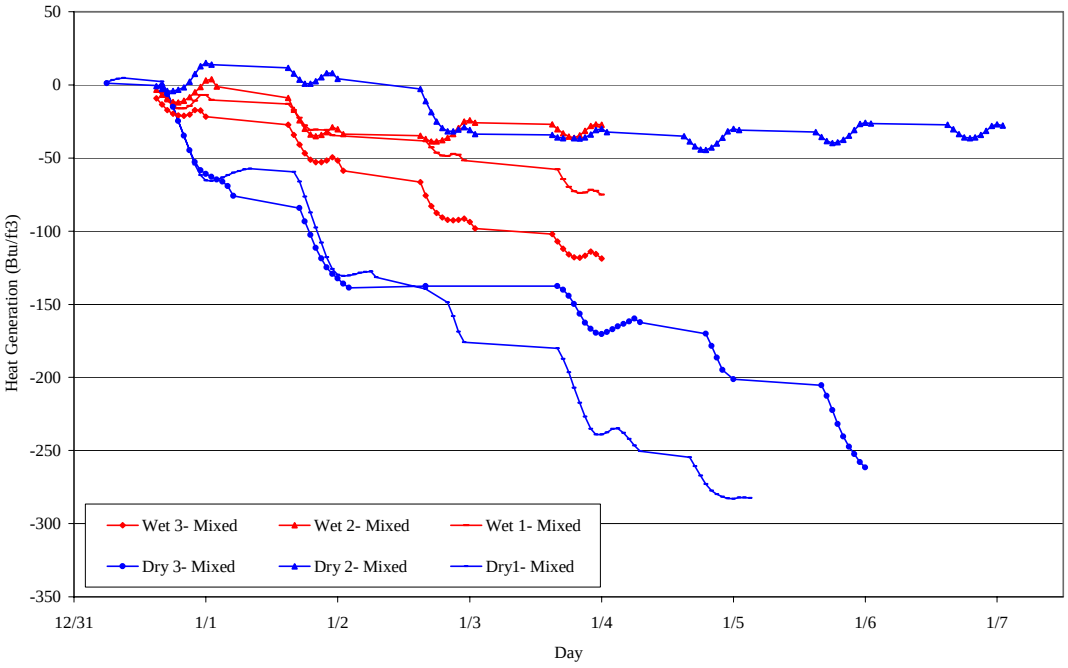

Cumulative Heat Generation
Tire Shred Pile

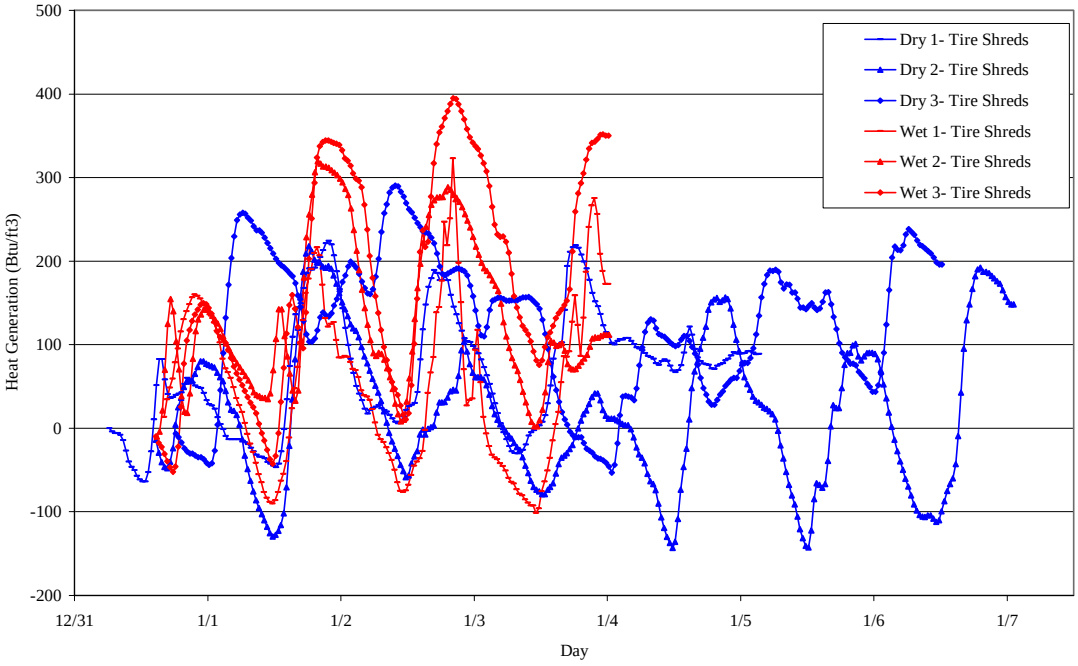

Dry Time Period #1
Heat Generation Correlations
Heat Generation Rate versus Internal Temperature

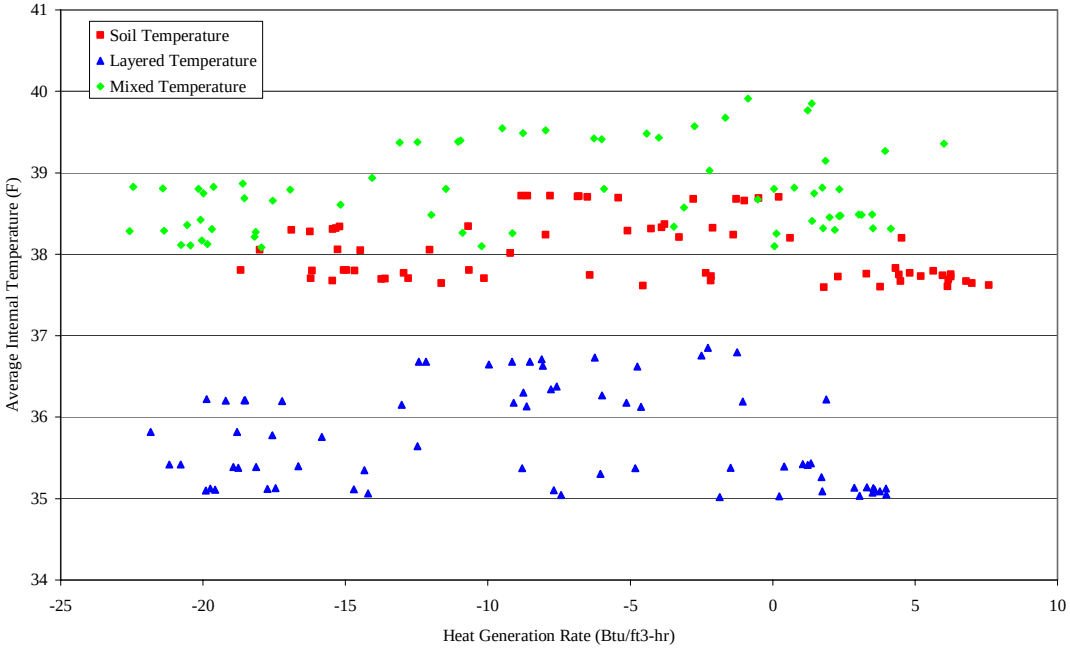

Dry Time Period #2
Heat Generation Correlations
Heat Generation Rate versus Internal Temperature

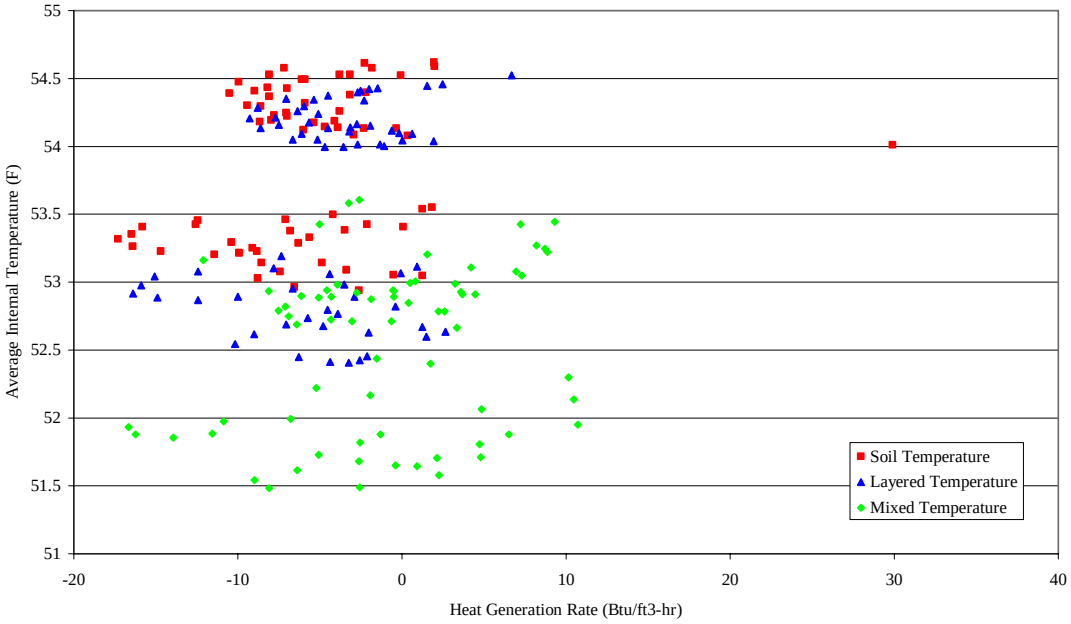

Dry Time Period #3
Heat Generation Correlations
Heat Generation Rate versus Internal Temperature

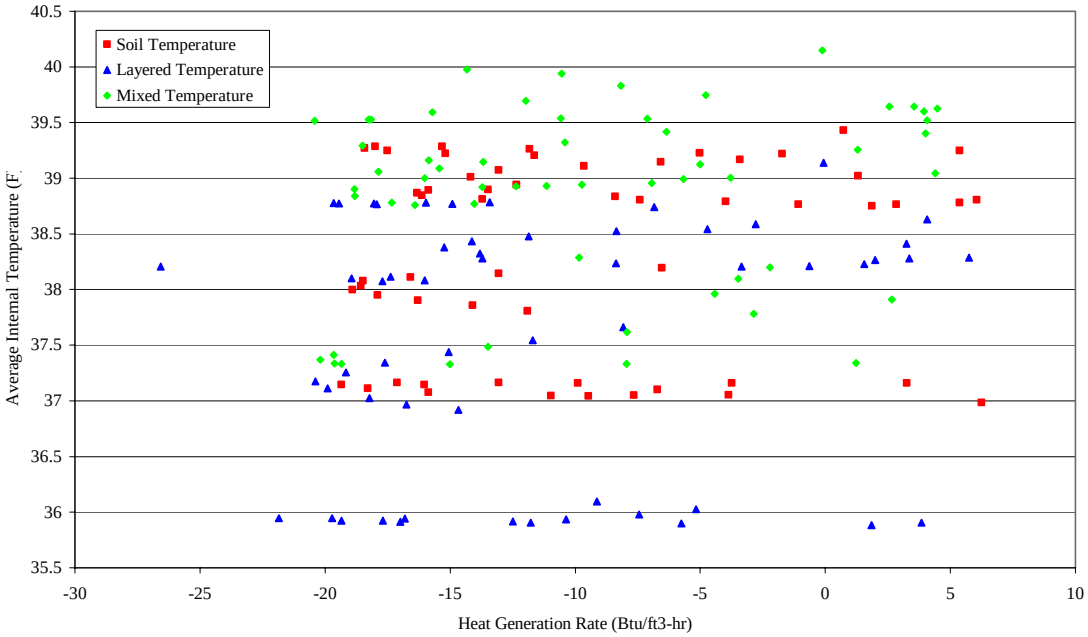

Wet Time Period #1
Heat Generation Correlations
Heat Generation Rate versus Internal Temperature

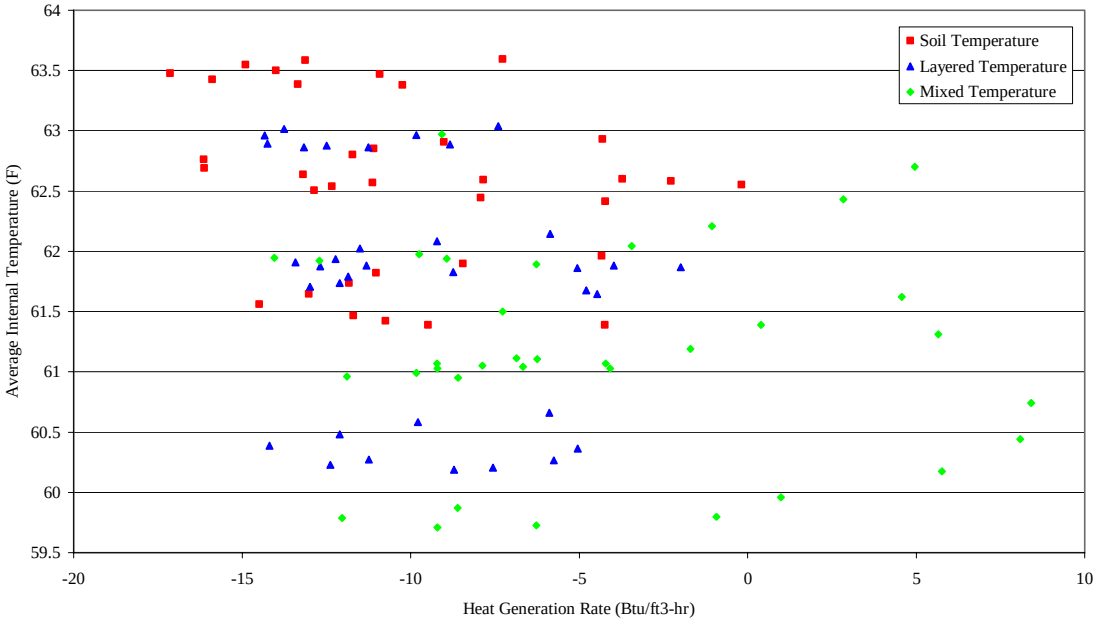

Wet Time Period #2
Heat Generation Correlations
Heat Generation Rate versus Internal Temperature

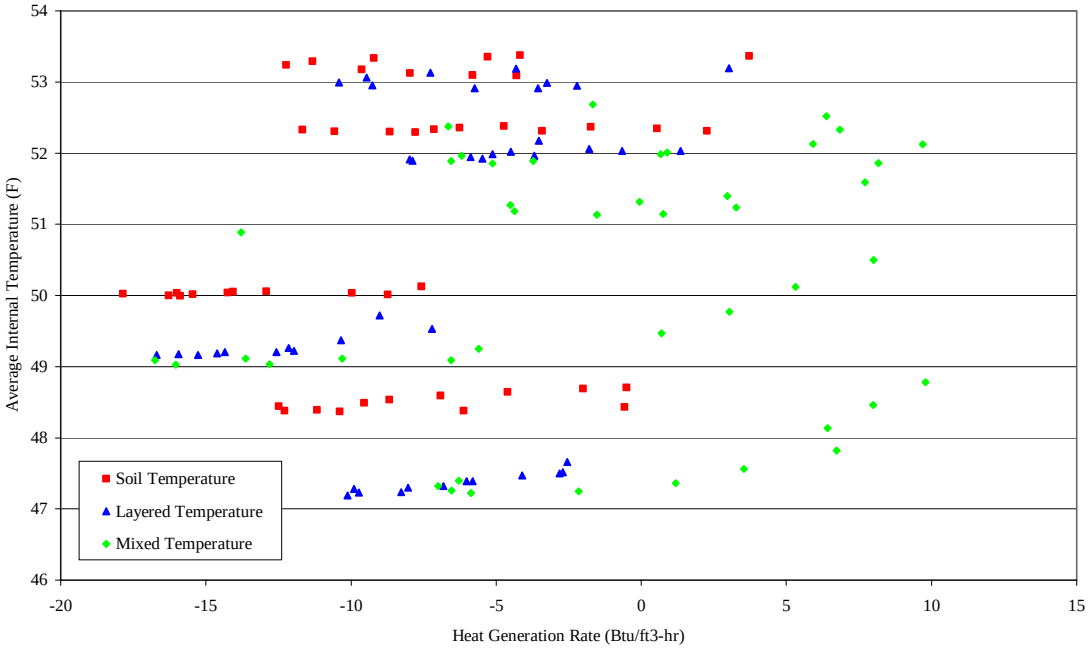

Wet Time Period #3
Heat Generation Correlations
Heat Generation Rate versus Internal Temperature

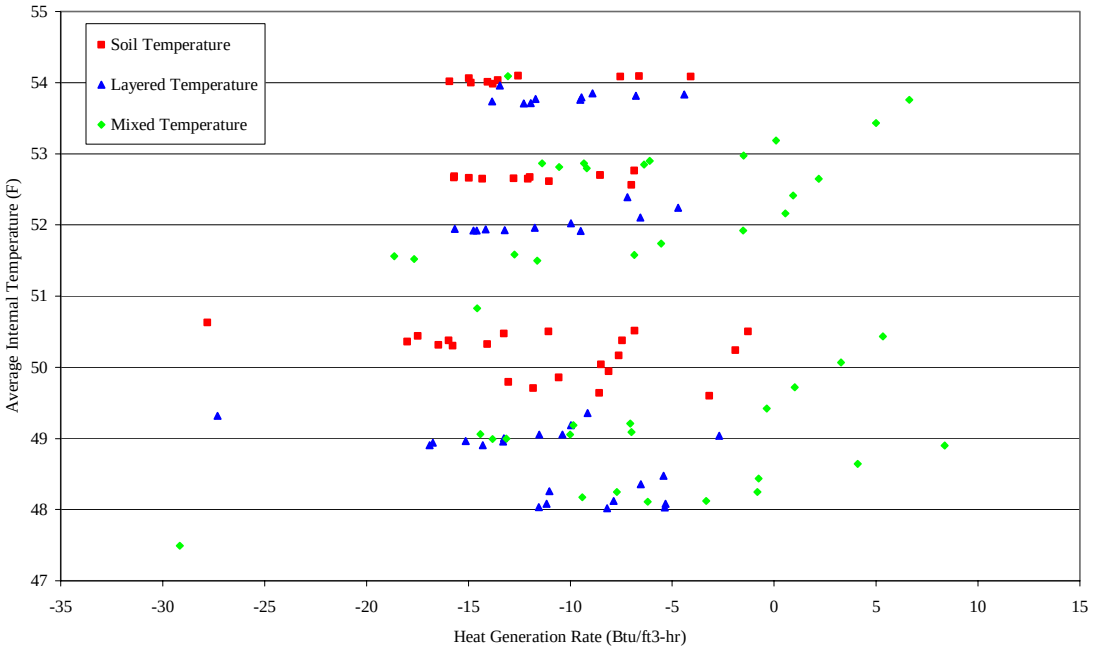

Dry Time Period #1
Heat Generation Correlations
Heat Generation Rate versus Water Content

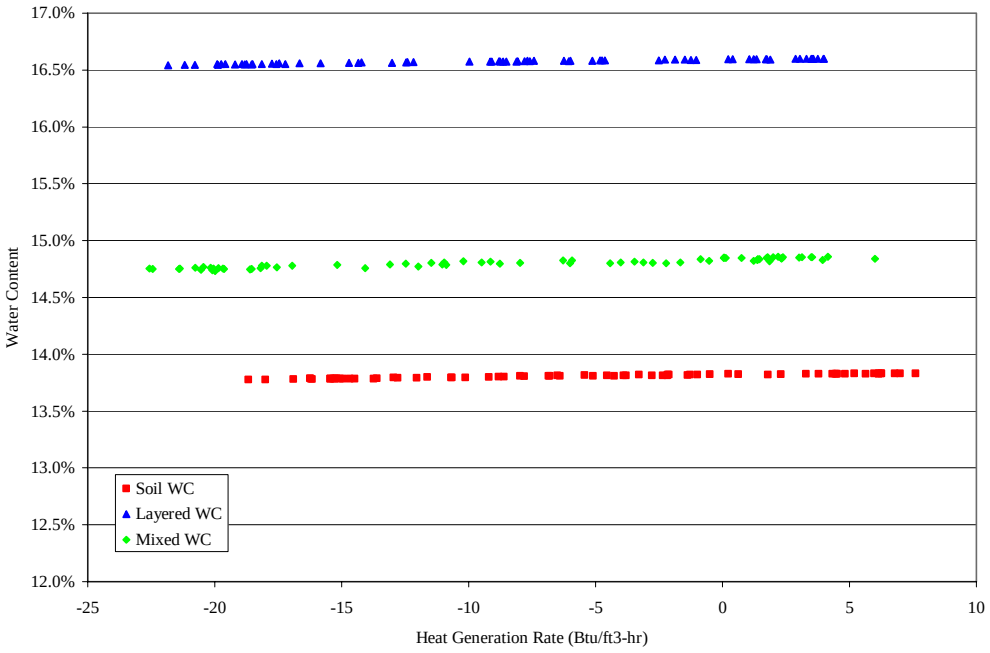

Dry Time Period #2
Heat Generation Correlations
Heat Generation Rate versus Water Content

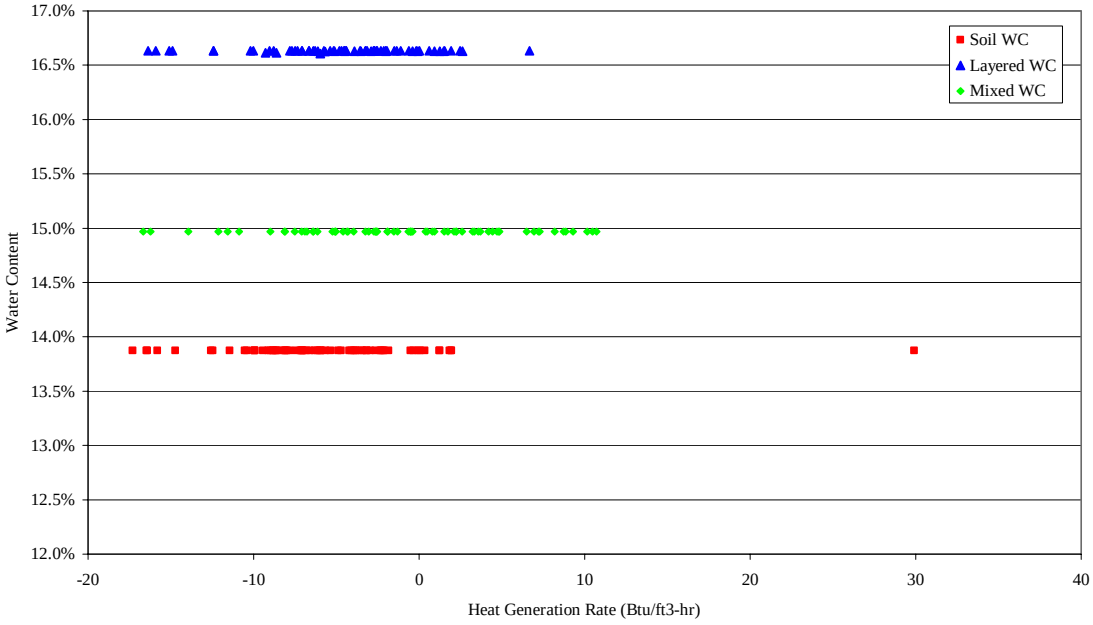

Dry Time Period #3
Heat Generation Correlations
Heat Generation Rate versus Water Content

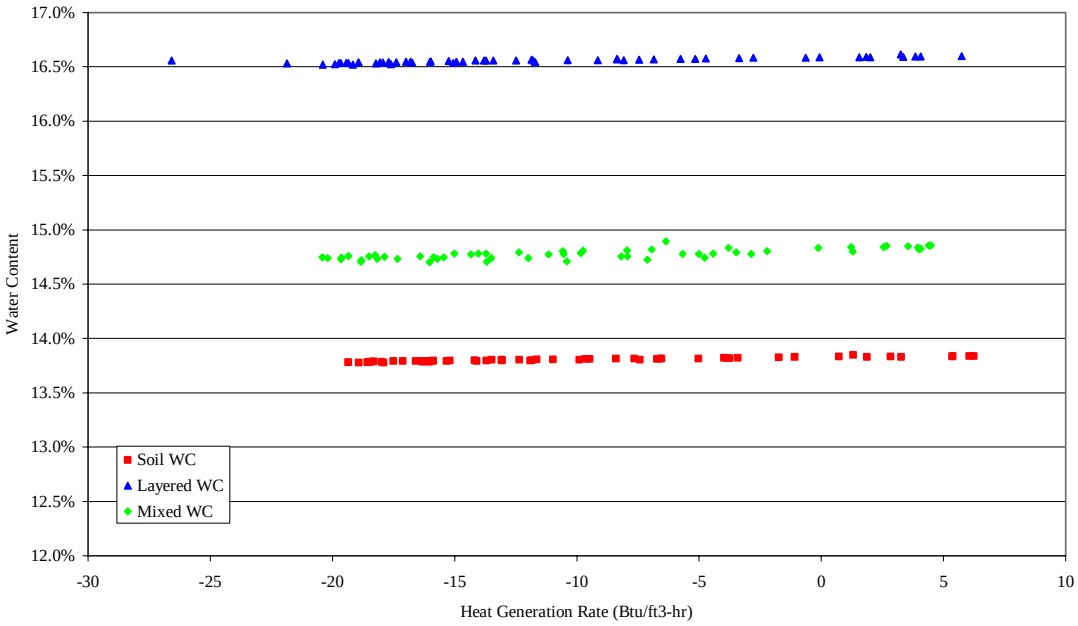

Wet Time Period #1
Heat Generation Correlations
Heat Generation Rate versus Water Content

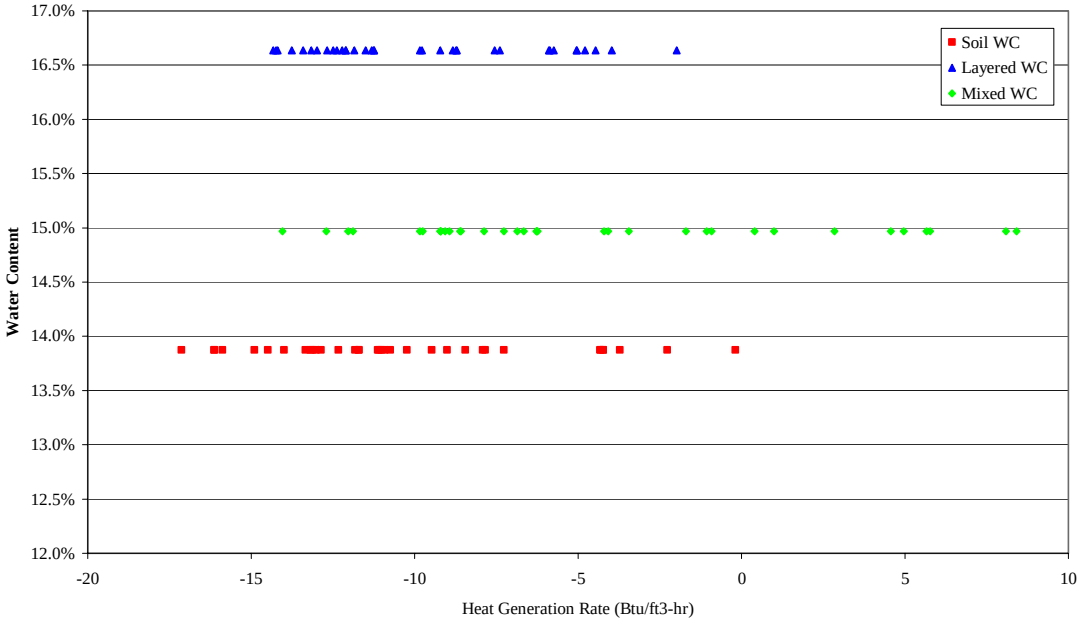

Wet Time Period #2
Heat Generation Correlations
Heat Generation Rate versus Water Content

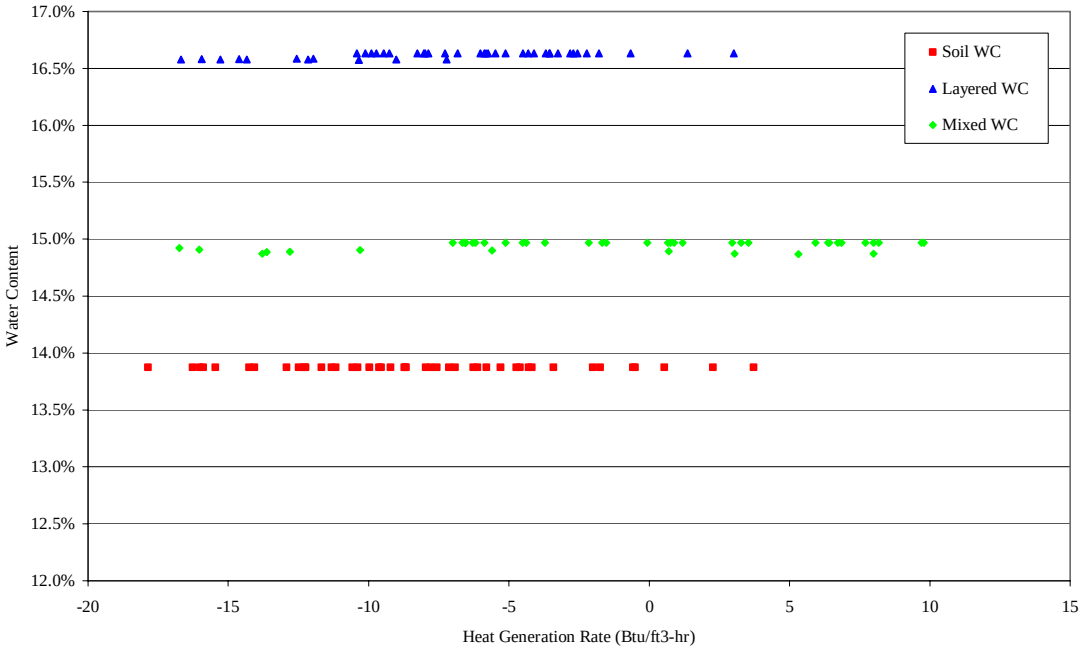

Wet Time Period #3
Heat Generation Correlations
Heat Generation Rate versus Water Content

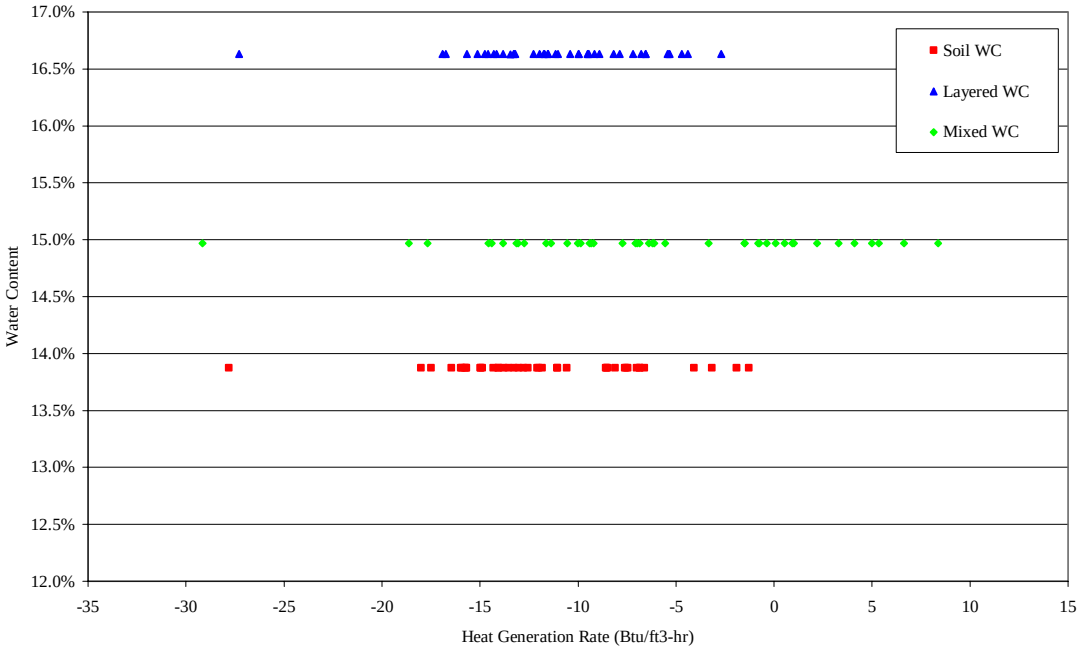

Dry Time Period #1
Heat Generation Correlations
Heat Generation Rate versus Soil Suction

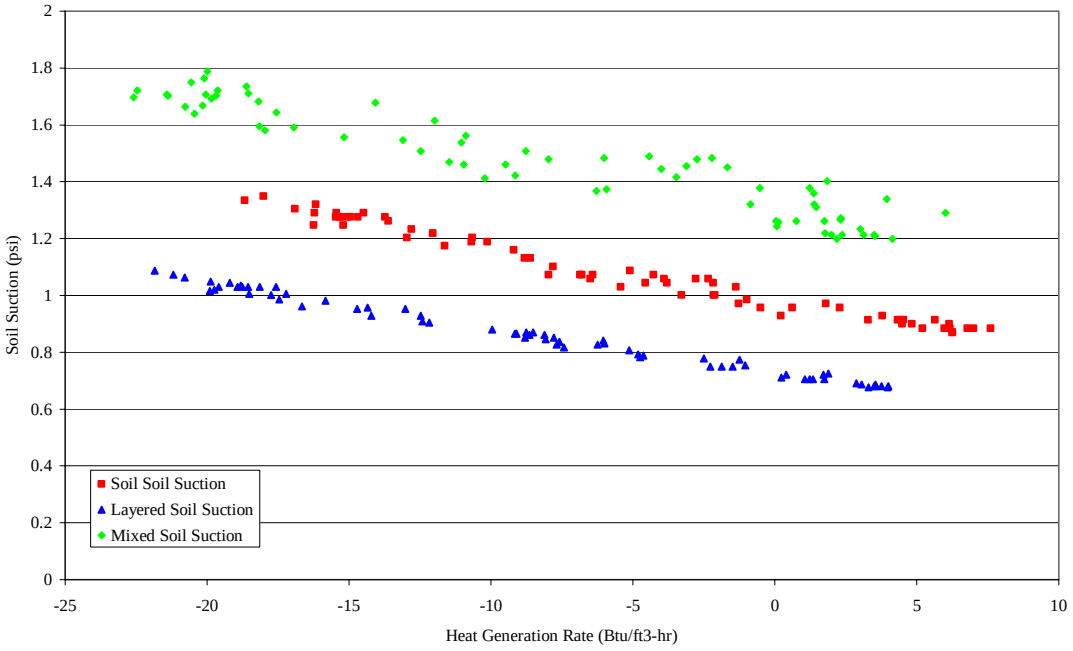

Dry Time Period #2
Heat Generation Correlations
Heat Generation Rate versus Soil Suction

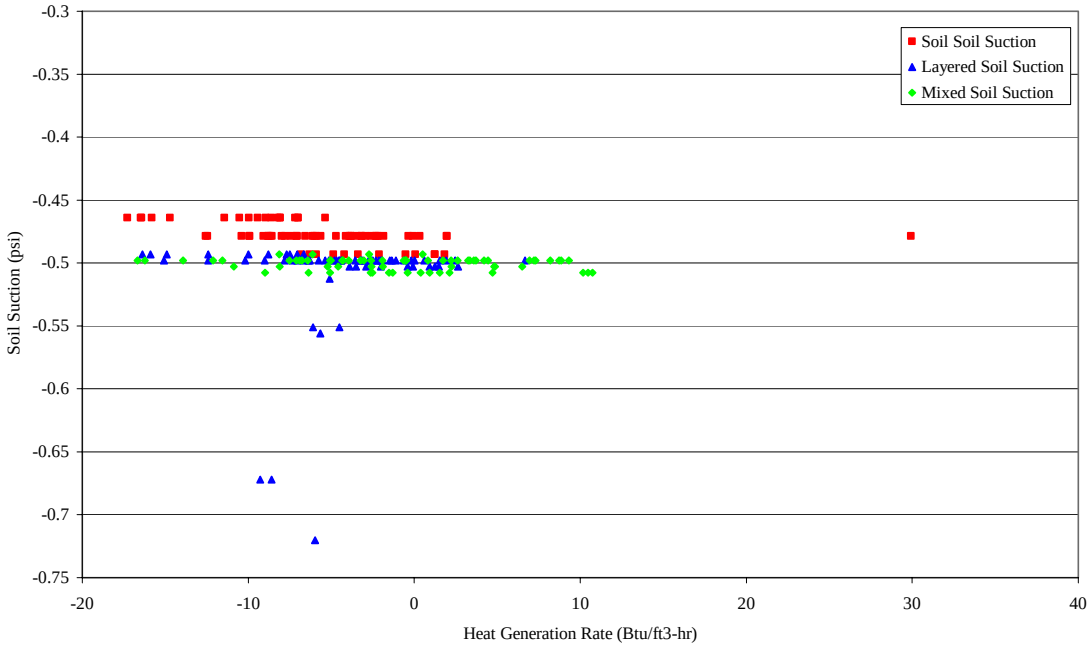

Dry Time Period #3
Heat Generation Correlations
Heat Generation Rate versus Soil Suction

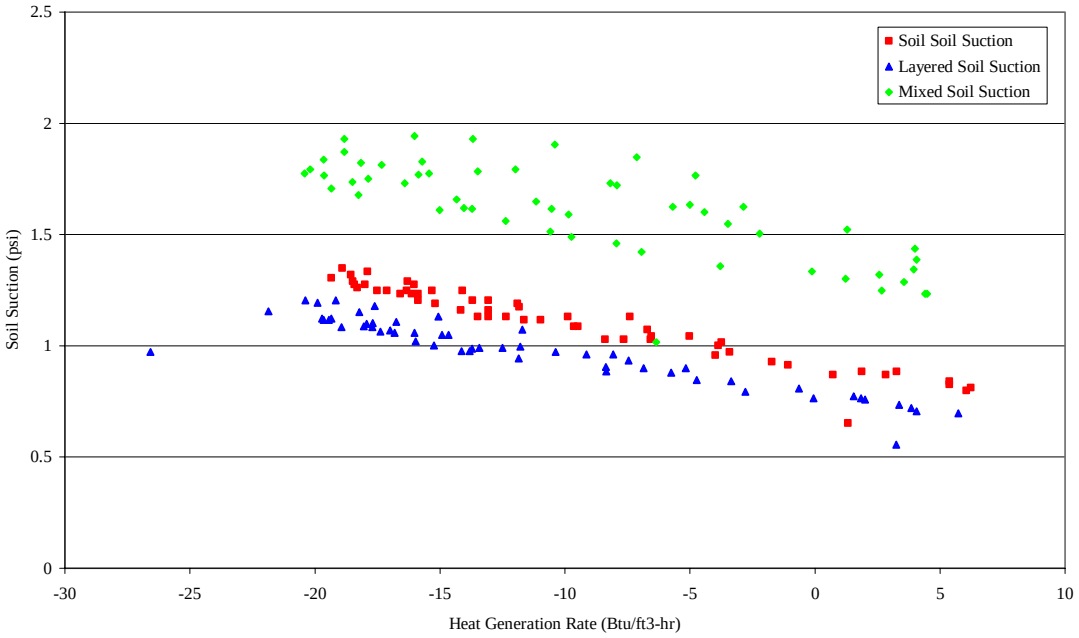

Wet Time Period #1
Heat Generation Correlations
Heat Generation Rate versus Soil Suction

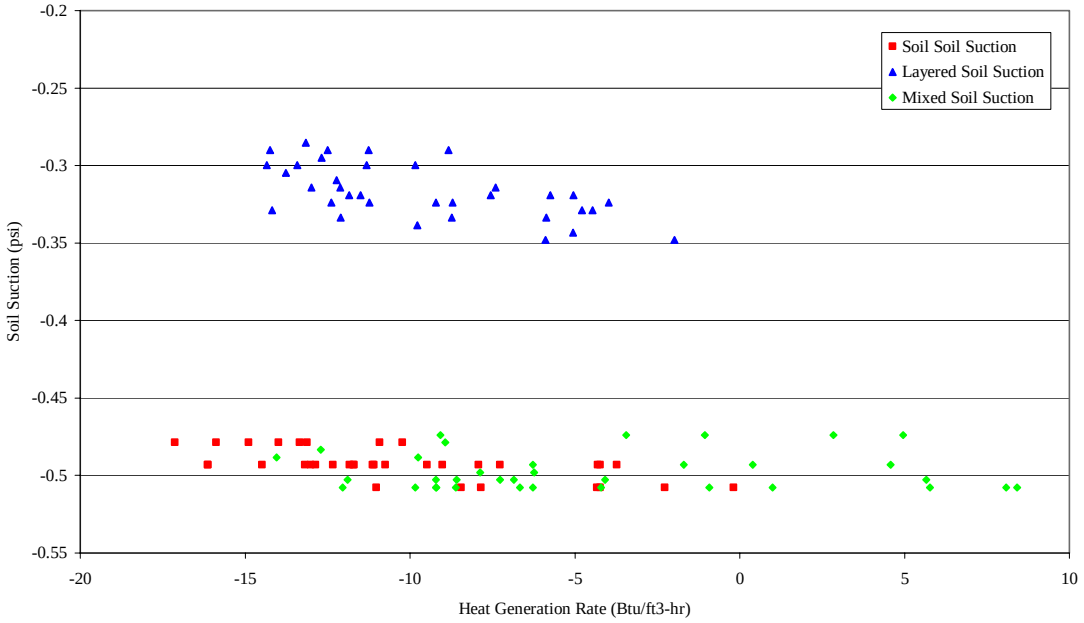

Wet Time Period #2
Heat Generation Correlations
Heat Generation Rate versus Soil Suction

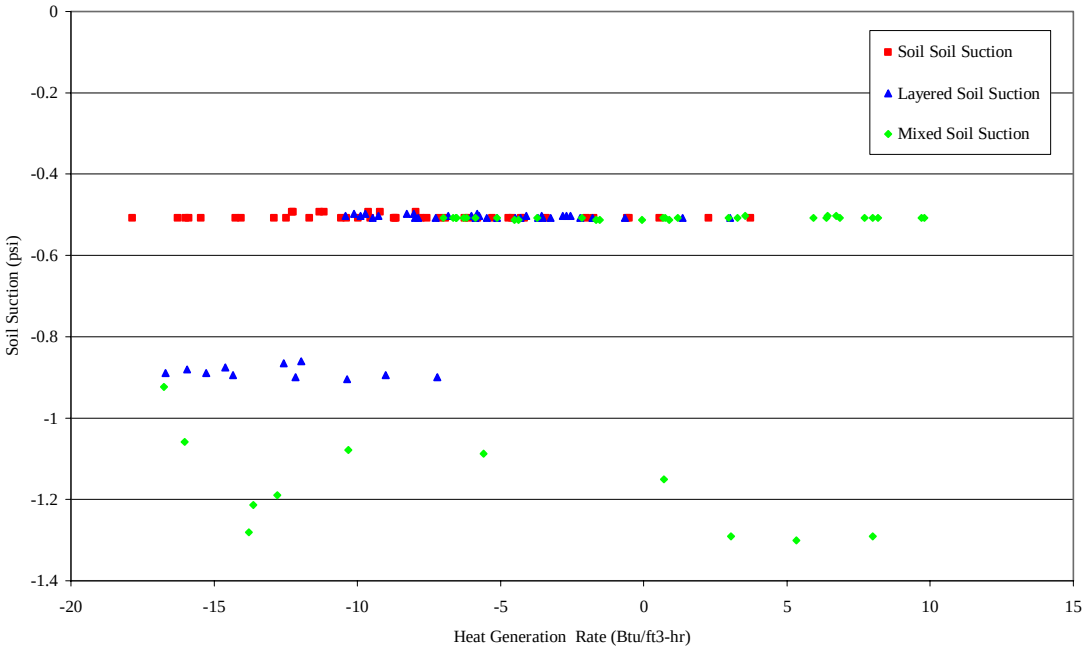

Wet Time Period #3
Heat Generation Correlations
Heat Generation Rate versus Soil Suction

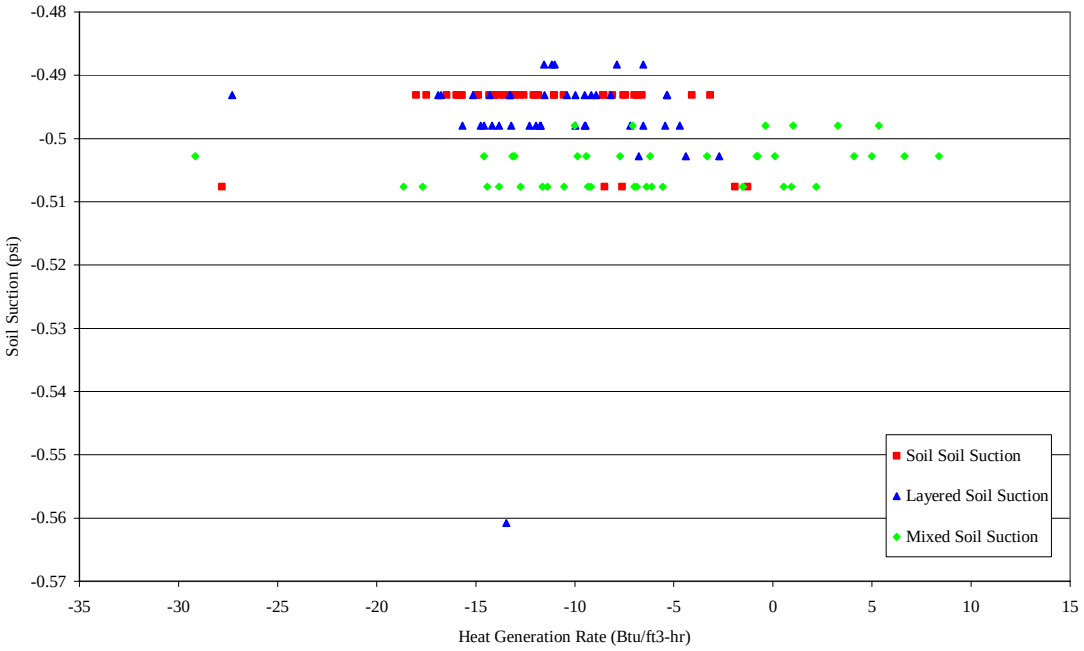

Dry Time Period #1
Heat Generation Correlations
Heat Generation Rate versus Layered Section Relative Humidity

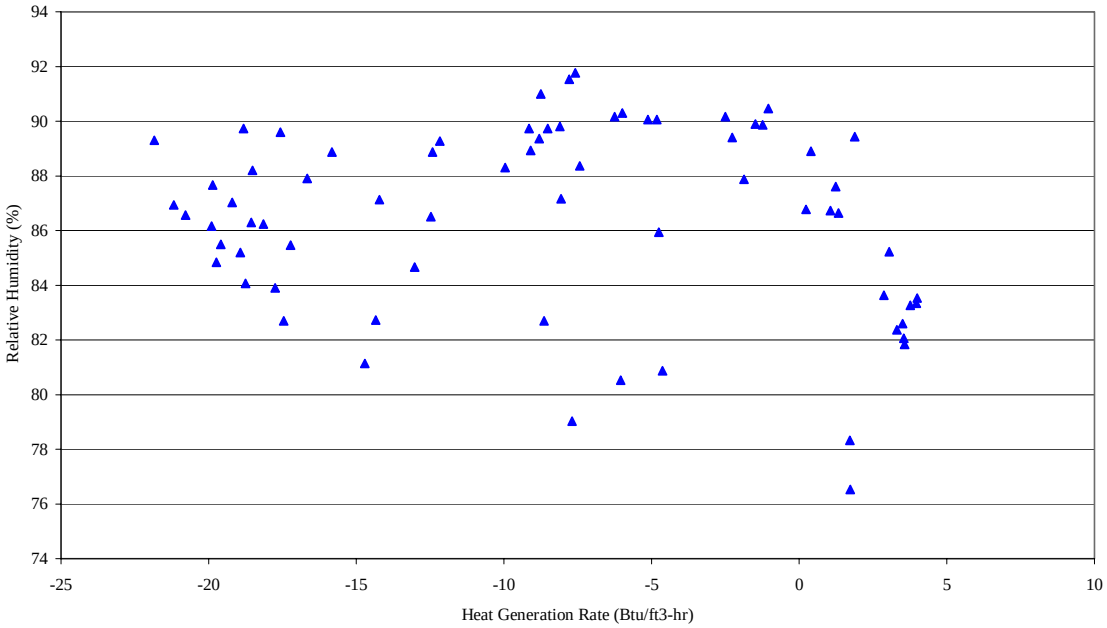

Dry Time Period #2
Heat Generation Correlations
Heat Generation Rate versus Layered Section Relative Humidity

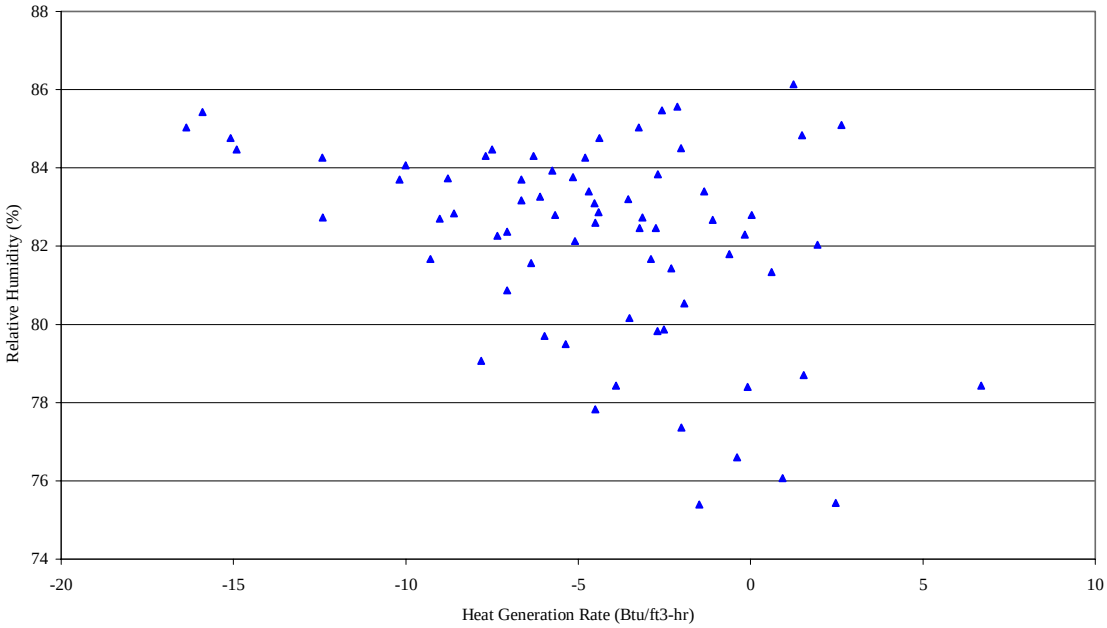

Dry Time Period #3
Heat Generation Correlations
Heat Generation Rate versus Layered Section Relative Humidity

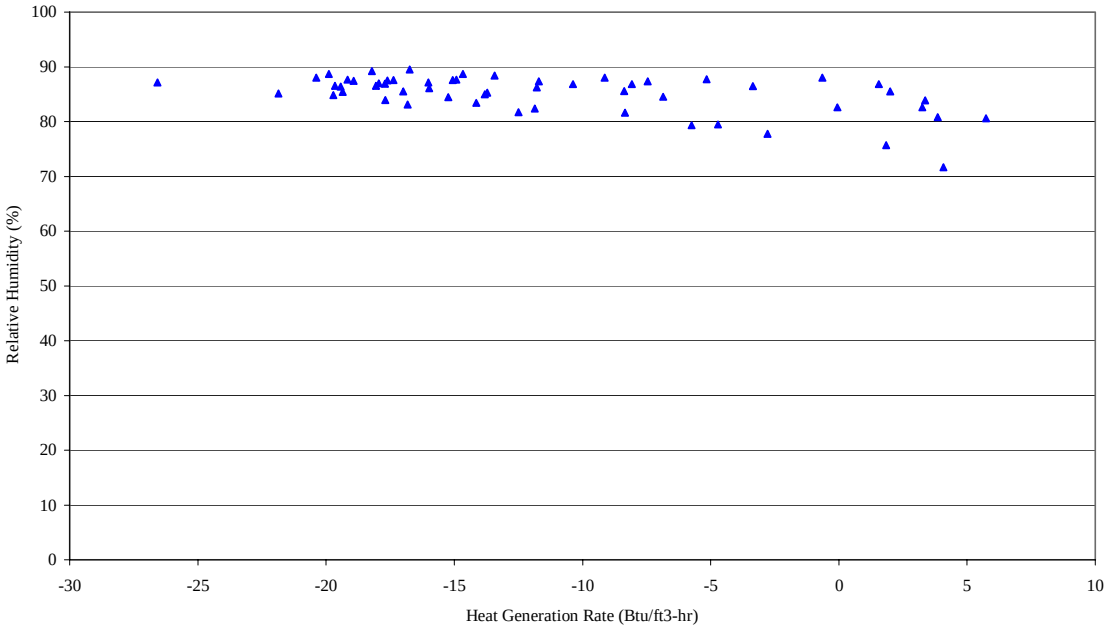

Wet Time Period #1
Heat Generation Correlations
Heat Generation Rate versus Layered Section Relative Humidity

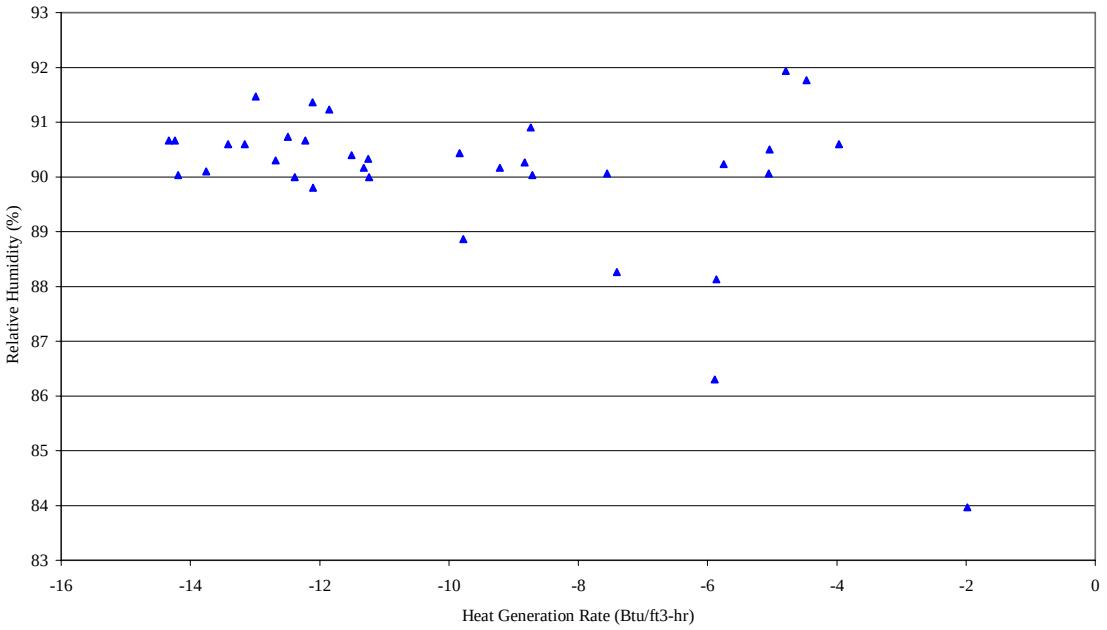

Wet Time Period #2
Heat Generation Correlations
Heat Generation Rate versus Layered Section Relative Humidity